

NPS ARCHIVE
1964
WILSON, P.

USE OF MITROVIC'S METHOD IN PREDICTING
LIMIT CYCLES IN FEEDBACK CONTROL SYSTEMS
WITH ONE AND TWO GAIN VARIABLE
NONLINEARITIES

PAUL L. WILSON

DUDLEY KNOX LIBRARY
NAVAL POSTGRADUATE SCHOOL
MONTEREY CA 93943-5101

Library
U. S. Naval Postgraduate School
Monterey, California

USE OF MITROVIC'S METHOD IN
PREDICTING LIMIT CYCLES IN FEEDBACK
CONTROL SYSTEMS WITH ONE AND TWO
GAIN VARIABLE NONLINEARITIES

* * * * *

Paul L. Wilson

USE OF MITROVIC'S METHOD IN
PREDICTING LIMIT CYCLES IN FEEDBACK
CONTROL SYSTEMS WITH ONE AND TWO
GAIN VARIABLE NONLINEARITIES

by

Paul L. Wilson

Lieutenant, United States Navy

Submitted in partial fulfillment of
the requirements for the degree of

MASTER OF SCIENCE
IN
ELECTRICAL ENGINEERING

United States Naval Postgraduate School
Monterey, California

1 9 6 4

THE UNIVERSITY OF CALIFORNIA
LIBRARY
DIVERSITY
AND
CULTURE

by

Paul L. Wilson

Department of Political Science

Submitted in partial fulfillment of
the requirements for the degree of

Master of Arts

Political Science

United States Naval Postgraduate School
Monterey, California

1964

Library
U. S. Naval Postgraduate School
Monterey, California

USE OF MITROVIC'S METHOD IN
PREDICTING LIMIT CYCLES IN FEEDBACK
CONTROL SYSTEMS WITH ONE AND TWO
GAIN VARIABLE NONLINEARITIES

by

Paul L. Wilson

This work is accepted as fulfilling
the thesis requirements for the degree of
MASTER OF SCIENCE
IN
ELECTRICAL ENGINEERING
from the
United States Naval Postgraduate School

ABSTRACT

Analysis and design of linear feedback control systems by application of the basic Mitrovic method is well established. However, little has been done in applying the basic Mitrovic method to nonlinear systems. The objective of this work was twofold. First, Mitrovic's method as applied to systems with a single gain-variable nonlinearity predicts limit cycles with results comparable to existing analysis methods. Secondly, an analog computer study was made on a system with two gain-variable nonlinearities and the results interpreted by Mitrovic's method.

The analog computer results were obtained by a Donner Scientific Corporation analog computer, Model 3100, at the U. S. Naval Postgraduate School, Monterey, California. The writer wishes to express his appreciation for the assistance and encouragement given him in this endeavor by Professor George Thaler of the U. S. Naval Postgraduate School.

TABLE OF CONTENTS

| Section | Title | Page |
|-------------|--|------|
| Part I | Prediction of Limit Cycles for Systems with One Gain Variable Nonlinearity | |
| | Introduction | 1 |
| Ch. I. | Saturation in the Error Channel | 5 |
| Ch. II. | Dead Zone in the Error Channel | 41 |
| Ch. III | Ideal Relay in the Error Channel | 71 |
| Ch. IV | Relay with Dead Zone in the Error Channel | 113 |
| Ch. V | Nonlinearity in a Feedback Path | 147 |
| Part II | A Study of the Two Nonlinearity Problem | |
| | Introduction | 187 |
| Ch. VI | Description of the Study and Analog Computer Results | 195 |
| Ch. VII | Explanation of the Results Using Mitrovic's Method and Some Prediction Schemes | 227 |
| Ch. VIII | Attempted Extension of the Prediction Schemes to Include More Systems | 257 |
| Ch. IX | Miscellaneous Ideas Concerning the Two Nonlinearity Problem | 267 |
| | Bibliography | 274 |
| Appendix A. | Mitrovic's Basic Equations | 277 |
| Appendix B. | Tabulation of the Experimental Results of the Two Nonlinearity Study | 277 |

LIST OF ILLUSTRATIONS

| Figure | | Page |
|----------|--|------|
| I. | Typical Coefficient Plane of Mitrovic's Method | 2 |
| I-A | Block Diagram of Error Channel Saturation, Loop Transfer Function with No Zeros | 5 |
| I-A-1.1 | Graphical Solution by Mitrovic's Method | 7 |
| I-A-2.1 | Sketch of Root Locus Solution | 10 |
| I-A-3.1 | Gain-Phase Plane of Describing Function Solution | 14 |
| I-A-4.1 | Analog Computer Simulation | 17 |
| I-A-4.2 | Saturation Static Characteristic | 19 |
| I-A-4.3 | Phase Portrait of the System of Figure I-A | 23 |
| I-B | Block Diagram of Error Channel Saturation, Loop Transfer Function with One Zero | 25 |
| I-B-1.1 | Graphical Solution by Mitrovic's Method | 28 |
| I-B-2.1 | Sketch of Root Locus Solution | 30 |
| I-B-3.1 | Gain-Phase Plane of Describing Function Solution | 33 |
| I-B-4.1 | Analog Computer Simulation | 35 |
| I-B-4.2 | Phase Portrait of the System of Figure I-B | 39 |
| II-A | Block Diagram of Dead Zone in the Error Channel, Loop Transfer Function with No Zeros | 41 |
| II-A-1.1 | Sketch of Dead Zone Static Characteristic Showing Relationship of Approximate E_{\max} to N_{ave} | 43 |
| II-A-1.2 | Graphical Solution by Mitrovic's Method | 45 |
| II-A-2.1 | Sketch of Root Locus Solution | 47 |
| II-A-3.1 | Gain-Phase Plane of Describing Function Method | 50 |
| II-A-4.1 | Analog Computer Simulation | 52 |
| II-A-4.2 | Dead Zone Static Characteristic | 54 |
| II-A-4.3 | Phase Portrait of the System of Figure II-A | 58 |

List of Illustrations (Cont'd)

| Figure | | Page |
|-----------|---|------|
| II-B | Block Diagram of Dead Zone in the Error Channel, Loop Transfer Function with One Zero | 60 |
| II-B-1.1 | Graphical Solution by Mitrovic's Method | 64 |
| II-B-2.1 | Sketch of Root Locus Solution | 66 |
| II-B-3.1 | Gain-Phase Plane of Describing Function Method | 69 |
| II-B-4.1 | Analog Computer Simulation | 71 |
| II-B-4.2 | Phase Portrait of System of Figure II-B | 75 |
| III-A | Block Diagram of Ideal Relay in Error Channel, Loop Transfer Function with No Zeros | 77 |
| III-A-1.1 | Graphical Solution by Mitrovic's Method | 81 |
| III-A-2.1 | Sketch of Root Locus Solution | 83 |
| III-A-3.1 | Gain-Phase Plane of Describing Function Method | 86 |
| III-A-4.1 | Analog Computer Simulation | 88 |
| III-A-4.2 | Ideal Relay Static Characteristic | 90 |
| III-A-4.3 | Phase Portrait of System of Figure III-A | 93 |
| III-B | Block Diagram of Ideal Relay in the Error Channel, Loop Transfer Function with One Zero | 95 |
| III-B-1.1 | Graphical Solution by Mitrovic's Method | 100 |
| III-B-2.1 | Sketch of Root Locus Solution | 102 |
| III-B-3.1 | Gain-Phase Plane of Describing Function Method | 105 |
| III-B-4.1 | Analog Computer Simulation | 107 |
| III-B-4.2 | Phase Portrait of the System of Figure III-B | 111 |
| IV-A | Block Diagram of Relay with Dead Zone in Error Channel, Loop Transfer Function with No Zeros | 113 |
| IV-A-1.1 | Graphical Solution by Mitrovic's Method | 117 |
| IV-A-2.1 | Sketch of Root Locus Solution | 119 |

List of Illustrations (Cont'd)

| Figure | | Page |
|----------|--|------|
| IV-A-3.1 | Gain-Phase Plane of Describing Function Method | 122 |
| IV-A-4.1 | Analog Computer Simulation | 124 |
| IV-A-4.2 | Relay with Dead Zone Static Characteristic | 126 |
| IV-A-4.3 | Phase Portrait of System of Figure IV-4 | 129 |
| IV-B | Block Diagram of Relay with Dead Zone in Error Channel, Loop Transfer Function with One Zero | 131 |
| IV-B-1.1 | Graphical Solution by Mitrovic's Method | 134 |
| IV-B-2.1 | Sketch of Root Locus Solution | 136 |
| IV-B-3.1 | Gain-Phase Plane of Describing Function Method | 139 |
| IV-B-4.1 | Analog Computer Simulation | 141 |
| IV-B-4.2 | Phase Portrait of System of Figure IV-B | 145 |
| V-A | Block Diagram of Saturation in a Velocity Feedback Path | 147 |
| V-A-1.1 | Graphical Solution by Mitrovic's Method | 150 |
| V-A-2.1 | Sketch of Root Locus Solution | 153 |
| V-A-3.1 | Block Diagram Manipulation | 155 |
| V-A-3.2 | Gain-Phase Plane of Describing Function Method | 158 |
| V-A-4.1 | Analog Computer Simulation | 161 |
| V-A-4.2 | Phase Portrait of System of Figure V-A | 168 |
| V-B | Block Diagram of Saturation in an Acceleration Feedback Path | 170 |
| V-B-1.1 | Graphical Solution by Mitrovic's Method | 172 |
| V-B-2.1 | Sketch of Root Locus Solution | 175 |
| V-B-3.1 | Gain-Phase Plane of Describing Function Method | 179 |
| V-B-4.1 | Analog Computer Simulation | 181 |
| V-B-4.2 | Phase Portrait of the System of Figure V-B | 187 |

List of Illustrations (Cont'd)

| Figure | | Page |
|--------|---|------|
| VI | Block Diagram of a System with Two Saturations | 189 |
| VI-1 | Analog Computer Simulation of the System of Figure VI | 193 |
| VI-2 | Typical Output Signal of a Saturation Simulation for Large Input Signals | 204 |
| VI-3 | Coefficient plane of System of Figure VI with Constant K_e and K_t Grid | 195 |
| VI-4 | Plot of Analog Computer Results - X_{2max} vs. Linear M-Point K_t with K_e constant | 220 |
| VI-5 | Plot of Analog Computer Results - X_{1max} vs. Linear M-Point K_t with K_e constant | 221 |
| VI-6 | Plot of Analog Computer Results - X_{2max} vs. Linear M-Point K_e with K_t Constant | 222 |
| VI-7 | Plot of Analog Computer Results - X_{1max} vs. Linear M-Point K_e with K_t Constant | 223 |
| VI-8 | Plot of Analog Computer Results - Limit Cycle Wave vs. Linear M-Point K_t with K_e Constant | 224 |
| VI-9 | Plot of Analog Computer Results - Limit Cycle Wave vs. Linear M-Point K_e with K_t Constant | 225 |
| VI-10 | Plot of Various Quantities of the Two Saturation System vs. Elapsed Peaks for a Linear M-Point Just Above No. 2 Dividing Line | 226 |
| VII-1 | Linear System Root Locus of the System of Figure VI, Inner Loop Reduced First | 228 |
| VII-2 | Typical M-Point Loci for Stable Linear Systems with Small Step Inputs | 235 |
| VII-3 | Typical M-Point Loci for Stable Linear Systems with Large Step Inputs | 235 |
| VII-4 | Possible Waveshapes of the Initial Plant Driving Signal for a Large Step Input Signal | 237 |
| VII-5 | Sketch of Phenomenon Occurring at No. 2 Dividing Line | 245 |

List of Illustrations (Cont'd)

| Figure | | Page |
|--------|--|------|
| VII-6 | Proposed Approximate Closed Loop Transfer Function for Stable Linear Systems with Large Step Inputs | 251 |
| VIII-1 | Complete Set of Dividing Lines for Any E_{s2}/E_{s1} Ratio | 262 |
| VIII-2 | Possible Shapes of the Intersection of the Dividing Lines with the Right Side of the Stability Curve | 263 |
| IX-1 | Proposed Method of Calculating the Average M-Point Locus for a Linear M-Point in Region II | 273 |

LIST OF ANALOG COMPUTER RESPONSES

| Recorder Trace | | Page |
|----------------------------|--|---------|
| I-A-4.1 thru I-A-4.3 | Stable Limit Cycle of the System with Error Channel Saturation and No Zeros in the Loop Transfer Function | 20-22 |
| I-B-4.1 and I-B-4.2 | Stable Limit Cycle of the System with Error Channel Saturation and One Zero in the Loop Transfer Function | 37-38 |
| II-A-4.1 thru II-A-4.3 | Unstable Limit Cycle of the System with Dead Zone in the Error Channel and No Zeros in the Loop Transfer Function | 55-57 |
| II-B-4.1 thru II-B-4.3 | Unstable Limit Cycle of the System with Dead Zone in the Error Channel and One Zero in the Loop Transfer Function | 73-74 |
| III-A-4.1 and III-A-4.2 | Stable Limit Cycle of the System with an Ideal Relay in the Error Channel and No Zeros in the Loop Transfer Function | 91-92 |
| III-B-4.1 and III-B-4.2 | Stable Limit Cycle of the System with an Ideal Relay in the Error Channel and One Zero in the Loop Transfer Function | 109-110 |
| IV-A-4.1 and IV-A-4.2 | Stable Limit Cycle of the System with a Relay with Dead Zone in the Error Channel and No Zeros in the Loop Transfer Function | 127-128 |
| IV-B-4.1 and IV-B-4.2 | Stable Limit Cycle of the System with a Relay with Dead Zone in the Error Channel and One Zero in the Loop Transfer Function | 143-.44 |
| V-A-4.1 thru V-A-4.5 | Stable and Unstable Limit Cycles of the System with Saturation in the Velocity Feedback Path | 163-167 |
| V-B-4.1 thru V-B-4.3 | Unstable Limit Cycle of the System with Saturation in the Acceleration Feedback Path | 184-186 |
| VI-1 thru VI-6 | Responses of Stable Linear Systems to Large and Small Step Inputs | 205-210 |
| VI-7 and VI-8 | Responses Showing a Stable Limit Cycle Resulting from Stable Linear Systems with Repeated Disturbances | 211-212 |
| VI-9 thru VI-11 | Responses Showing Dependency of the Limit Cycle on the Linear M-Point but not the Magnitude of Input Step | 213-215 |

LIST OF ANALOG COMPUTER RESPONSES (Cont'd)

| Recorder Trace | | Page |
|--------------------|--|---------|
| VI-12 and VI-13 | Responses Showing the Change in the Limit Cycle as the Linear M-Point Moves Across No. 1 Dividing Line | 216-217 |
| VI-14 and VI-15 | Responses Showing the Change in the Limit Cycle as the Linear M-Point Crosses No. 2 Dividing Line | 218-219 |

LIST OF SYMBOLS

| | |
|---------------------------|---|
| $B_o, B_1, B_2 \dots B_n$ | Designation of an assumed variable coefficient of the characteristic equation |
| B_{nave} | The "pseudo average" value of an assumed variable coefficient over a cycle or half cycle. |
| B_{nmin} | The instantaneous minimum value of an assumed variable coefficient during a half cycle. |
| N | The instantaneous value of the gain of the nonlinear element over a cycle or half cycle of oscillation. |
| N_{ave} | The "pseudo average" gain of the nonlinear element over a cycle or half cycle of oscillation. |
| N_{min} | The instantaneous minimum gain of the nonlinear element over a cycle or half cycle of oscillation. |
| X | The input signal to the nonlinear element |
| Y | The output signal of the nonlinear element |
| θ_i or E_i | The magnitude of the step input signal to the system |
| | The error signal |
| θ_o | The output signal |
| K | The linear plant gain |
| K_e | The linear gain of the error channel |
| K_t | The linear gain of the tachometer channel |

PART I

PREDICTION OF LIMIT CYCLES BY MITROVIC'S METHOD FOR CONTROL SYSTEMS WITH ONE GAIN VARIABLE NONLINEARITY

Introduction.

Mitrovic's method is easily applied to nonlinear control systems if the nonlinearity can be described by an input-output characteristic in which the output is an odd single-valued function of the input. Such a nonlinearity can then be expressed as an instantaneous variable gain with zero phase shift. This property allows the nonlinear effect to be expressed as a variable coefficient of the system characteristic equation. For the nonlinearity in the error channel, such a system can only have limit cycles if the linear system is unstable since the nonlinearity contributes no phase shift.

Mitrovic's method determines absolute stability for a linear system, which has fixed coefficients in the characteristic equation, by assuming two of the coefficients to be variable. The method derives equations for two coefficients with ζ and ω_n of the S-plane as parameters. With the $j\omega$ axis ($\zeta = 0$) as the S-plane mapping contour, the curve of one coefficient versus the other coefficient is plotted using different values of ω_n . If this curve encircles a point defined as the working point or M-point in a clockwise direction for increasing ω_n , the system is stable. The working point is determined by the fixed values of the two coefficients which were assumed variable.

For a nonlinearity, as described above, one or more coefficients of the characteristic equation are variable. This manifests itself on the variable coefficient plane as a locus of possible working point locations.

Thus a limit cycle for the nonlinear system exists for the conditions at the intersection of the working point locus and the stability ($\zeta = 0$) curve. A typical Mitrovic plot is shown in Figure I. The frequency of the limit cycle is read from the stability curve at the intersection. The amplitude is determined approximately from the gain of the nonlinearity obtained from the working point locus.

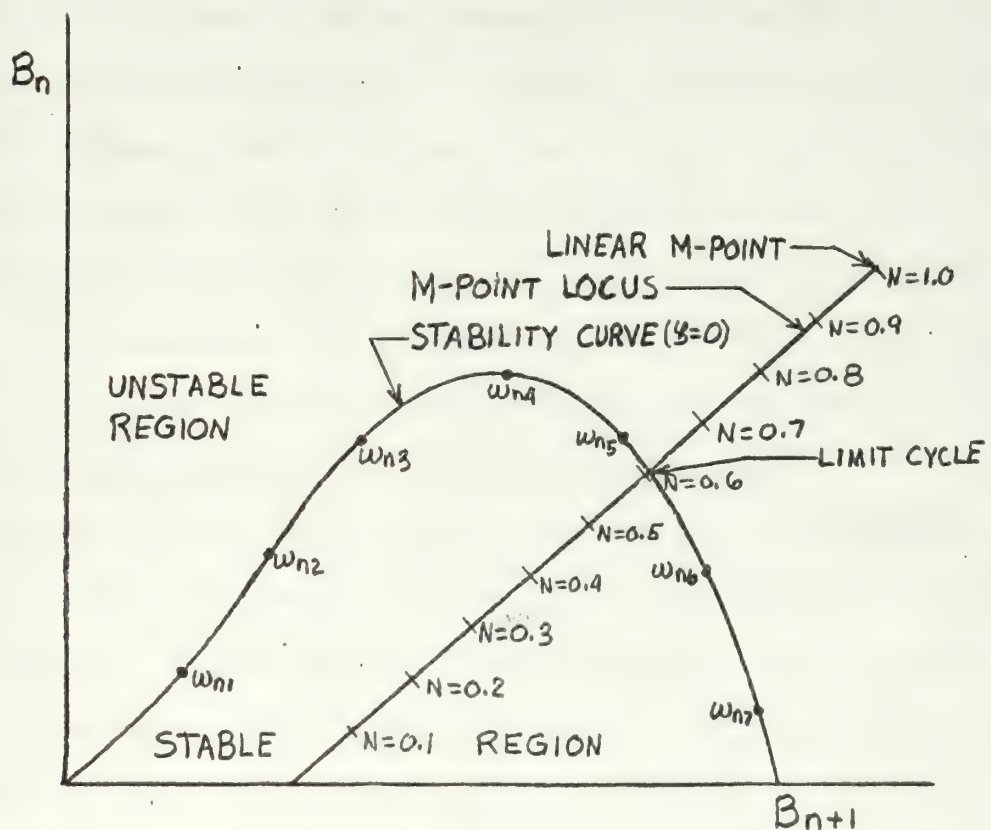


Figure I

Coefficient Plane of Mitrovic's Method

The amplitude determined in this manner will necessarily be less than the actual amplitude. The gain of the nonlinearity is defined as the ratio of the instantaneous output to the instantaneous input and the actual amplitude could be determined accurately if during a cycle the

minimum/maximum instantaneous gain could be determined. However, the non-linear gain determined from the Mitrovic plot is a "psuedo - average" gain over a complete cycle, since this "psuedo - average" gain is determined from an "average" M-point position over a cycle.

The shape of the stability curve on a coefficient plane depends on the two coefficients chosen and the order of the characteristic equation. If the coefficients of the S^0 and S^1 are chosen variable, then the stability curve for a third order system is a straight line on the B_0 versus B_1 plane, for a fourth order system the stability curve is a parabola, and so on. If different coefficients are chosen variable, then the stability curve has a different shape on the corresponding coefficient plane.

The working point locus depends also on the linear system and specifically the number of zeros in the loop transfer function. For no zeros in the loop transfer function and the nonlinearity in the forward path, the working point locus is as straight line segment parallel to the B_0 axis since the variable nonlinear gain appears only in the constant coefficient of the characteristic equation. For a linear system with one zero in the loop transfer function, the working point locus is again a straight line segment with a specific slope on the B_0 versus B_1 plane. Other systems can be conceived with different placements of the nonlinearity but the basic working point locus is always a straight line segment on the appropriate coefficients plane.

The use of Mitrovic's method for a nonlinear system for which the linear loop transfer function has two or more zeros becomes more complicated. In this case the nonlinear gain appears in three or more coefficients of the characteristic equation. With only two assumed variable

coefficients, the stability curve becomes a family of curves with the nonlinear gain a parameter. To determine the limit cycles for such a system the intersection of the straight line working point locus and the family of stability curves must be found.

The various systems chosen to analyze in the chapters of Part One are completely arbitrary. The author had no specific system or specific device in mind when the block diagram was drawn. Consequently, all signals in the various systems are referred to in volts. The following guidelines were followed in order to simplify the analysis without disrupting the arbitrary nature of the system:

1. The poles and zeros of the linear loop transfer function were in general chosen one octave apart. This was done in order to sketch the actual Bode magnitude curve in the describing function analysis from the asymptotic plot by applying the usual corrections at the corner frequency and two octaves either side of the corner frequency.

2. The magnitudes of the poles, zeros, and gain constants were chosen to eliminate magnitude and time scaling procedures in the analog computer simulations of the system.

CHAPTER I

SATURATION IN ERROR CHANNEL

I-A Loop Transfer Function with No Zeros.

The block diagram of the system chosen to analyze is given in Figure I-A.

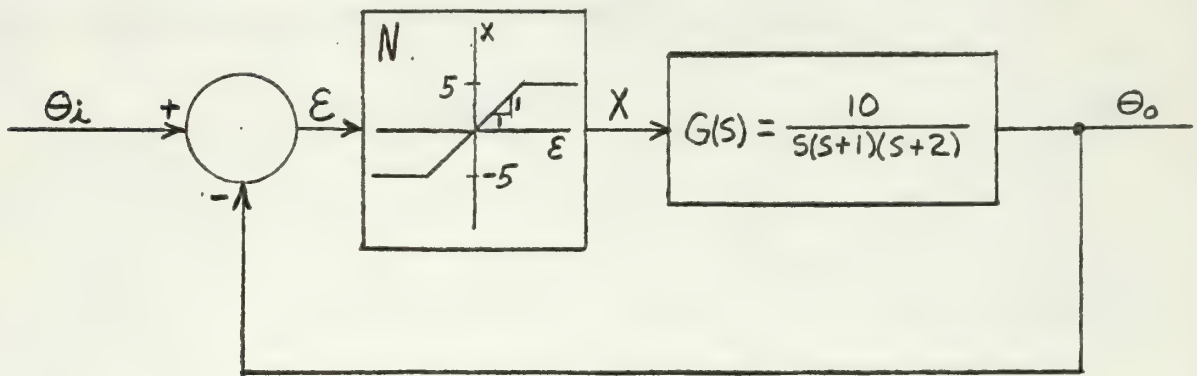


Figure I-A

Saturation in Error Channel
Loop Transfer Function with No Zeros

I-A-1. Mitrovic's Method.

Assigning the variable gain N to the nonlinearity, the characteristic equation becomes,

$$s^3 + 3s^2 + 2s + 10N = 0. \quad (\text{I-A-1.1})$$

Assuming the last two coefficients variable the characteristic equation is rewritten,

$$s^3 + 3s^2 + B_1s + B_0 = 0 \quad (\text{I-A-1.2})$$

From Appendix A, Mitrovic's equations for B_0 and B_1 are,

$$B_0 = -[3\omega_n^2 \phi_1(\xi) + \omega_n^3 \phi_2(\xi)] \quad (\text{I-A-1.3})$$

and

$$B_1 = 3\omega_n \phi_2(\xi) + \omega_n^2 \phi_3(\xi) . \quad (\text{I-A-1.4})$$

Substitution of the values of the ϕ functions Appendix A for $\xi = 0$ gives the parametric equations of the stability curve as

$$B_0 = 3\omega_n^2 \quad (\text{I-A-1.5})$$

and

$$B_1 = \omega_n^2 . \quad (\text{I-A-1.6})$$

From comparison of equations I-A-1.1 and I-A-1.2, it is seen that the equations describing the M-point locus are

$$B_0 = 10N \quad (\text{I-A-1.7})$$

and

$$B_1 = 2 . \quad (\text{I-A-1.8})$$

Thus the set of four parametric equations I-A-1.5 through I-A-1.8 describe the two curves whose intersection is desired for limit cycle determination.

At the intersection, Equation I-A-1.5 equals Equation I-A-1.7 and Equation I-A-1.6 equals Equation I-A-1.8. Thus,

$$\omega_n^2 = 2 \quad (\text{I-A-1.9})$$

and

$$10 N_{ave} = 3 \omega_n^2. \quad (\text{I-A-1.10})$$

Solution of these two simultaneous equations yields,

$$\omega_n = 1.414 \text{ rad/sec} \quad (\text{I-A-1.11})$$

and

$$N_{ave} = 0.6. \quad (\text{I-A-1.12})$$

Since the nonlinear gain N is defined as the ratio of the output to the input,

$$\epsilon_{max} = \frac{5}{N_{ave}}. \quad (\text{I-A-1.13})$$

Thus the frequency of the limit cycle is given by equation I-A-1.11 and the approximate amplitude by I-A-1.13 or

$$\epsilon_{max} = 8.33 \text{ Volts}. \quad (\text{I-A-1.14})$$

The above solution is presented graphically in Figure I-A-1.1.

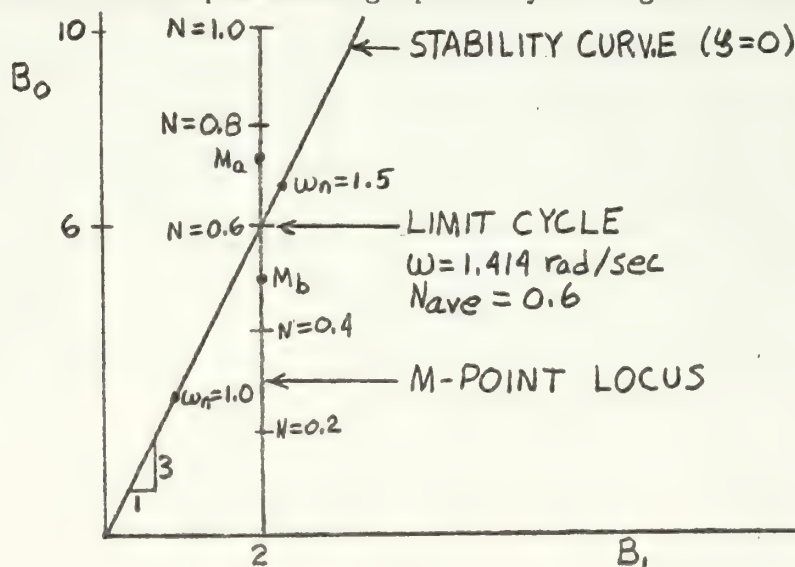


Figure I-A-1.1

Graphical Solution for Saturation in Error Channel, Loop Transfer Function with no Zeros

The limit cycle is a stable limit cycle as determined by the following reasoning. If the input signal, Θ_{λ} , is large enough such that N is small enough to place the instantaneous M-point at say M_b in Figure I-A-1.1. The system is instantaneously stable and the oscillations decrease. As the oscillations decrease, N increases moving the instantaneous M-point above the stability curve. Here the system is unstable and the oscillations increase thereby decreasing N and moving the M-point back into the stable region. Eventually a dynamic equilibrium will occur in which the "pseudo average" M-point lies on the intersection of the two curves. If the input signal is small enough, N will be large enough such that the instantaneous M-point lies at say M_a at which point the system is unstable. By similar reasoning as above, the "pseudo - average" M-point will again eventually end up at the intersection.

I-A-2. Root Locus Method.

The root locus method of analyzing a system with such a non-linearity consists of construction of the linear root locus and determining the point where the root locus crosses the $J\omega$ axis.

The system characteristic equation is

$$s^3 + 3s^2 + 2s + 10N = 0 . \quad (\text{I-A-2.1})$$

Substitution of $s = J\omega$ and simplifying

$$-J\omega^3 - 3\omega^2 + J2\omega + 10N = 0 . \quad (\text{I-A-2.2})$$

By requiring that both the real and imaginary part of equation I-A-2.2 go to zero independently,

$$-J\omega^3 + J2\omega = 0 \quad (\text{I-A-2.3})$$

and

$$-3\omega^2 + 10N = 0 . \quad (\text{I-A-2.4})$$

Dividing equation I-A-2.3 by $J\omega$ the frequency is obtained as

$$\omega = 1.414 \text{ rad/sec.}$$

By substituting ω into equation I-A-2.4 the "pseudo - average" gain over a complete cycle is obtained as

$$N_{ave} = 0.6$$

from which the approximate amplitude of the limit cycle is determined as

$$\mathcal{E}_{max} = \frac{5}{0.6} = 8.33 \text{ Volts} .$$

A sketch of the root locus solution is given in Figure I-A-2.1.

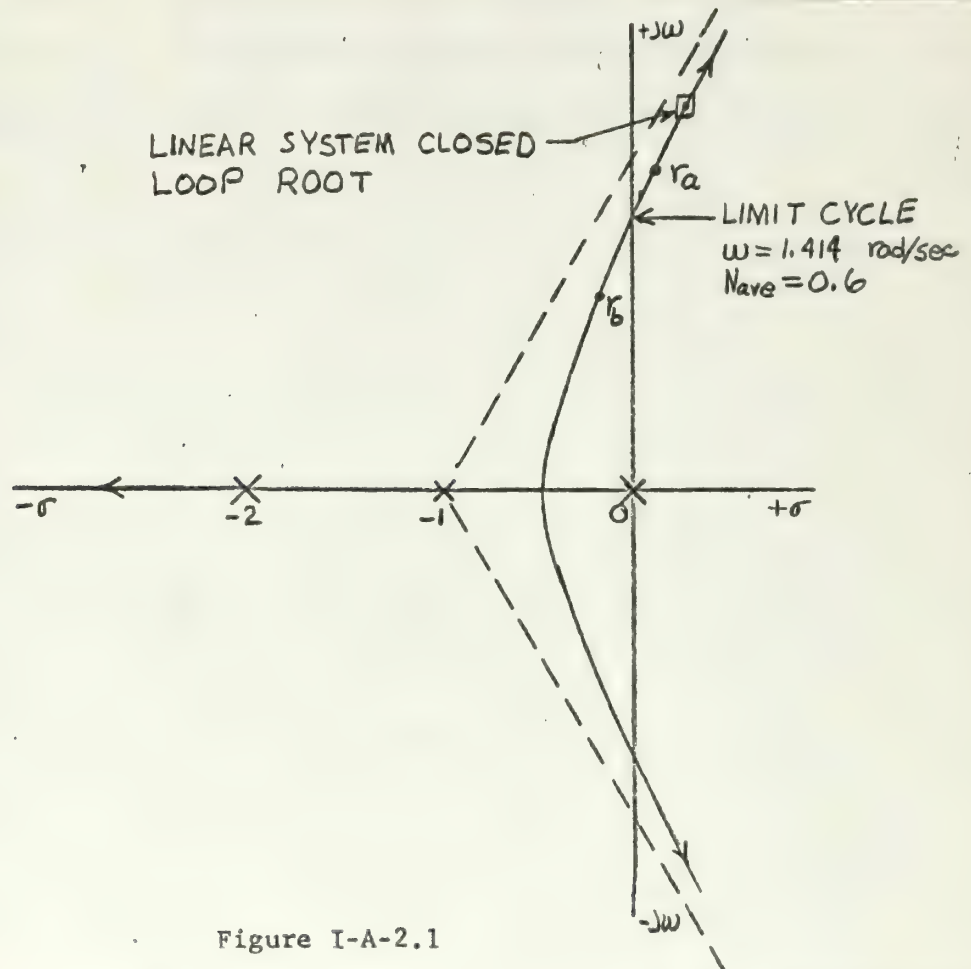


Figure I-A-2.1

Root Locus Solution for Saturation in Error Channel

Loop Transfer Function with No Zeros

The root locus method also gives a stable limit cycle by the following reasoning. If the input signal is large enough, N will be small enough such that the instantaneous root location is at r_b in Figure I-A-2.1. The system is stable and the oscillations decrease. As the oscillations decrease N increases moving the instantaneous root into the right half plane. The system is now unstable, the oscillations increase causing N to decrease, and the instantaneous root moves back into left

half plane. Eventually a dynamic equilibrium is established in which the "average" root location is at the imaginary axis cross-over. If the input signal is small, N is large placing the instantaneous root in the right half plane at r_a . By a similar reasoning the "average" root location over a cycle will again lie at the imaginary axis cross-over.

I-A-3. Describing Function Method.

Application of describing function theory to the given system entails plotting the linear loop transfer function and the negative reciprocal of the describing function on the gain-phase plane (Nichols plot). Limit cycles of the system are then given by the intersections of the two curves on the gain-phase plane.

The describing function for a saturating element with unity gain in the linear region is

$$G_D = \frac{2}{\pi} [\sin^{-1} R + R \sqrt{1-R^2}] \angle 0^\circ \quad (\text{I-A-3.1})$$

where

$$R = \frac{E_{\text{sat}}}{E_{\text{max}}} \quad (\text{I-A-3.2})$$

The linear loop transfer function in frequency response form is

$$G(j\omega) = \frac{5}{j\omega(j\omega+1)(0.5j\omega+1)} \quad (\text{I-A-3.3})$$

Since G_D has no phase shift then $1/G_D$ has an associated phase angle of -180° , and the $1/G_D$ curve lies entirely on the -180° axis of the gain-phase plane. Consequently, the only region of the linear loop transfer function which is of interest is the region in which the phase shift is -180° . The values of gain in db and phase of the linear loop transfer function in the region of -180° which were used to plot on the gain-phase plane are given in Table I-A-3.1. These values were obtained from a Bode diagram plot of the linear loop transfer function.



TABLE I-A-3.1

| ω | $ G(j\omega) _{db}$ | $\angle G(j\omega)$ deg |
|----------|---------------------|-------------------------|
| 1.0 | 9.8 | -162 |
| 1.1 | 8.5 | -167.5 |
| 1.2 | 7.1 | -172 |
| 1.3 | 5.8 | -176 |
| 1.4 | 4.5 | -179.5 |
| 1.5 | 3.3 | -183 |
| 1.6 | 2.2 | -186 |

The values of $1/G_D$ in db were calculated for various values of R according to equation I-A-3.1 and appear in Table I-A-3.2. The gain-phase plane of the system is shown in Figure I-A-3.1.

TABLE I-A-3.2

| R | G_D | $1/G_D$ | $1/G_D$ db |
|------|-------|----------|------------|
| 0.0 | 0 | ∞ | ∞ |
| 0.1 | 0.127 | 7.88 | 17.92 |
| 0.2 | 0.253 | 3.95 | 11.94 |
| 0.3 | 0.376 | 2.66 | 8.5 |
| 0.4 | 0.496 | 2.02 | 6.1 |
| 0.5 | 0.609 | 1.642 | 4.32 |
| 0.6 | 0.716 | 1.396 | 2.9 |
| 0.49 | 0.598 | 1.673 | 4.48 |

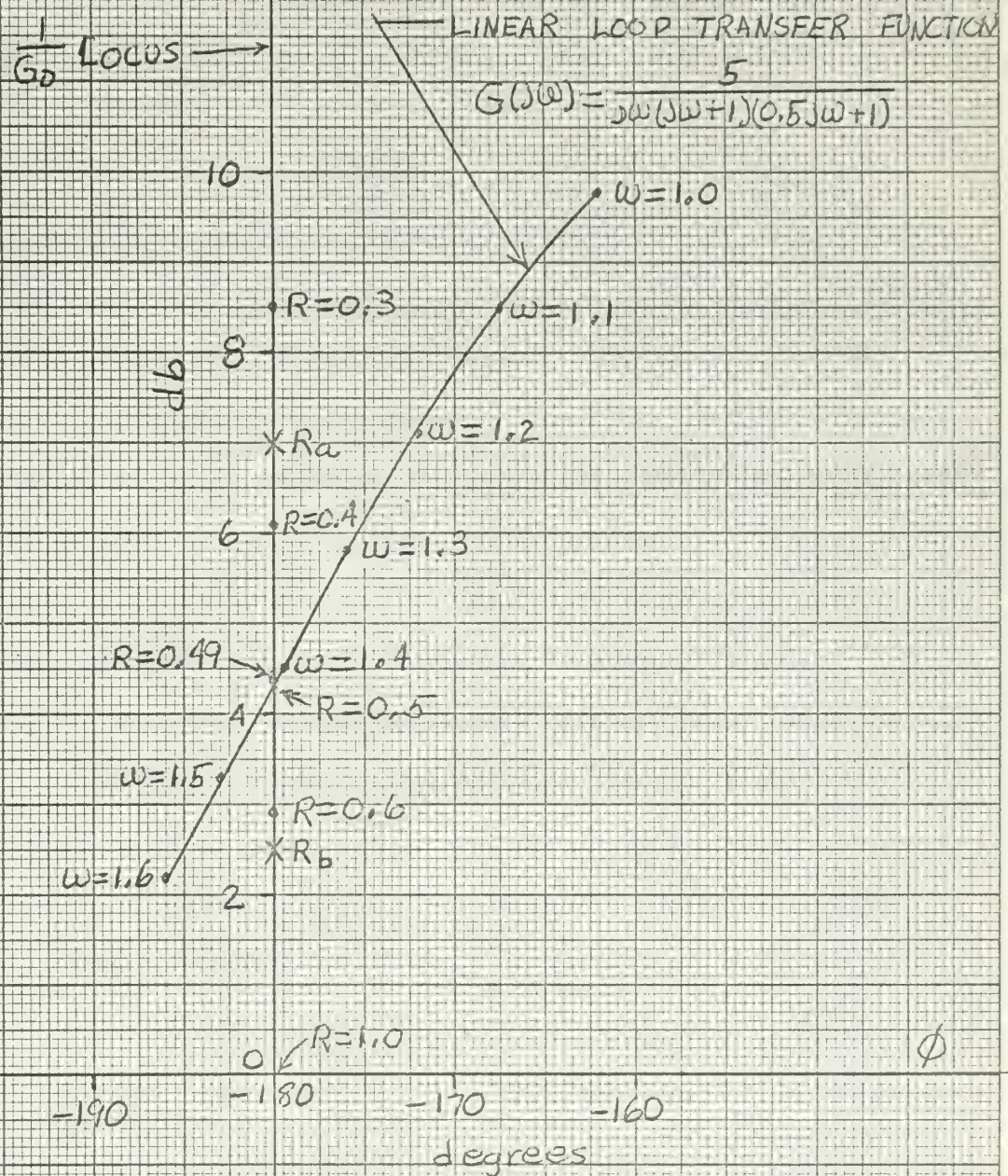


FIGURE 1 A 3.1

GAIN-PHASE PLANE - SATURATION IN
ERROR CHANNEL, LOOP TRANSFER
FUNCTION WITH NO ZEROS

By interpolation of Figure I-A-3.1, the intersection occurs at

$$\omega = 1.41 \text{ rad/sec}$$

and

$$R = 0.495 \quad \bullet$$

Thus from Equation I-A-3.2 the amplitude of the limit cycle is

$$E_{\max} = 10.1 \text{ volts} \quad \bullet$$

Assuming the $1/G_D$ curve to be the locus of the critical point of the system, the describing function method predicts a stable limit cycle by the following reasoning. If the input signal, Θ_i , is large R will be small and the instantaneous critical point lies above the $G(j\omega)$ curve say at point R_a in I-A-3.1. The system is momentarily stable due to a positive phase margin and the oscillations will decrease. As the oscillations decrease, R increases and the critical point moves below the $G(j\omega)$ curve. The system is now unstable due to a negative phase margin and the oscillations increase moving the critical point above the $G(j\omega)$ curve. Eventually a dynamic equilibrium is reached in which the "average" critical point over a cycle lies at the intersection of the two curves. If the input signal is small, R is large and the critical point is momentarily below the $G(j\omega)$ curve at R_b . The system is unstable and the oscillations increase. Similar reasoning shows again that the "average" critical point over a cycle will eventually lie at the intersection of the two curves.

I-A-4. Analog Computer Simulation.

The simulation of the given nonlinear system is given in Figure I-A-4.1. The coefficient pot settings with associated resistances and capacitances for real time and real magnitude scaling are given in Table I-A-4.1.

TABLE I-A-4.1

| Pot Setting | Associated Elements |
|----------------------------------|--|
| $a_1 = \frac{E_1}{100}$ | For Input Step of E_1 volts and $R_1 = 1 \text{ Meg}, \quad R_{f1} = 1 \text{ Meg}$ |
| $a_2 = 1.0$ | $R_2 = 1 \text{ Meg} \quad R_{f1} = 1 \text{ Meg}$ |
| $a_3 = 1.0$ | $R_3 = 1 \text{ Meg} \quad R_{f2} = 1 \text{ Meg}$ |
| $a_4 = 1.0$ | $R_4 = 1 \text{ Meg} \quad C_{f1} = 1 \text{ uf}$ |
| $a_5 = 1.0$ | $R_5 = 1 \text{ Meg} \quad C_{f1} = 1 \text{ uf}$ |
| $a_6 = 1.0$ | $R_6 = 0.1 \text{ Meg} \quad C_{f2} = 1 \text{ uf}$ |
| $a_7 = 1.0$ | $R_7 = 0.5 \text{ Meg} \quad C_{f2} = 1 \text{ uf}$ |
| $a_8 = 1.0$ | $R_8 = 1 \text{ Meg} \quad C_{f3} = 1 \text{ uf}$ |
| $a = 0.05$ Initial Setting | For a 5 Volt Saturation Voltage |

To accurately set the back-biasing pots, "a", a sine wave generator was connected to the input of the saturation simulator. The two pots were then adjusted until the saturated output voltage was exactly 5 volts on a recording device. The frequency of the generator was set at 0.01 cps and the static characteristic of the saturation simulation was obtained by an X-Y recorder. This characteristic appears as Figure I-A-4.2.

The system was first excited with a 2 volt step input signal. The

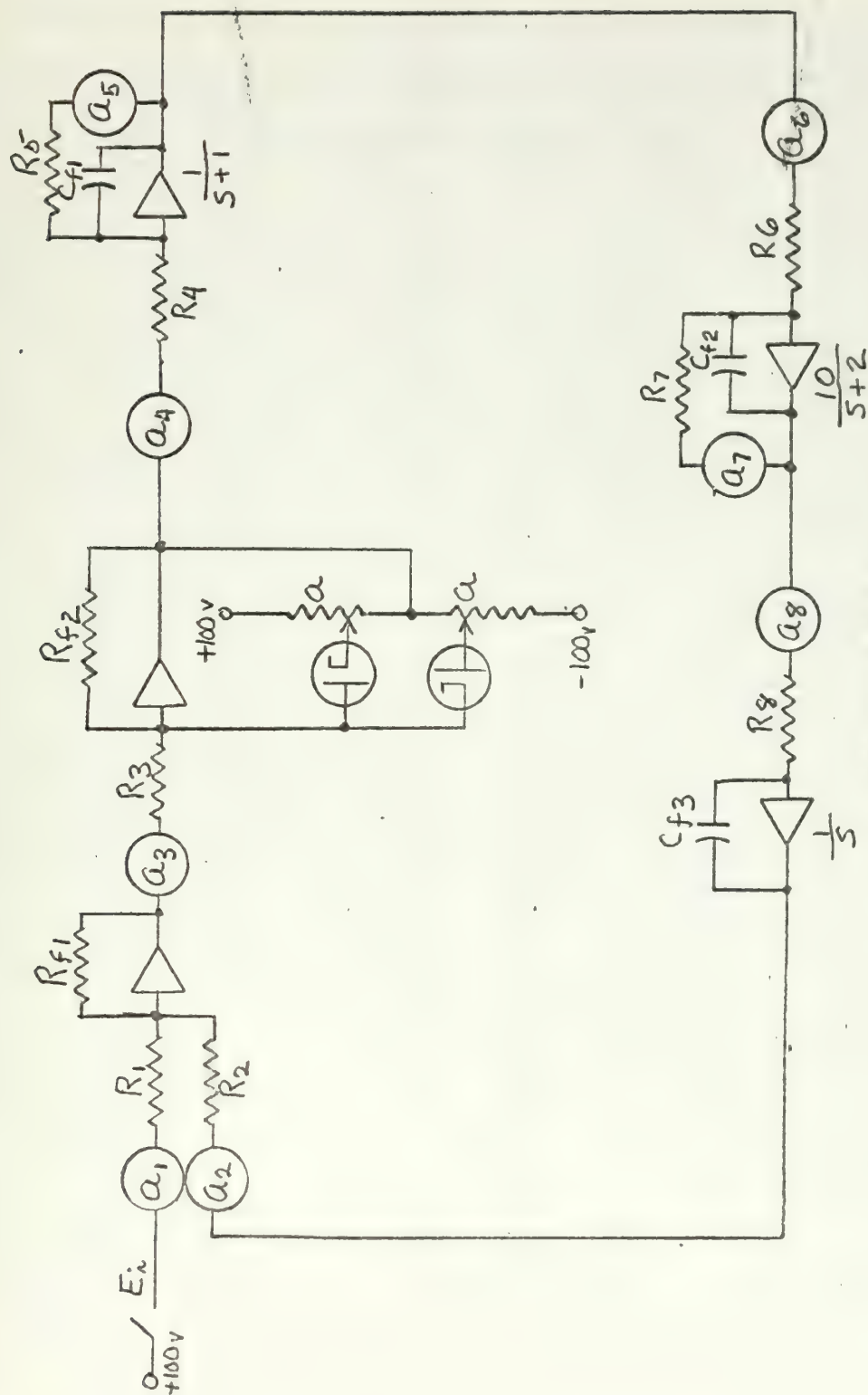


Figure 1A-4.1

Analog Computer Simulation of Error Amplifier Saturation, Loop Transfer Function with No Zeros.

system was found to go in to the limit cycle shown in recorder trace I-A-4.1. The system was then excited with a 20 volt step input and was found to go into the same limit cycle (recorder trace I-A-4.2). From the recorder traces the limit cycle is a stable limit cycle with an angular frequency of 1.395 rad/sec and 10.0 volts amplitude. The phase portrait for the system appears in Figure I-A-4.3.

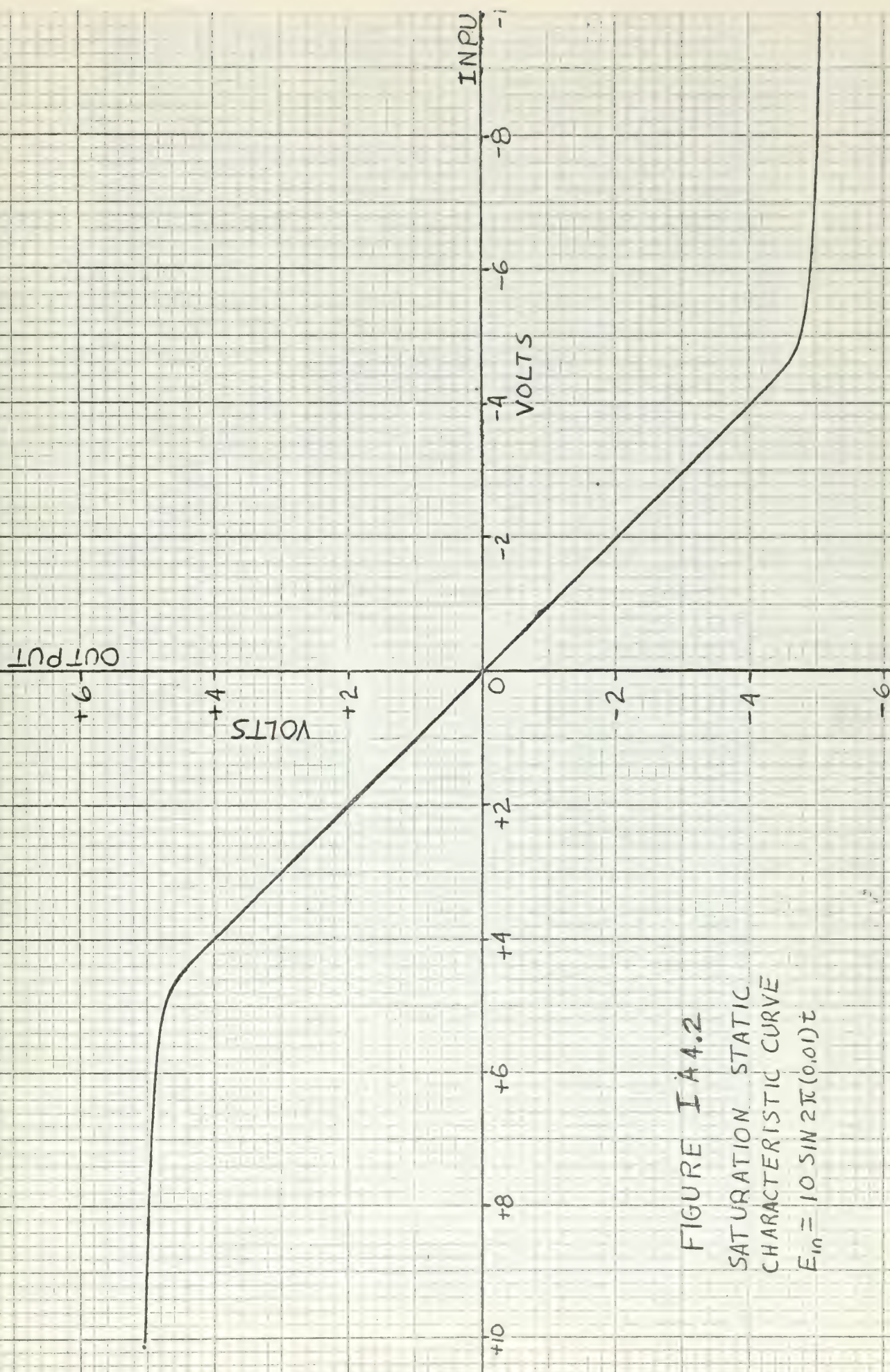
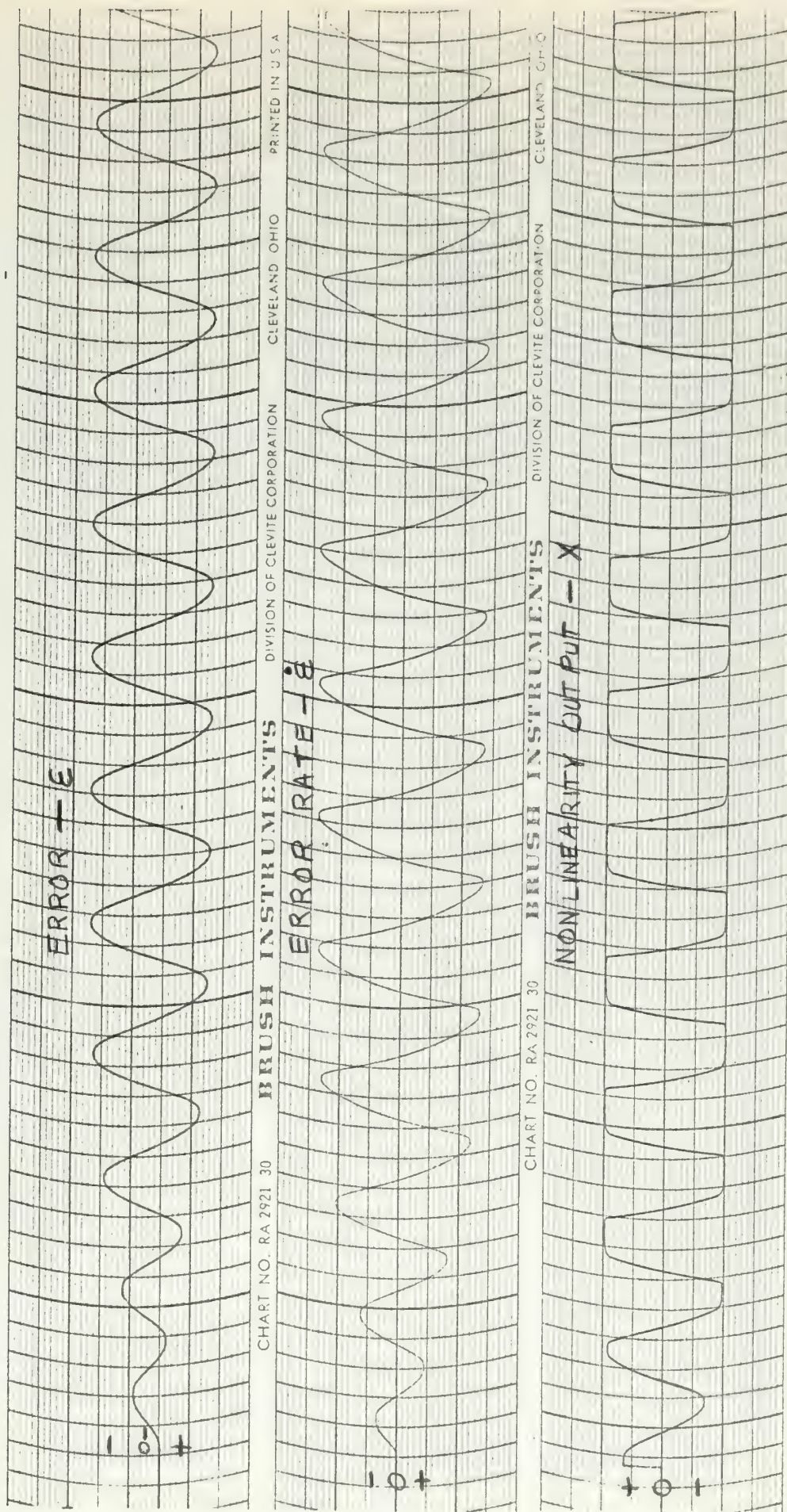
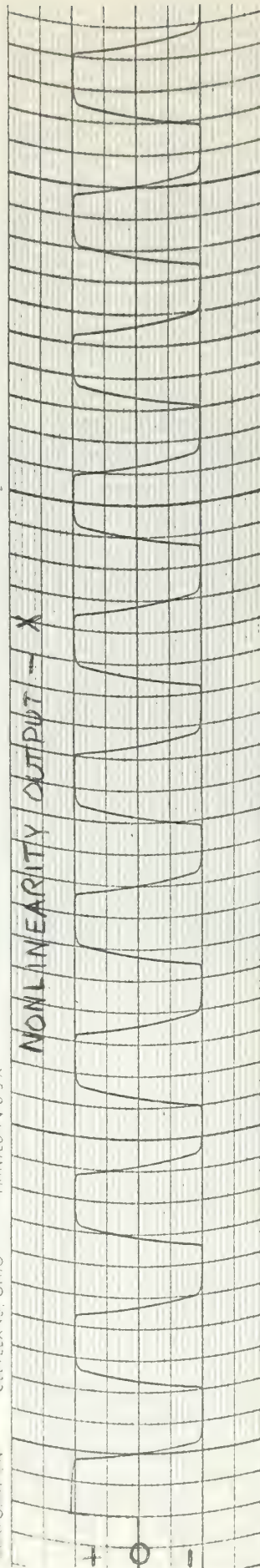
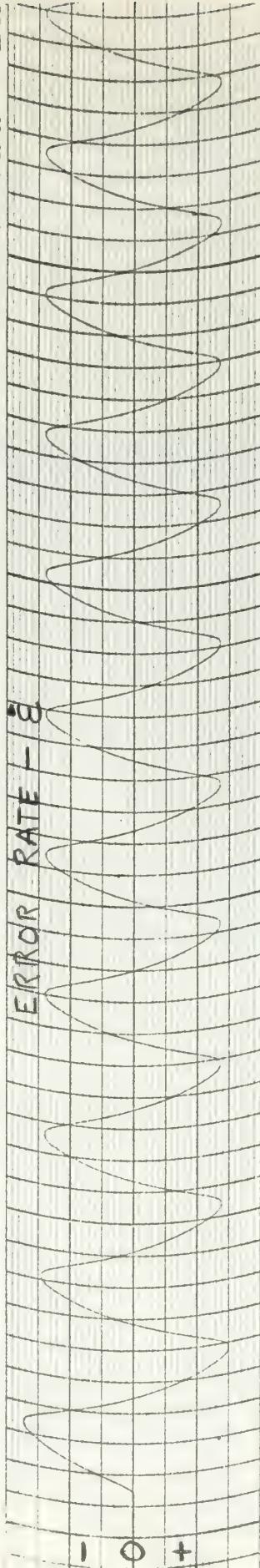
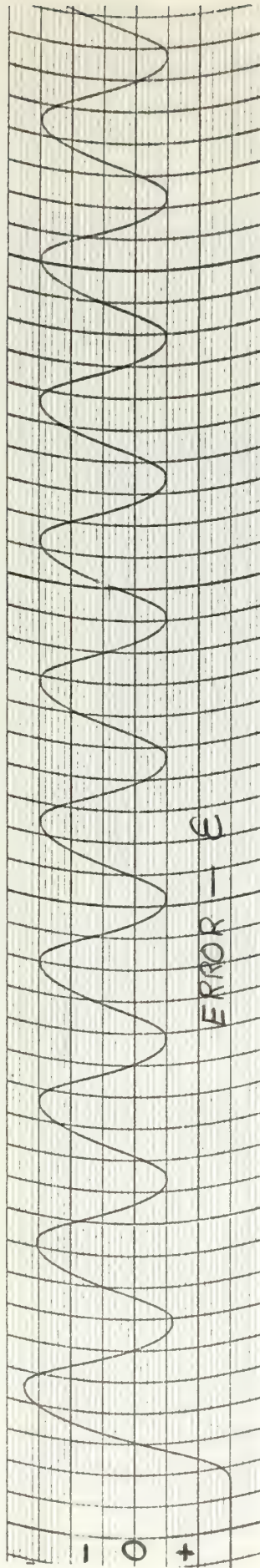


FIGURE 1A4.2
SATURATION STATIC
CHARACTERISTIC CURVE
 $E_{in} = 10 \sin 2\pi(0.01)t$



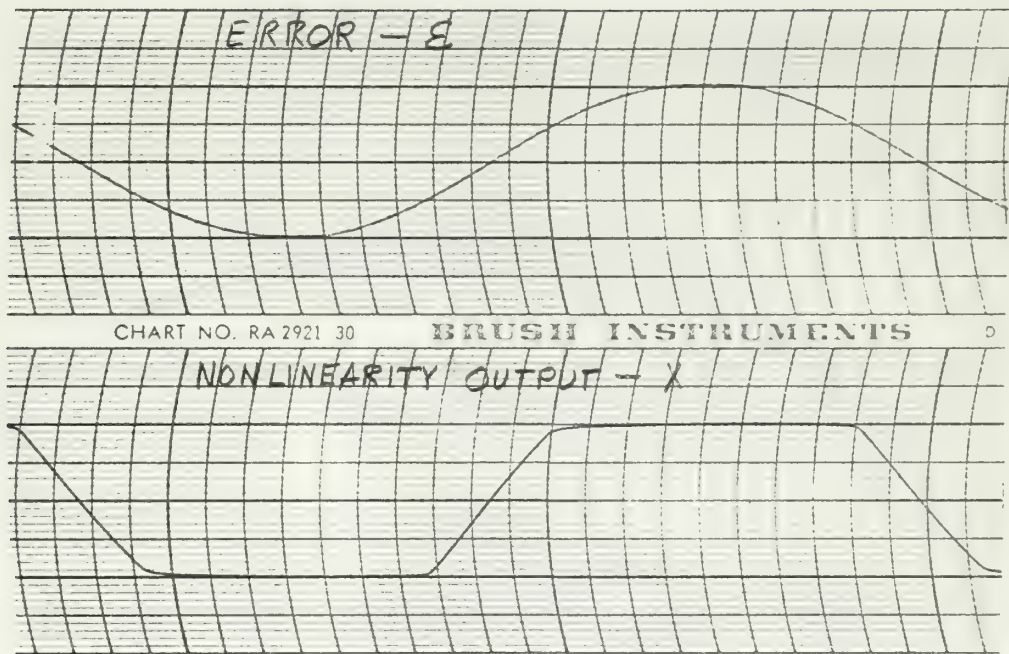
Recorder Trace 1-A-4.1
 Error Channel Saturation, Loop Transfer Function with No Forcs, 2 Volts Step Input
 SCALES: $E = \text{Volts/Line}$ $\dot{E} = 1 \text{ Volt/Line}$ $X = 0.4 \text{ Volts/Line}$



Recorder Trace T-A-4.2

Error Channel Saturation, Loop Transfer Function with No Delay, 20 V/10 Step Input

SCALES: $E = 1 \text{ V/10/10}^{-4}$ $\dot{E} = 1 \text{ V/10/10}^{-4}$ $X = 1 \text{ V/10/10}^{-4}$ Time = 1 Second/10



Recorder Trace I-A-4.3

Limit Cycle Measurement, Error Channel Saturation, Loop
Transfer Function with No Zeros.

Scales: E - 1 Volt/Line X - 0.5 Volts/Line

Time - 0.2 Second/Division

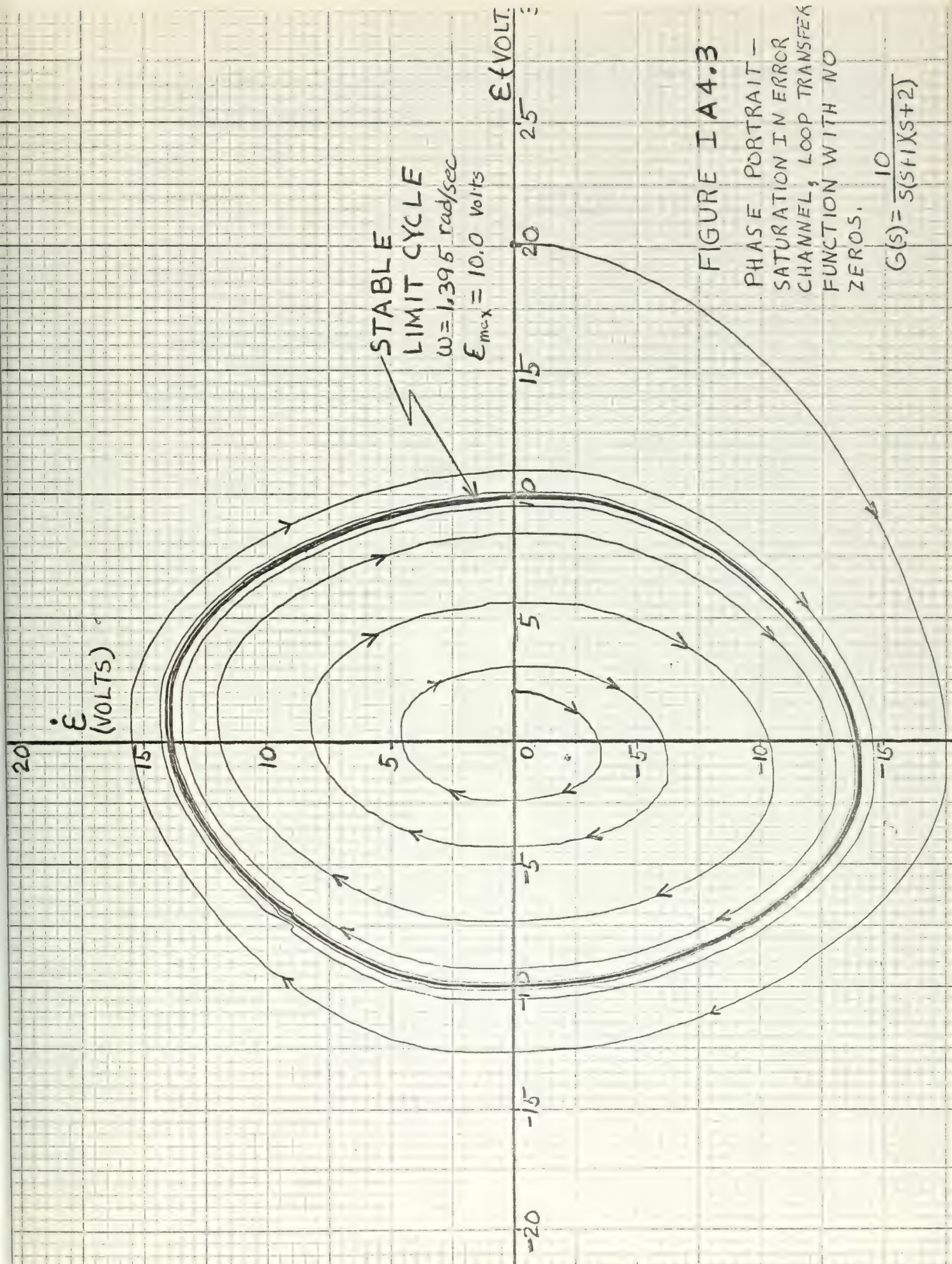


FIGURE I A 4.3

PHASE PORTRAIT -
 SATURATION IN ERROR
 CHANNEL, LOOP TRANSFER
 FUNCTION WITH NO
 ZEROS.

$$G(s) = \frac{10}{s(s+1)(s+2)}$$

I-A-5. Comparison of the Four Analytic Methods in Limit Cycle Prediction for the System of Figure I-A.

| Method | Frequency (rad/sec) | Amplitude (volts) |
|---------------------|------------------------|----------------------|
| Mitrovic's | 1.414 | 8.33 |
| Root Locus | 1.414 | 8.33 |
| Describing Function | 1.41 | 10.1 |
| Analog Simulation | 1.395 | 10.0 |

I-B. Loop Transfer Function with One Zero.

The block diagram of the system chosen to analyze is shown in Figure I-B.

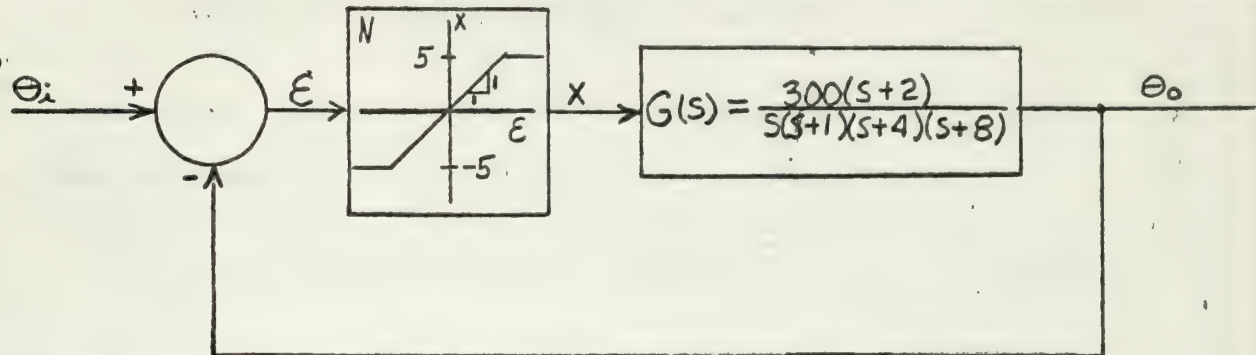


Figure I-B

Saturation in Error Channel Loop

Transfer Function with One Zero



I-B-1. Mitrovic's Method.

If N is the instantaneous gain of the nonlinearity the characteristic equation for the system is

$$s^4 + 13s^3 + 44s^2 + (32 + 300N)s + 600N = 0 \quad (I-B-1.1)$$

Assuming the last two coefficients to be variable, the characteristic equation becomes,

$$s^4 + 13s^3 + 44s^2 + B_1s + B_0 = 0 \quad (I-B-1.2)$$

where

$$B_1 = 32 + 300N \quad (I-B-1.3)$$

and

$$B_0 = 600N \quad (I-B-1.4)$$

From Appendix A, Mitrovic's equations for B_0 and B_1 are,

$$B_0 = -[44\omega_n^2\phi_1(\xi) + 13\omega_n^3\phi_2(\xi) + \omega_n^4\phi_3(\xi)] \quad (I-B-1.5)$$

and

$$B_1 = 44\omega_n\phi_2(\xi) + 13\omega_n^2\phi_3(\xi) + \omega_n^3\phi_4(\xi) \quad (I-B-1.6)$$

Substitution of the values of the ϕ functions from Appendix A for

$\xi = 0$ gives,

$$B_0 = 44\omega_n^2 - \omega_n^4 \quad (I-B-1.7)$$

and

$$B_1 = 13\omega_n^2 \quad (I-B-1.8)$$

Thus the sets of parametric equations I-B-1.3, I-B-1.4, I-B-1.7, and I-B-1.8 describe the stability curve and the working point locus on

the B_0 versus B_1 plane. To find the intersection of two curves solve Equation I-B-1.8 for ω_n^2 and substitute in Equation I-B-1.7 to obtain

$$B_0 = \frac{44}{13} B_1 - \frac{B_1^2}{169} \quad (\text{I-B-1.9})$$

Solving Equation I-B-1.4 for N and substituting in Equation I-B-1.3 gives,

$$B_1 = 32 + 0.5 B_0 \quad (\text{I-B-1.10})$$

At the intersection, equations I-B-1.9 and I-B-1.10 must be satisfied simultaneously. Solving Equation I-B-1.10 for B_0 and substituting in Equation I-B-1.9 yields,

$$B_1^2 - 234 B_1 - 10816 = 0 \quad (\text{I-B-1.11})$$

Solving for B_1 gives

$$B_1 = 273.54, \text{ and } B_1 = -39.54$$

The negative value is meaningless, thus substitution of the positive value into equations I-B-1.8 and I-B-1.3 gives the frequency and the "average" gain respectively, as

$$\omega_n = 4.587 \text{ rad/sec}$$

and

$$N_{ave} = 0.8051$$

The approximate amplitude of the limit cycle is given by

$$E_{\max} = \frac{E_{\text{sat}}}{N}$$

or

$$E_{\max} = \frac{5.0}{0.8051} = 6.21 \text{ Volts}$$

The graphical representation of the solution is shown in Figure I-B-1.1.



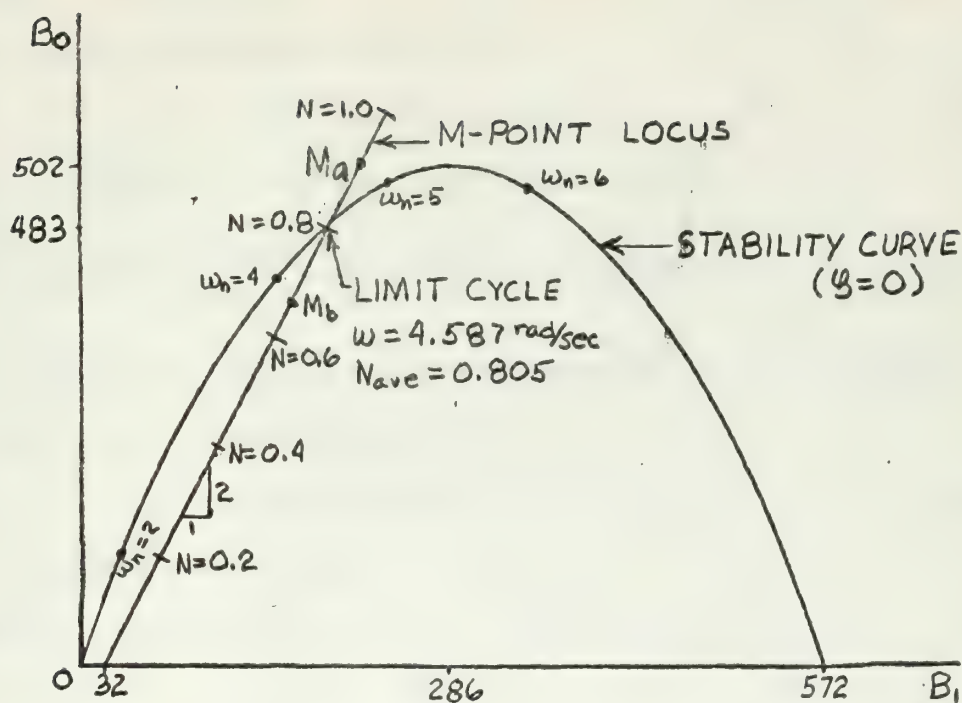


Figure I-B-1.1

Graphical Solution for Saturation in Error Channel,
Loop Transfer Function with One Zero

Mitrovic's method predicts a stable limit cycle by following similar reasoning to that given in Section I-A-1 of this chapter.



I-B-2. Root Locus Method.

The system characteristic Equation is

$$s^4 + 13s^3 + 44s^2 + (32 + 300N)s + 600N = 0. \quad (\text{I-B-2.1})$$

Substitution of $s = j\omega$ and simplifying, yields

$$\omega^4 - j13\omega^3 - 44\omega^2 + j(32 + 300N)\omega + 600N = 0. \quad (\text{I-B-2.2})$$

By requiring that both the real and imaginary parts of equation I-B-2.1 go to zero simultaneously, then

$$\omega^4 - 44\omega^2 + 600N = 0 \quad (\text{I-B-2.3})$$

and
$$-j13\omega^3 + 32\omega + j300\omega N = 0. \quad (\text{I-B-2.4})$$

Dividing Equation I-B-2.4 by $j\omega$ and solving for N gives

$$N = \frac{13}{300}\omega^2 - \frac{32}{300}. \quad (\text{I-B-2.5})$$

Substituting this into Equation I-B-2.3 gives the following equation for ω

$$\omega^4 - 18\omega^2 - 64 = 0. \quad (\text{I-B-2.6})$$

Solution of Equation I-B-2.6 for ω^2 gives

$$\omega^2 = 21.042,$$

from which

$$\omega = 4.587 \text{ rad/sec.}$$

Substitution of ω^2 into Equation I-B-2.5 gives the "average" non-linear gain over a cycle as

$$N_{\text{ave}} = 0.8051$$

From this the approximate amplitude is obtained as

$$\epsilon_{\text{max}} = \frac{5}{0.8051} = 6.21 \text{ Volts}$$

A pictorial representation of the root locus solution appears in Figure I-B-2.1.



The root locus method also predicts a stable limit cycle by following similar reasoning to that given in Section I-A-1 of this Chapter.

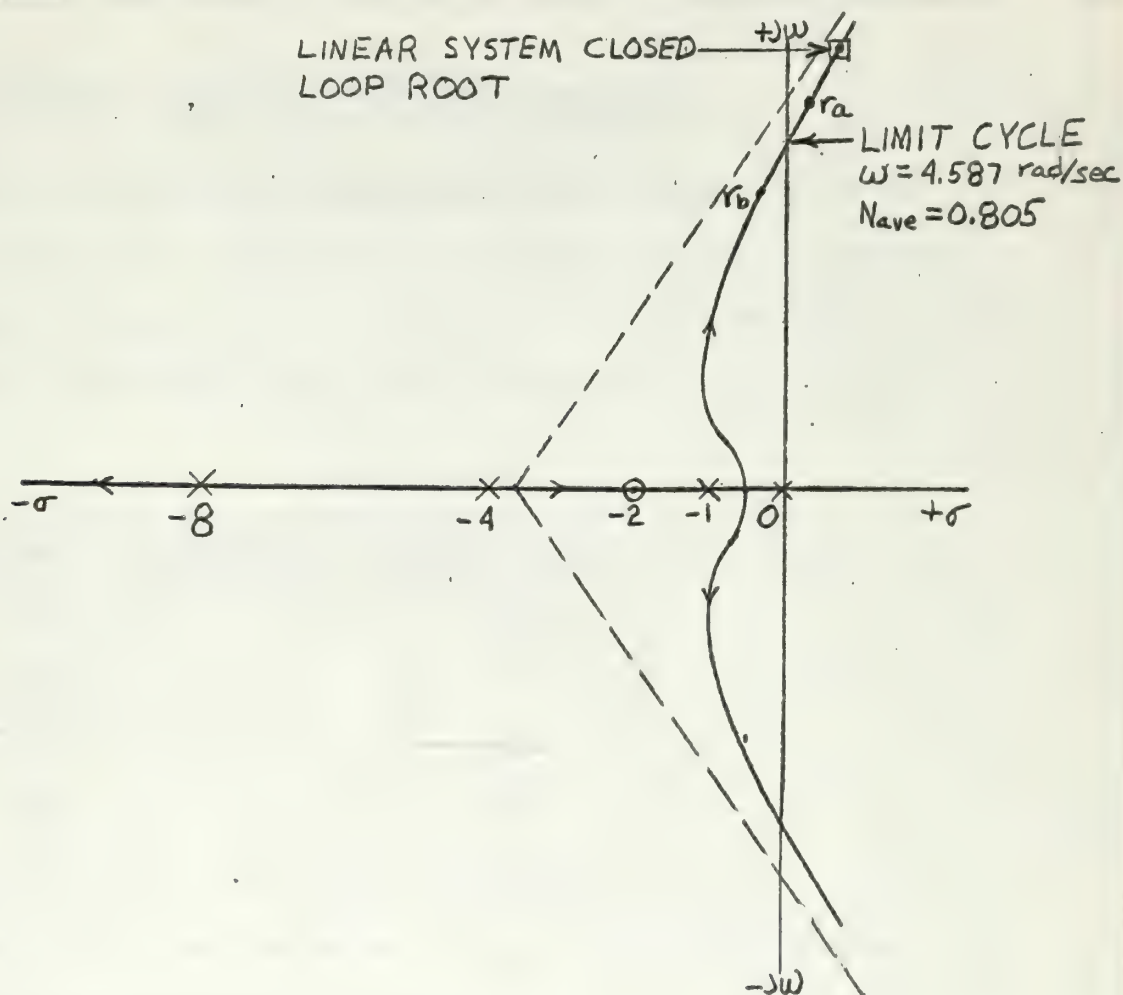


Figure I-B-2.1

Root Locus Solution for Saturation in Error Channel

Loop Transfer Function with One Zero



I-B-3. Describing Function Method.

The describing function is the same as that given in Equation I-A-3.1 of this Chapter.

The linear loop transfer function in frequency response form is,

$$G(j\omega) = \frac{18.75(0.5j\omega + 1)}{j\omega(j\omega + 1)(0.25j\omega + 1)(0.125j\omega + 1)} \quad (I-B-3.1)$$

Table I-B-3.1 gives the magnitude and phase of Equation I-B-3.1 which were used to plot the linear loop transfer function on the gain-phase plane of Figure I-B-3.1. These values were obtained from a Bode diagram plot of the linear loop transfer function.

TABLE I-B-3.1

| ω | $ G(j\omega) _{db}$ | $\angle G(j\omega)$ deg |
|----------|---------------------|-------------------------|
| 4.05 | 4 | -174.5 |
| 4.3 | 3 | -177 |
| 4.55 | 2 | -180 |
| 4.85 | 1 | -183 |
| 5.15 | 0 | -190.5 |

Table I-B-3.2 gives the values of $1/G_D$ in the area of interest.

These values were obtained from Equation I-A-3.1.

TABLE I-B-3.2

| R | G_D | $1/G_D$ | $1/G_D$ db |
|------|-------|---------|------------|
| 0.6 | 0.716 | 1.396 | 2.9 |
| 0.68 | 0.794 | 1.26 | 2.01 |
| 0.69 | 0.803 | 1.246 | 1.92 |
| 0.7 | 0.812 | 1.232 | 1.83 |



By interpolation of Figure I-B-3.1, the intersection and thus the limit cycle occurs at

$$\omega = 4.55 \text{ rad/sec.}$$

and

$$R = 0.682$$

From Equation I-A-3.2, the amplitude of the limit cycle is then

$$\mathcal{E}_{\max} = \frac{5}{0.682} = 7.33 \text{ Volts}$$

The describing function predicts a stable limit cycle by following similar reasoning to that given in Section I-A-3 of this Chapter.



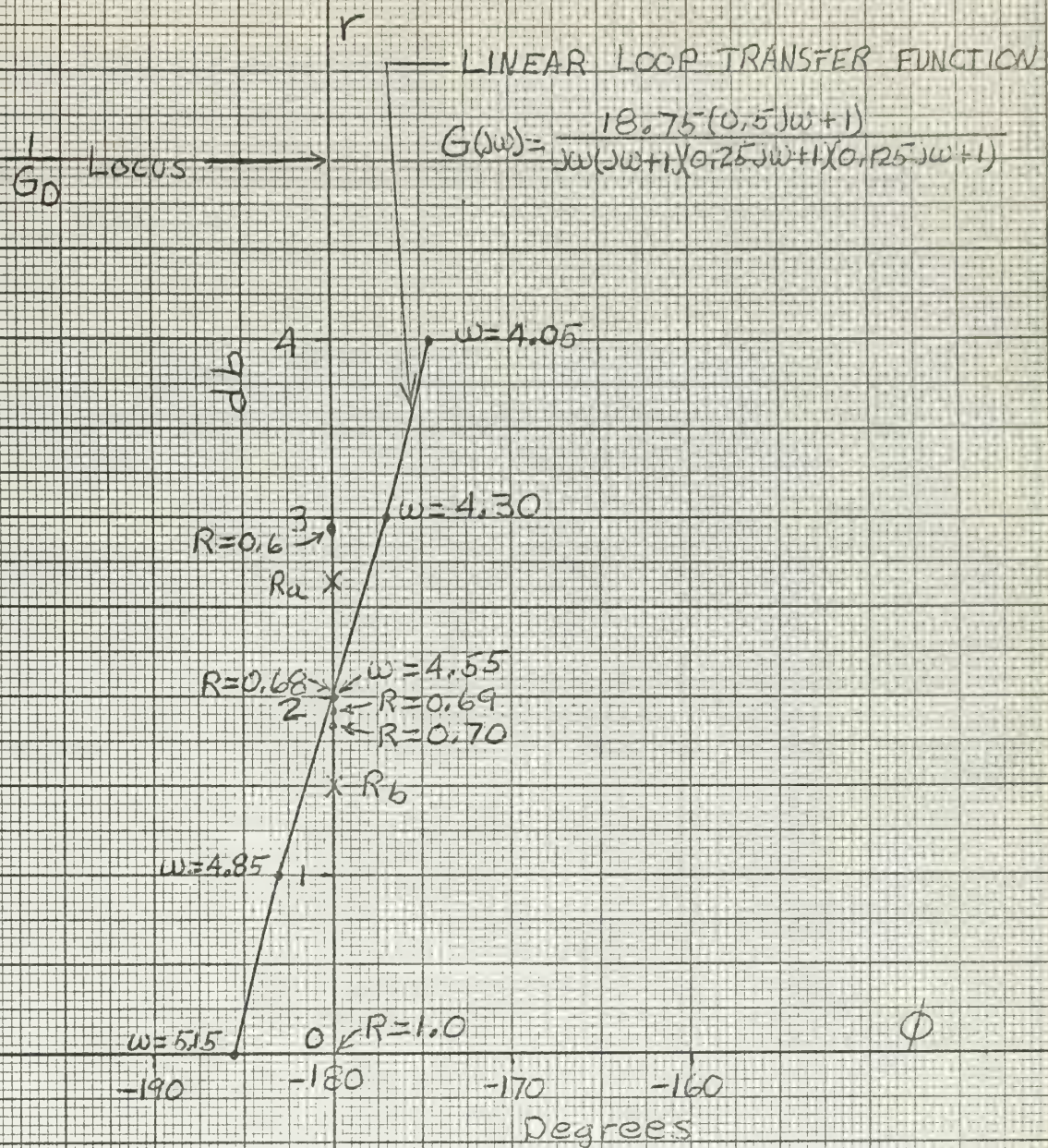


FIGURE 1B3.1
GAIN-PHASE PLANE - SATURATION IN
ERROR CHANNEL, LOOP TRANSFER
FUNCTION WITH ONE ZERO



I-B-4. Analog Computer Simulation.

The analog simulation of the given nonlinear system is shown in Figure I-B-4.1. The coefficient pot settings with associated resistances and capacitances for real time and real magnitude scaling are given in Table I-B-4.1.

TABLE I-B-4.1

| Pot Setting | Associated Elements |
|-------------------------------|---|
| $a_1 = \frac{E_i}{100}$ | For Input Step of E_i Volts and $R_1 = 1 \text{ Meg}$, $R_{f1} = 1 \text{ Meg}$ |
| $a_2 = 1.0$ | $R_2 = 1 \text{ Meg}$, $R_{f1} = 1 \text{ Meg}$ |
| $a_3 = 1.0$ | $R_3 = 1 \text{ Meg}$, $R_{f2} = 1 \text{ Meg}$ |
| $a_4 = 1.0$ | $R_4 = 0.5 \text{ Meg}$, $C_{f1} = 1 \text{ uf}$ |
| $a_5 = 0.4$ | $R_5 = 0.1 \text{ Meg}$, $C_{f1} = 1 \text{ uf}$ |
| $a_6 = 1.0$ | $R_6 = 0.1 \text{ Meg}$, $R_{f3} = 1 \text{ Meg}$ |
| $a_7 = 1.0$ | $R_7 = 0.1 \text{ Meg}$, $R_{f3} = 1 \text{ Meg}$ |
| $a_8 = 0.3$ | $R_8 = 0.1 \text{ Meg}$, $C_{f2} = 1 \text{ uf}$ |
| $a_9 = 1.0$ | $R_9 = 1 \text{ Meg}$, $C_{f2} = 1 \text{ uf}$ |
| $a_{10} = 1.0$ | $R_{10} = 0.1 \text{ Meg}$, $C_{f3} = 1 \text{ uf}$ |
| $a_{11} = 0.8$ | $R_{11} = 0.1 \text{ Meg}$, $C_{f3} = 1 \text{ uf}$ |
| $a_{12} = 1.0$ | $R_{12} = 1 \text{ Meg}$, $C_{f4} = 1 \text{ uf}$ |
| $a_{13} = 1.0$ | $R_{13} = 1 \text{ Meg}$, $R_{f4} = 1 \text{ Meg}$ |
| $a = 0.05$ initial Setting | For a 5 volt Saturation Voltage |

To accurately set the back-bias pots "a" a sine wave generator was connected to the input of the saturation simulator. The two pots were then adjusted until the saturated output voltage was 5 volts on a recording device.



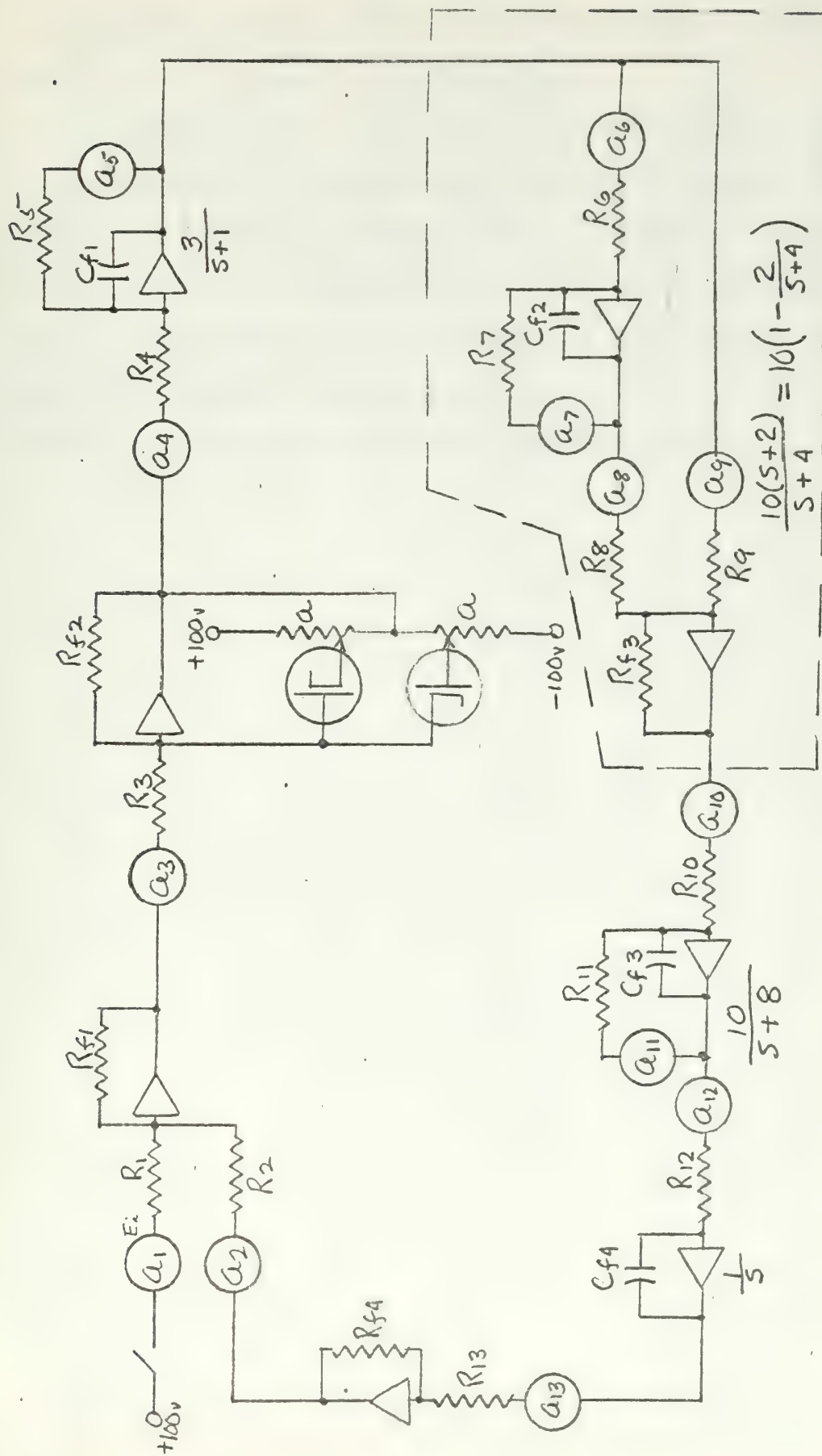


Figure 1-B-4.1
ADALM Computer Simulation of Error Channel Situation. Loop Transfer Function with $O_1 = Z_1$.



The static characteristic for the saturation simulator appears as Figure I-A-4.2 in Section I-A-4 of this Chapter.

The system was first excited with a 4 volt input signal. The system was found to go into the limit cycle shown in recorder trace I-B-4.1. The system was then excited with a 10 volt step input signal. The system was found to go into the same limit cycle (recorder trace I-B-4.2). From these two recorder traces, the limit cycle is seen to be stable with an angular frequency of 4.58 rad/sec and 7.2 volts amplitude. The phase portrait for the system appears in Figure I-B-4.2.



ERROR - E

+ 0 -

K II CHART NO. RA 2921 32

BRUSH IN'S

DIVISION OF CLEVITE CORPORATION

CLEVELAND, OHIO

PRINTED IN U.S.A.

ERROR RATE - E

- 0 +

NON LINEARITY OUTPUT - X

- 0 +

Recorder Trace I-B-4.1

Error Channel Saturation, Loop Transfer Function with One Zero, 4-Volt Step Input.

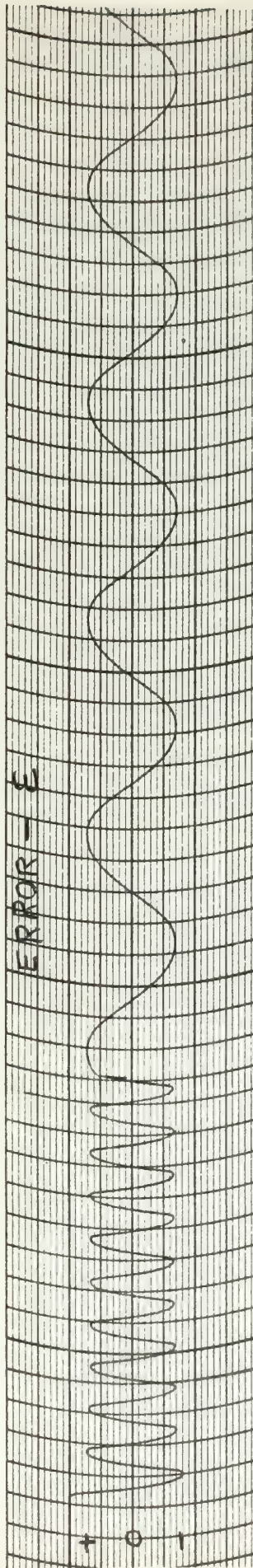
SCALES E - 1 volts/Line

E - 2 Volts/Line

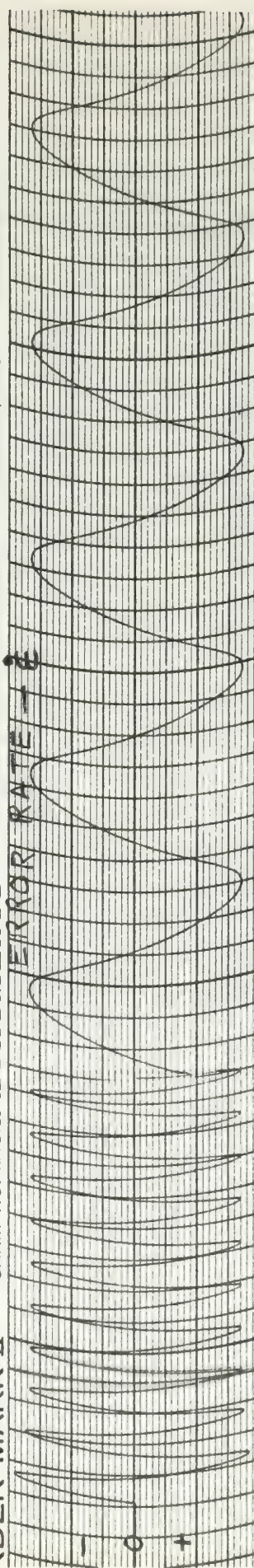
X - 0.5 Volts/Line

Time - 1 Second/Division
0.2 Second/Division

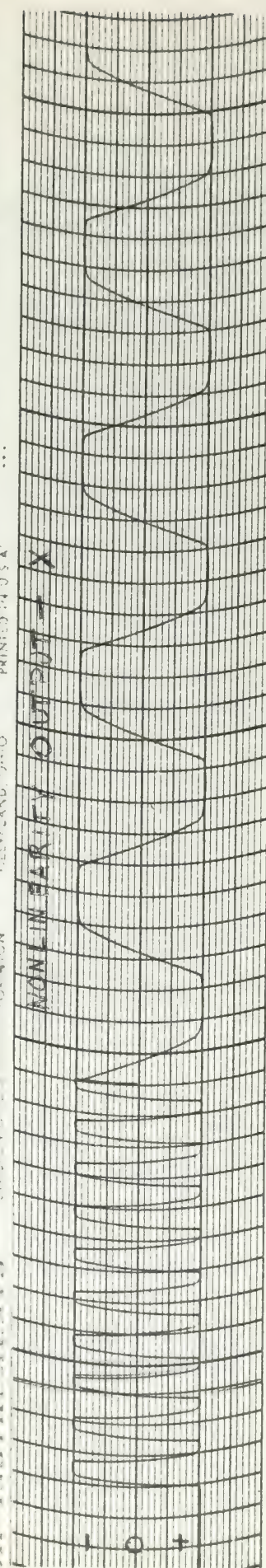




ORDER MARK II CHART NO. RA 2921 33 TRUMENT'S DIVISION OF CLEVITE CORPORATION CLEVELAND, OHIO PRINTED IN U.S.A.



III INSTRUMENTS DIVISION OF CLEVITE CORPORATION CLEVELAND, OHIO PRINTED IN U.S.A.

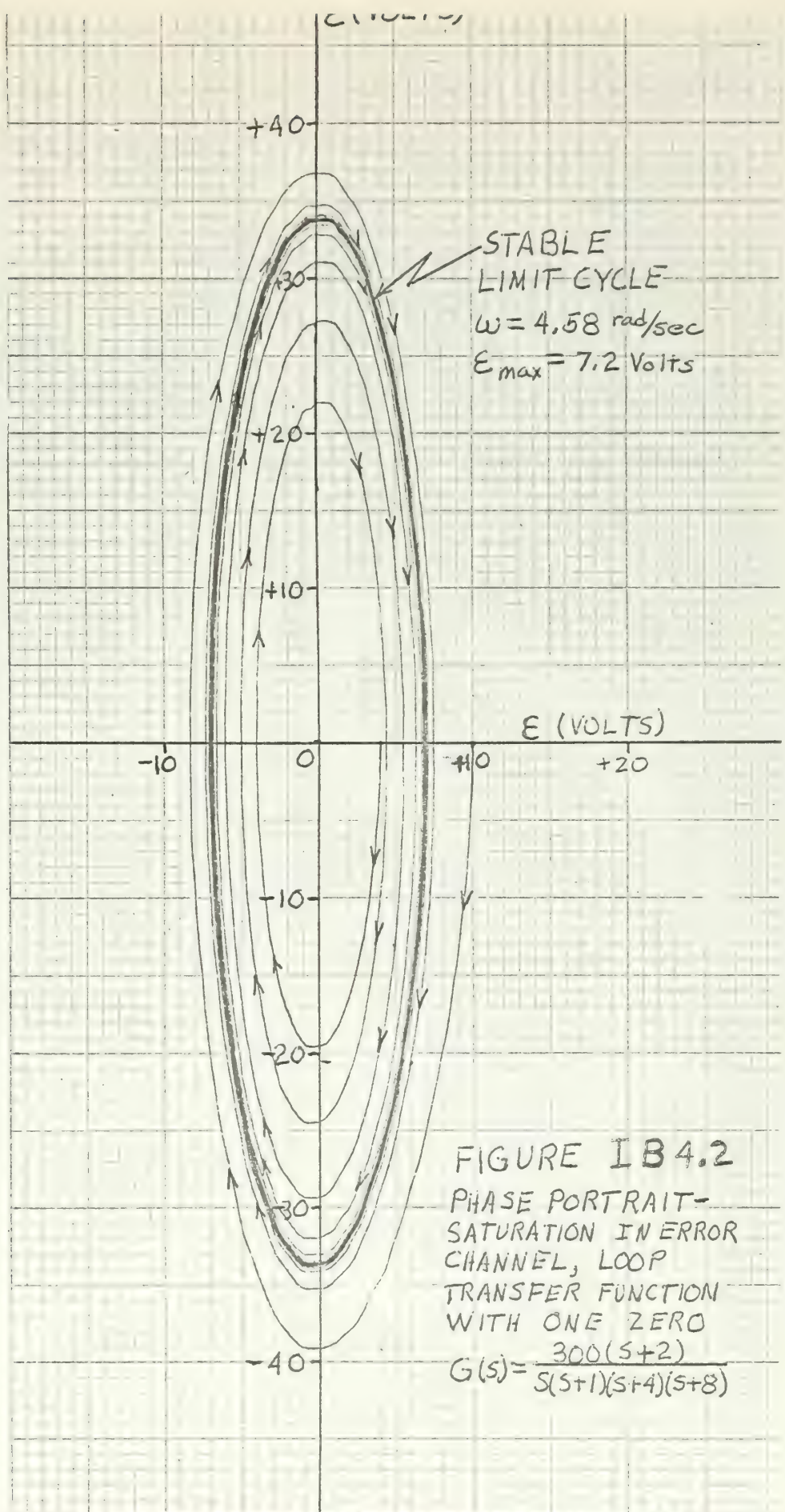


Recorder Type I-B 4.2

Error Signal Saturation, Step Transfer Function with One Zero, 10 Volt Step Input.

Scale: $\epsilon = 1 \text{ volt/line}$ $\dot{\epsilon} = 1 \text{ volt/line}$ $X = 0.5 \text{ volts/line}$ Time: 1 sec/div 0.1 sec/div







I-B-5. Comparison of the Four Analytic Methods In Limit Cycle Prediction
for the System Given in Figure I-B.

| Method | Frequency rad/sec | Amplitude (volts) |
|---------------------|----------------------|----------------------|
| Mitrovic | 4.587 | 6.21 |
| Root Locus | 4.587 | 6.21 |
| Describing Function | 4.55 | 7.33 |
| Analog Simulation | 4.58 | 7.2 |



CHAPTER II

DEAD ZONE IN ERROR CHANNEL

II-A Loop Transfer Function with No Zeros.

The block diagram of the arbitrarily chosen system which is to be analyzed is given in Figure II-A.

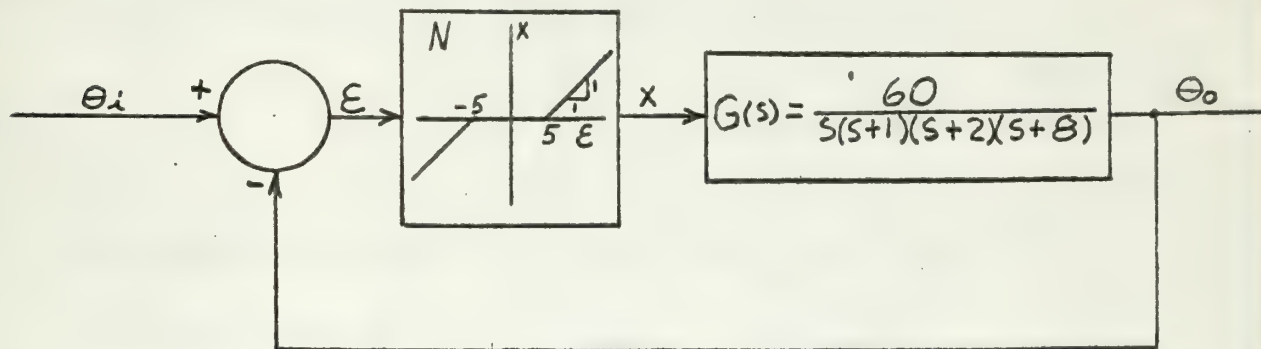


Figure II-A

Dead Zone in Error Channel Loop
Transfer Function with No Zeros



II-A-1. Mitrovic's Method.

The characteristic Equation of the given system is,

$$s^4 + 11s^3 + 26s^2 + 16s + 60N = 0. \quad (\text{II-A-1.1})$$

Assuming the last two coefficients variable the characteristic equation becomes,

$$s^4 + 11s^3 + 26s^2 + B_1s + B_0 = 0 \quad (\text{II-A-1.2})$$

where the parametric equations of the working point locus are,

$$B_0 = 60N \quad (\text{II-A-1.3})$$

and

$$B_1 = 16. \quad (\text{II-A-1.4})$$

From Appendix A, Mitrovic's equations for B_0 and B_1 are,

$$B_0 = -[26\omega_n^2\phi_1(\xi) + 11\omega_n^3\phi_2(\xi) + \omega_n^4\phi_3(\xi)] \quad (\text{II-A-1.5})$$

and

$$B_1 = 26\omega_n\phi_2(\xi) + 11\omega_n^2\phi_3(\xi) + \omega_n^3\phi_4(\xi). \quad (\text{II-A-1.6})$$

Substitution of the values of the ϕ functions from Appendix A for

$\xi = 0$ gives the parametric equations of the stability curve as

$$B_0 = 26\omega_n^2 - \omega_n^4 \quad (\text{II-A-1.7})$$

and

$$B_1 = 11\omega_n^2. \quad (\text{II-A-1.8})$$

At the intersection of the M-point locus and the stability curve, equations II-A-1.3 and II-A-1.4 and Equations II-A-1.7 and II-A-1.8 must be satisfied simultaneously. Thus at the intersection,

$$11\omega_n^2 = 16 \quad (\text{II-A-1.9})$$



from which the angular frequency of the limit cycle is determined to be,

$$\omega_n = 1.206 \text{ rad/sec.}$$

Also at the intersection

$$26\omega_n^2 - \omega_n^4 = 60N \quad (\text{II-A-1.10})$$

Substitution of, ω_n^2 from Equation II-A-1.9 into Equation II-A-1.10 gives the "average" gain of the nonlinearity over the cycle as,

$$N_{\text{ave}} = 0.595$$

To obtain the approximate amplitude of the limit cycle, reference is made to Figure II-A-1.1 which is a sketch of the nonlinearity static characteristic.

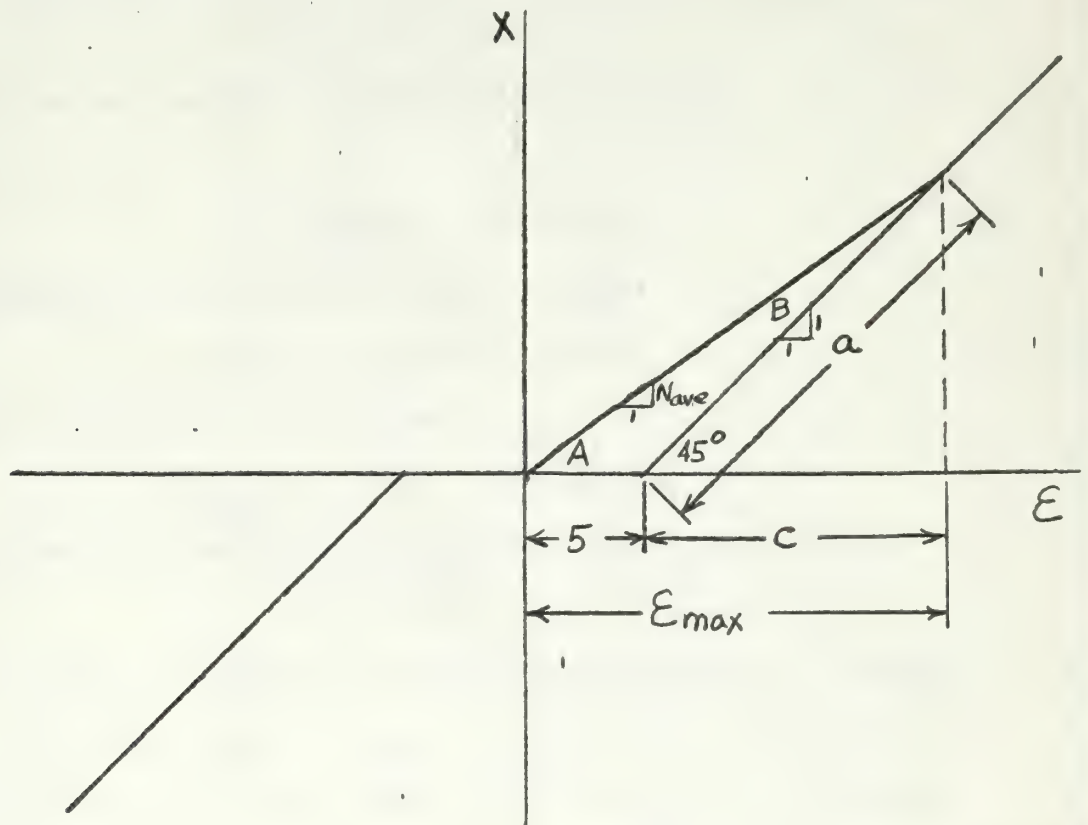


Figure II-A-1.1

Limit Cycle Amplitude Calculation from the
Dead Zone Characteristic Knowing N_{ave}



From the figure the following equations are obtained,

$$\mathcal{E}_{\max} = 5 + c \quad (\text{II-A-1.11})$$

$$c = a \cos 45^\circ = 0.707a \quad (\text{II-A-1.12})$$

$$a = \frac{5 \sin A}{\sin B} \quad (\text{II-A-1.13})$$

$$A = \tan^{-1} N_{\text{ave}} \quad (\text{II-A-1.14})$$

and

$$B = 180 - A - (180 - 45) \quad (\text{II-A-1.15})$$

Entering equation II-A-1.14 with the "average" gain over a cycle,

$$A = \tan^{-1} 0.595 = 30.8^\circ$$

Substituting this in Equation II-A-1.15 gives

$$B = 45^\circ - 30.8^\circ = 14.2^\circ$$

Substituting for A and B in Equation II-A-1.13 gives,

$$a = 5 \frac{\sin 30.8}{\sin 14.2} = 10.469$$

Substituting for "a" in Equation II-A-1.12 gives

$$c = 0.707 (10.469) = 7.402$$

And finally Equation II-A-1.11 gives

$$\mathcal{E}_{\max} = 5 + 7.402 = 12.402 \text{ Volts}$$

The graphical solution of the intersection is sketched in Figure II-A-1.2.

Mitrovic's method predicts an unstable limit cycle by the following reasoning. If the input signal is small, N will be small and the instantaneous M-point will be in the stable region such as M_b in Figure II-A-1.2. The system is stable and the oscillations will decrease in amplitude. As the oscillations decrease, N becomes even smaller driving the M-point even further into the stable region. Consequently the M-point



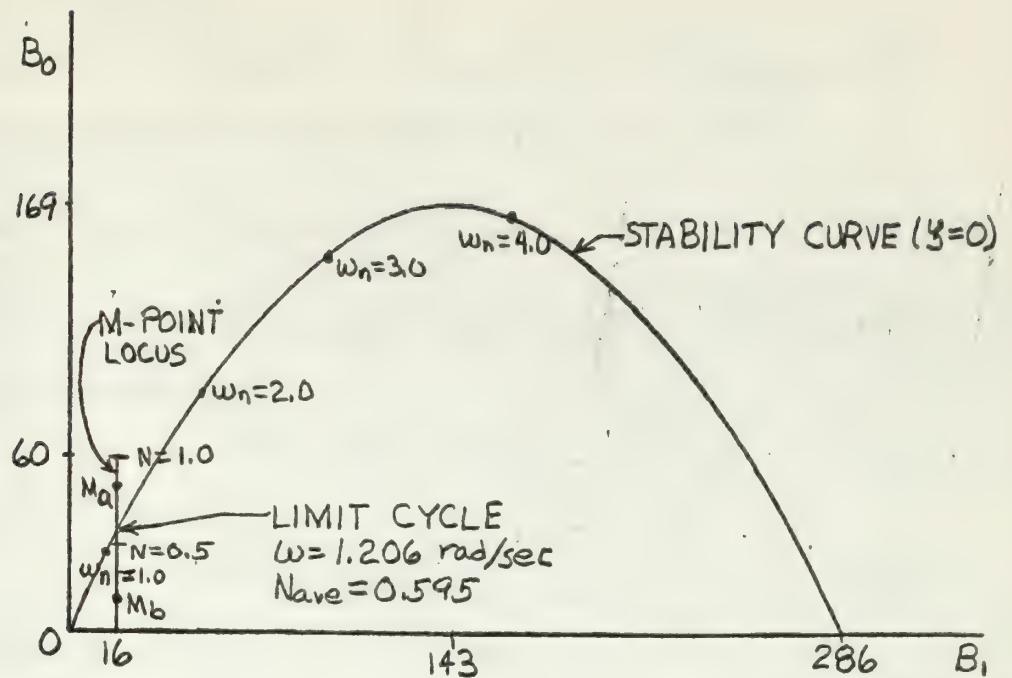


Figure II-A-1.2

Graphical Solution for Dead Zone in Error Channel,

Loop Transfer Function with No Zeros

can never go into the unstable region and all oscillations will eventually die out. If the input signal is large, N is relatively large and the instantaneous M -point lies in the unstable region such as M_a . The system is unstable and the oscillations increase, N increases toward $N = 1.0$, and the M -point moves farther into the unstable region. Consequently, the oscillations increase indefinitely in magnitude.



II-A-2. Root Locus Method.

Substitution of $s = j\omega$ into the characteristic equation given in Equation II-A-1.1 and evaluating the higher powers of j gives,

$$\omega^4 - j11\omega^3 - 26\omega^2 + j16\omega + 60N = 0. \quad (\text{II-A-2.1})$$

By requiring that both the real and imaginary parts of Equation II-A-2.1 go to zero independently,

$$\omega^4 - 26\omega^2 + 60N = 0 \quad (\text{II-A-2.2})$$

and

$$-j11\omega^3 + j16\omega = 0. \quad (\text{II-A-2.3})$$

Dividing Equation II-A-2.3 by $j\omega$, gives

$$11\omega^2 - 16 = 0 \quad (\text{II-A-2.4})$$

from which the angular frequency of the limit cycle is obtained as

$$\omega = 1.206 \text{ rad/sec.}$$

Substitution of ω^2 from Equation II-A-2.4 into Equation II-A-2.2 and solving for N_{ave} yields

$$N_{\text{ave}} = 0.595.$$

To determine the approximate amplitude of the limit cycle, Equations II-A-1.11 through II-A-1.15 are again used. Thus,

$$\mathcal{E}_{\text{max}} = 12.402 \text{ Volts}$$

A graphical presentation of the root locus solution is given in Figure II-A-2.1.

The root locus method predicts an unstable limit cycle by the following reasoning. If the input signal is small, N is small and the loop gain is small placing the instantaneous root at r_b in Figure II-A-2.1. The system is stable and the oscillations decrease in magnitude. As the



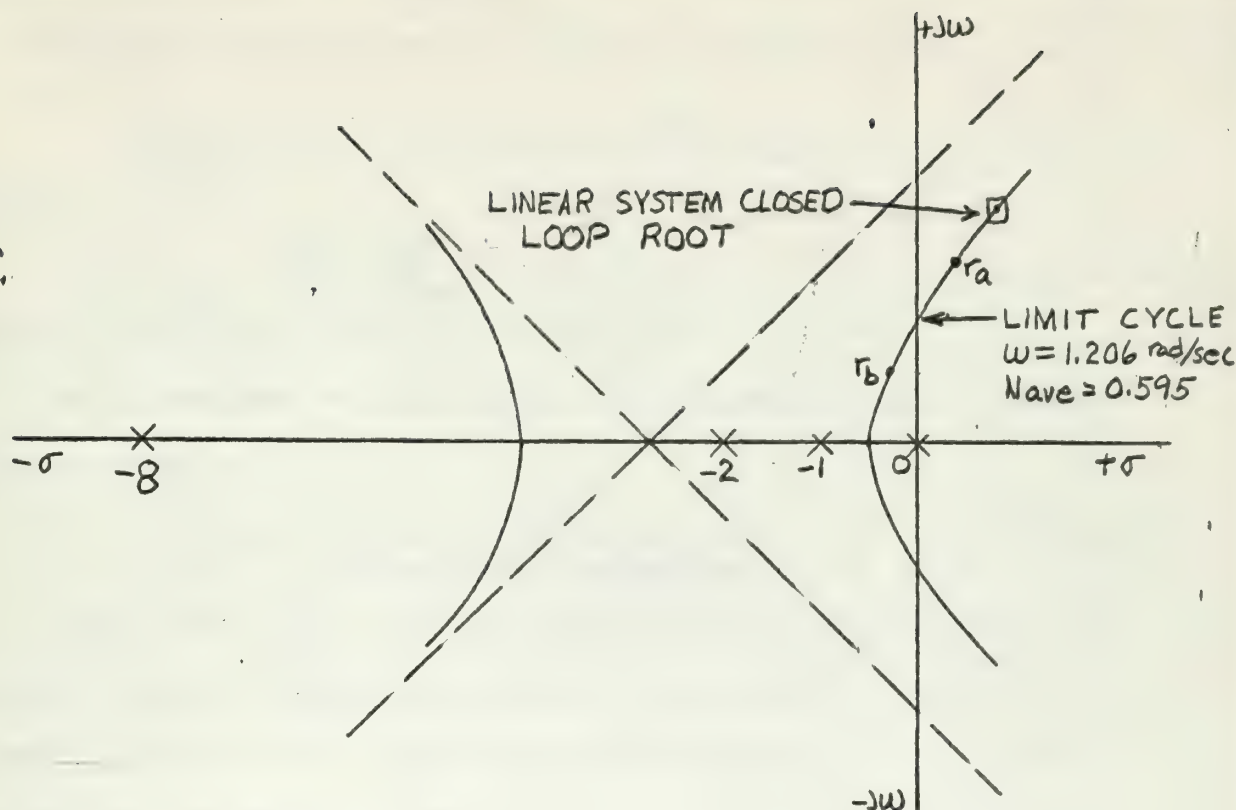


Figure II-A-2.1

Root Locus Solution for Dead Zone in Error Channel,

Loop Transfer Function with No Zeros

oscillations decrease, N also decreases, driving the root location farther into the left half plane. Consequently, the system is always stable and the oscillations eventually die out. If the input signal is large, N is also relatively large making the loop gain high. The instantaneous root location is at r_a . The system is unstable and the oscillations increase. As the oscillations increase, N increases toward $N = 1$. The root location moves farther into the right half plane. Thus the system is always unstable and the oscillations will increase indefinitely.



II-A-3. Describing Function Method.

The describing function for a dead zone nonlinearity is

$$G_D = \frac{2}{\pi} \left[\frac{\pi}{2} - \sin^{-1} R - R \sqrt{1-R^2} \right] \angle 0^\circ \quad (\text{II-A-3.1})$$

with

$$R = \frac{b}{2 \varepsilon_{\max}} \quad (\text{II-A-3.2})$$

where b is the total minus to plus dead zone.

The linear loop transfer function for the given system in frequency response form is

$$G(j\omega) = \frac{3.75}{j\omega(j\omega+1)(0.5j\omega+1)(0.125j\omega+1)} \quad (\text{II-A-3.3})$$

Table II-A-3.1 gives the magnitude and phase of Equation II-A-3.3 for the different frequencies which were used to plot the linear loop transfer function on the gain-phase plane of Figure II-A-3.1. These values are obtained from a Bode diagram plot of Equation II-A-3.3.

TABLE II-A-3.1

| ω | $ G(j\omega) \text{ db}$ | $\angle G(j\omega) \text{ deg}$ |
|----------|---------------------------|---------------------------------|
| 1.0 | 7.7 | -168 |
| 1.1 | 6.2 | -174 |
| 1.2 | 4.7 | -179.5 |
| 1.3 | 3.5 | -184 |
| 1.4 | 2.0 | -189.5 |

TABLE II-A-3.2

| R | G_D | $1/G_D$ | $1/G_D \text{ db}$ |
|------|-------|---------|--------------------|
| 0 | 1 | 1 | 0 |
| 0.2 | 0.746 | 1.34 | 2.55 |
| 0.3 | 0.624 | 1.60 | 4.10 |
| 0.32 | 0.61 | 1.64 | 4.29 |
| 0.35 | 0.577 | 1.73 | 4.78 |
| 0.4 | 0.504 | 1.98 | 5.94 |

Table II-A-3.2 gives the values of $1/G_D$ in the area of interest.

These values were obtained from equation II-A-3.1.



By interpolation of Figure II-A-3.1, the intersection and thus the limit cycle occurs at

$$\omega = 1.21 \text{ rad/sec.}$$

and

$$R = 0.34$$

From Equation II-A-3.2, the amplitude of the limit cycle is then

$$\mathcal{E}_{\max} = \frac{b}{2R}$$

or

$$\mathcal{E}_{\max} = 14.71 \text{ Volts}$$

The describing function method predicts an unstable limit cycle by the following reasoning. For small input signals, R is relatively large. Assuming the $-1/G_D$ curve to be the locus of the system critical point, then the instantaneous critical point is at R_a in Figure II-A-3.1 and the system is stable due to a positive phase margin. The oscillations will decrease causing R to decrease, thus moving the critical point farther up the -180° axis. This motion of the critical point increases the positive phase margin. Thus the system is always stable for small signals and all oscillations will eventually die out. For large input signals R is small placing the instantaneous critical point at R_b . The system is unstable due to a negative phase margin and the oscillations increase. As the oscillations increase R becomes even smaller moving the critical point down the -180° axis and increasing the negative phase margin. Consequently, for large signals the system is always unstable and the oscillations increase indefinitely.



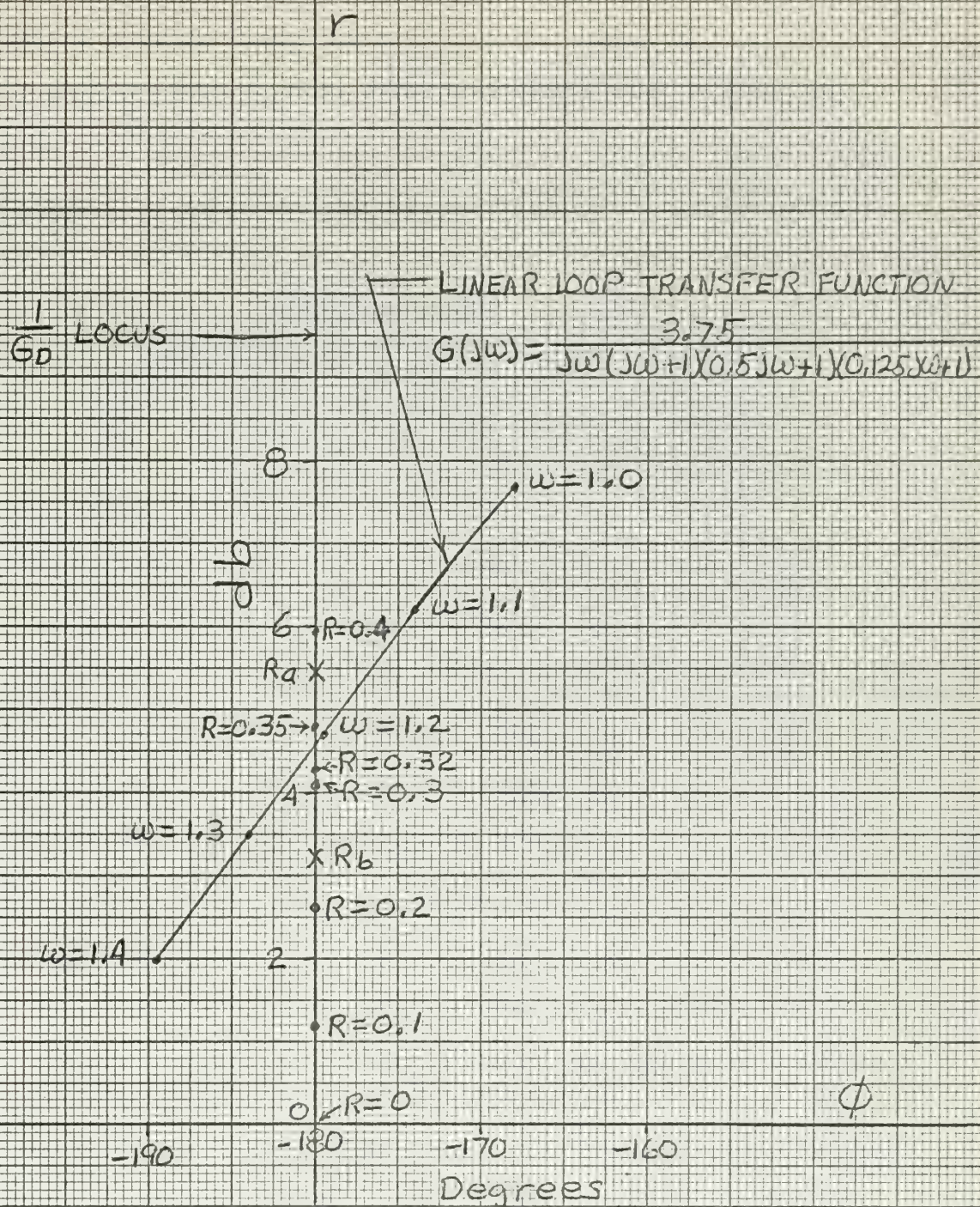


FIGURE 11A3.1

GAIN-PHASE PLANE — DEAD ZONE IN
ERROR CHANNEL, LOOP TRANSFER
FUNCTION WITH NO ZEROS



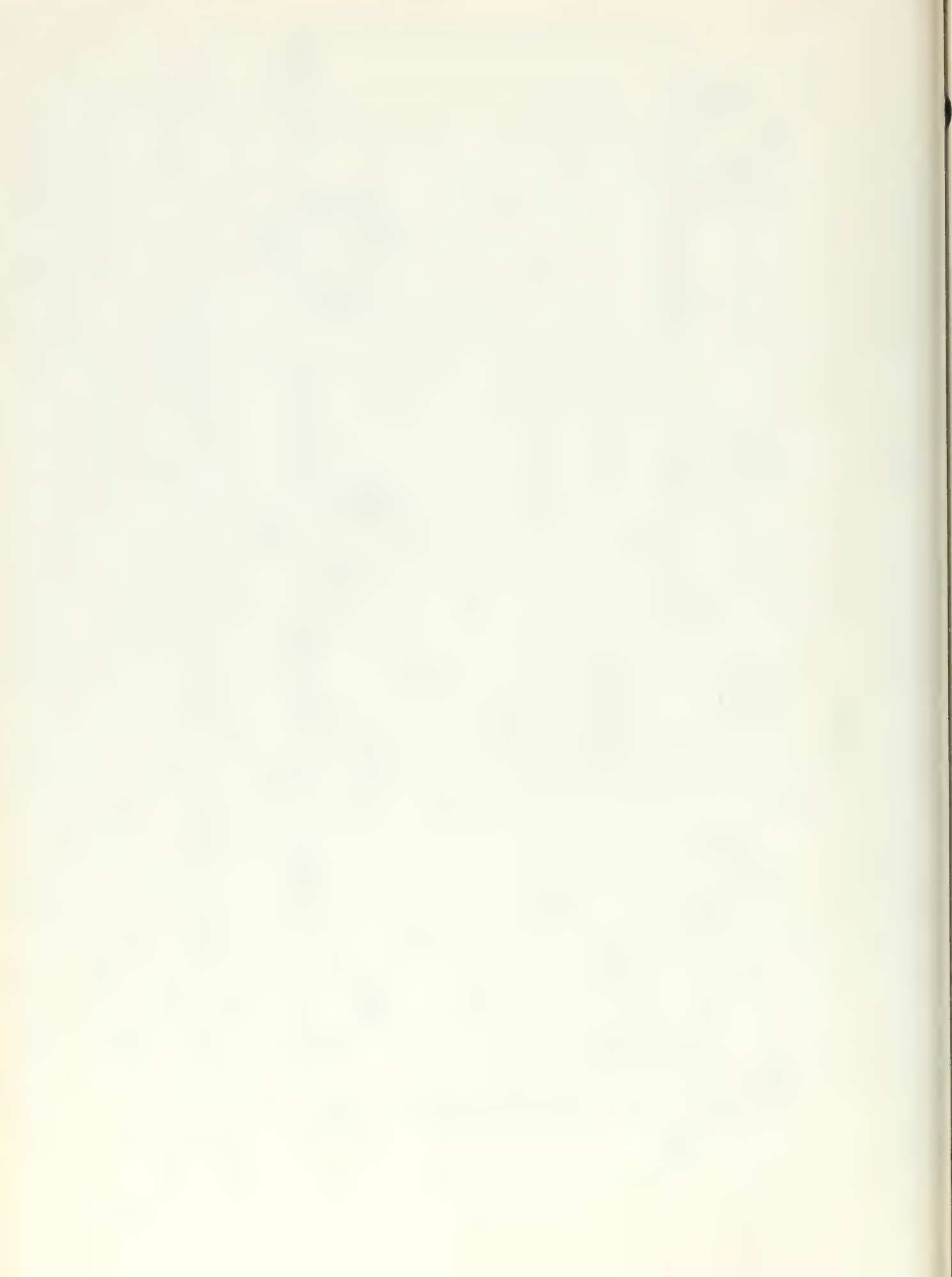
II-A-4 Analog Computer Simulation.

The analog simulation of the given nonlinear system is shown in Figure II-A-1. The coefficient pot settings with associated resistances and capacitances for real time and real magnitude scaling are given in Table II-A-4.1.

TABLE II-A-4.1

| Pot Setting | Associated Elements |
|------------------------------|--|
| $a_1 = \frac{E_i}{100}$ | For Input Step of E_i Volts $R_1 = 1 \text{ Meg}, R_{f1} = 1 \text{ Meg}$ |
| $a_2 = 1.0$ | $R_2 = 1 \text{ Meg}, R_{f1} = 1 \text{ Meg}$ |
| $a_3 = 1.0$ | $R_3 = 1 \text{ Meg}, R_{f2} = 1 \text{ Meg}$ |
| $a_4 = 1.0$ | $R_4 = 1 \text{ Meg}, C_{f1} = 1 \text{ uf}$ |
| $a_5 = 1.0$ | $R_5 = 1 \text{ Meg}, C_{f1} = 1 \text{ uf}$ |
| $a_6 = 0.6$ | $R_6 = 0.1 \text{ Meg}, C_{f2} = 1 \text{ uf}$ |
| $a_7 = 1.0$ | $R_7 = 0.5 \text{ Meg}, C_{f2} = 1 \text{ uf}$ |
| $a_8 = 1.0$ | $R_8 = 0.1 \text{ Meg}, C_{f3} = 1 \text{ uf}$ |
| $a_9 = 0.8$ | $R_9 = 0.1 \text{ Meg}, C_{f3} = 1 \text{ uf}$ |
| $a_{10} = 1.0$ | $R_{10} = 1 \text{ Meg}, C_{f4} = 1 \text{ uf}$ |
| $a_{11} = 1.0$ | $R_{11} = 1 \text{ Meg}, R_{f3} = 1 \text{ Meg}$ |
| $a = 0.5$ Initial Setting | For a 5 Volt Dead Zone Each Side of Zero |

To accurately set the back-bias pots "a", a sine wave generator was connected to the input of the dead zone simulator. An X-Y recorder was then calibrated for 5 volts per inch on each axis. The input and output of the simulator was then connected to the X-Y recorder and pots "a" were adjusted until both break voltages of the static characteristic curve were 5 volts. The static characteristic curve appears as Figure II-A-4.2.



The system was first excited with a 15 volt step input signal and the system was found to be stable as shown in recorder trace II-A-4.1. The system was then excited with a 17 volt step input and was found to be unstable as shown in recorder trace II-A-4.2. The unstable limit cycle was found to occur for an input step of 17.07 and is shown in recorder trace II-A-4.3. From recorder trace II-A-4.3 the limit cycle is seen to have an angular frequency of 1.207 rad/sec and an amplitude of 15 volts.

The phase portrait of the system is shown in Figure II-A-4.3.

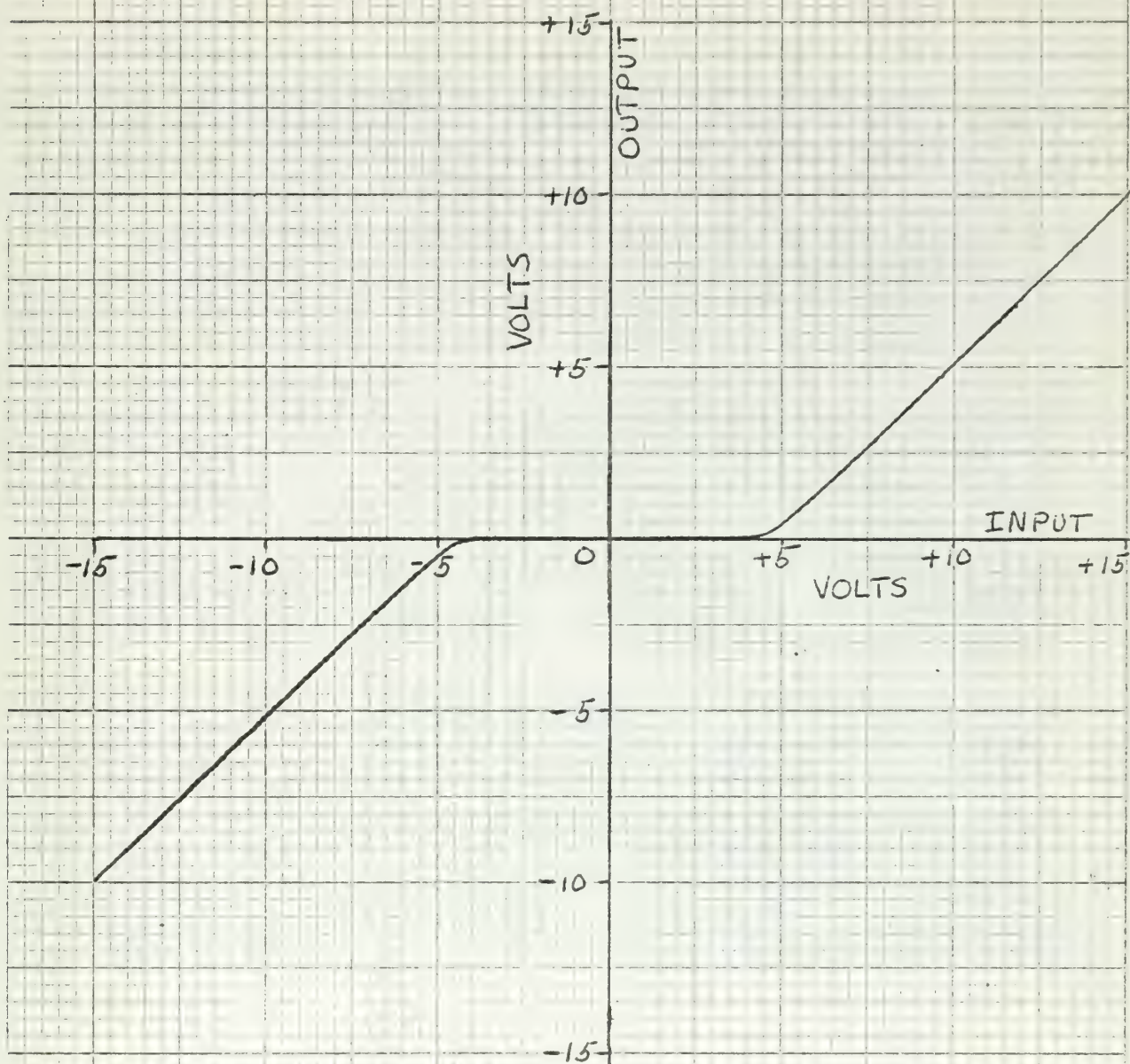
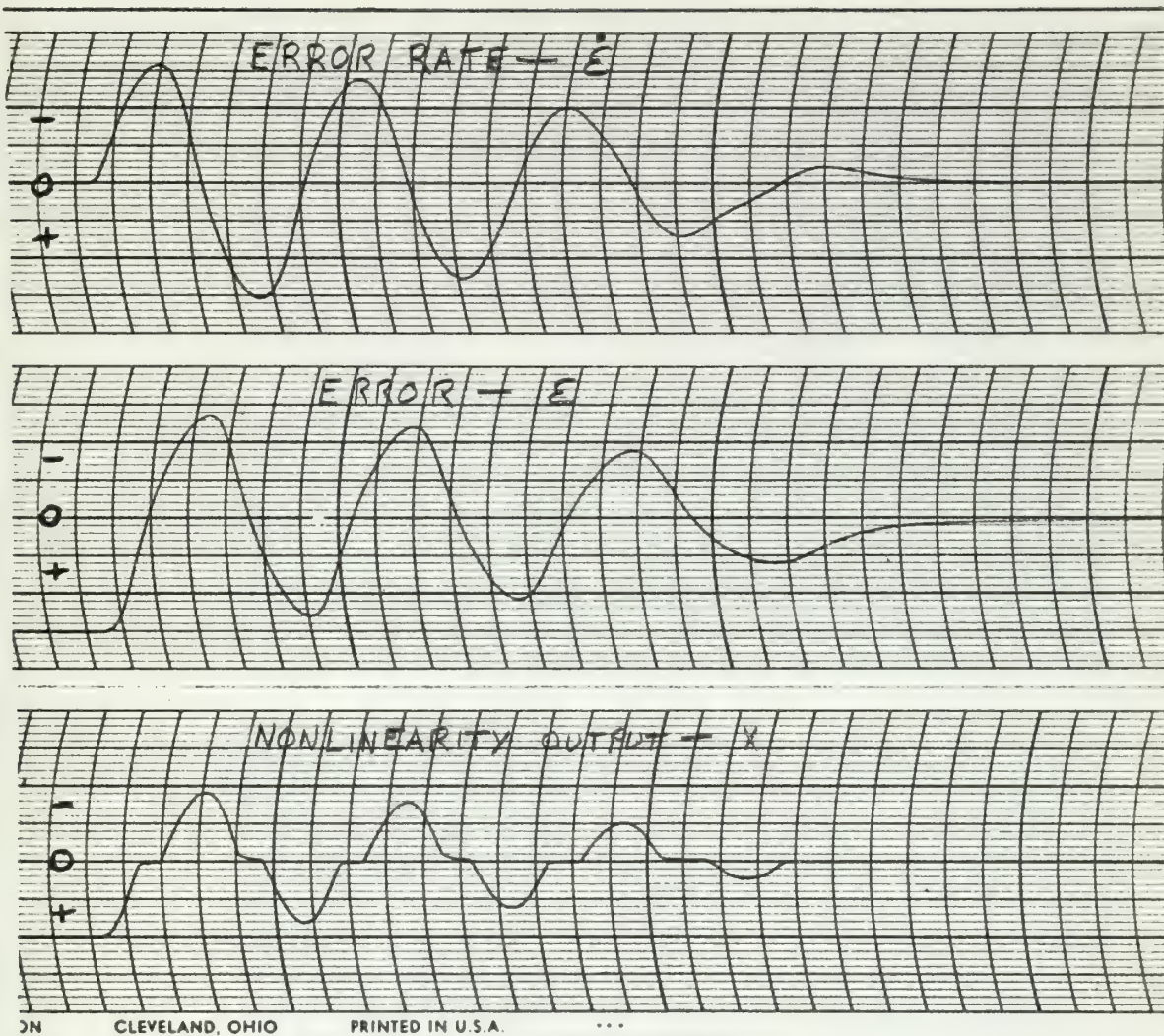


FIGURE II A 4.2

DEAD ZONE STATIC
CHARACTERISTIC CURVE

$$E_m = 15 \sin 2\pi(0.01)t$$





Recorder Trace II-A-4.1

Dead Zone in Error Channel, Loop Transfer Function with No Zeros, 15 Volt Step Input

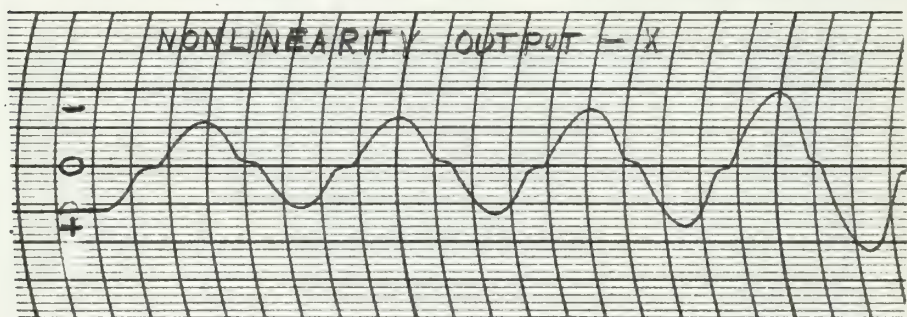
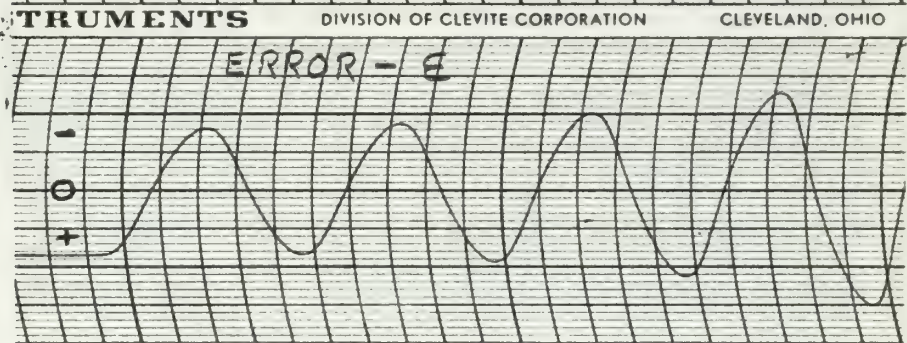
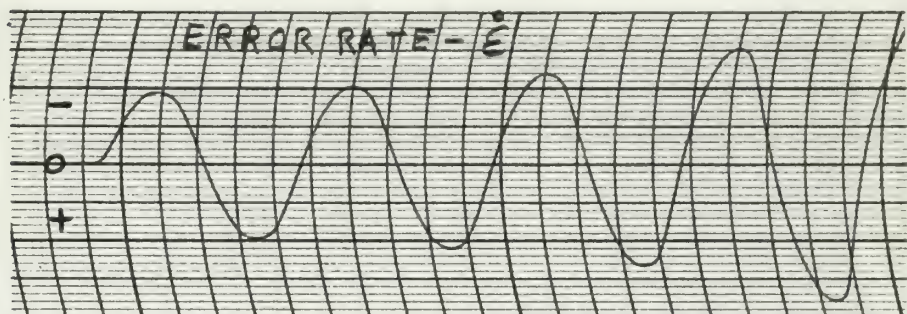
SCALE: \dot{E} - 1 Volt/Line

E - 1 Volt/Line

X - 1 Volt/Line

Time - 1 Second/Division





BRUSH INSTRUMENTS DIVISION OF CLEVITE CORPORATION

Recorder Trace II-A-4.2

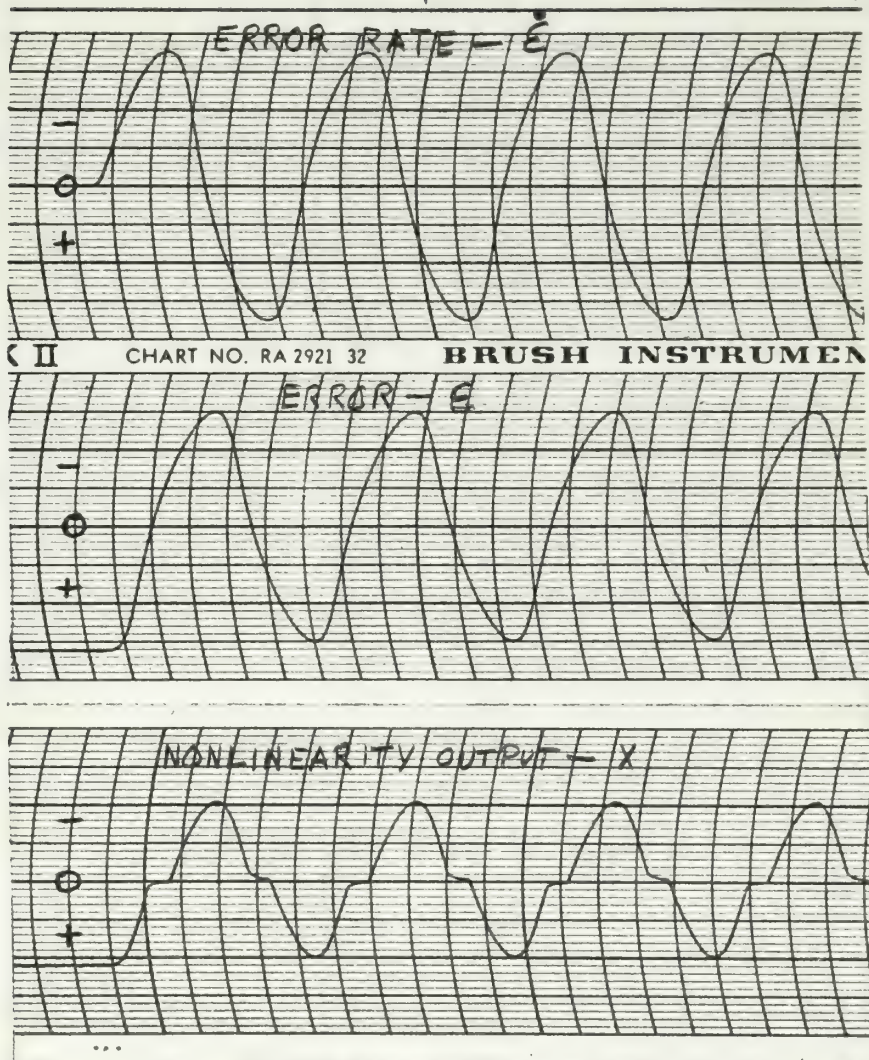
Dead Zone in Error Channel, Loop Transfer Function with No Zeros, 17 Volt Step Input

SCALE: \dot{E} - 2 Volts/line

E - 2 Volts/line

X - 2 Volts/line

Time - 1 Second/Division



Recorder Trace II-A-4.3

Limit Cycle, Dead Zone in Error Channel, Loop Transfer Function with No Zeros, 16.07 Volt Step Input

SCALES:

\dot{E} - 1 Volt/Line

E - 1 Volt/Line

X - 1 Volt/Line

Time - 1 Second/Division

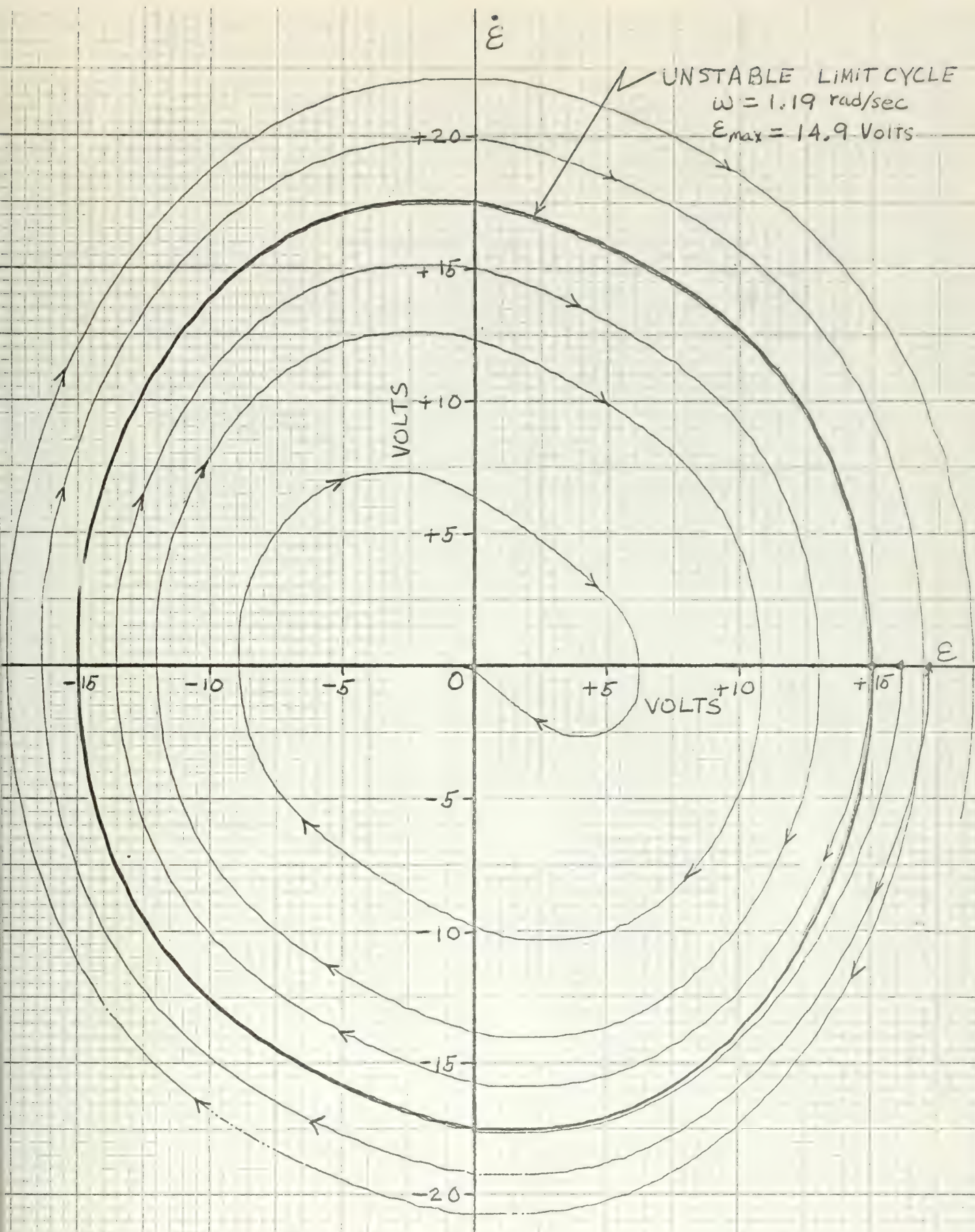


FIGURE II A 4.3

PHASE PORTRAIT - DEAD ZONE IN ERROR CHANNEL,
LOOP TRANSFER FUNCTION WITH NO ZEROS

$$G(s) = \frac{60}{s(s+1)(s+2)(s+8)}$$

II-A-5 Comparison of the four analytic methods in limit cycle prediction for the system of Figure II-A.

| Method | Frequency (rad/sec) | Amplitude (volts) |
|---------------------|------------------------|----------------------|
| Mitrovic | 1.206 | 12.402 |
| Root Locus | 1.206 | 12.402 |
| Describing Function | 1.21 | 14.71 |
| Analog Simulation | 1.207 | 15.0 |



II-B Loop Transfer Function with One Zero.

The block diagram of the system chosen to analyze is shown in Fig.

II-B.

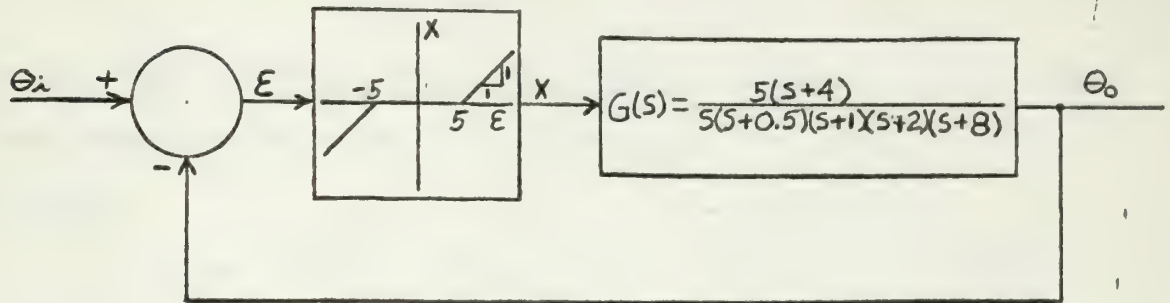


Figure II-B

Dead Zone in Error Channel Loop

Transfer Function with One Zero

II-B-1. Mitrovic's Method.

If N is the instantaneous gain of the nonlinearity the characteristic equation for the system is

$$s^5 + 11.5s^4 + 31.5s^3 + 29s^2 + (8 + 5N)s + 20N = 0. \quad (\text{II-B-1.1})$$

Assuming the last two coefficients to be variable, the characteristic equation becomes,

$$s^5 + 11.5s^4 + 31.5s^3 + 29s^2 + B_1s + B_0 = 0 \quad (\text{II-B-1.2})$$

where

$$B_1 = 8 + 5N \quad (\text{II-B-1.3})$$

and

$$B_0 = 20N. \quad (\text{II-B-1.4})$$

From Appendix A, Mitrovic's equations for B_0 and B_1 are,

$$B_0 = -[29\omega_n^2\phi_1(\xi) + 31.5\omega_n^3\phi_2(\xi) + 11.5\omega_n^4\phi_3(\xi) + \omega_n^5\phi_4(\xi)] \quad (\text{II-B-1.3})$$

and

$$B_1 = 29\omega_n\phi_2(\xi) + 31.5\omega_n^2\phi_3(\xi) + 11.5\omega_n^3\phi_4(\xi) + \omega_n^4\phi_5(\xi). \quad (\text{II-B-1.4})$$

Substitution of the values of the ϕ functions from Appendix A for

$\xi = 0$ gives,

$$B_0 = 29\omega_n^2 - 11.5\omega_n^4 \quad (\text{II-B-1.5})$$

and

$$B_1 = 31.5\omega_n^2 - \omega_n^4. \quad (\text{II-B-1.6})$$

The sets of parametric equations II-B-1.3, II-B-1.4, II-B-1.7, and II-B-1.8 describe the M-point locus and the stability curve on the B_0 versus B_1 plane. Direct solution of these equations for the intersection becomes fairly complicated; consequently, a straight graphical solution is performed.

Table II-B-1.1 gives the values of B_0 and B_1 for values of ω_n plotted in Figure II-B-1.1. Elimination of N from Equations II-B-1.3 and II-B-1.4 yields

$$B_1 = 8 + \frac{B_0}{4} \quad (\text{II-B-1.7})$$

which is a straight line with a B_1 intercept of + 8 and a slope of + 4.

The intersection of the two curves is seen to be approximately at $\omega_n = 0.96$ rad/sec.

To accurately determine the intersection more values of stability curve are calculated and the value of B_1 thus determined is substituted in Equation II-B-1.9.

TABLE II-B-1.1

| ω_n | B_o | B_1 |
|------------|-------|-------|
| 0.5 | 6.53 | 7.81 |
| 0.6 | 8.95 | 11.21 |
| 0.8 | 13.85 | 19.75 |
| 1.0 | 17.5 | 30.50 |
| 1.2 | 17.9 | 43.23 |
| 1.4 | 12.6 | 57.86 |
| 1.588 | 0 | 73.0 |

The intersection occurs when the two values of B_o are equal. These additional calculations appear in Table II-B-1.2

TABLE II-B-1.2

| ω_n | B_1 | B_o | B_o' |
|------------|----------|---------|---------|
| 0.55 | 9.43724 | 8.72017 | 5.74897 |
| 0.567 | 10.02355 | 8.13459 | 8.09419 |
| 0.568 | 10.05857 | 8.15910 | 8.23428 |
| 0.57 | 10.12679 | 8.20816 | 8.50716 |

By interpolation the intersection occurs at

$$\omega_n = 0.5673 \text{ rad/sec}$$

and

$$B_o = 8.140$$

From Equation II-B-1.4, the average nonlinear gain over a cycle is

$$N_{ave} = 0.407$$

Since the nonlinearity is the same as the one of Section A-1 of this chapter, Equations II-A-1.11 through II-A-1.15 are used to obtain the approximate amplitude of the limit cycle. Substituting N_{ave} into Equation II-A-1.14 yields

$$A = \tan^{-1} 0.407 = 22.15^\circ ,$$

Substituting A into Equation II-A-1.15 yields

$$B = 22.85^\circ ,$$

Substituting A and B in Equation II-A-1.13 gives

$$a = 5 \frac{\sin 22.15}{\sin 22.85} = 4.85 .$$

Substituting "a" into Equation II-A-1.12 gives

$$c = 0.707 (4.85) = 3.42 .$$

Finally Equation II-A-1.11 gives

$$E_{max} = 5 + 3.42 = 8.42 \text{ volts} .$$

Applying the same reasoning as given in Section II-A-1 to Figure II-B-1.2, Mitrovic's method predicts an unstable limit cycle.

II-B-2. Root Locus Method.

Substitution of $S=j\omega$ into Equation II-B-1.1 and simplifying the higher order J terms gives

$$J\omega^5 + 11.5\omega^4 - J31.5\omega^3 - 29\omega^2 + J(8+5N)\omega + 20N = 0. \quad (\text{II-B-2.1})$$

By requiring that both the real and imaginary parts of Equation II-B-2.1 go to zero independently gives

$$J\omega^5 - J31.5\omega^3 + J(8+5N)\omega = 0 \quad (\text{II-B-2.2})$$

and

$$11.5\omega^4 - 29\omega^2 + 20N = 0. \quad (\text{II-B-2.3})$$

Dividing Equation II-B-2.2 by $J\omega$ and solving for $5N$ gives

$$5N = -\omega^4 + 31.5\omega^2 - 8. \quad (\text{II-B-2.4})$$

Substitution of Equation II-B-2.4 into Equation II-B-2.3 and simplifying gives

$$7.5\omega^4 + 97\omega^2 - 32 = 0.$$

Solving this equation for ω^2 gives

$$\omega^2 = 0.3219$$

from which

$$\omega = 0.567 \text{ rad/sec}.$$

Substituting the value of ω^2 back into Equation II-B-2.4 gives the "average" nonlinear gain over a cycle as,

$$N_{\text{ave}} = 0.4072.$$

To find the approximate amplitude of the limit cycle, Equations II-A-1.11 through II-A-1.15 are again used. These equations yield

$$E_{\text{max}} = 8.41 \text{ volts}$$



A graphical presentation of the solution is sketched in Figure II-B-

2.1.

Applying the same reasoning as given in Section II-A-2 to Figure II-B-2.1, the root locus method predicts an unstable limit cycle.

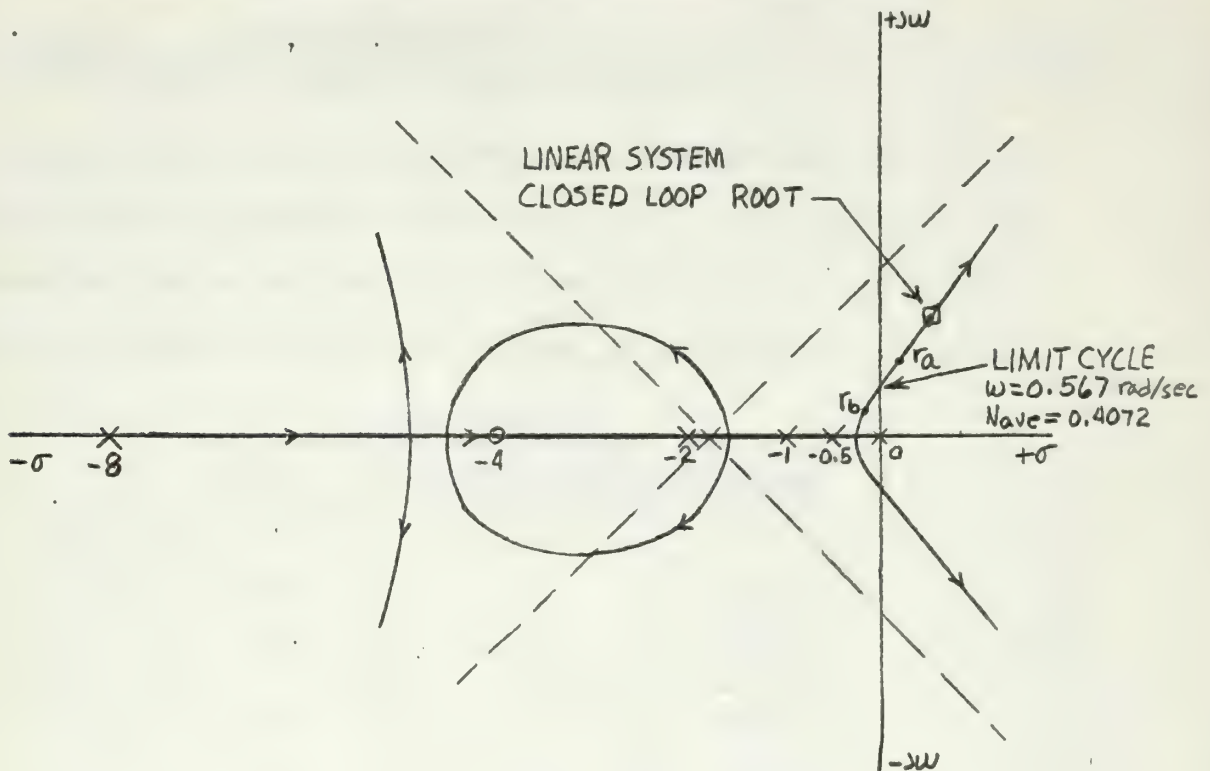


Fig. II-B-2.1

Root Locus Solution for Dead Time System. The

Loop transfer function with the zero



II-B-3. Describing Function Method.

The describing function for dead zone is given in Equation II-A-3.1.

The linear loop transfer function for the given system in frequency response form is

$$G(j\omega) = \frac{2.5(0.25j\omega + 1)}{j\omega(2j\omega + 1)(j\omega + 1)(0.5j\omega + 1)(0.125j\omega + 1)} \quad (\text{II-B-3.1})$$

Table II-B-3.1 gives the magnitude and phase of Equation II-B-3.1 for the different frequencies which were used to plot the linear loop transfer function on the gain-phase plane of Figure II-B-3.1. These values are obtained from the Bode diagram plot of Equation II-B-3.1.

TABLE II-B-3.1

| ω | $ G(j\omega) \text{ db}$ | $\angle G(j\omega) \text{ deg}$ |
|----------|---------------------------|---------------------------------|
| 0.495 | + 10 | -172 |
| 0.53 | + 9 | -176 |
| 0.56 | + 8 | -180 |
| 0.60 | + 7 | -184 |
| 0.638 | + 6 | -188 |

Table II-B-3.2 gives the values of $1/G_D$ plotted in Figure II-B-3.1. These values are obtained from Equation II-A-3.1 for various values of R .

TABLE II-B-3.2

| R | G_D | $1/G_D$ | $1/G_D \text{ db}$ |
|------|--------|---------|--------------------|
| 0.4 | 0.5044 | 1.983 | 5.94 |
| 0.45 | 0.447 | 2.237 | 6.99 |
| 0.48 | 0.4132 | 2.420 | 7.48 |
| 0.49 | 0.4021 | 2.4817 | 7.91 |
| 0.5 | 0.3910 | 2.558 | 8.16 |

By interpolation of Figure II-B-3.1 the intersection and thus the limit cycle occurs at



$$\omega = 0.56 \text{ rad/sec}$$

and

$$R = 0.495$$

From Equation II-A-3.2, the amplitude of the limit cycle is then

$$E_{\max} = \frac{10}{2(0.495)} = 10.1 \text{ volts.}$$

Applying the same reasoning given in Section II-A-3 to Figure II-B-3.1, the describing function predicts an unstable limit cycle.



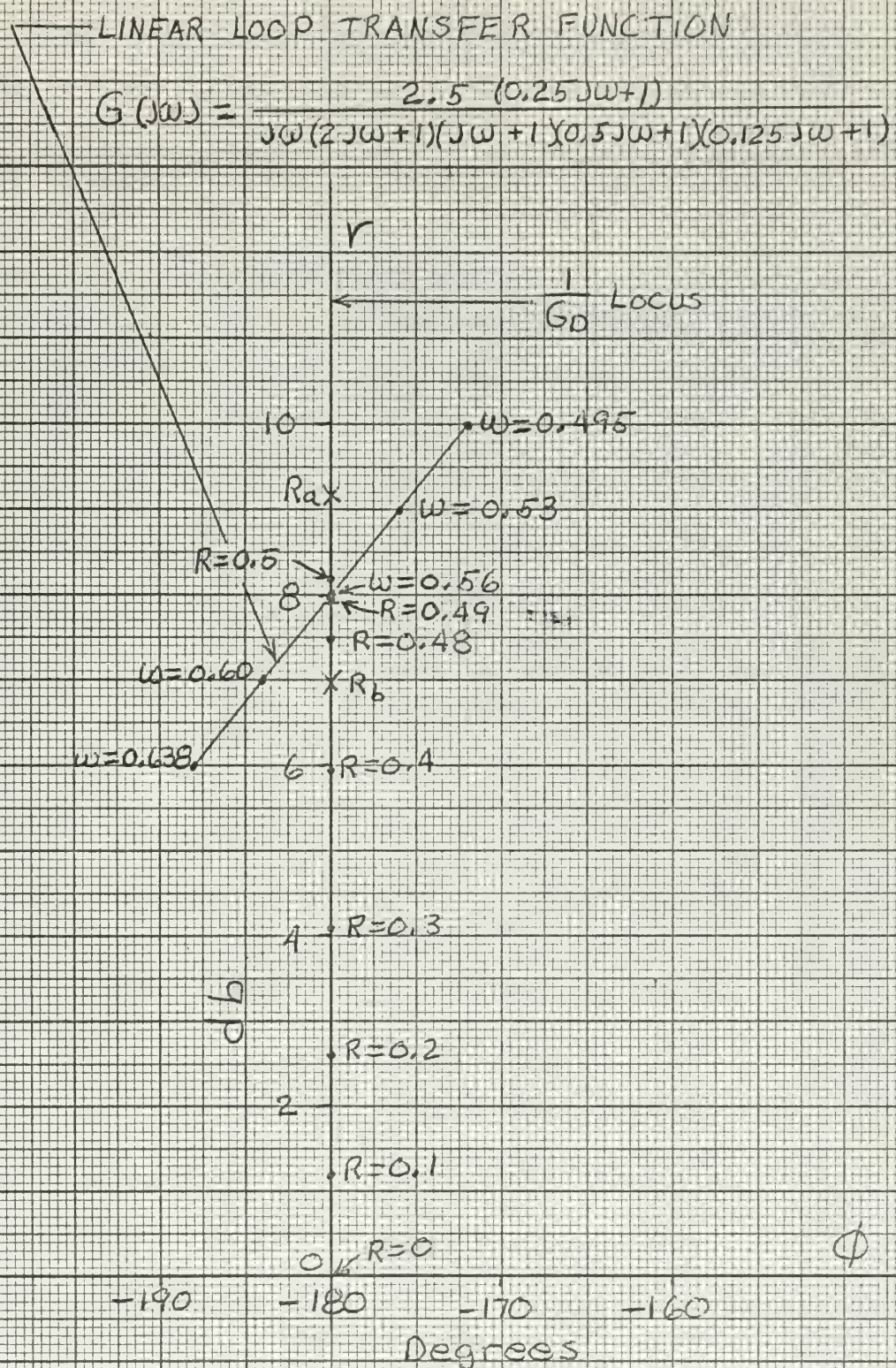


FIGURE IB 3.1

GAIN-PHASE PLANE - DEAD ZONE IN
ERROR CHANNEL; LOOP TRANSFER
FUNCTION WITH ONE ZERO



II-B-4 Analog Computer Simulation.

The analog simulation of the given nonlinear system is shown in Figure II-A-4.1. The coefficient pot settings with associated resistances and capacitances for real time and real magnitude scaling are given in Table II-A-4.1.

TABLE II-A-4.1

| Pot Setting | Associated Elements |
|-------------------------------|--|
| $a_1 = \frac{E_i}{100}$ | For Input Step of E_i volts $R_1 = 1 \text{ Meg}, R_{f1} = 1 \text{ Meg}$ |
| $a_2 = 1.0$ | $R_2 = 1 \text{ Meg}, R_{f1} = 1 \text{ Meg}$ |
| $a_3 = 1.0$ | $R_3 = 1 \text{ Meg}, R_{f2} = 1 \text{ Meg}$ |
| $a_4 = 0.4$ | $R_4 = 0.4 \text{ Meg}, C_{f1} = 1 \text{ uf}$ |
| $a_5 = 0.8$ | $R_5 = 0.1 \text{ Meg}, C_{f1} = 1 \text{ uf}$ |
| $a_6 = 1.0$ | $R_6 = 1 \text{ Meg}, R_{f3} = 1 \text{ Meg}$ |
| $a_7 = 1.0$ | $R_7 = 1 \text{ Meg}, R_{f3} = 1 \text{ Meg}$ |
| $a_8 = 0.5$ | $R_8 = 0.1 \text{ Meg}, C_{f2} = 1 \text{ uf}$ |
| $a_9 = 1.0$ | $R_9 = 0.5 \text{ Meg}, C_{f2} = 1 \text{ uf}$ |
| $a_{10} = 1.0$ | $R_{10} = 1 \text{ Meg}, C_{f3} = 1 \text{ uf}$ |
| $a_{11} = 1.0$ | $R_{11} = 1 \text{ Meg}, C_{f3} = 1 \text{ uf}$ |
| $a_{12} = 1.0$ | $R_{12} = 1 \text{ Meg}, C_{f4} = 1 \text{ uf}$ |
| $a_{13} = 0.5$ | $R_{13} = 1 \text{ Meg}, C_{f4} = 1 \text{ uf}$ |
| $a_{14} = 1.0$ | $R_{14} = 1 \text{ Meg}, C_{f5} = 1 \text{ uf}$ |
| $a = 0.05$ Initial setting | For a 5 volt Dead Zone Each Side of Zero |

The back-bias pots "a" were accurately set in the same manner as described in Section II-A-4. The static characteristic of the nonlinearity is shown in Figure II-A-4.1.

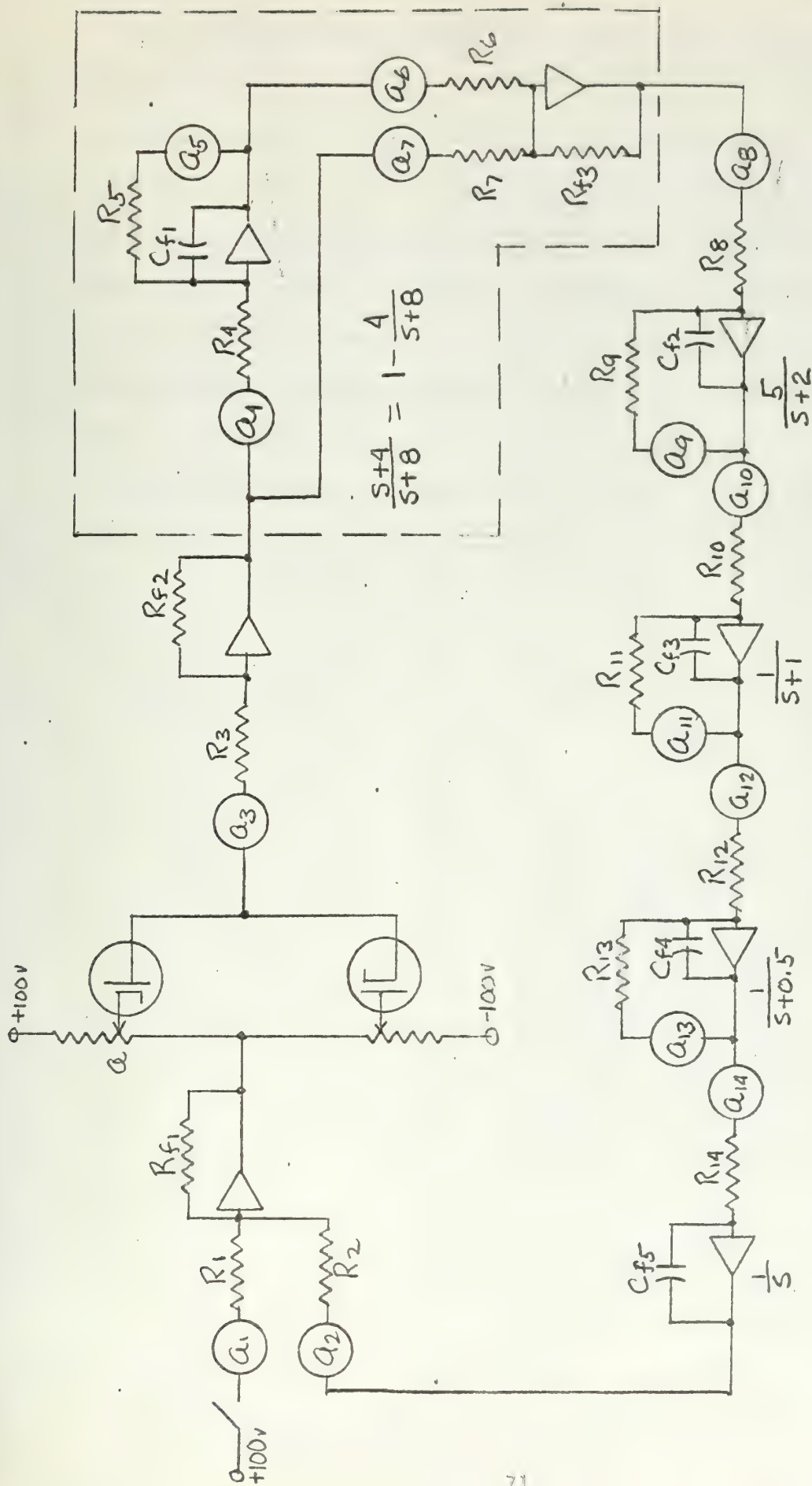


Figure 11-B-4.1

analog computer simulation of dead zone in error channel, loop transfer function with one zero.



The system was first excited with a 10.2 volt step input and was found to be stable as shown in recorder trace II-B-4.1. The system was then excited with a 10.6 volt step input and found to be unstable, as shown in recorder trace II-B-4.2. The unstable limit cycle was difficult to obtain but was found to lie between step inputs of 10.3 volts and 10.4 volts. These two responses are shown in recorder traces II-B-4.3 and II-B-4.4. The average of the two traces show the angular frequency to be 0.552 rad/sec and the amplitude, using the first two peaks of each trace, to be 9.9 volts.

The phase portrait of the system is shown in Figure II-B-4.2.

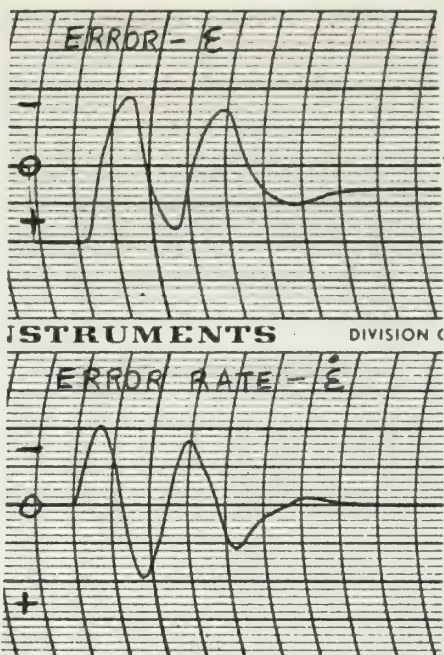


Recorder Trace II-B-4.1

Dead Zone in Error Channel,
Loop Transfer Function with
One Zero, 10.2 Volt Step
Input.

SCALES:

\dot{E} - 1 Volt/Line
 E - 0.5 Volts/Line
Time - 5 Seconds/Division

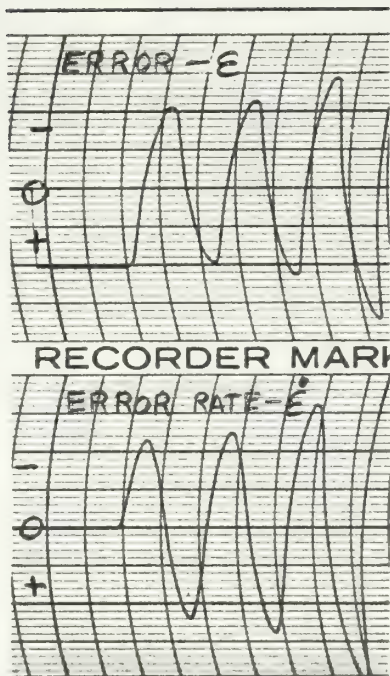


Recorder Trace II-B-4.2

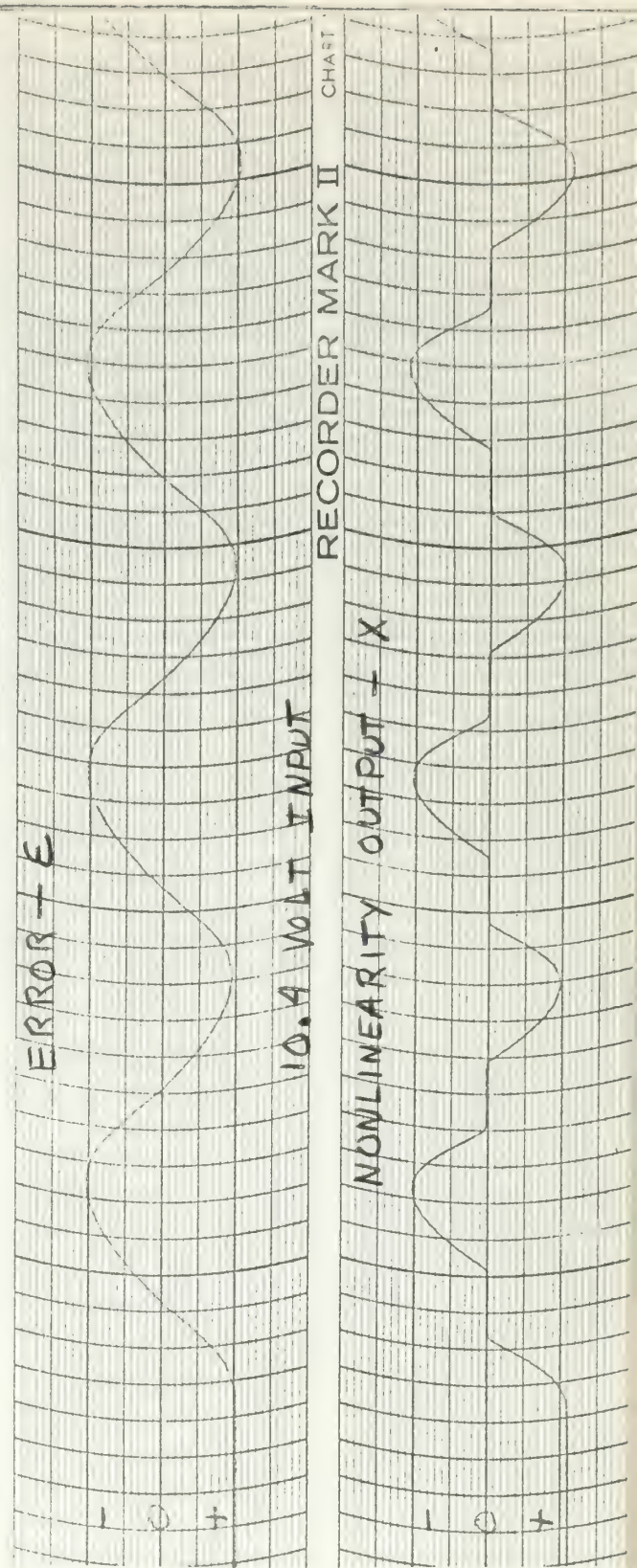
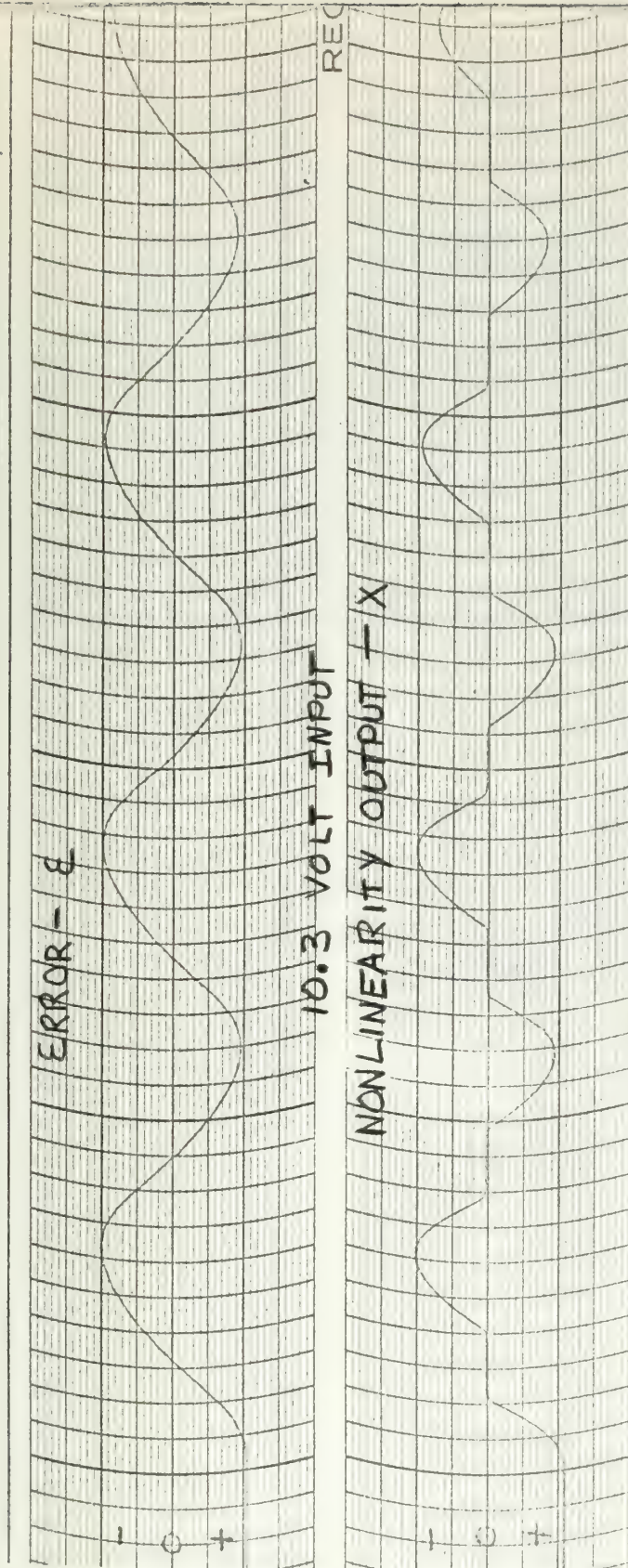
Dead Zone in Error Channel,
Loop Transfer Function with
One Zero, 10.6 Volt Step Input

SCALES:

\dot{E} - 1 Volt/Line
 E - 0.5 Volts/Line
Time - 5 Seconds/Division







Recorder Trace II-B-4.3

LIMIT CYCLE, Dead Zone in Error Channel, Loop Transfer Function with One Zero

SCALES: ϵ - 1 volt/line X - 0.5 Volt/line Time - 1 Second/division

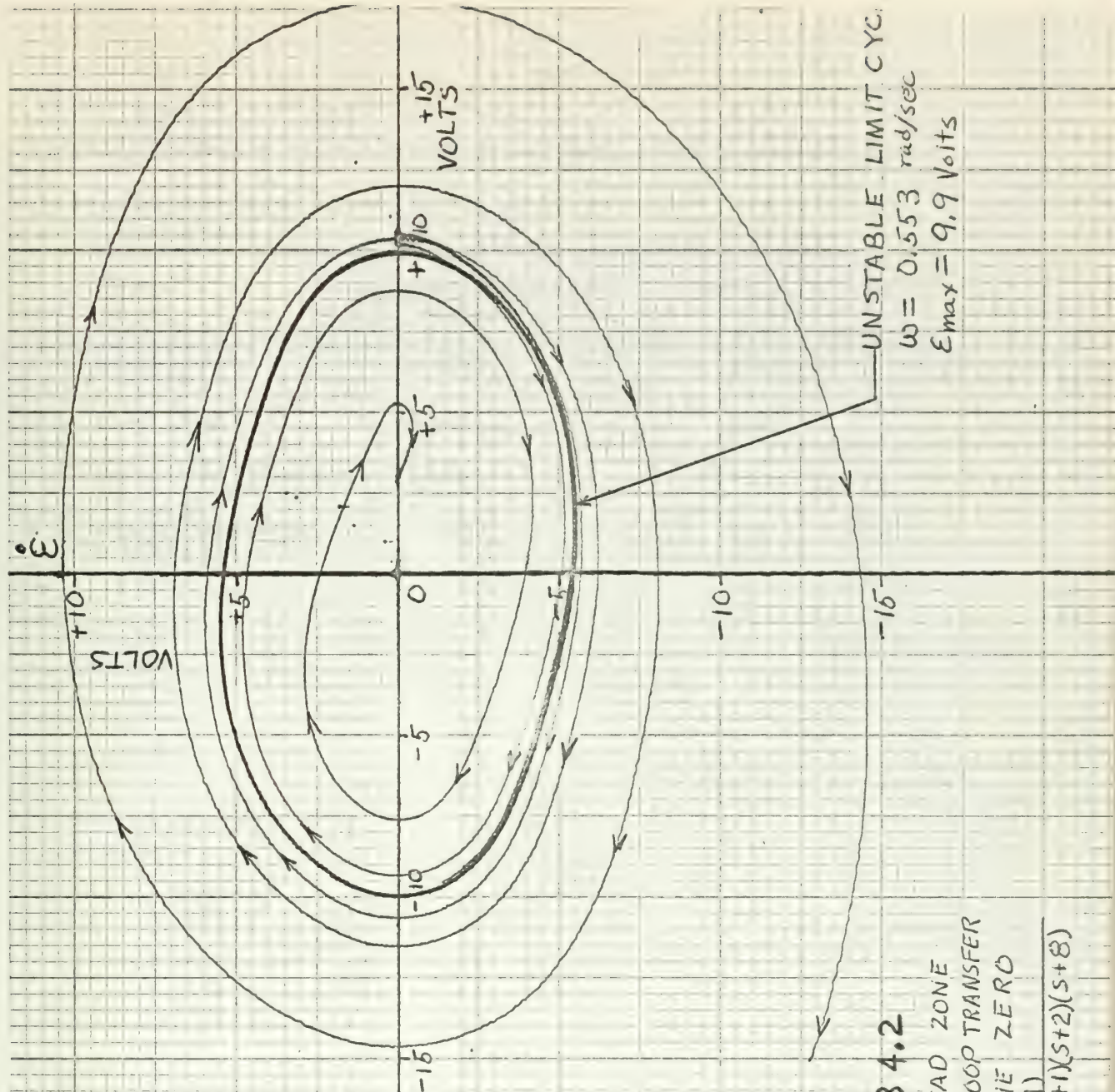


FIGURE II B 4.2

PHASE PORTRAIT- DEAD ZONE
 IN ERROR CHANNEL, LOOP TRANSFER
 FUNCTION WITH ONE ZERO

$$G(s) = \frac{5(s+4)}{s(s+0.5)(s+1)(s+2)(s+8)}$$



II-B-5 Comparison of the Four Analytic Methods in Predicting Limit
Cycles for the System Shown in Figure II-B.

| Method | Angular Frequency rad/sec | Amplitude Volts |
|---------------------|------------------------------|--------------------|
| Mitrovic's | 0.5673 | 8.42 |
| Root Locus | 0.567 | 8.41 |
| Describing Function | 0.560 | 10.1 |
| Analog Simulation | 0.552 | 9.9 |



CHAPTER III

IDEAL RELAY IN ERROR CHANNEL

III-A Loop Transfer Function With No Zeros

The system arbitrarily chosen to analyze is shown in the block diagram of Figure III-A.

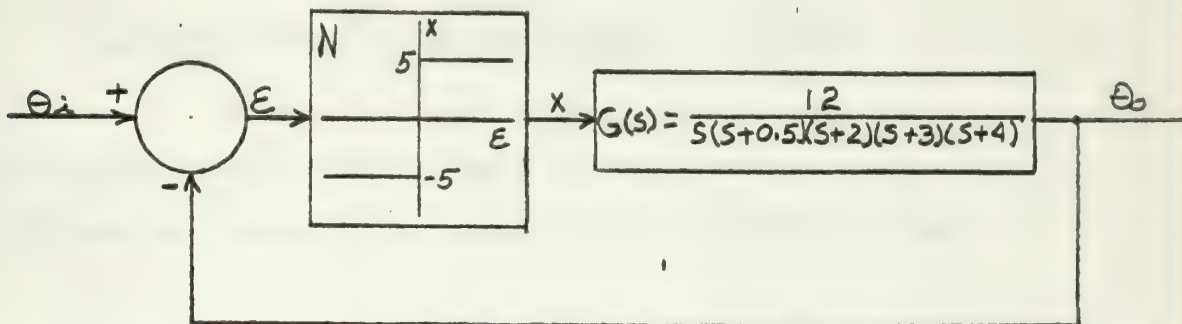


Figure III-A

Ideal Relay in Error Channel

Loop Transfer Function With No Zeros

III-A-1 Mitrovic's Method

Assigning N as the instantaneous gain of the relay, the characteristic equation can be written as

$$s^5 + 9.5s^4 + 30.5s^3 + 37s^2 + 12s + 12N = 0. \quad (\text{III-A-1.1})$$

Assuming the last two coefficients variable, the characteristic equation becomes,

$$s^5 + 9.5s^4 + 30.5s^3 + 37s^2 + B_1s + B_0 = 0, \quad (\text{III-A-1.2})$$

where

$$B_0 = 12N \quad (\text{III-A-1.3})$$

and

$$B_1 = 12 \quad . \quad (\text{III-A-1.4})$$

From Appendix A, Mitrovic's equation for B_0 and B_1 are,

$$B_0 = -[37\omega_n^2\phi_1(\zeta) + 30.5\omega_n^3\phi_2(\zeta) + 9.5\omega_n^4\phi_3(\zeta) + \omega_n^5\phi_4(\zeta)] \quad (\text{III-A-1.5})$$

and

$$B_1 = 37\omega_n\phi_2(\zeta) + 30.5\omega_n^2\phi_3(\zeta) + 9.5\omega_n^3\phi_4(\zeta) + \omega_n^4\phi_5(\zeta) \quad . \quad (\text{III-A-1.6})$$

Substitution of the values of the ϕ functions from Appendix A for

$\zeta = 0$ gives the parametric equations of the stability curve as,

$$B_0 = 37\omega_n^2 - 9.5\omega_n^4 \quad (\text{III-A-1.7})$$

and

$$B_1 = 30.5\omega_n^2 - \omega_n^4 \quad . \quad (\text{III-A-1.8})$$

To find the intersection between the M-point locus (Equations III-A-1.3 and III-A-1.4) and the stability curve (Equations III-A-1.7 and III-A-1.8), the graphical approach is chosen. Table III-A-1.1 gives the values of B_0 and B_1 for various ω_n that are plotted in Figure III-A-1.1. The M-point locus is seen to be a straight line parallel to the B_0 axis at $B_1 = 12$. From Figure III-A-1.1, the intersection is seen to occur at about $\omega_n = 0.62$.



TABLE III-A-1.1

| ω_n | B_o | B_1 |
|------------|-------|-------|
| 0.5 | 8.65 | 7.56 |
| 0.6 | 12.08 | 10.85 |
| 0.7 | 15.85 | 15.70 |
| 0.8 | 19.8 | 19.2 |
| 1.0 | 27.5 | 29.5 |
| 1.2 | 33.6 | 41.8 |
| 1.4 | 36.0 | 56.0 |
| 1.6 | 32.5 | 71.4 |
| 1.8 | 20.3 | 88.2 |
| 1.974 | 0 | 103.6 |

To accurately determine the intersection more values of B_o and B_1 are calculated for ω_n close to 0.62. These values appear in Table III-A-1.2. By interpolation from Table III-A-1.2 the intersection and thus the limit cycle occurs at

$$\omega_n = 0.6315 \text{ rad/sec}$$

and

$$B_o = 13.24$$

TABLE III-A-1.2

| ω_n | B_o | B_1 |
|------------|---------|---------|
| 0.62 | 12.8191 | 11.5764 |
| 0.63 | 13.1891 | 11.9480 |
| 0.631 | 13.2259 | 11.9854 |
| 0.632 | 13.2631 | 12.0229 |

The "average" nonlinear gain over a cycle is determined from

Equation III-A-1.3 as,

$$N_{ave} = 1.103$$

From this the approximate amplitude of the limit cycle is

$$\mathcal{E}_{max} = 4.53 \text{ volts}$$

Note that the M-point of the linear system in Figure III-A-1.1 shows that the linear system is stable. It is well known that an ideal relay gives a limit cycle for a linear system of order three or above and the occurrence of a limit cycle is independent of linear system stability. This is easily explainable on the B_0 versus B_1 plane. The ideal relay has an infinite maximum instantaneous gain whereas the nonlinearity used in Chapters I and II have a maximum instantaneous gain of one. This on the B_0 versus B_1 plane the M-point locus is unlimited for the ideal relay but does have a maximum value for the other nonlinearities. Consequently, an infinite straight line segment must necessarily intersect the stability curve at some point producing a limit cycle.

Mitrovic's method predicts a stable limit by the same reasoning used in Chapter I, Section I-A-1. This same argument can be applied to the ideal relay since this nonlinearity can be envisioned as saturation with an infinite gain in the linear region.

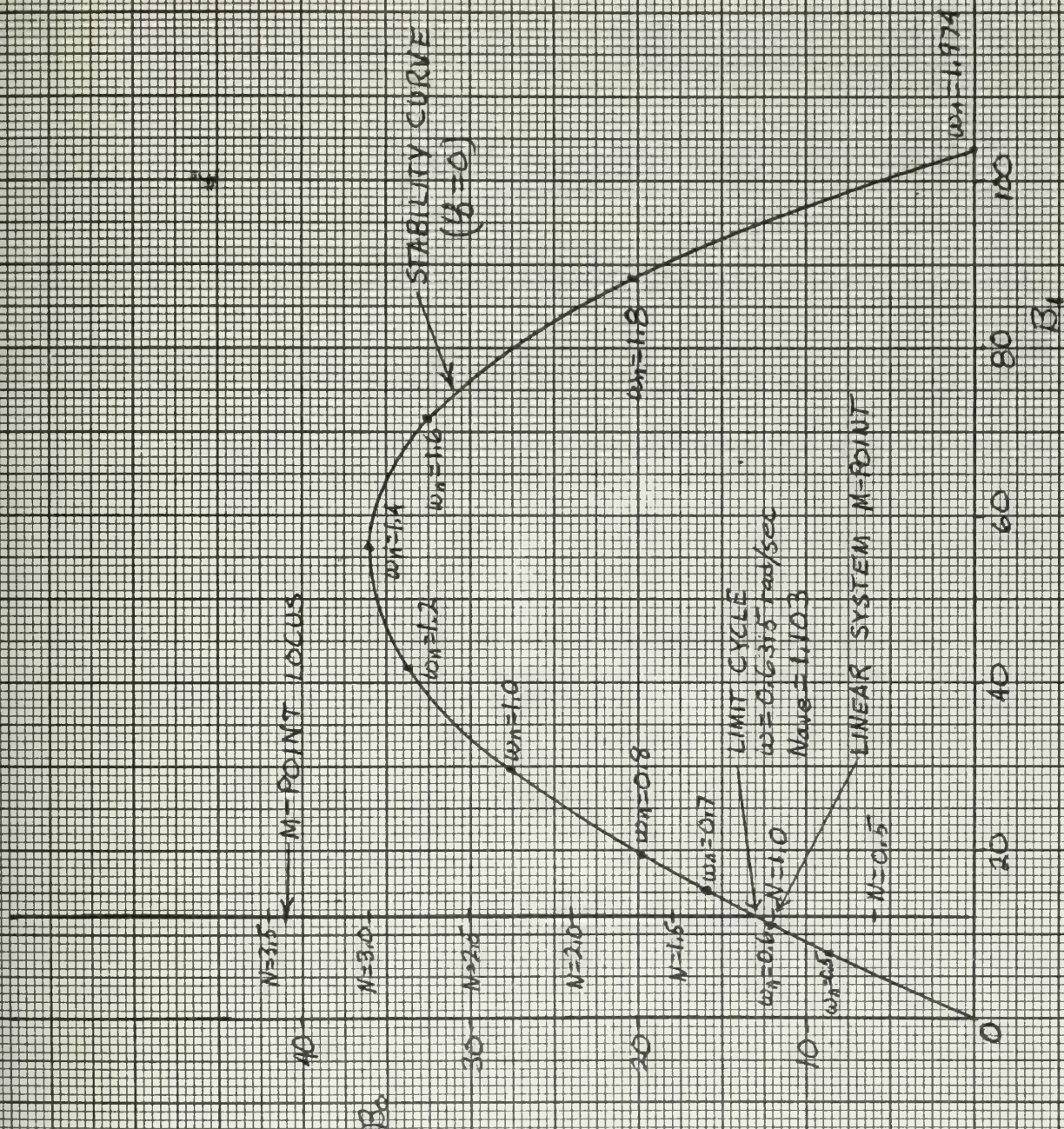


FIGURE III A.1.1
GRAPHICAL SOLUTION FOR RELAY IN ERROR CHANNEL
LOOP TRANSFER FUNCTION WITH NO ZEROS



III-A-2 Root Locus Method.

Substituting $S = j\omega$ into the characteristic Equation III-A-1.1 and evaluating the higher order powers of j yields,

$$j\omega^5 + 9.5\omega^4 - j30.5\omega^3 - 37\omega^2 + j12\omega + 12N = 0. \quad \text{III-A-2.1}$$

Requiring that the real and imaginary parts of Equation III-A-2.1 go to zero independently gives,

$$j\omega^5 - j30.5\omega^3 + j12\omega = 0 \quad \text{III-A-2.2}$$

and

$$9.5\omega^4 - 37\omega^2 + 12N = 0. \quad \text{III-A-2.3}$$

Dividing Equation III-A-2.2 by $j\omega$ and solving for ω^2 gives

$$\omega^2 = 0.3986,$$

from which

$$\omega = 0.6314 \text{ rad/sec.}$$

Substituting ω^2 into Equation III-A-2.3 and solving for N gives,

$$N_{ave} = 1.1032$$

From this "average" nonlinearity gain over a cycle, the approximate amplitude is determined as,

$$E_{max} = 4.533 \text{ volts}$$

The graphical presentation of the solution by root locus method is shown in Figure III-A-2.1.

The root locus method predicts a stable limit cycle by applying the same arguments to Figure III-A-2.1 that are given in Chapter I, Section I-A-2.



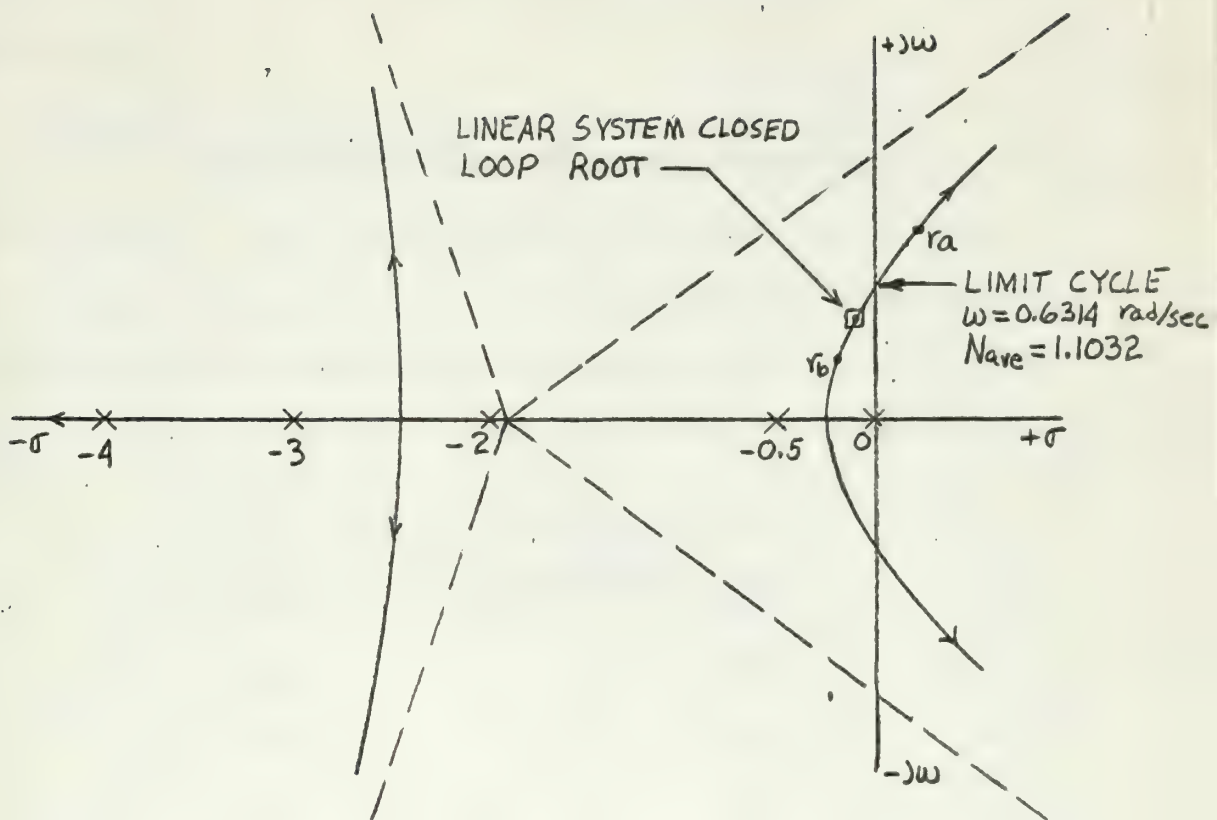


Fig. IIT-A-2.

Root Locus Solution for Ideal Relay in Error Channel
 Loop Transfer Function with n Zeros



III-A-3 Describing Function Method.

The describing function for an ideal relay is

$$G_D = \frac{4V}{\pi E_{max}} \angle 0^\circ \quad . \quad (\text{III-A-3.1})$$

The linear loop transfer function for the given system in frequency response form is,

$$G(j\omega) = \frac{1}{j\omega(2j\omega+1)(0.5j\omega+1)(0.333j\omega+1)(0.25j\omega+1)} \quad . \quad (\text{III-A-3.2})$$

Table III-A-3.1 gives the magnitude and phase of Equation III-A-3.2 for the different frequencies which were used to plot the linear loop transfer function on the gain-phase plane of Figure III-A-3.1. These values are obtained from a Bode diagram plot of Equation III-A-3.2.

TABLE III-A-3.1

| ω | $ G(j\omega) \text{ db}$ | $\angle G(j\omega) \text{ deg}$ |
|----------|---------------------------|---------------------------------|
| 0.527 | 2.0 | -167.5 |
| 0.565 | 1.0 | -172 |
| 0.605 | 0 | -176.5 |
| 0.625 | -0.5 | -178.5 |
| 0.648 | -1.0 | -181 |
| 0.69 | -2.0 | -185.5 |
| 0.735 | -3.0 | -190 |

Table III-A-3.2 gives the values of $1/G_D$ in the area of interest as obtained from Equation III-A-3.1 for various values of error.

TABLE III-A-3.2

| E_{max} | G_D | $1/G_D$ | $1/G_D \text{ db}$ |
|-----------|-------|---------|--------------------|
| 5 | 1.273 | 0.7854 | -2.10 |
| 6 | 1.061 | 0.942 | -0.52 |
| 5.8 | 1.098 | 0.911 | -0.80 |



By interpolation of Figure III-A-3.1, the intersection and thus the limit cycle occurs at

$$\omega = 0.635 \text{ rad/sec}$$

and

$$\epsilon_{\text{max}} = 5.6 \text{ volts}$$

The describing function method predicts a stable limit cycle by applying the same arguments in Section I-A-3 of Chapter I to Figure III-A-3.1



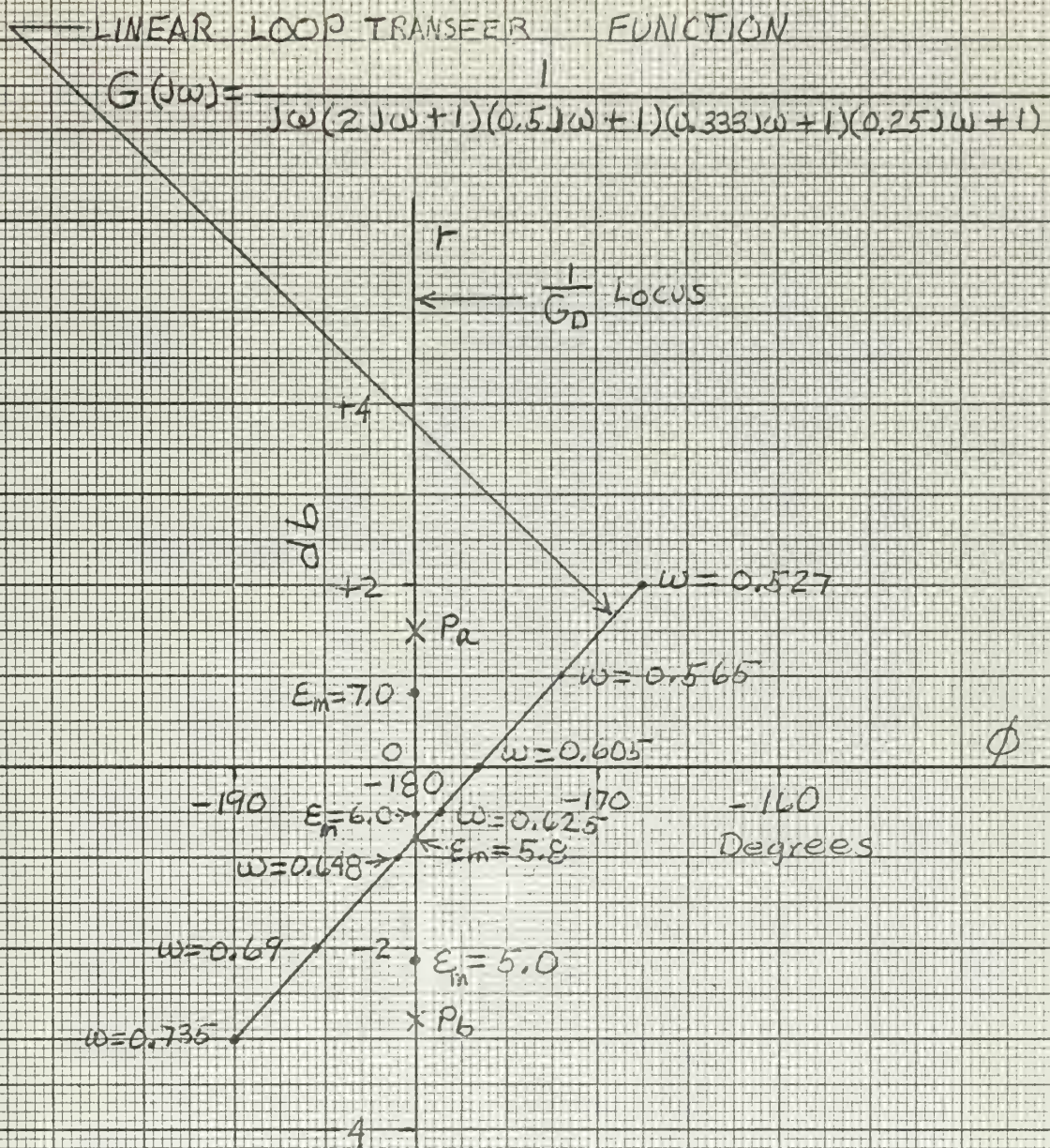


FIGURE III A 3.2
GAIN-PHASE PLANE - IDEAL RELAY IN
ERROR CHANNEL, LOOP TRANSFER
FUNCTION WITH NO ZEROS

III-A-4 Analog Computer Simulation.

The analog simulation of the given nonlinear system is shown in Figure III-A-4.1. The coefficient pot settings with associated resistances and capacitances for real time and real magnitude scaling are given in Table III-A-4.1.

TABLE III-A-4.1

| Pot Setting | Associated Elements |
|---------------------------------|--|
| $a_1 = \frac{E_1}{100}$ | For Input Step of E_1 Volt $R_1 = 1 \text{ Meg}$, $R_{f1} = 1 \text{ Meg}$ |
| $a_2 = 1.0$ | $R_2 = 1 \text{ Meg}$, $R_{f1} = 1 \text{ Meg}$ |
| $a_3 = (\text{See discussion})$ | $R_3 = 0.1 \text{ Meg}$, $R_{f2} = 1 \text{ Meg}$ |
| $a_4 = 0.4$ | $R_4 = 0.1 \text{ Meg}$, $C_{f1} = 1 \text{ uf}$ |
| $a_5 = 0.5$ | $R_5 = 1 \text{ Meg}$, $C_{f1} = 1 \text{ uf}$ |
| $a_6 = 0.3$ | $R_6 = 0.1 \text{ Meg}$, $C_{f2} = 1 \text{ uf}$ |
| $a_7 = 1.0$ | $R_7 = 0.5 \text{ Meg}$, $C_{f2} = 1 \text{ uf}$ |
| $a_8 = 1.0$ | $R_8 = 1 \text{ Meg}$, $C_{f3} = 1 \text{ uf}$ |
| $a_9 = 0.3$ | $R_9 = 0.1 \text{ Meg}$, $C_{f3} = 1 \text{ uf}$ |
| $a_{10} = 1.0$ | $R_{10} = 1 \text{ Meg}$, $C_{f4} = 1 \text{ uf}$ |
| $a_{11} = 0.4$ | $R_{11} = 0.1 \text{ Meg}$, $C_{f4} = 1 \text{ uf}$ |
| $a_{12} = 1$ | $R_{12} = 1 \text{ Meg}$, $C_{f5} = 1 \text{ uf}$ |
| $a = 0.05$ (Initial setting) | For 5 Volt Voltage |

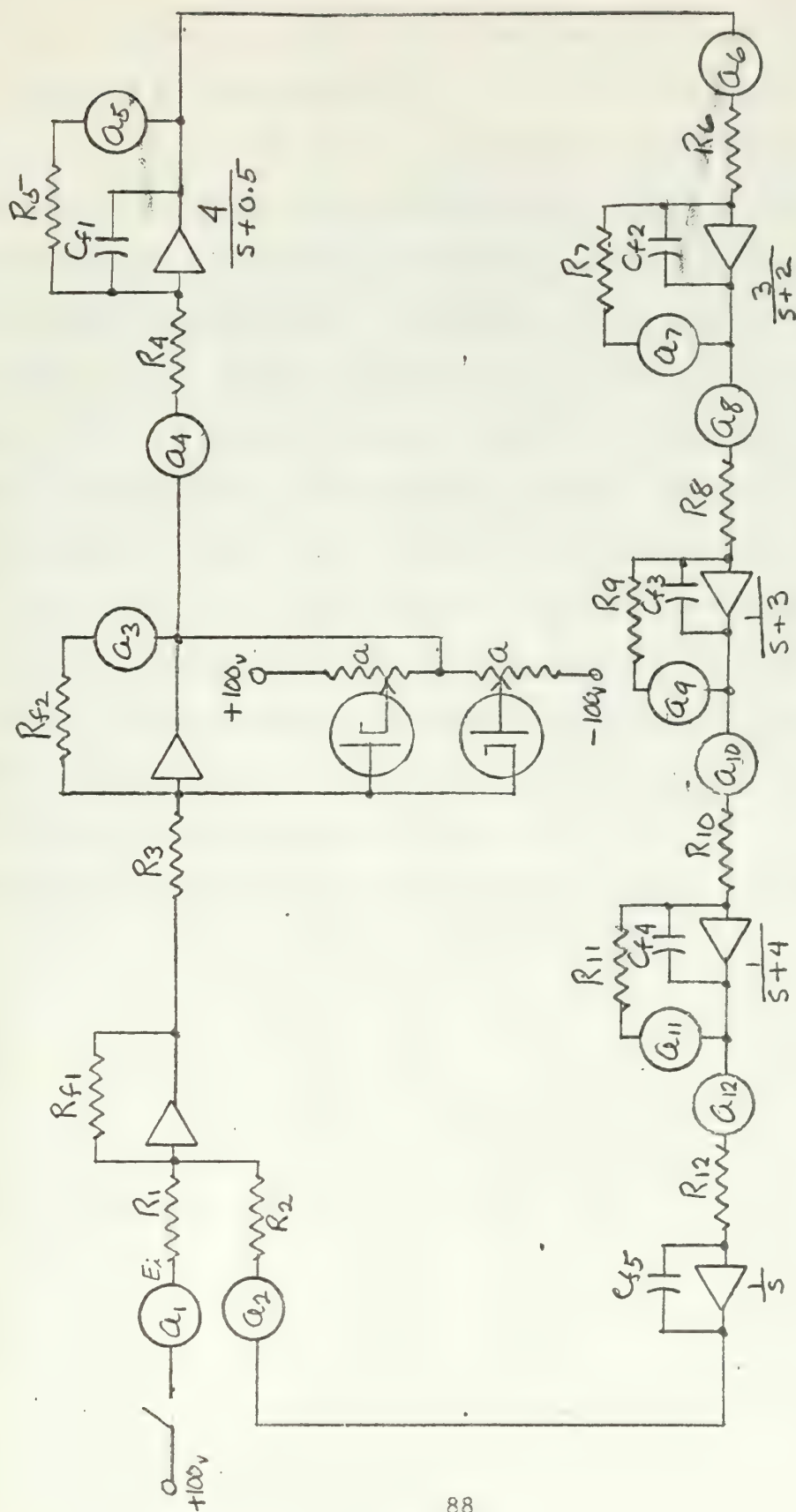


Figure IIT-A-4.1

Analog Computer Simulation of Ideal Relay in Error Channel, Loop Transfer Function with No Zeros.

The simulation of the ideal relay is seen to be a simple saturation simulation. However, the gain of the linear portion is made very high by the insertion of coefficient pot a_3 . To set the back-bias pots "a" and pot a_3 , a sine wave generator was connected to the input of the relay simulator. The output was monitored and the back-bias pots "a" were then adjusted until the output was limited at ± 5 volts. The output and input was then connected to an X - Y recorder to obtain a static characteristic curve. Pot a_3 was then adjusted until the slope of the linear portion was as nearly vertical as possible without the amplifier overloading. The static characteristic curve appears as Figure III-A-4.2.

The system was first excited with a 1 volt input signal and was found to build up to the limit cycle as shown in recorder trace III-A-4.1. The system was then excited with a 10 volt step input and was found to go into the same limit cycle as shown in recorder trace III-A-4.2. From these two recorder traces the limit cycle is seen to be stable with an angular frequency of 0.628 rad/sec and an amplitude of 5.7 volts.

The phase portrait of the system is shown in Figure III A-4.3.

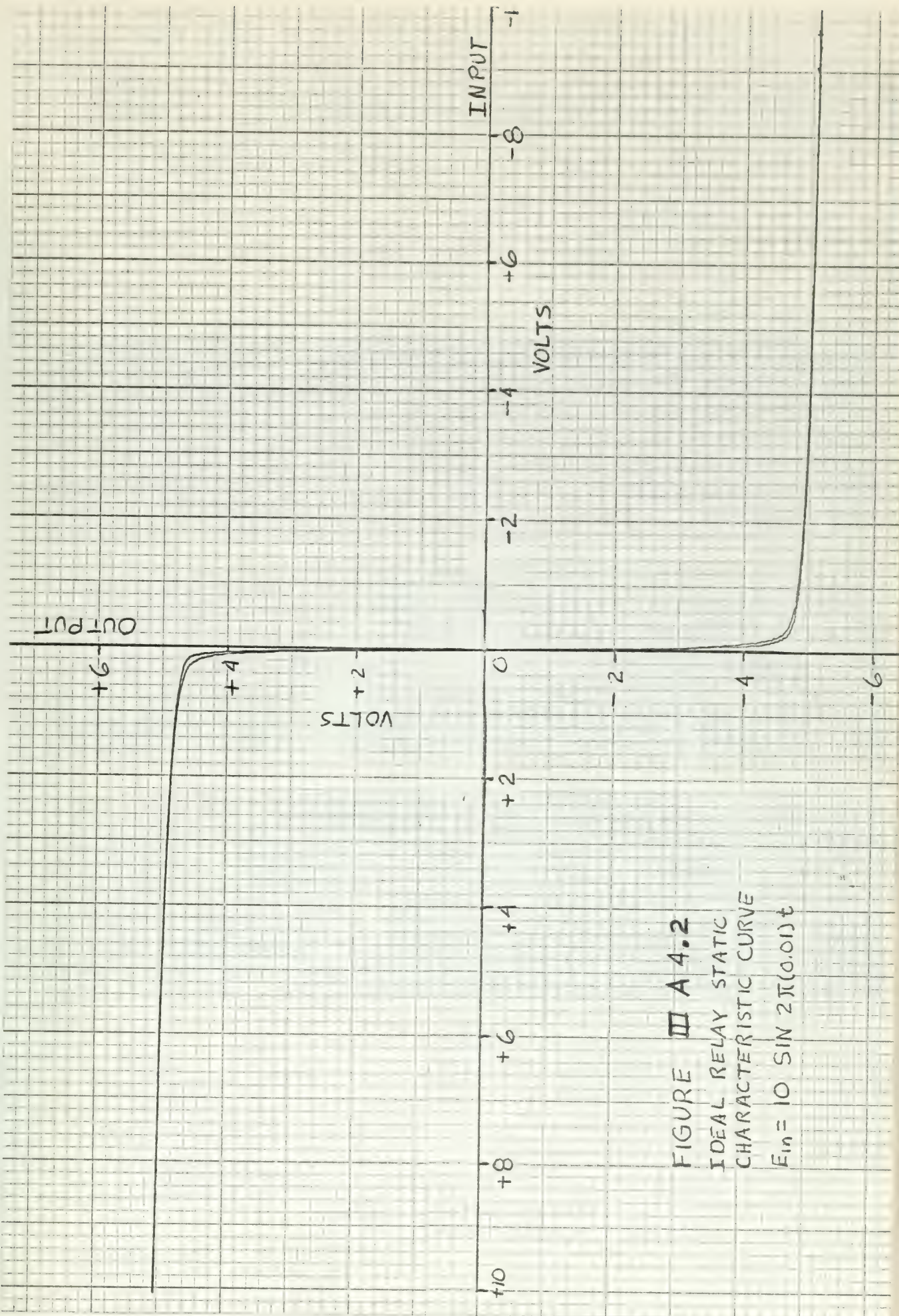
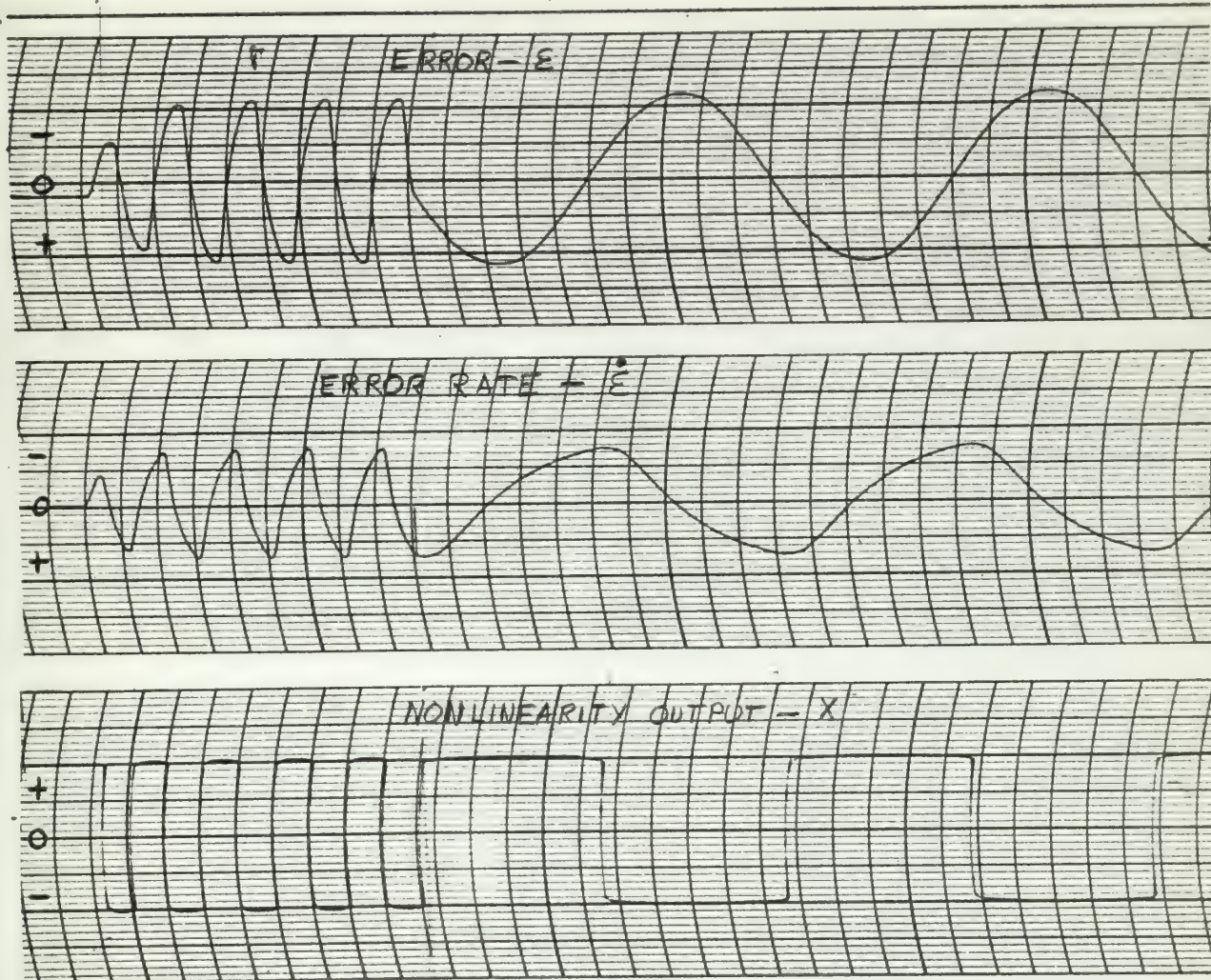


FIGURE III A 4.2
 IDEAL RELAY STATIC
 CHARACTERISTIC CURVE
 $E_{in} = 10 \sin 2\pi(0.01)t$



Recorder Trace III-A-4.1

Ideal Relay in Error Channel, Loop Transfer Function with No Zeros,
1 Volt Step Input

SCALES:

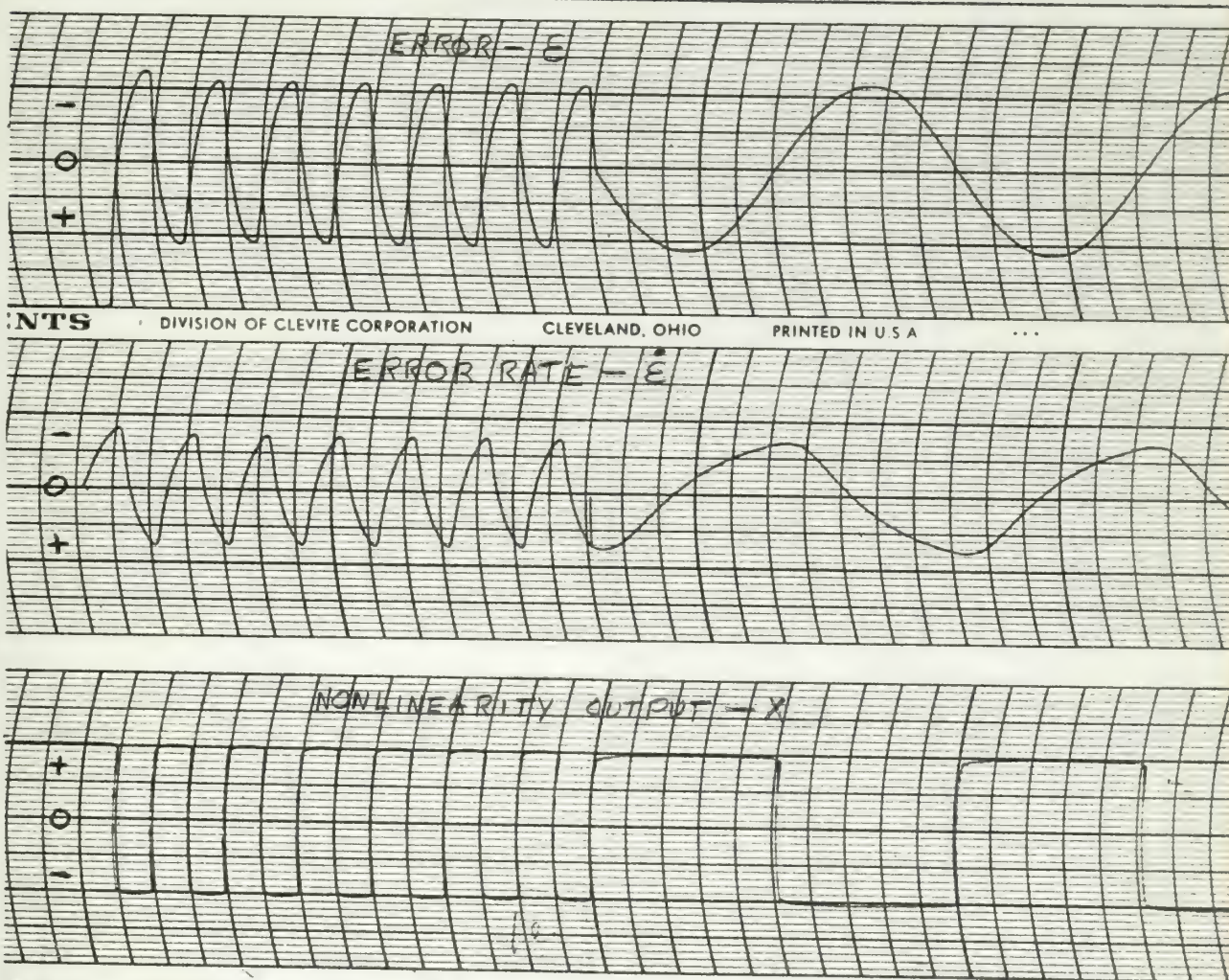
E - 0.5 Volts/ Line

\dot{E} - 0.5 Volts/line

X - 0.5 Volts/line

Time - 5 Seconds/Division

1 Second/Division



Recorder Trace TTYA-4.2

Ideal Relay in Error Channel, Loop Transfer Function with No Zeros,
10 Volt Step Input.

SCALES:

E - 0.5 Volts/Line

\dot{E} - 0.5 Volts/line

X - 0.5 Volts/line

Time - 5 Seconds/Division

1 Second/Division

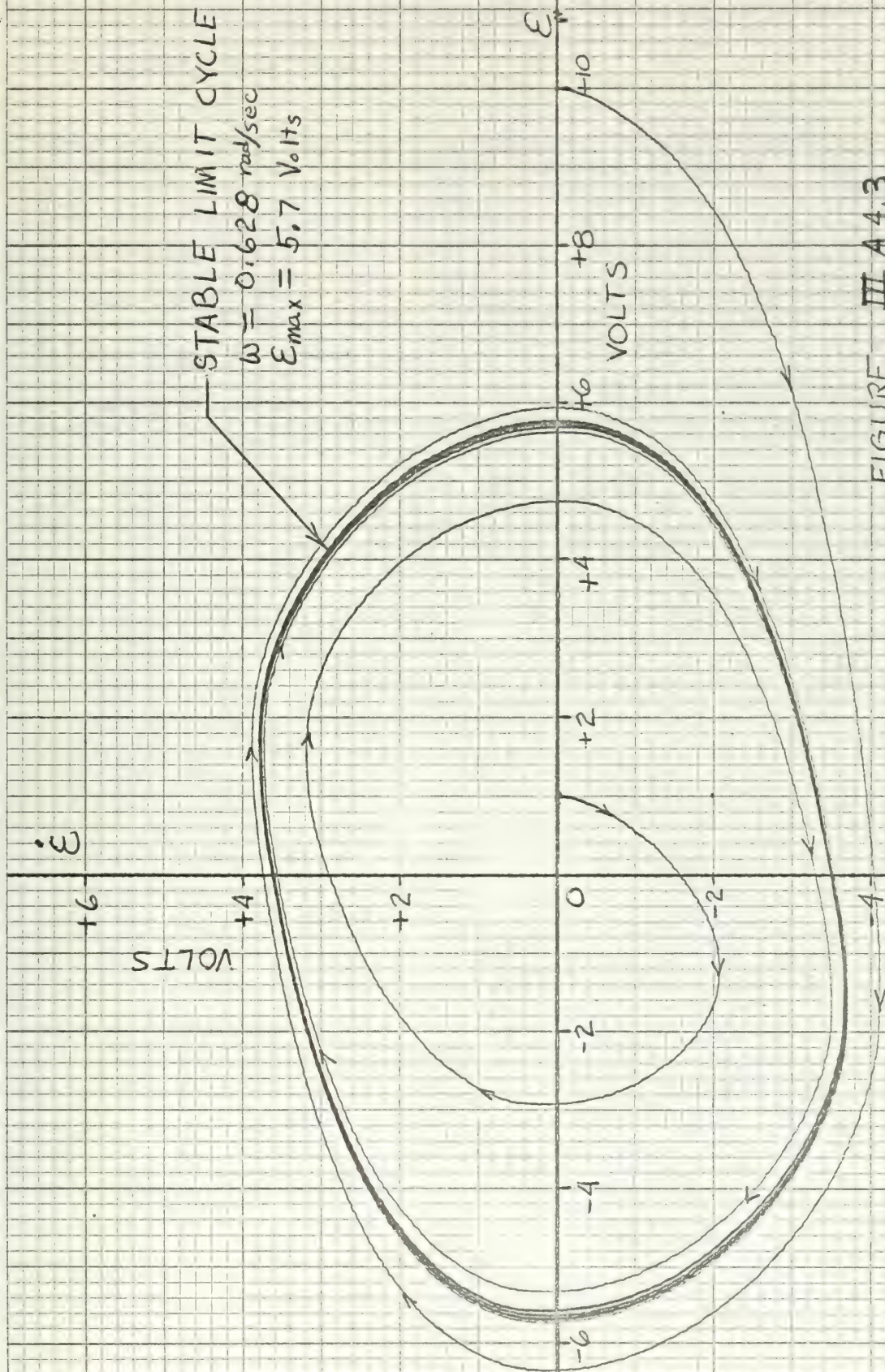


FIGURE III A 4.3
 IDEAL RELAY IN ERROR CHANNEL, LOOP
 TRANSFER FUNCTION WITH NO ZEROS

$$G(s) = \frac{12}{s(s+0.5)(s+2)(s+3)(s+4)}$$

III-A-5 Comparison of the Four Methods in Predicting Limit Cycles for the System of Figure III-A.

| Method | Angular Frequency rad/sec | Amplitude Volts |
|----------------------|------------------------------|--------------------|
| Mitrovic's | 0.6315 | 4.53 |
| Root Locus | 0.6314 | 4.533 |
| Describing Functions | 0.635 | 5.8 |
| Analog Simulation | 0.628 | 5.7 |

III-B Loop Transfer Function with One Zero.

The system to analyze is shown in the block diagram of Figure III-B.

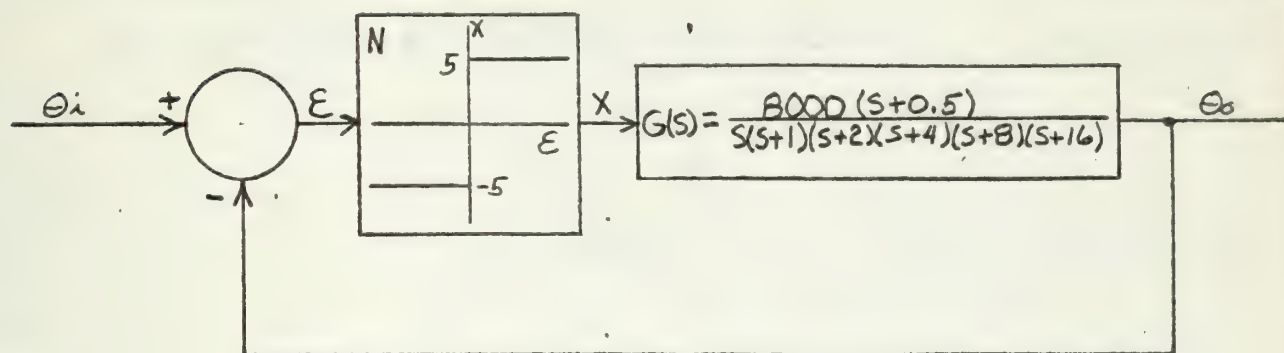


Figure III-B

Ideal Relay in Error Channel Loop

Transfer Function with One Zero

III-B-1. Mitrovic's Method.

Assigning N as the instantaneous gain of the relay, the characteristic Equation can be written as

$$s^6 + 31s^5 + 310s^4 + 1240s^3 + 1984s^2 + (1024 + 8000N)s + 4000N = 0. \quad (\text{III-B-1.1})$$

Assuming the last two coefficients are variable, the characteristic equation becomes,

$$s^6 + 31s^5 + 310s^4 + 1240s^3 + 1984s^2 + B_1s + B_0 = 0 \quad (\text{III-B-1.2})$$

where

$$B_0 = 4000N \quad (\text{III-B-1.3})$$

and

$$B_1 = 1024 + 8000N \quad (\text{III-B-1.4})$$

From Appendix A, Mitrovic's equations for B_0 and B_1 are.

$$B_0 = -[1984\omega_n^2\phi_1(\zeta) + 1240\omega_n^3\phi_2(\zeta) + 310\omega_n^4\phi_3(\zeta) + 31\omega_n^5\phi_4(\zeta) + \omega_n^6\phi_5(\zeta)] \quad (\text{III-B-1.5})$$

and

$$B_1 = 1984\omega_n\phi_2(\zeta) + 1240\omega_n^2\phi_3(\zeta) + 310\omega_n^3\phi_4(\zeta) + 31\omega_n^4\phi_5(\zeta) + \omega_n^5\phi_6(\zeta). \quad (\text{III-B-1.6})$$

Substituting the values of the functions from Appendix A for $\zeta = 0$ gives the parametric equations of the stability curve as,

$$B_0 = 1984\omega_n^2 - 310\omega_n^4 + \omega_n^6 \quad (\text{III-B-1.7})$$

and

$$B_1 = 1240\omega_n^2 - 31\omega_n^4 \quad (\text{III-B-1.8})$$

To find the intersection between the M-point locus (Equations III-B-1.1)

and III-B-1.4) and the stability curve, the graphical approach is chosen. Table III-B-1.1 gives the values of B_0 and B_1 for the stability curve as plotted in Figure III-B-1.1.

TABLE III-B-1.1

| ω_n | B_0 | B_1 |
|------------|-------|-------|
| 0.5 | 227 | 308 |
| 0.8 | 1143 | 780 |
| 1.0 | 1675 | 1239 |
| 1.2 | 2219 | 1722 |
| 1.4 | 2708 | 2311 |
| 1.6 | 3067 | 2962 |
| 1.8 | 3200 | 3695 |
| 2.0 | 3040 | 4464 |
| 2.2 | 2454 | 5275 |
| 2.3 | 1968 | 5892 |
| 2.5 | 544 | 6540 |

To obtain the M-point locus solve Equation III-B-1.4 for N and substitute into Equation III-B-1.3.

$$B_0 = 0.5 B_1 - 512 \quad (\text{III-B-1.9})$$

Equation III-B-1.9 is seen to be a straight line with a slope of 0.5 and

a B_1 intercept of 1024.

It is seen from Figure III-B-1.1 that the intersection occurs at roughly $\omega_n = 2.24$. To more accurately determine the intersection, values of B_0 and B_1 are calculated for ω_n close to 2.24. The value of B_1 is then substituted into Equation III-B-1.9 and the intersection occurs when the two B's are equal. These additional values are given in Table III-B-1.2.

TABLE III-B-1.2

| ω_n | B_0 (Stability curve) | B_1 | B_0 (M-point Locus) |
|------------|-------------------------|--------|-----------------------|
| 2.24 | 2266 | 5439 | 2208 |
| 2.249 | 2233.5 | 5478.8 | 2227.4 |
| 2.25 | 2228.7 | 5483.0 | 2229.5 |

Thus from Table III-B-1.2, the frequency of the limit cycle is

$$\omega_n = 2.25 \text{ rad/sec}$$

Substituting B_0 at $\omega_n = 2.25$ into Equation III-B-1.2, the "average" gain over a cycle is determined as

$$N_{ave} = \frac{2229}{4000} = 0.5573 ,$$

from which the approximate amplitude is determined as

$$\varepsilon_{max} = \frac{5}{0.5573} = 8.973 \text{ volts.}$$

Mitrovic's method predicts a stable limit cycle by the same arguments applied to Figure III-B-1.1 as were given in Chapter I, Section I-A-1.

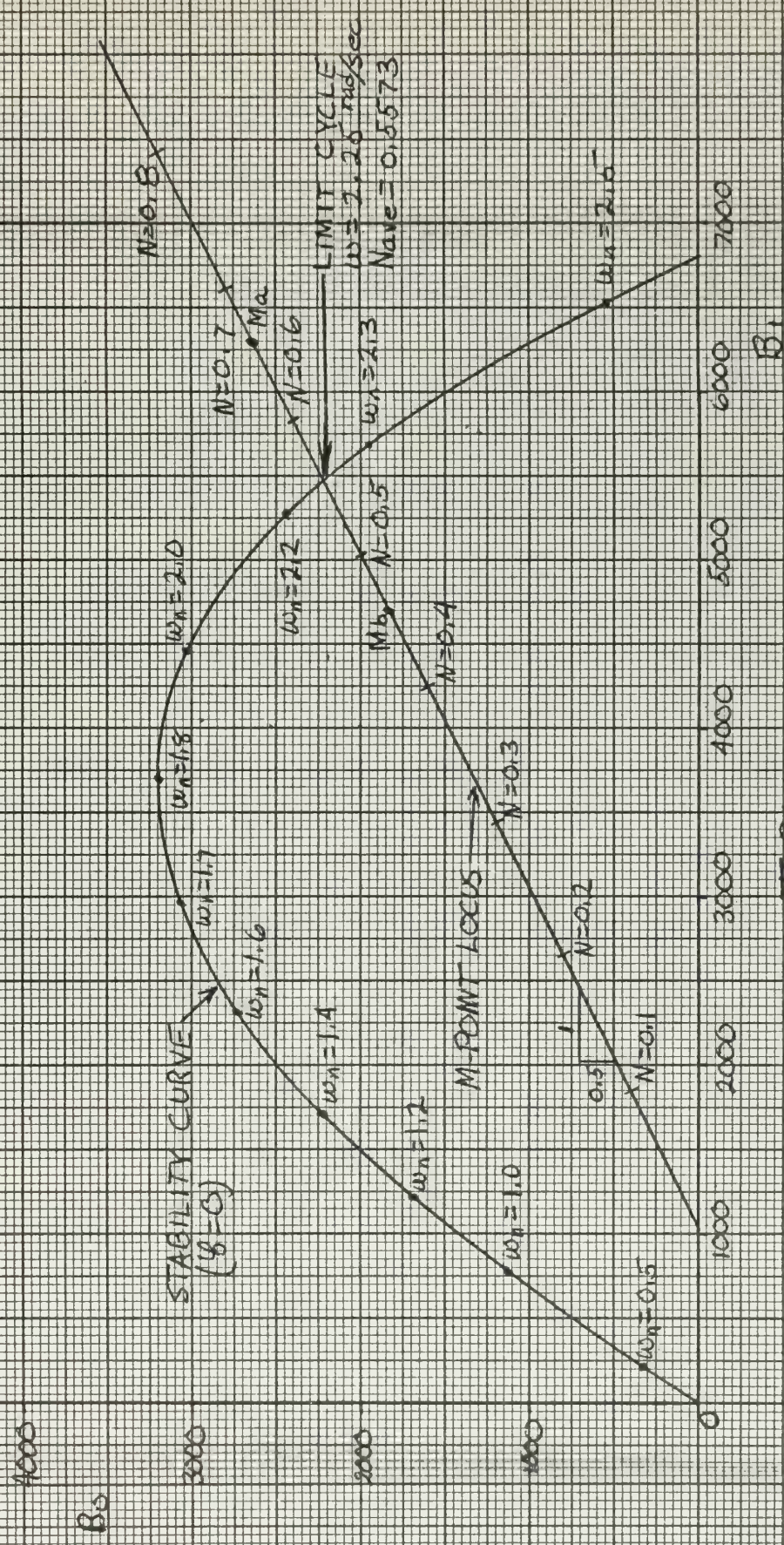


FIGURE III B1.1
GRAPHICAL SOLUTION OF IDEAL RELAY INNER ERROR CHANNEL
LOOP TRANSFER FUNCTION WITH ONE ZERO

III-B-2 Root Locus Method.

Substituting $s = j\omega$ into the characteristic Equation III-B-1.1 and evaluating the higher powers of j yields,

$$-\omega^6 + j31\omega^5 + 310\omega^4 - j1240\omega^3 - 1984\omega^2 + j(1024 + 8000N)\omega + 4000N = 0. \quad \text{III-B-2.1}$$

Requiring that the real and imaginary parts of Equation III-B-2.1 go to zero independently, gives

$$-\omega^6 + 310\omega^4 - 1984\omega^2 + 4000N = 0 \quad \text{III-B-2.2}$$

and

$$j31\omega^5 - j1240\omega^3 + j(1024 + 8000N)\omega = 0. \quad \text{III-B-2.3}$$

Dividing Equation III-B-2.3 by $j\omega$ and solving this for $4000N$ gives,

$$4000N = 620\omega^2 - 512 - 15.5\omega^4. \quad \text{III-B-2.4}$$

Combining Equations III-B-2.3 and III-B-2.4 gives

$$\omega^6 - 299.5\omega^4 + 136\omega^2 + 512 = 0. \quad \text{III-B-2.5}$$

To solve for ω^2 from Equation III-B-2.5, a digital computer program was used and gave the roots,

$$\omega^2 = 5.062$$

$$\omega^2 = -0.55$$

$$\omega^2 = -299.53$$

Only the first value is of use and gives

$$\omega = 2.50 \text{ rad/sec.}$$

Substituting ω^2 into equation III-B-2.4 gives the average gain of the relay over a cycle as

$$N_{ave} = 0.5574$$

from which the approximate amplitude of the limit cycle is determined to be

$$\epsilon_{\max} = 8.972 \text{ volts}$$

A graphical presentation of the solution is sketched in Figure III-B-2.1. The root locus method predicts a stable limit cycle by, applying to Figure III-B-2.1 the same arguments given in Chapter I, Section II-A-2.

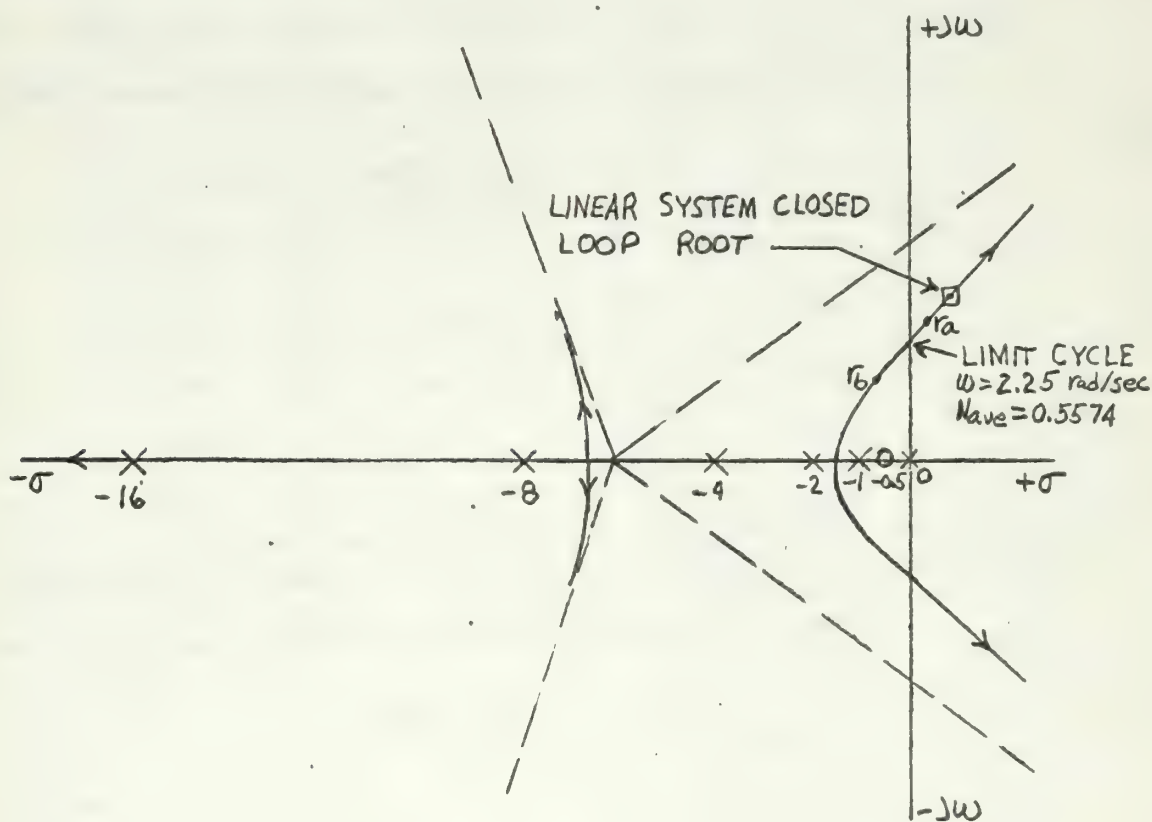


Figure III-B-2.1

Root Locus Solution for Ideal Relay in Error Channel,
Loop Transfer Function with One Zero.

III-B-3 Describing Function Method.

The describing function for the ideal relay is given in Equation III-A-3.1. The linear loop transfer function for the given system in frequency response form is

$$G(j\omega) = \frac{3.91(2j\omega + 1)}{j\omega(j\omega + 1)(0.5j\omega + 1)(0.25j\omega + 1)(0.125j\omega + 1)(0.0625j\omega + 1)} \quad \text{(III-B-3.1)}$$

Table III-B-3.1 gives the magnitude and phase of Equation III-B-3.1 for the different frequencies which were used to plot the linear loop transfer function on the gain-phase curve of Figure III-B-3.1. These values are obtained from a Bode diagram plot of Equation III-B-3.1.

TABLE III-B-3.1

| ω | $ G(j\omega) $ db | $\angle G(j\omega)$ deg |
|----------|-------------------|-------------------------|
| 1.97 | 7 | -168 |
| 2.1 | 6 | -174.5 |
| 2.24 | 5 | -180 |
| 2.38 | 4 | -185 |
| 2.52 | 3 | -190 |

Table III-B-3.2 gives the values of $1/G_D$ in the area of interest as obtained from Equation III-A-3.1 for various values of error.

TABLE III-B-3.2

| E_{\max} | G_D | $1/G_D$ | $1/G_D$ db |
|------------|-------|---------|------------|
| 8 | 0.796 | 1.257 | 1.99 |
| 10 | 0.634 | 1.571 | 3.93 |
| 11 | 0.579 | 1.729 | 4.75 |
| 11.3 | 0.563 | 1.775 | 4.98 |
| 12 | 0.531 | 1.885 | 5.51 |

By interpolation of Figure III-B-3.1, the intersection and thus the limit cycle occurs at

$$\omega = 2.24 \text{ rad/sec.}$$

and

$$E_{\max} = 11.31 \text{ volts ,}$$

The describing function method predicts a stable limit cycle by applying to Figure III-B-3.1 the same arguments given in Chapter I, Section I-A-3.

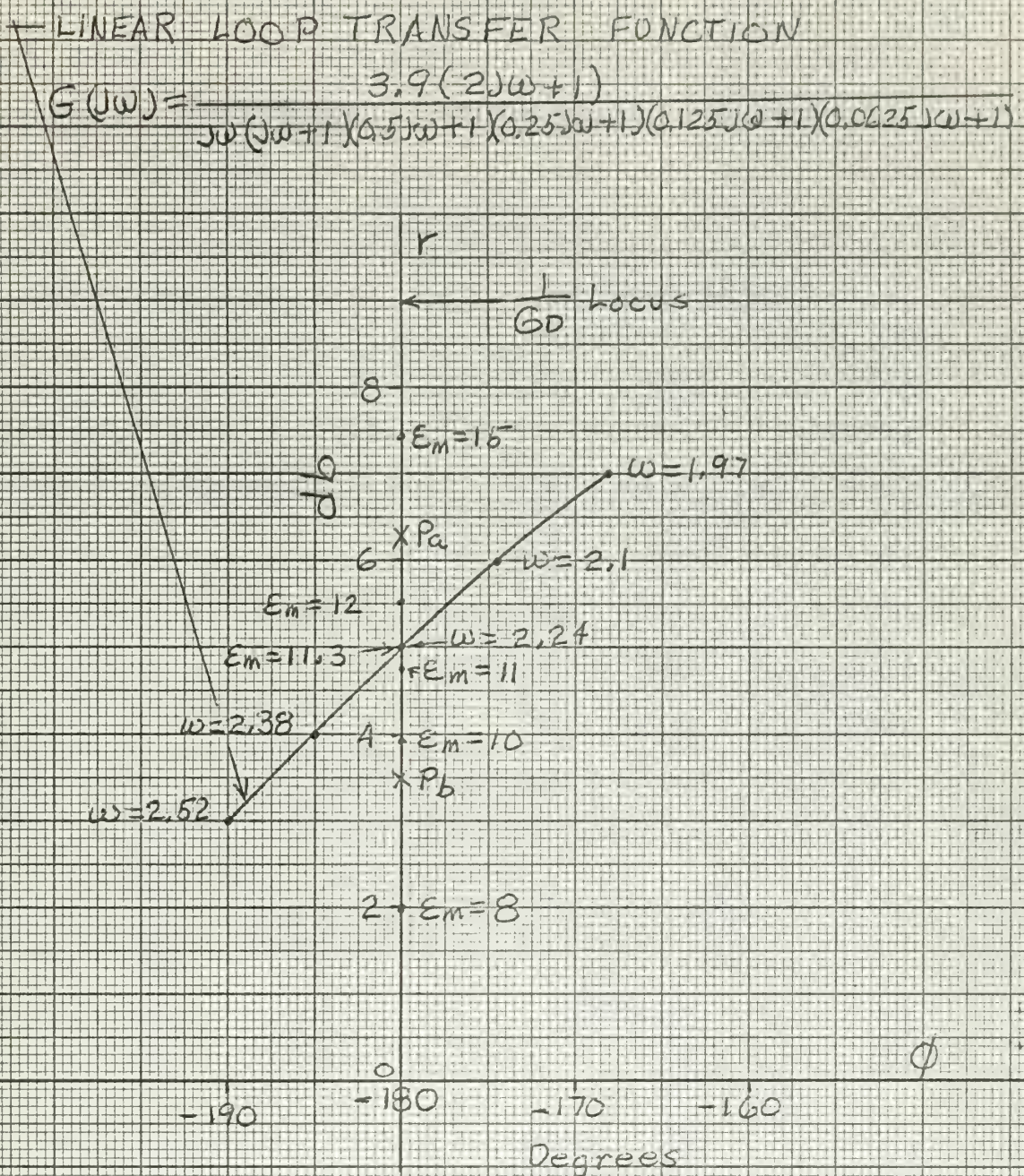


FIGURE B 3.1
GAIN-PHASE PLANE—IDEAL RELAY IN
ERROR CHANNEL, LOOP TRANSFER
FUNCTION WITH ONE ZERO

III-B-4 Analog Computer Simulation.

The analog simulation of the given nonlinear system is shown in Figure III-B-4.1. The coefficient pot settings with associated resistances and capacitances for real time and real magnitude scaling are given in Table III-B-4.1.

TABLE III-B-4.1.

| Pot Setting | Associated Elements |
|---------------------------------|--|
| $a_1 = \frac{E_i}{100}$ | For a Step Input of E_i Volts $R_1 = 1 \text{ Meg}, R_{f1} = 1 \text{ Meg}$ |
| $a_2 = 1.0$ | $R_2 = 1 \text{ Meg}, R_{f1} = 1 \text{ Meg}$ |
| $a_3 = (\text{See discussion})$ | $R_3 = 0.1 \text{ Meg}, R_{f2} = 1 \text{ Meg}$ |
| $a_4 = 0.5$ | $R_4 = 1 \text{ Meg}, C_{f1} = 1 \text{ uf}$ |
| $a_5 = 1.0$ | $R_5 = 1 \text{ Meg}, C_{f1} = 1 \text{ uf}$ |
| $a_6 = 1.0$ | $R_6 = 1 \text{ Meg}, R_{f3} = 1 \text{ Meg}$ |
| $a_7 = 1.0$ | $R_7 = 1 \text{ Meg}, R_{f3} = 1 \text{ Meg}$ |
| $a_8 = 1.0$ | $R_8 = 0.1 \text{ Meg}, C_{f2} = 1 \text{ uf}$ |
| $a_9 = 1.0$ | $R_9 = 0.5 \text{ Meg}, C_{f2} = 1 \text{ uf}$ |
| $a_{10} = 1.0$ | $R_{10} = 0.1 \text{ Meg}, C_{f3} = 1 \text{ uf}$ |
| $a_{11} = 0.4$ | $R_{11} = 0.1 \text{ Meg}, C_{f3} = 1 \text{ uf}$ |
| $a_{12} = 1.0$ | $R_{12} = 0.1 \text{ Meg}, C_{f4} = 1 \text{ uf}$ |
| $a_{13} = 0.8$ | $R_{13} = 0.1 \text{ Meg}, C_{f4} = 1 \text{ uf}$ |
| $a_{14} = 0.8$ | $R_{14} = 1 \text{ Meg}, C_{f5} = 0.1 \text{ uf}$ |
| $a_{15} = 0.8$ | $R_{15} = 0.5 \text{ Meg}, C_{f5} = 0.1 \text{ uf}$ |
| $a_{16} = 1.0$ | $R_{16} = 1 \text{ Meg}, C_{f6} = 1 \text{ uf}$ |
| $a_{17} = 1.0$ | $R_{17} = 1 \text{ Meg}, R_{f4} = 1 \text{ Meg}$ |
| $a = 0.05$ (Initial Setting) | For 5 Volt relay voltage |

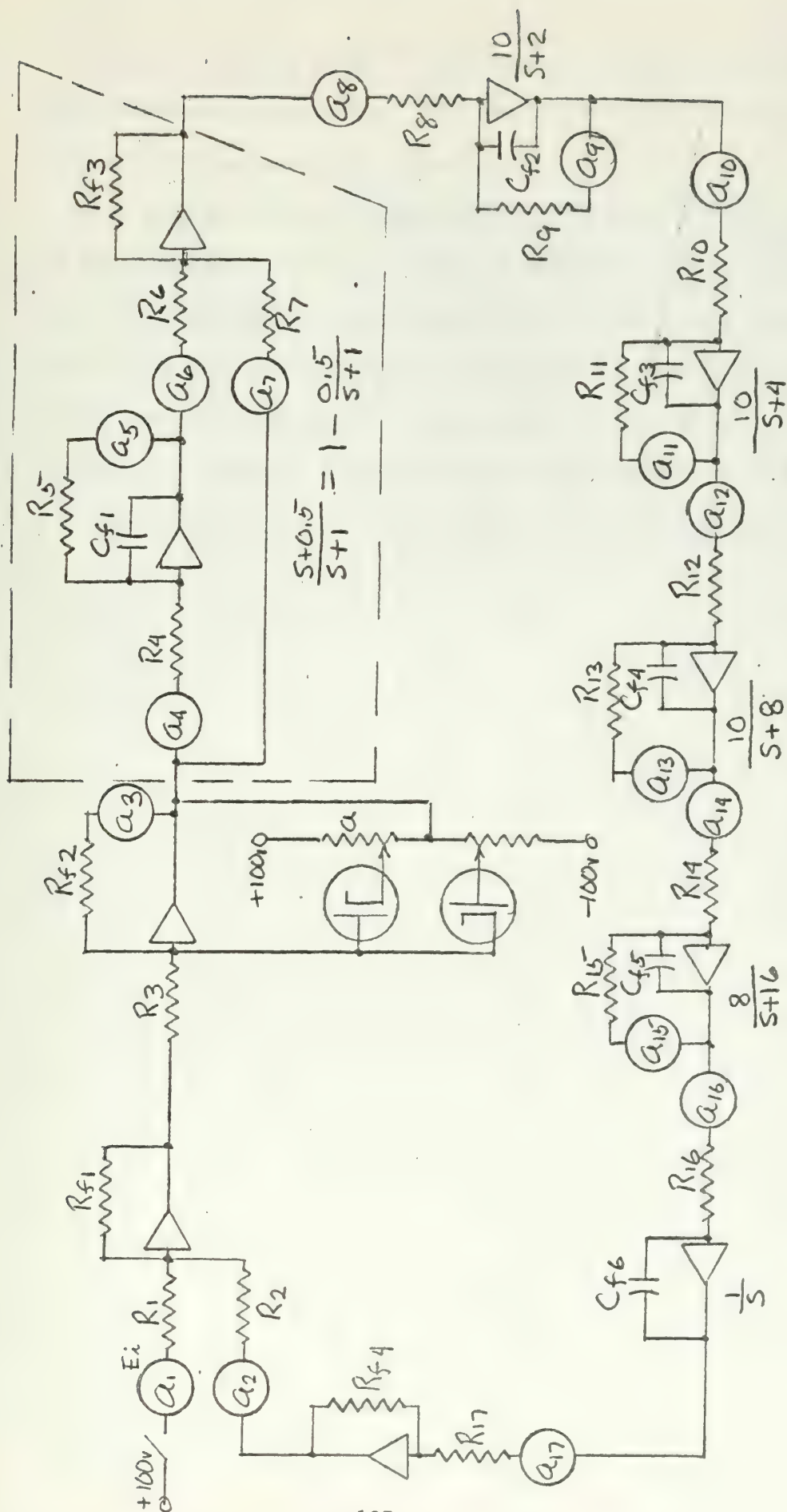


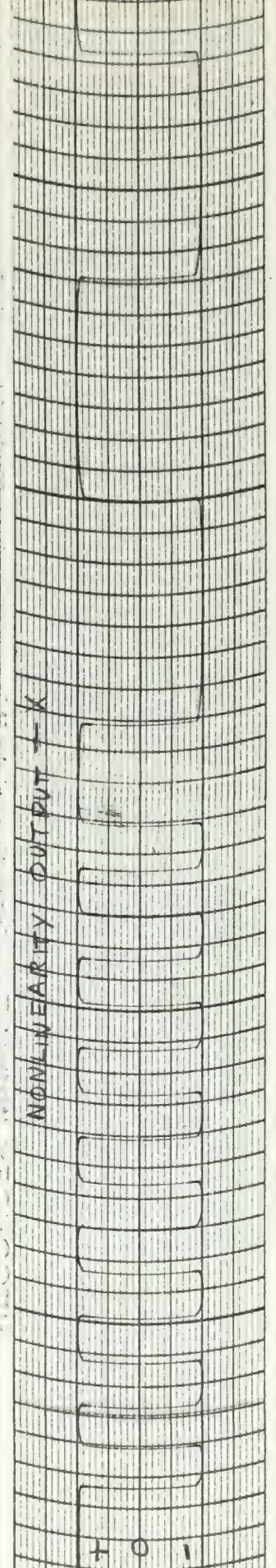
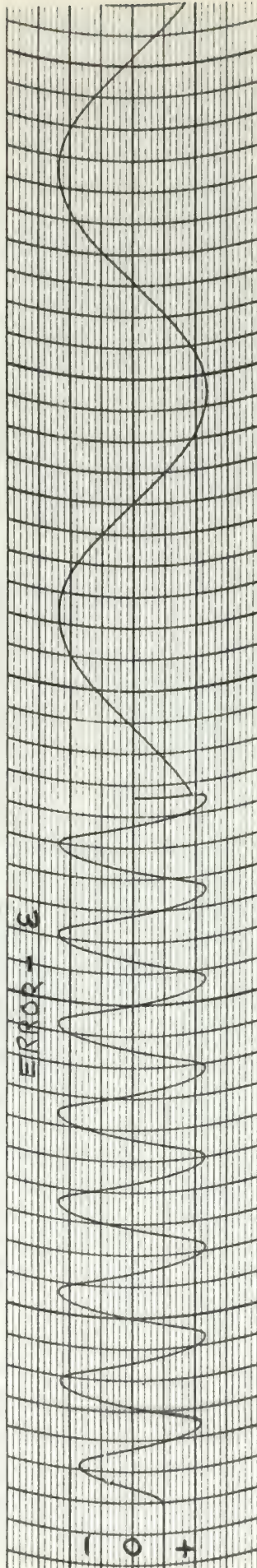
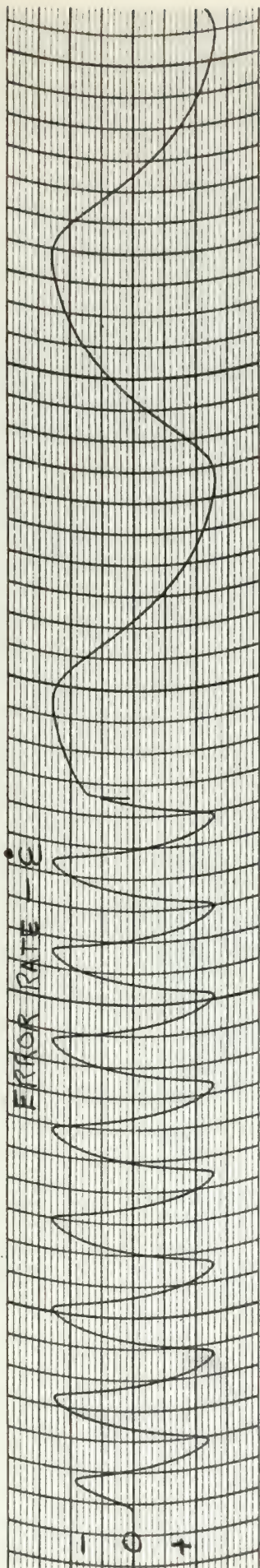
Figure III-B-4.1

Analog Computer Simulation of Ideal Relay in Error Channel 1. Loop Transfer Function with One Zero.

The back-biasing pots "a" and pot a_3 were set in the same way described in Section III-A-4. The static characteristic curve is also the same as shown in Figure III-A-4.1.

The system was first excited with a 5 volt step input signal and was found to build up to the limit cycle shown in recorder trace III-B-4.1. The system was then excited with a 20 volt step signal and found to go into the same limit cycle as shown in recorder trace III-B-4.2. From these two recorder traces the limit cycle is seen to be stable with angular frequency of 2.22 rad/sec and an amplitude of 11.7 Volts.

The phase portrait of the system is shown in Figure III-B-4.2.

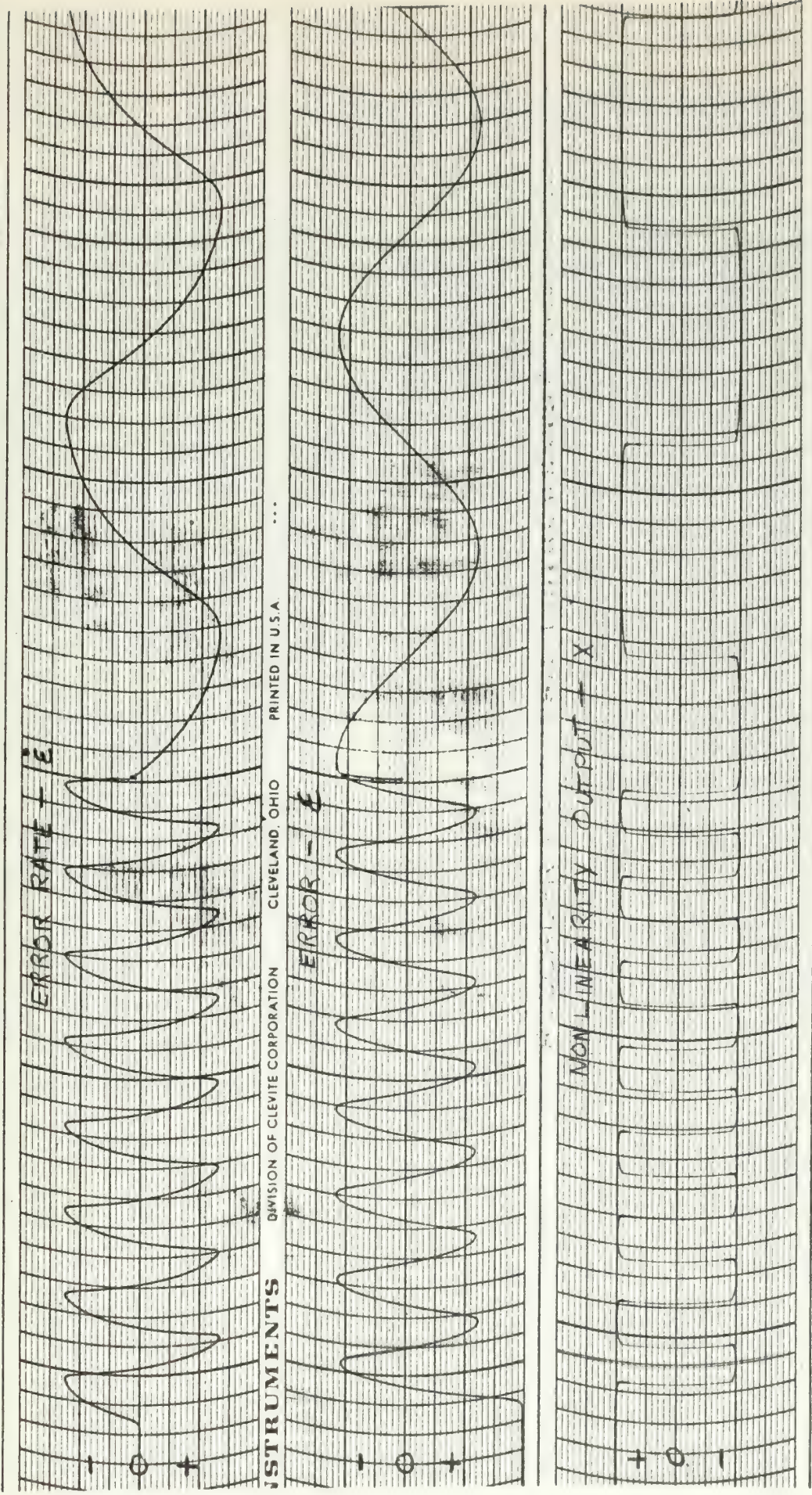


Recorder Trace III-B-4.1

Ideal Relay in Error Channel, Loop Transfer Function with One Zero, 5 Volt Step Input.

SAMPLE

| | | |
|------------------|--------------------|--|
| E - 2 Volts/Line | X = 0.8 Volts/Line | Time . 1 Second/Division 0.2 Seconds/Division |
|------------------|--------------------|--|



INSTRUMENTS DIVISION OF CLEVITE CORPORATION CLEVELAND, OHIO PRINTED IN U.S.A.

Recorder Trace III-B-4, 2

Ideal Relay in Error Channel, Loop Transfer Function with One Zero, 20 Volt Step Input.

SCALES $\dot{\epsilon}$ - 2 Volts/Line ϵ - 1 Volt/Line X - 0.5 Volts/Line Time - 1 Second/Division 0.2 Second/Division

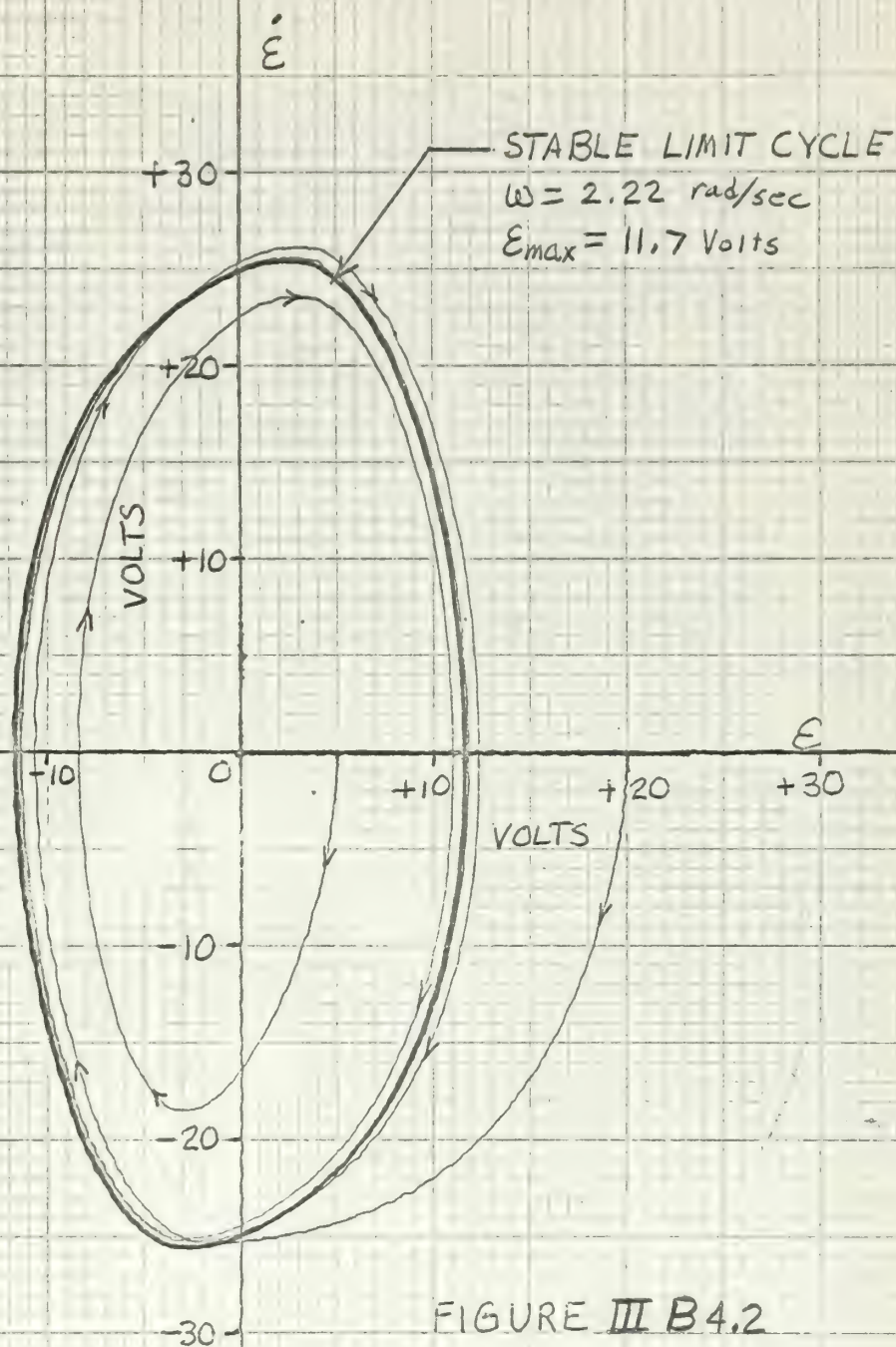


FIGURE III B4.2

IDEAL RELAY IN ERROR CHANNEL, LOOP TRANSFER FUNCTION WITH ONE ZERO

$$G(s) = \frac{8000(s+0.5)}{s(s+1)(s+2)(s+4)(s+8)(s+16)}$$

III-B-5. Comparison of the Four Methods in Predicting Limit Cycles for the System Shown in Figure III-B.

| Method | Angular Frequency rad/sec | Amplitude Volts |
|---------------------|------------------------------|--------------------|
| Mitrovic's | 2.25 | 8.973 |
| Root Locus | 2.250 | 8.972 |
| Describing Function | 2.24 | 11.31 |
| Analog Simulation | 2.22 | 11.7 |

CHAPTER IV

RELAY WITH DEAD ZONE IN ERROR CHANNEL

IV-A. Loop Transfer Function with No Zeros.

The block diagram of system chosen is shown in Figure IV-A.

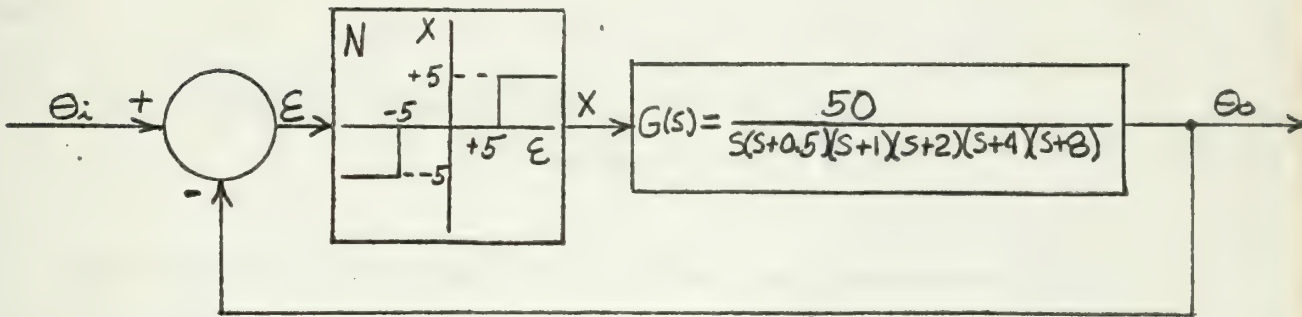


Figure IV-A,

Relay with Dead Zone in Error Channel Loop

Transfer Function with No Zeros

IV-A-1 Mitrovic's Method

The characteristic equation of the given system is,

$$s^6 + 15.5s^5 + 77.5s^4 + 155s^3 + 124s^2 + 32s + 50N = 0.$$

(IV-A-1.1)

Assuming the last two coefficients variable, the characteristic equation becomes

$$s^6 + 15.5s^5 + 77.5s^4 + 155s^3 + 124s^2 + B_1s + B_0 = 0$$

(IV-A-1.2)

where

$$B_0 = 50 \text{ N} \quad (\text{IV-A-1.3})$$

and

$$B_1 = 32 \quad (\text{IV-A-1.4})$$

From Appendix A, Mitrovic's equations for B_0 and B_1 are,

$$B_0 = -[24\omega_n^2\phi_1(\zeta) + 155\omega_n^3\phi_2(\zeta) + 77.5\omega_n^4\phi_3(\zeta) + 15.5\omega_n^5\phi_4(\zeta) + \omega_n^6\phi_5(\zeta)] \quad (\text{IV-A-1.5})$$

and

$$B_1 = 124\omega_n\phi_2(\zeta) + 155\omega_n^2\phi_3(\zeta) + 77.5\omega_n^3\phi_4(\zeta) + 15.5\omega_n^4\phi_5(\zeta) + \omega_n^5\phi_6(\zeta). \quad (\text{IV-A-1.6})$$

Substitution of the values of the ϕ functions from Appendix A for

$\zeta = 0$ gives the parametric equations of the stability curve as,

$$B_0 = 124\omega_n^2 - 77.5\omega_n^4 + \omega_n^6 \quad (\text{IV-A-1.7})$$

and

$$B_1 = 155\omega_n^2 - 15.5\omega_n^4. \quad (\text{IV-A-1.8})$$

Table IV-A-1.1 gives the points of stability curve plotted in Figure IV-A-1.1. These points are calculated from Equation IV-A-1.7 and IV-A-1.8 for various ω_n .

From Equations IV-A-1.3 and IV-A-1.4, the M-point locus is seen to be a straight line parallel to the B_0 axis with a maximum of $B_0 = 50$. From Figure IV-A-1.1, the intersection of the M-point locus with the stability curve is seen to occur at roughly $\omega_n = 0.46$ rad/sec. To more accurately determine the intersection more points in the area of the intersection are calculated in Table IV-A-1.2.

TABLE IV-A-1.1

| ω_n | B_1 | B_0 |
|------------|-------|-------|
| 0.2 | 6.18 | 4.76 |
| 0.4 | 24.0 | 17.9 |
| 0.5 | 37.8 | 26.3 |
| 0.6 | 53.8 | 34.6 |
| 0.7 | 72.2 | 42.4 |
| 0.8 | 92.9 | 48.1 |
| 0.9 | 115.4 | 50.1 |
| 1.0 | 139.5 | 47.5 |
| 1.1 | 164.8 | 38.3 |
| 1.2 | 190.9 | 25.5 |

TABLE IV-A-1.2

| ω_n | B_0 | B_1 |
|------------|-------|-------|
| 0.45 | 21.94 | 30.75 |
| 0.46 | 22.78 | 31.59 |
| 0.461 | 22.86 | 32.24 |
| 0.47 | 23.62 | 33.48 |

By interpolation of Table IV-A-1.2 using Equation IV-A-1.4, the intersection and thus the limit cycle occurs at

$$\omega_n = 0.4607 \text{ rad/sec}$$

and

$$B_0 = 22.84 \bullet$$

From Equation IV-A-1.3, the "average" nonlinear gain over a cycle is determined as,

$$N_{a,e} = 0.457$$

from which the approximate amplitude of the limit cycle is determined to be

$$\mathcal{E}_{\max} = 10.95 \text{ Volts ,}$$

Mitrovic's method predicts a stable limit cycle by the following reasoning. The input signal must be larger than the dead zone for the system to respond at all. Once the input signal becomes larger than the dead zone, the characteristic of the relay is for practical purposes similar to saturation. Thus the same arguments given in Chapter I, Section I-A-1 can be applied to Figure IV-A-1.1.

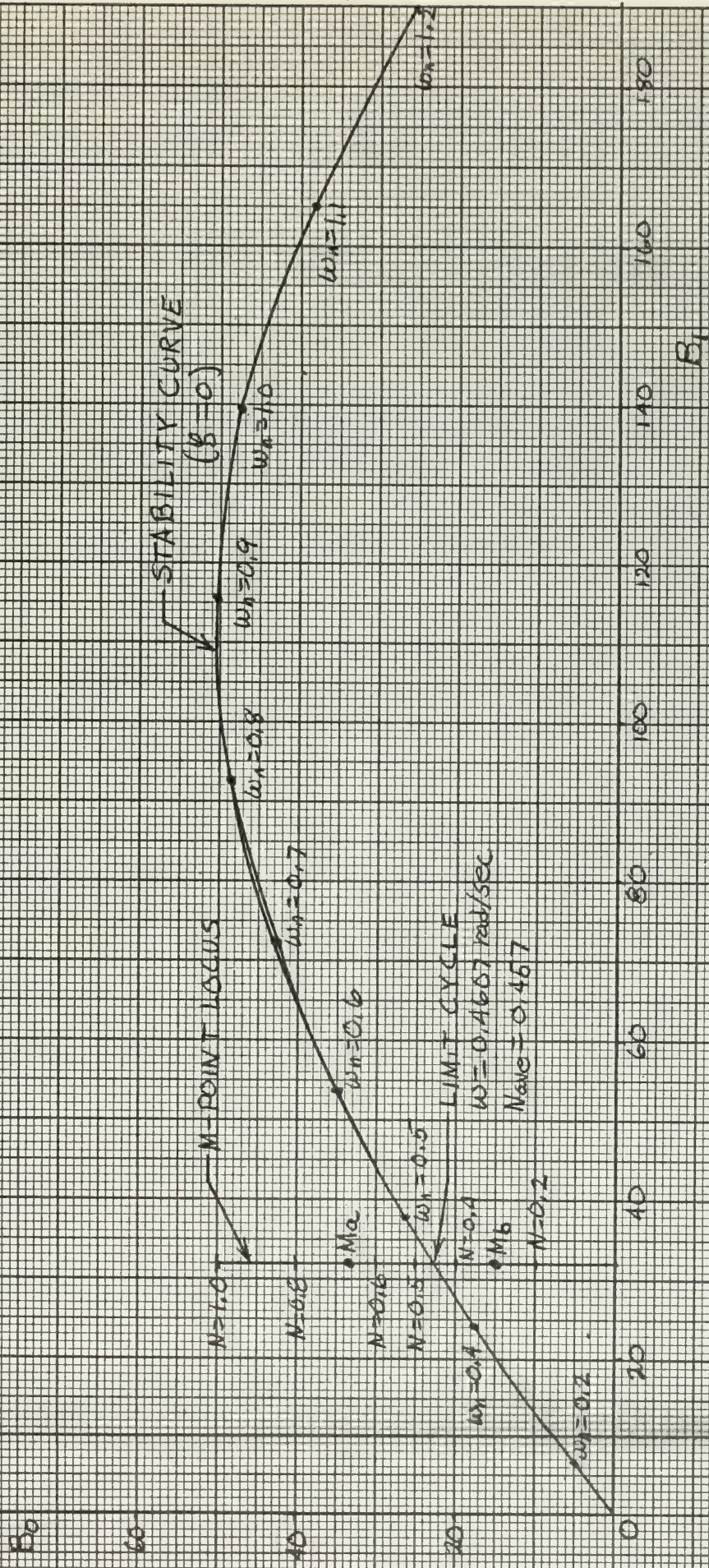


FIGURE IX A 1.1
 GRAPHICAL SOLUTION FOR RELAY WITH DEAD ZONE IN ERROR CHANNEL
 LOOP TRANSFER FUNCTION WITH NO ZEROS

IV-A-1.2 Root Locus Method.

Substituting $S = j\omega$ in the characteristic Equation IV-A-1.1 and evaluating the higher powers of j gives,

$$-\omega^6 + j15.5\omega^5 + 77.5\omega^4 - j155\omega^3 - 124\omega^2 + j32\omega + 50N = 0. \quad (\text{IV-A-2.1})$$

Requiring that the real and imaginary parts of Equation IV-A-2.1 go to zero independently, yields the following two equations,

$$-\omega^6 + 77.5\omega^4 - 124\omega^2 + 50N = 0 \quad (\text{IV-A-2.2})$$

and

$$j15.5\omega^5 - j155\omega^3 + j32\omega = 0, \quad (\text{IV-A-2.3})$$

Dividing Equation IV-A-2.3 by $j\omega$ and using the quadratic formula to solve for ω^2 yields,

$$\omega^2 = 0.210899$$

as the only meaningful root. Thus the frequency of the limit cycle is

$$\omega = 0.4592 \text{ rad/sec.}$$

Substituting ω^2 back into Equation IV-A-2.2 and solving for N as the "average" gain of the nonlinearity, gives

$$N_{\text{ave}} = 0.4543$$

from which the approximate amplitude is found to be

$$E_m = 11.01 \text{ volts.}$$

A graphical presentation of the root locus solution is shown in Figure IV-A-2.1.

The root locus method predicts a stable limit cycle by the following

arguments. For an input signal larger than the dead zone, the relay characteristic is similar to saturation and the arguments given in Chapter I, Section I-A-2 can be applied to Figure IV-A-2.1.

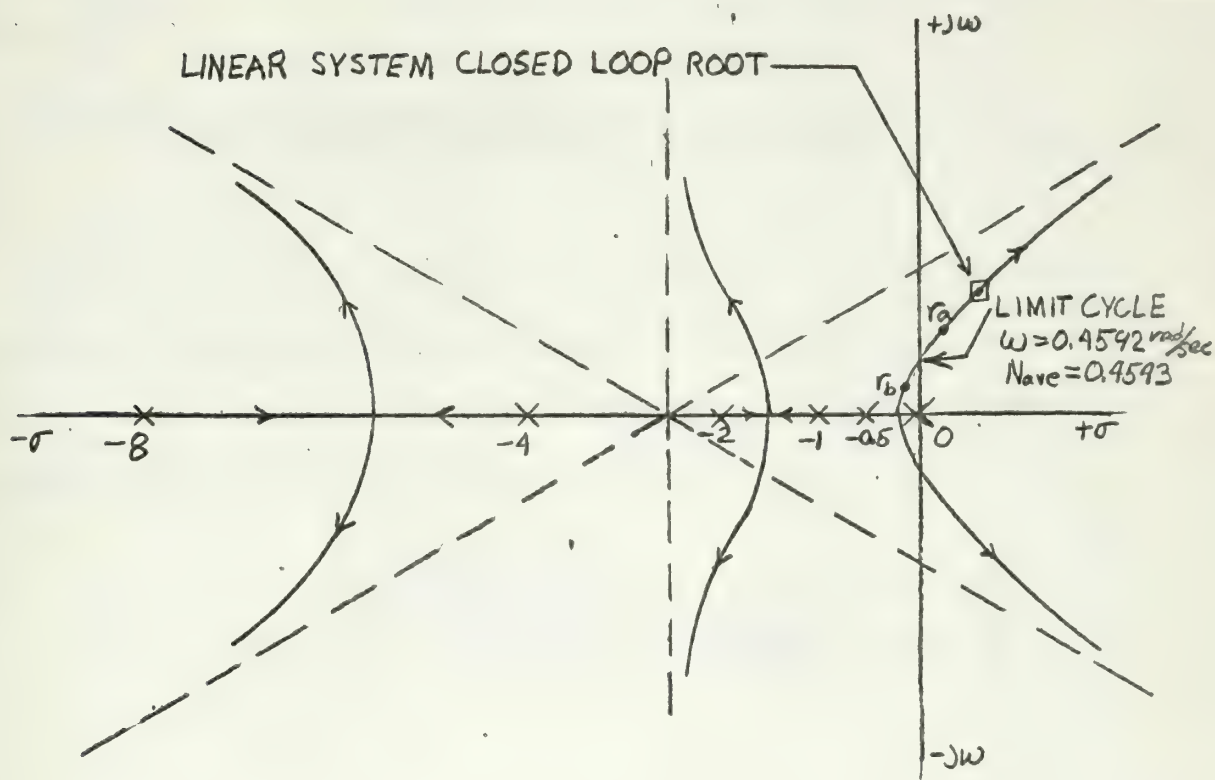


Figure IV-A-2.1.

Root Locus Solution for Relay with Dead Zone
in Error Channel, Loop Transfer Function with
No Zeros

IV-A-3. Describing Function Method.

The describing function for a relay with dead zone is

$$G_D = \frac{4V}{\pi E_{max}} \sqrt{1 - \left(\frac{d}{2E_{max}}\right)^2} \angle 0^\circ \quad (IV-A-3.1)$$

where V is the signal controlled by the relay

E_{max} is the relay input signal

d is the total dead zone minus to plus.

The linear loop transfer function for the given system in frequency response is

$$G(j\omega) = \frac{1.562}{j\omega(2j\omega+1)(j\omega+1)(0.5j\omega+1)(0.25j\omega+1)(0.125j\omega+1)} \quad (IV-A-3.2)$$

Table IV-A-3.1 gives the magnitude and phase of Equation IV-A-3.2 for the various frequencies that are used to plot the linear loop transfer function on the gain-phase plane of Figure IV-A-3.1. These values are obtained from a Bode diagram plot of Equation IV-A-3.2.

TABLE IV-A-3.1

| ω | $ G(j\omega) $ db | $\angle G(j\omega)$ deg |
|----------|-------------------|-------------------------|
| 0.4 | 9 | -172 |
| 0.43 | 8 | -177.5 |
| 0.455 | 7.5 | -180 |
| 0.463 | 7 | -182 |
| 0.49 | 6 | -186.5 |

Table IV-A-3.2 gives the values of $1/G_D$ which are plotted in Figure IV-A-3.1. These values are obtained from Equation IV-A-3.1.

TABLE IV-A-3.1

| E_{max} | G_D | $1/\omega$ | $1/\omega_{crit}$ |
|-----------|--------|------------|-------------------|
| 10 | 0.5513 | 1.524 | 1.17 |
| 12 | 0.4823 | 2.074 | 1.35 |
| 14 | 0.4247 | 2.324 | 1.44 |
| 15 | 0.4026 | 2.484 | 1.47 |

Inspection of Figure IV-A-3.1 shows the limit cycle will occur at,

$$\omega = 0.45 \text{ rad/sec}$$

and

$$E_{max} = 14.1 \text{ volts}.$$

The describing function method predicts a stable limit cycle at the following arguments. For an input signal greater than the dead zone, the relay characteristic is similar to saturation and the arguments given in Chapter I, Section I-A-3 can be applied to Figure IV-A-3.1.

LINEAR LOOP TRANSFER FUNCTION

$$G(j\omega) = \frac{50}{j\omega(2j\omega+1)(j\omega+1)(0.5j\omega+1)(0.25j\omega+1)(0.125j\omega+1)}$$

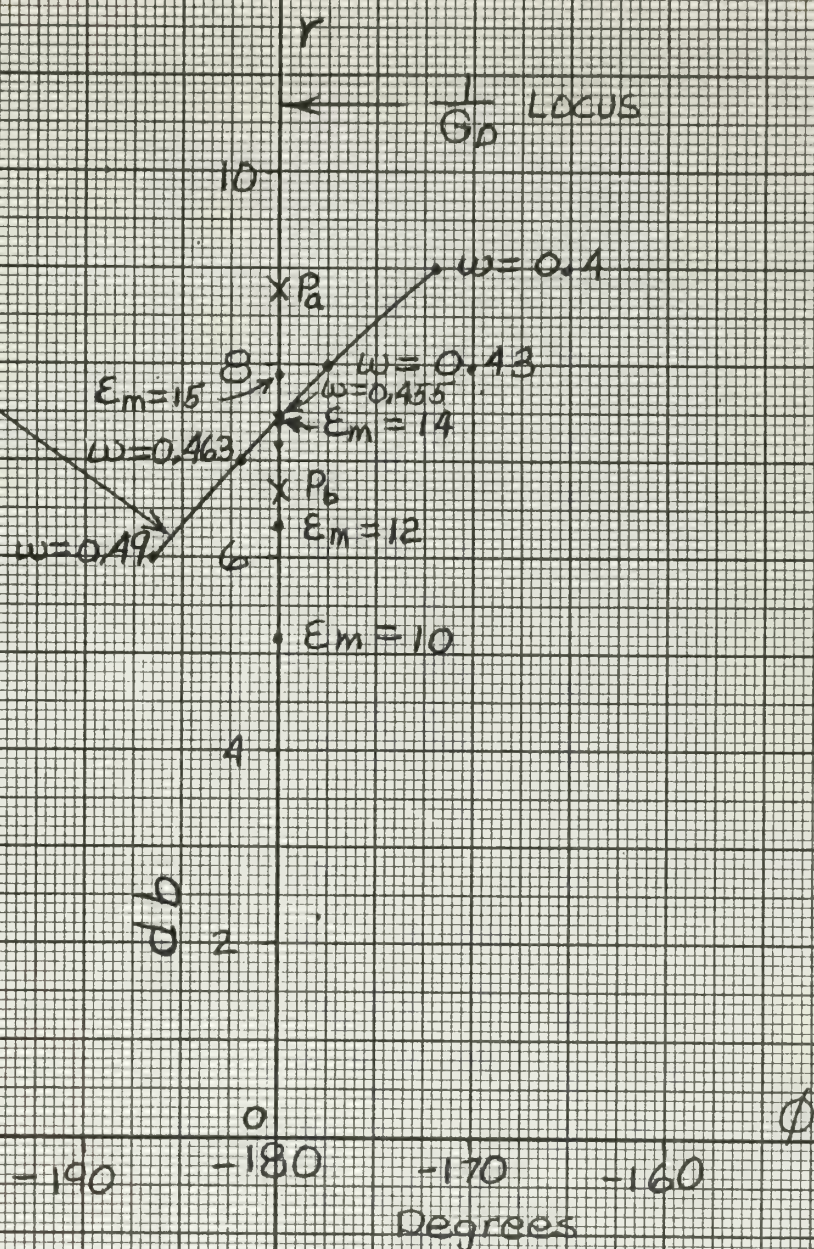


FIGURE A3.1
GAIN-PHASE PLANE - RELAY WITH DEAD ZONE
IN ERROR CHANNEL, LOOP TRANSFER
FUNCTION WITH NO ZEROS

IV-A-4 Analog Computer Simulation

The analog computer simulation of the given nonlinear system is shown in Figure IV-A-4.1. The coefficient pot settings with associated resistances and capacitances for real time and real magnitude scaling are given in Table IV-A-4.1.

TABLE IV-A-4.1

| Pot Settings | Associated Elements |
|-----------------------------------|---|
| $a_1 = \frac{E_1}{100}$ | For an input step of E_1 volts $R_1 = 1 \text{ Meg}, R_{11} = 1 \text{ Meg}$ |
| $a_2 = 1.0$ | $R_2 = 1 \text{ Meg}, R_{11} = 1 \text{ Meg}$ |
| $a_3 = 1.0$ | $R_3 = 0.1 \text{ Meg}, R_{12} = 1 \text{ Meg}$ |
| $a_4 = 1.0$ | $R_4 = 0.1 \text{ Meg}, R_{23} = 1 \text{ Meg}$ |
| $a_5 = 1.0$ | $R_5 = 1 \text{ Meg}, C_{11} = 1 \text{ sec}$ |
| $a_6 = 0.5$ | $R_6 = 1 \text{ Meg}, C_{11} = 1 \text{ sec}$ |
| $a_7 = 1.0$ | $R_7 = 1 \text{ Meg}, C_{12} = 1 \text{ sec}$ |
| $a_8 = 1.0$ | $R_8 = 1 \text{ Meg}, C_{11} = 1 \text{ sec}$ |
| $a_9 = 1.0$ | $R_9 = 1 \text{ Meg}, C_{13} = 1 \text{ sec}$ |
| $a_{10} = 1.0$ | $R_{10} = 0.5 \text{ meg}, C_{13} = 1 \text{ sec}$ |
| $a_{11} = 0.5$ | $R_{11} = 0.1 \text{ meg}, C_{11} = 1 \text{ sec}$ |
| $a_{12} = 0.4$ | $R_{12} = 0.1 \text{ Meg}, C_{11} = 1 \text{ sec}$ |
| $a_{13} = 1.0$ | $R_{13} = 0.1 \text{ Meg}, C_{13} = 1 \text{ sec}$ |
| $a_{14} = 0.8$ | $R_{14} = 0.1 \text{ Meg}, C_{13} = 1 \text{ sec}$ |
| $a_{15} = 1.0$ | $R_{15} = 1 \text{ Meg}, C_{14} = 1 \text{ sec}$ |
| $a = 0.05$ (Initial Setting) | for dead zone of 5 volts right side of zero |
| $a^1 = 0.05$ (Initial Setting) | For 5 volts steady state voltage |

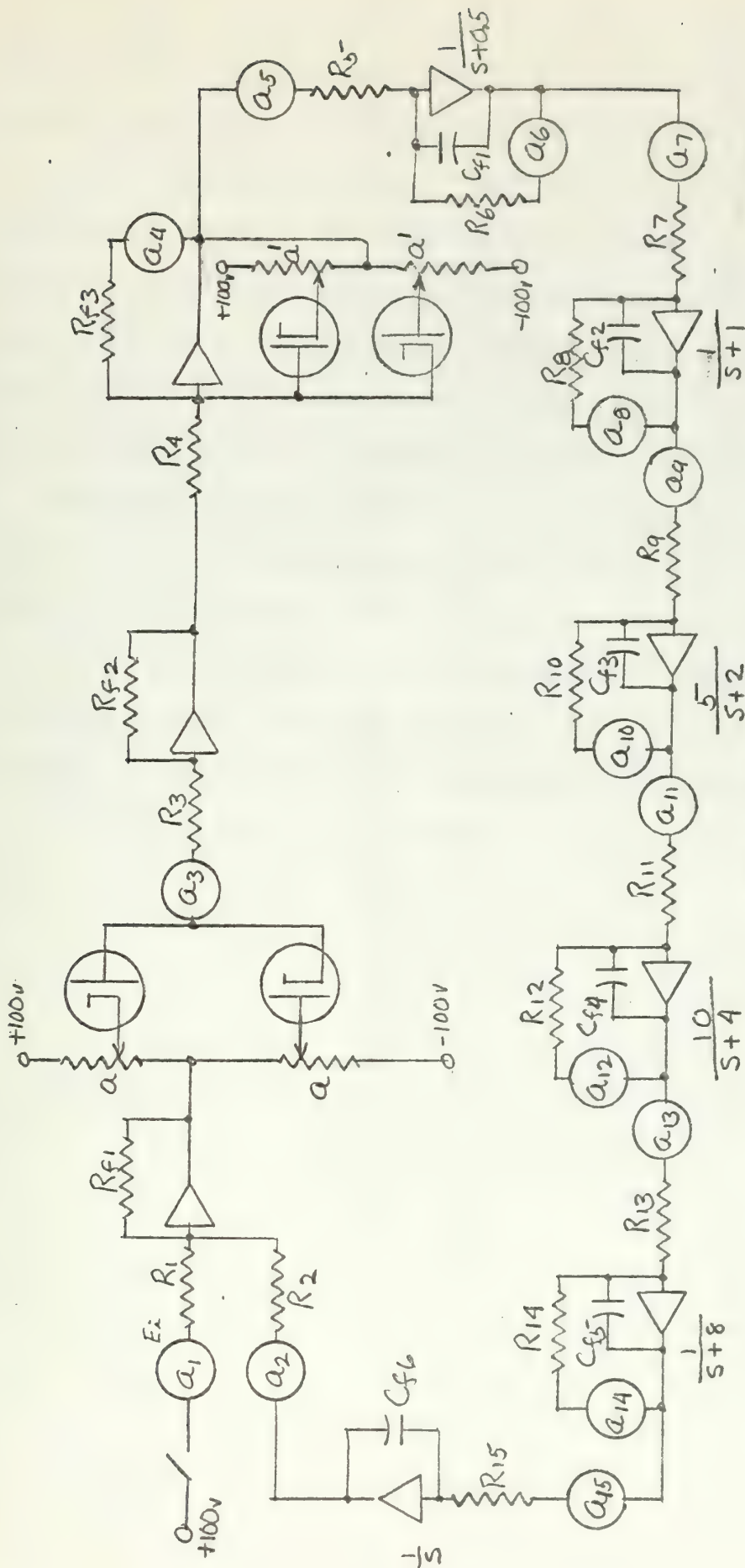


Fig. 11-5-1

11-5-1. A control system with multiple feedback loops and transfer functions.

to accurately set the back-biasing pots "a" and "b", a sine wave generator was connected to the input of the relay simulation.

An X-Y recorder was then calibrated to 2 volts per inch on both axes. The input and output of the relay simulator were then connected to the respective X and Y axis terminals. The pots "a" and "b" were then adjusted until the X - Y recorder plot closely approximated the static characteristic of the chosen relay with dead zone. The static characteristic obtained by the X - Y recorder is shown in Figure IV-A-4.2.

The system was first excited by a 10 volt step input signal and the system was found to build up into a limit cycle as shown in recorder trace IV-A-4.1. The system was then excited by a 20 volt step input signal and found to go into the same limit cycle as shown by recorder trace IV-A-4.1. From these recorder traces the limit cycle was found to have an angular frequency of 0.455 rad/sec and an amplitude of 14.3 volts.

The phase portrait of the system is shown in Figure IV-A-4.3.

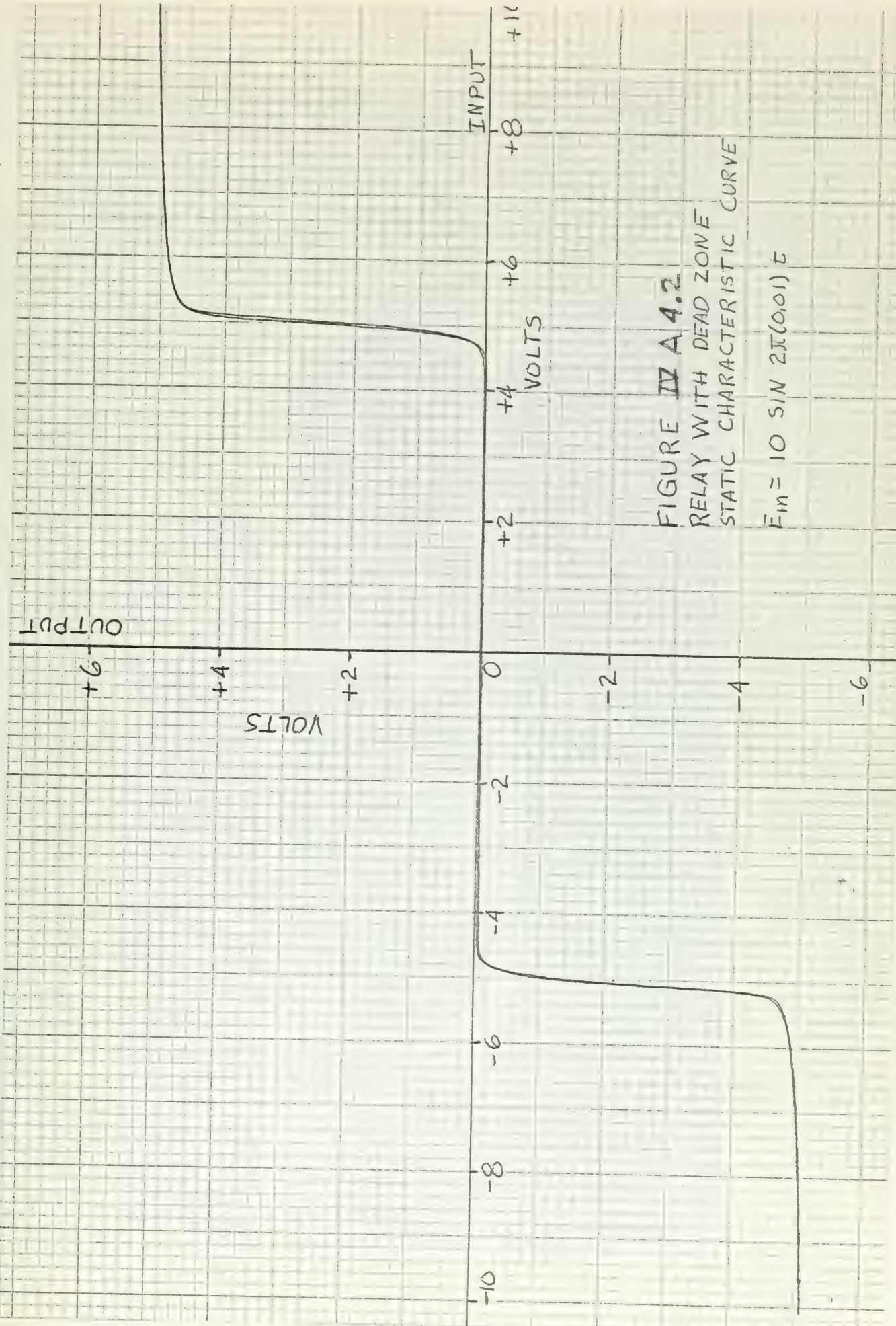
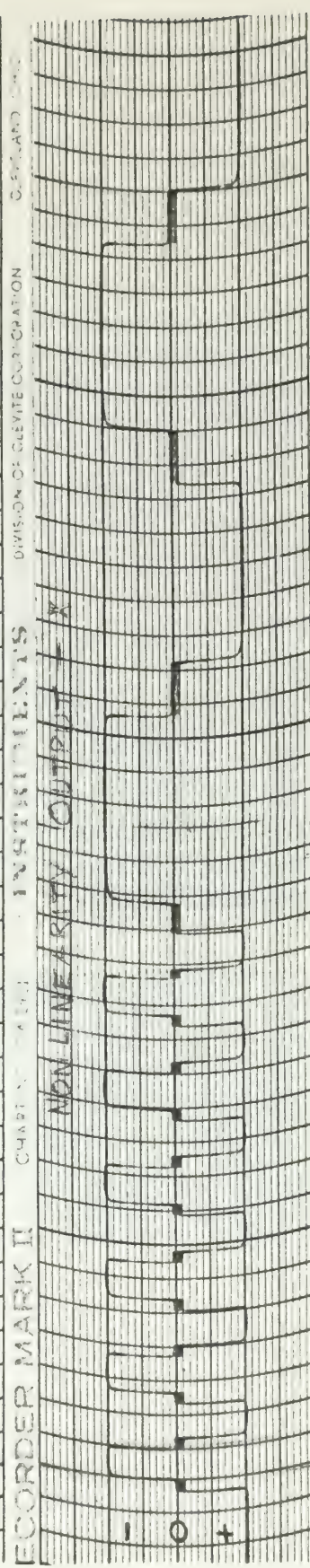
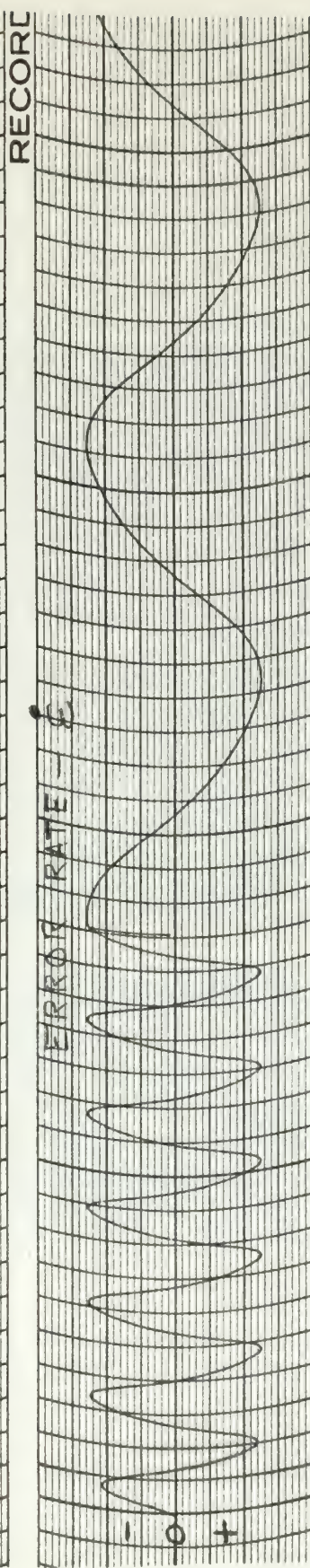


FIGURE IV A 4.2
RELAY WITH DEAD ZONE
STATIC CHARACTERISTIC CURVE

$$\bar{E}_m = 10 \sin 2\pi(0.01) t$$



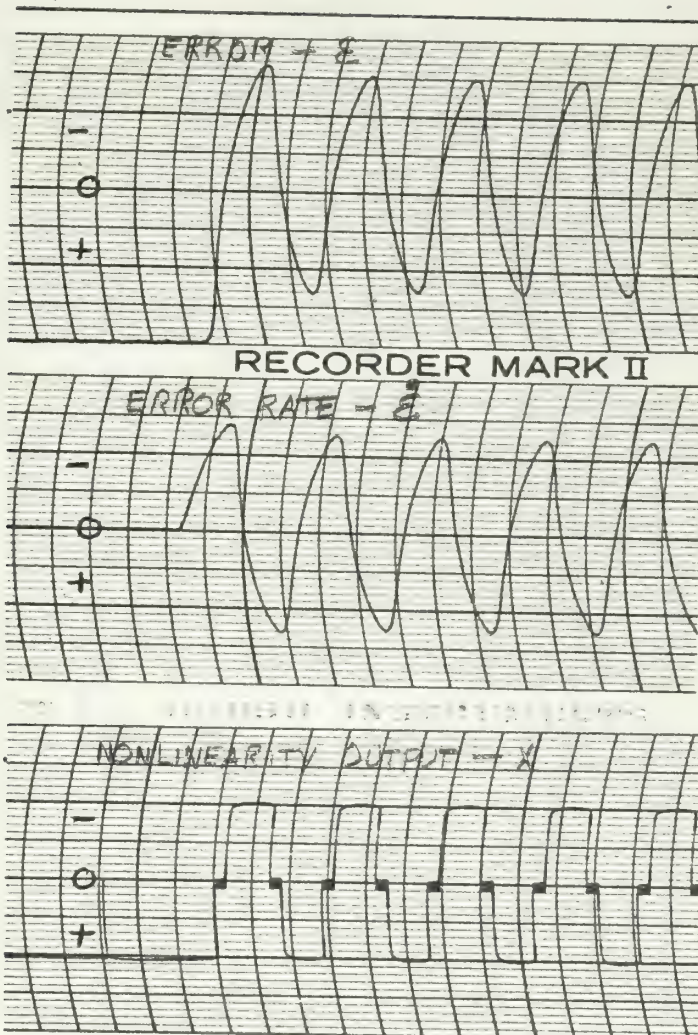
RECORDED ON RECORDER MARK II - A-4.1

RECORDED ON RECORDER MARK II - A-4.1. RECORDED ON RECORDER MARK II - A-4.1. RECORDED ON RECORDER MARK II - A-4.1.

RECORDED ON RECORDER MARK II - A-4.1. RECORDED ON RECORDER MARK II - A-4.1. RECORDED ON RECORDER MARK II - A-4.1.

RECORDED ON RECORDER MARK II - A-4.1. RECORDED ON RECORDER MARK II - A-4.1. RECORDED ON RECORDER MARK II - A-4.1.

RECORDED ON RECORDER MARK II - A-4.1. RECORDED ON RECORDER MARK II - A-4.1. RECORDED ON RECORDER MARK II - A-4.1.



Recorder Trace W-4-4, 1954

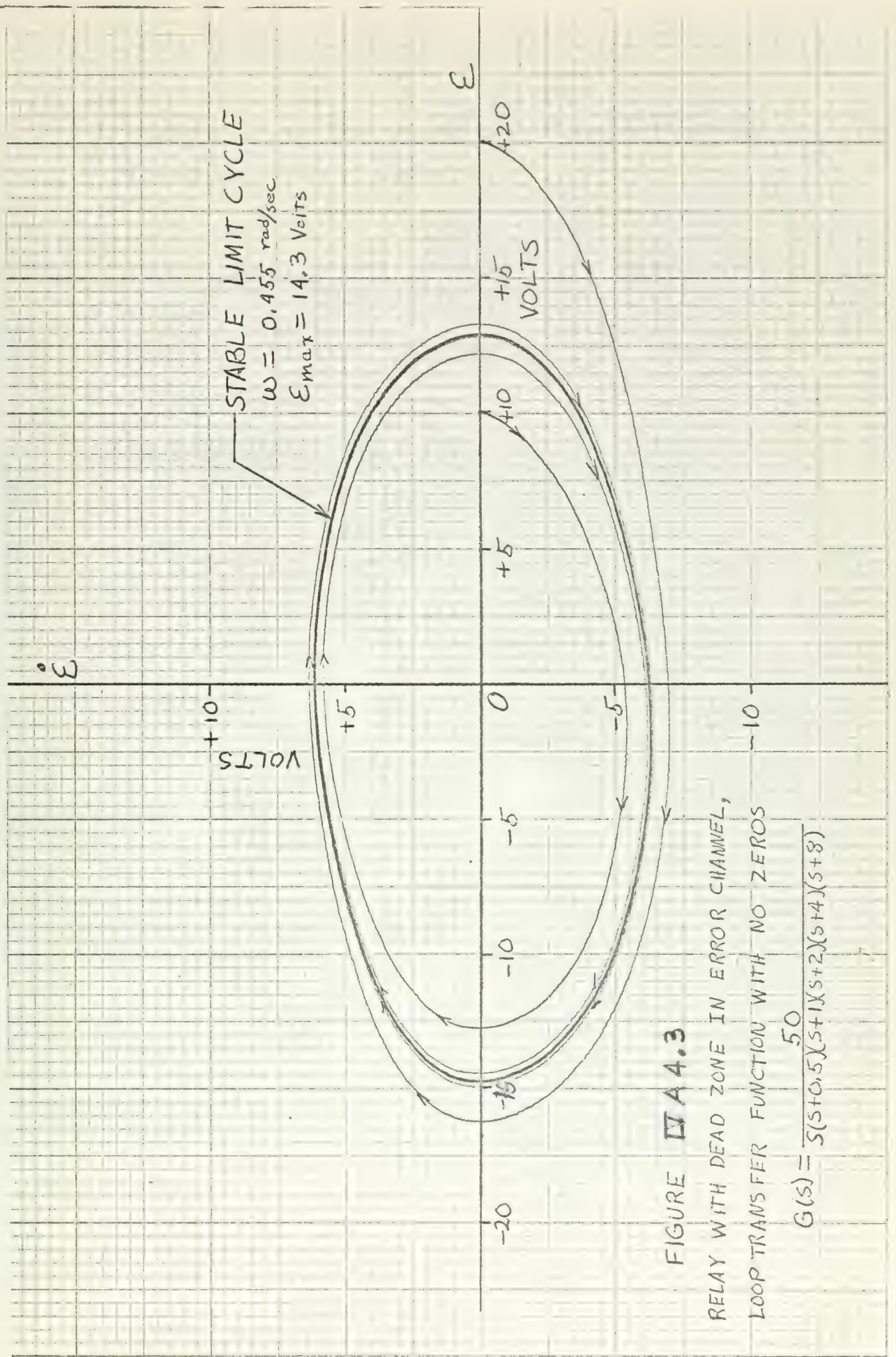
Relay with Dead Zone in Error Channel, 100 Hz, 20 Volt Step Input, with No Zeros, 20 Volt Step Input.

SCALES:

ϵ - 1 Volt/Line

$\dot{\epsilon}$ - 0.5 Volt/Line

X - 1 Volt/Line



IV-A-5 Comparison of the Four Methods in Limit Cycle Prediction for
a Nonlinear System of Figure IV-A.

| Method | Frequency rad/sec | Amplitude (Volts) |
|---------------------|----------------------|----------------------|
| Mitrovic's | 0.4507 | 13.5 |
| Root Locus | 0.4598 | 14.0 |
| Describing Function | 0.450 | 14.1 |
| Analog Simulation | 0.450 | 14.3 |

IV-B Loop Transfer Function with One Zero.

The block diagram of the system chosen is shown in Figure IV-B.

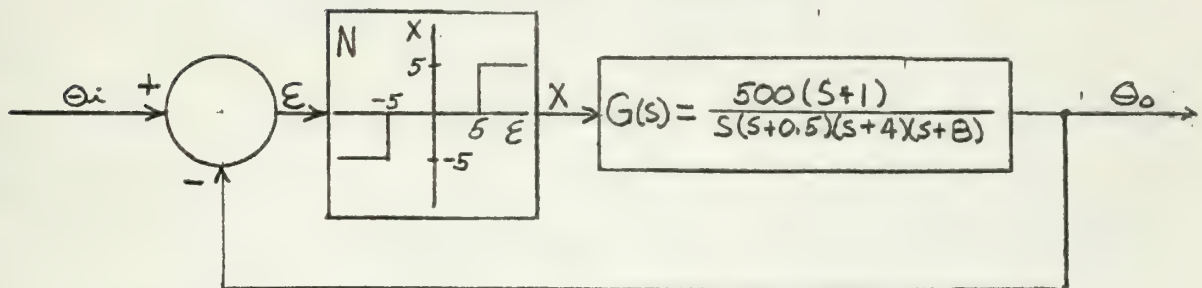


Figure IV-B

Relay with Dead Zone in Error Channel Loop

Transfer Function with One Zero

IV-B-1 Mitrovic's Method.

The characteristic equation of the given system is

$$s^4 + 12.5s^3 + 38s^2 + (16 + 500N)s + 500N = 0. \quad (\text{IV-B-1.1})$$

Assuming the last two coefficients variable, the characteristic equation becomes,

$$s^4 + 12.5s^3 + 38s^2 + B_1s + B_0 = 0 \quad (\text{IV-B-1.2})$$

where

$$B_0 = 500N \quad (\text{IV-B-1.3})$$

and

$$B_1 = 16 + 500N \quad (\text{IV-B-1.4})$$

From Appendix A, Mitrovic's equations for B_0 and B_1 are

$$B_0 = -[38\omega_n^2\phi_1(\gamma) + 12.5\omega_n^3\phi_2(\gamma) + \omega_n^4\phi_3(\gamma)] \quad (\text{IV-B-1.5})$$

and

$$B_1 = 38\omega_n\phi_2(\gamma) + 12.5\omega_n^2\phi_3(\gamma) + \omega_n^3\phi_4(\gamma). \quad (\text{IV-B-1.6})$$

Substitution of the values of the ϕ functions from Appendix A for

$\gamma = 0$ gives the parametric equations of the stability curve as,

$$B_0 = 38\omega_n^2 + \omega_n^4 \quad (\text{IV-B-1.7})$$

and

$$B_1 = 12.5\omega_n^2 \quad (\text{IV-B-1.8})$$

At the intersection of the M-point locus and the stability curve, equation IV-B-1.3 equals Equation IV-B-1.7 and Equation IV-B-1.4 equals Equation IV-B-1.8, thus

$$500N = 38\omega_n^2 + \omega_n^4 \quad (\text{IV-B-1.9})$$

and

$$16 + 500N = 12.5\omega_n^2 \quad (\text{IV-B-1.10})$$

Substituting Equation IV-B-1.9 into Equation IV-B-1.10 and combining terms yields

$$\omega_n^4 - 25.5 \omega_n^2 - 16 = 0 \quad . \quad (\text{IV-B-1.11})$$

Using the quadratic formula to solve Equation IV-B-1.11 for ω_n^2 yields

$$\omega_n^2 = 26.11$$

from which the frequency of the limit cycle is determined to be

$$\omega_n = 5.11 \text{ rad/sec.}$$

Substituting ω_n^2 back into Equation IV-B-1.9 the "average" gain of the nonlinearity over a cycle is determined as

$$N_{\text{ave}} = 0.6208$$

from which the approximate amplitude of the limit cycle is determined to be

$$E_{\text{max}} = 8.054 \text{ volts.}$$

A graphical presentation of the intersection is sketched in Figure IV-B-1.1.

Mitrovic's Method predicts a stable limit cycle by applying the same arguments given in Section IV-A-1 to Figure IV-B-1.1.

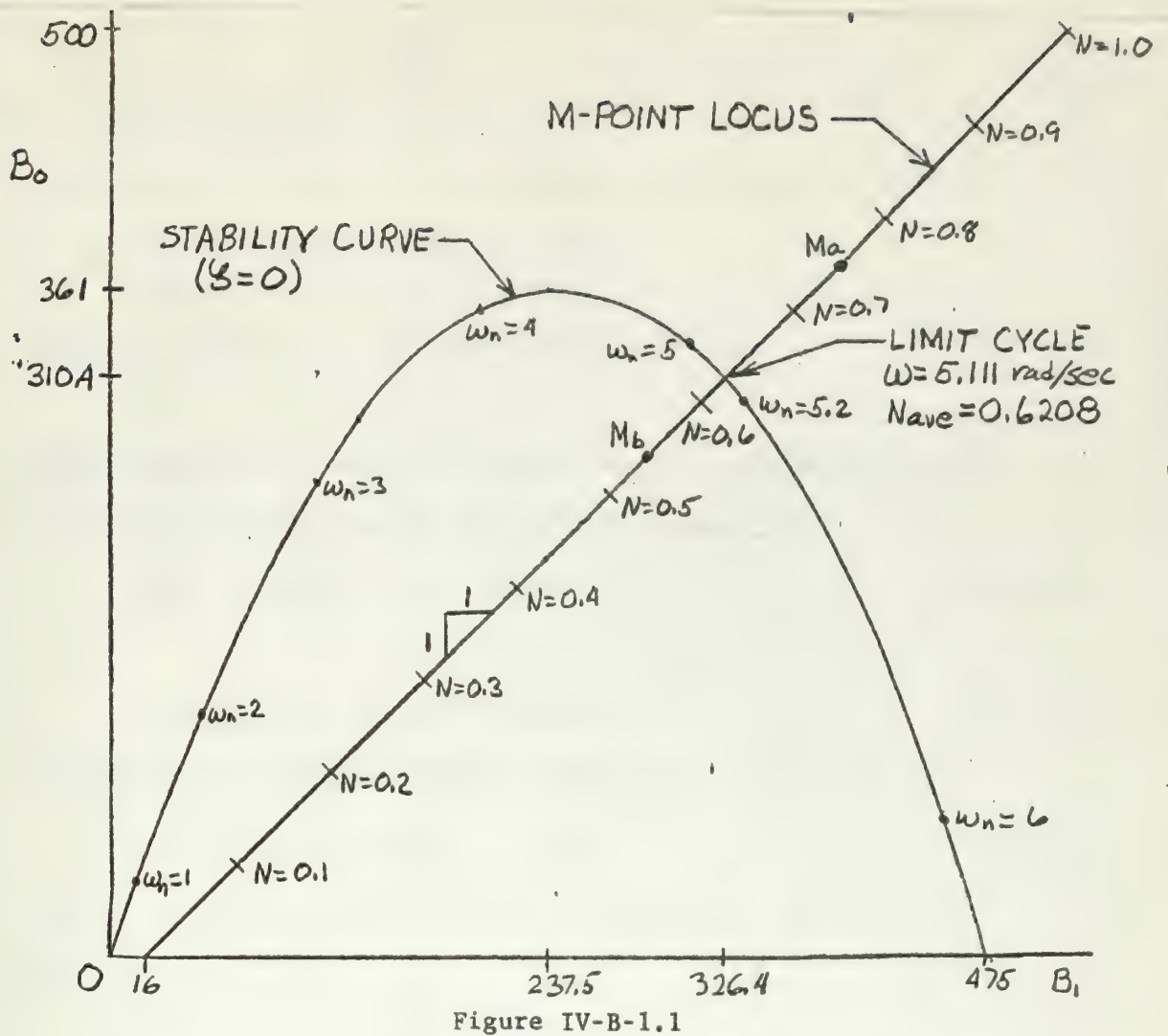


Figure IV-B-1.1

Graphical Solution for Relay with Dead Zone in Error
 Channel, Loop Transfer Function with One Zero

IV-B-2 Root Locus Method

Substituting $S = j\omega$ in the characteristic Equation IV-B-1.1 and evaluating the higher powers of j gives,

$$\omega^4 - j12.5\omega^3 - 38\omega^2 + j(16 + 500N)\omega + 500N = 0. \quad (\text{IV-B-2.1})$$

Requiring that the real and imaginary parts of Equation IV-B-2.1 go to zero independently yields the following equations,

$$\omega^4 - 38\omega^2 + 500N = 0 \quad (\text{IV-B-2.2})$$

and

$$-j12.5\omega^3 + j(16 + 500N)\omega = 0 \quad (\text{IV-B-2.3})$$

Eliminating N between equations IV-B-2.2 and IV-B-2.3 gives,

$$\omega^4 - 25.5\omega^2 - 16 = 0 \quad (\text{IV-B-2.4})$$

Using the quadratic formula to solve Equation IV-B-2.4 for ω^2 gives,

$$\omega^2 = 26.11$$

from which the frequency of the limit cycle is determined to be

$$\omega = 5.11 \text{ rad/sec.}$$

Substituting ω^2 back into Equation IV-B-2.2 gives, the "average" gain of the nonlinearity over a cycle as

$$N_{\text{ave}} = 0.6208$$

from which the approximate amplitude of the limit cycle is determined to be

$$\mathcal{E}_{\text{max}} = 8.054 \text{ volts.}$$

A graphical presentation of the root locus solution is sketched in Figure IV-B-2.1.

The root locus method predicts a stable limit cycle by applying the arguments given in Section IV-A-1 to Figure IV-B-2.1.

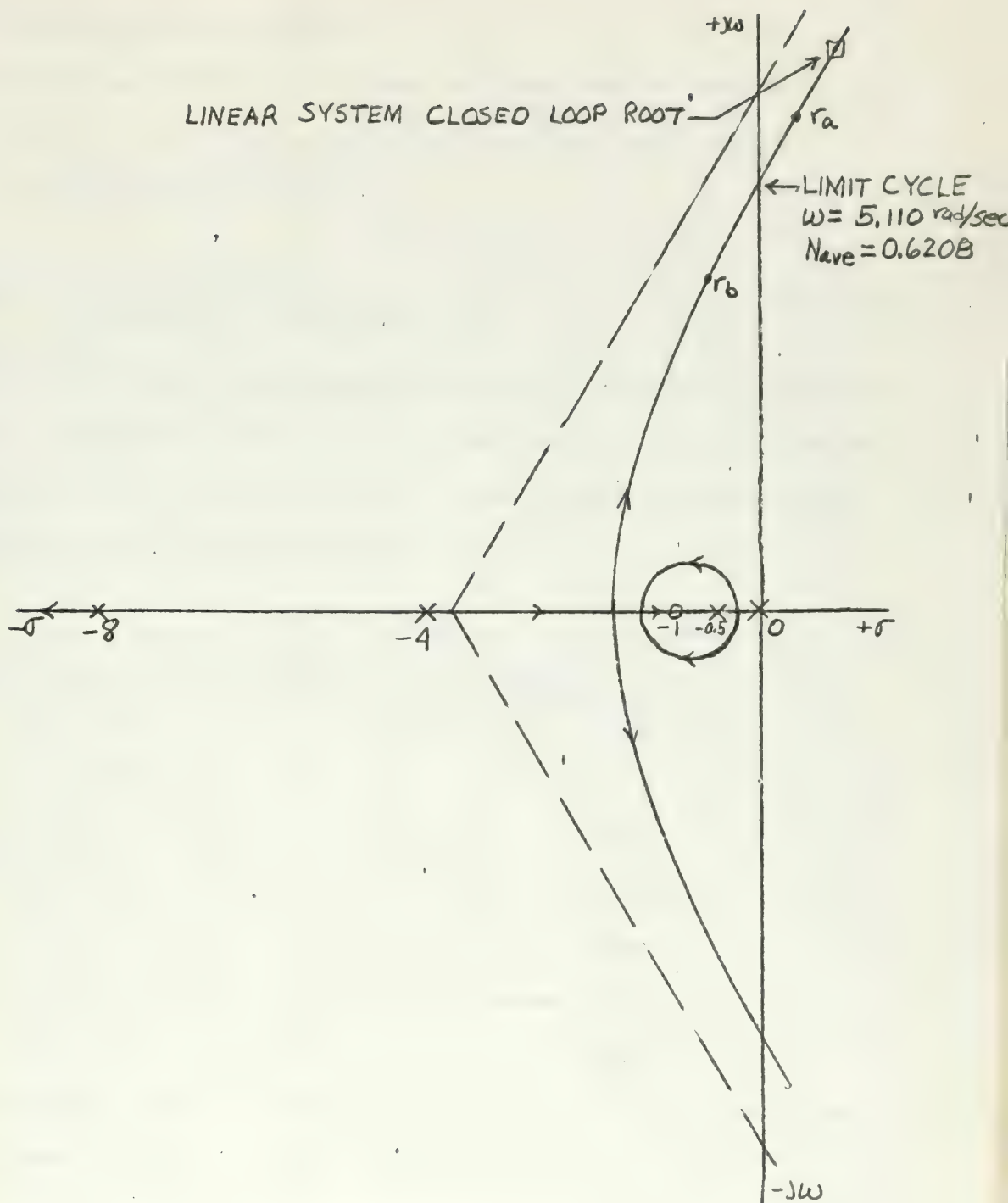


Figure IV-B-2.1

Root Locus Solution for Relay with Dead Zone in
Error Channel Loop Transfer Function with One Zero

IV-B-3 Describing Function Method.

The describing function for a relay with dead zone is given in Equation IV-A-3.1. The linear loop transfer function for the given system in frequency response form is

$$G(j\omega) = \frac{31.25(j\omega + 1)}{j\omega(2j\omega + 1)(0.25j\omega + 1)(0.125j\omega + 1)} \quad (IV-B-3.1)$$

Table IV-B-3.1 gives the magnitude and phase of Equation IV-B-3.1 for the various frequencies used to plot the linear loop transfer function on the gain-phase plane of Figure IV-B-3.1. These values are obtained from A Bode diagram plot of Equation IV-B-3.1.

TABLE IV-B-3.1

| ω | $ G(j\omega) $ db | $\angle G(j\omega)$ deg |
|----------|-------------------|-------------------------|
| 4.65 | 6 | -176 |
| 4.95 | 5 | -178.5 |
| 5.1 | 4.6 | -180 |
| 5.3 | 4 | -181.5 |
| 5.6 | 3 | -184 |
| 5.9 | 2 | -187 |

Table IV-B-3.2 gives the values of $1/G_D$ which are plotted in Figure IV-B-3.1. These values are determined from Equation IV-A-3.1.

TABLE IV-B-3.2

| \mathcal{E}_{max} | G_D | $1/G_D$ | $1/G_D$ db |
|---------------------|-------|---------|------------|
| 8 | 0.621 | 1.61 | 4.14 |
| 8.9 | 0.592 | 1.69 | 4.56 |
| 9 | 0.588 | 1.7 | 4.62 |
| 10 | 0.551 | 1.814 | 5.175 |

Inspection of Figure IV-B-3.1 shows the intersection and thus the limit cycle to occur at

$$\omega = 5.1 \text{ rad/sec.}$$

and

$$\epsilon_{\max} = 8.95 \text{ Volts.}$$

The describing function method predicts a stable limit cycle by applying the arguments given in Section IV-A-3 to Figure IV-B-3.1.

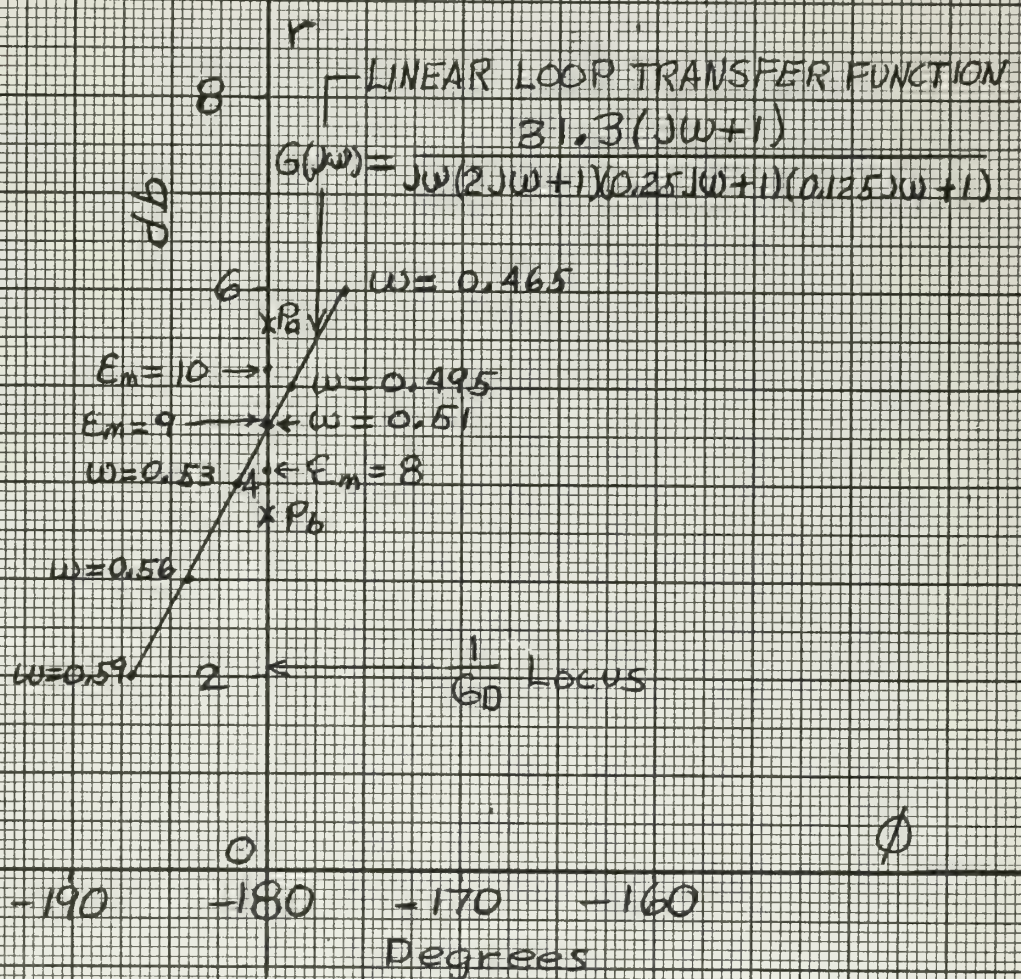


FIGURE II B3.1
GAIN-PHASE PLANE - RELAY WITH DEAD ZONE
IN ERROR CHANNEL, LOOP TRANSFER
FUNCTION WITH ONE ZERO

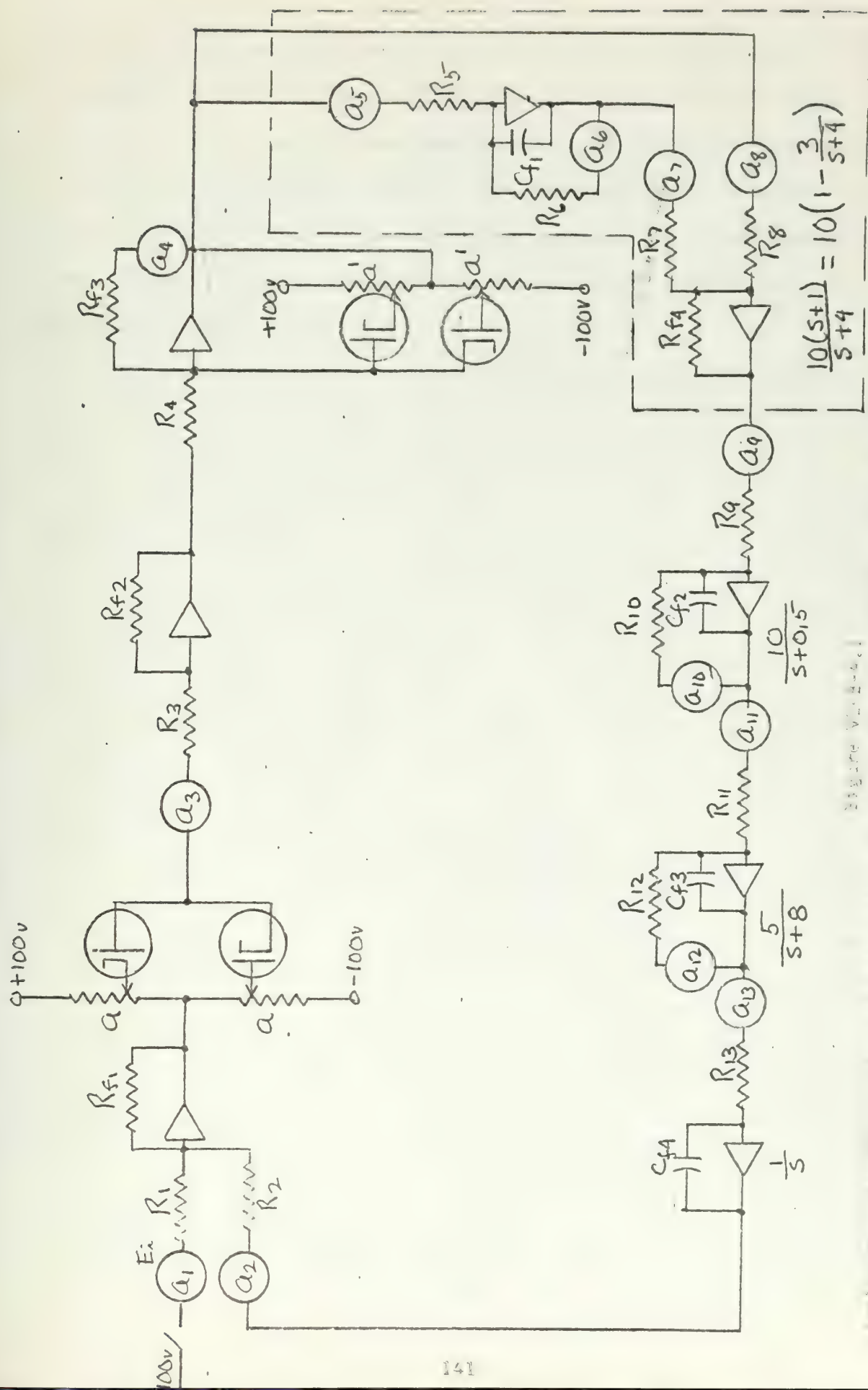
IV-B-4 Analog Computer Simulation.

The analog computer simulation of the given system is shown in Figure IV-B-4.1. The coefficient pot settings with associated resistances and capacitances for real time and real magnitude scaling are given in Table IV-B-4.1.

TABLE IV-B-4.1.

| Pot Setting | Associated Elements |
|--------------------------------|---|
| $a_1 = \frac{E_i}{100}$ | For an input step of E_i volts $R_1 = 1 \text{ Meg}, R_{f1} = 1 \text{ Meg}$ |
| $a_2 = 1.0$ | $R_2 = 1 \text{ Meg}, R_{f1} = 1 \text{ Meg}$ |
| $a_3 = 1.0$ | $R_3 = 0.1 \text{ Meg}, R_{f2} = 1 \text{ Meg}$ |
| $a_4 = 1.0$ | $R_4 = 0.1 \text{ Meg}, R_{f3} = 1 \text{ Meg}$ |
| $a_5 = 0.3$ | $R_5 = 0.1 \text{ Meg}, C_{f1} = 1 \text{ uf}$ |
| $a_6 = 0.4$ | $R_6 = 0.1 \text{ Meg}, C_{f1} = 1 \text{ uf}$ |
| $a_7 = 1.0$ | $R_7 = 0.1 \text{ Meg}, R_{f4} = 1 \text{ Meg}$ |
| $a_8 = 1.0$ | $R_8 = 0.1 \text{ Meg}, R_{f4} = 1 \text{ Meg}$ |
| $a_9 = 1.0$ | $R_9 = 0.1 \text{ Meg}, C_{f2} = 1 \text{ uf}$ |
| $a_{10} = 0.5$ | $R_{10} = 1 \text{ Meg}, C_{f2} = 1 \text{ uf}$ |
| $a_{11} = 0.5$ | $R_{11} = 0.5 \text{ Meg}, C_{f3} = 1 \text{ uf}$ |
| $a_{12} = 0.8$ | $R_{12} = 0.1 \text{ Meg}, C_{f3} = 1 \text{ uf}$ |
| $a_{13} = 1.0$ | $R_{13} = 1 \text{ Meg}, C_{f4} = 1 \text{ uf}$ |
| $a = 0.05$ (Initial Setting) | For 5 volt dead zone either side of Zero |
| $a^1 = 0.05$ (Initial Setting) | For 5 Volt relay output Voltage |

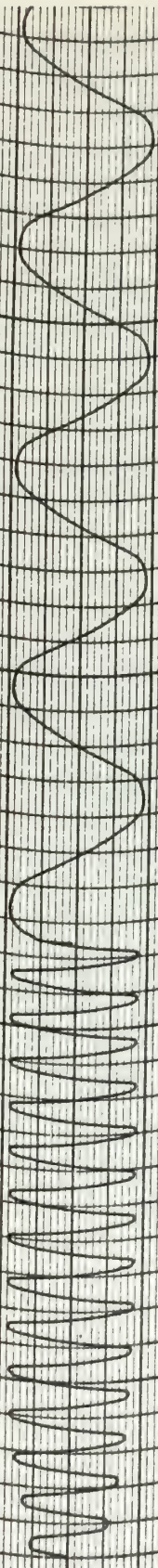
To accurately set the back-biasing pots "a" and " a^1 ", the same procedure as given in Section IV-A-4 was followed. The static characteristic of the relay is the same as that shown in Figure IV-A-4.2.



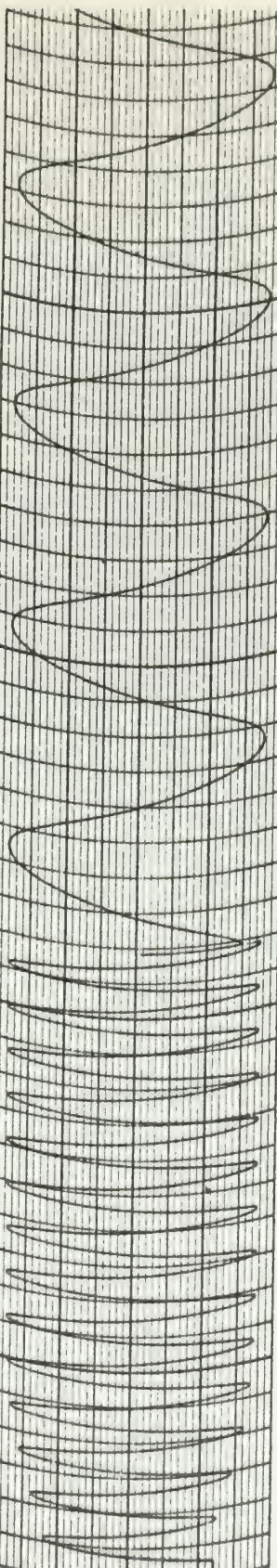
The system was first excited with a 6 volt step input signal and was found to build up into the limit cycle shown in recorder trace IV-E-4.1. The system was then excited with a 12 volt step input signal and the system was found to go into the same limit cycle as shown in recorder trace IV-E-4.2. From these two recorder traces the limit cycle was determined to have an angular frequency of 5.07 rad/sec and an amplitude of 9.0 volts.

The phase portrait of the system is shown in Figure IV-A-4.2.

ERROR RATE - $\dot{\epsilon}$



ERROR - ϵ



NON-LINEARITY OUTPUT - X

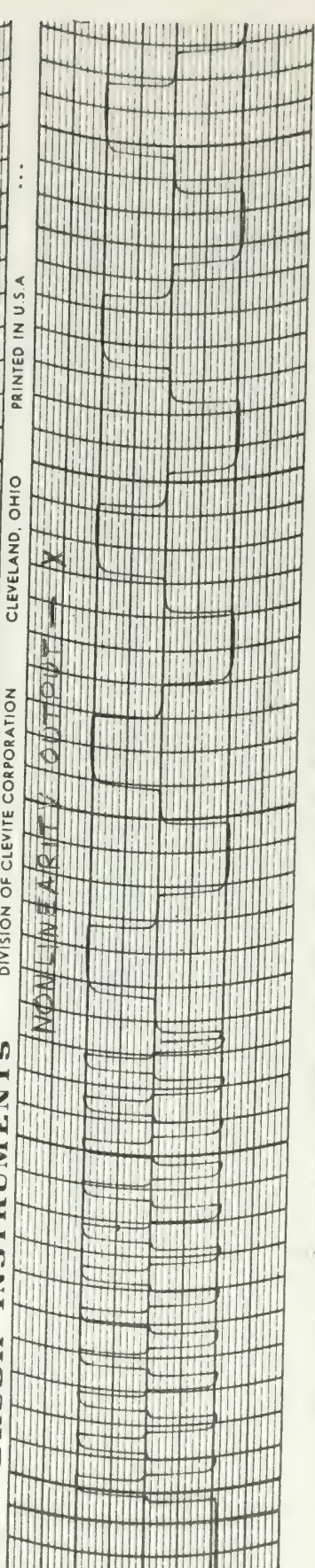
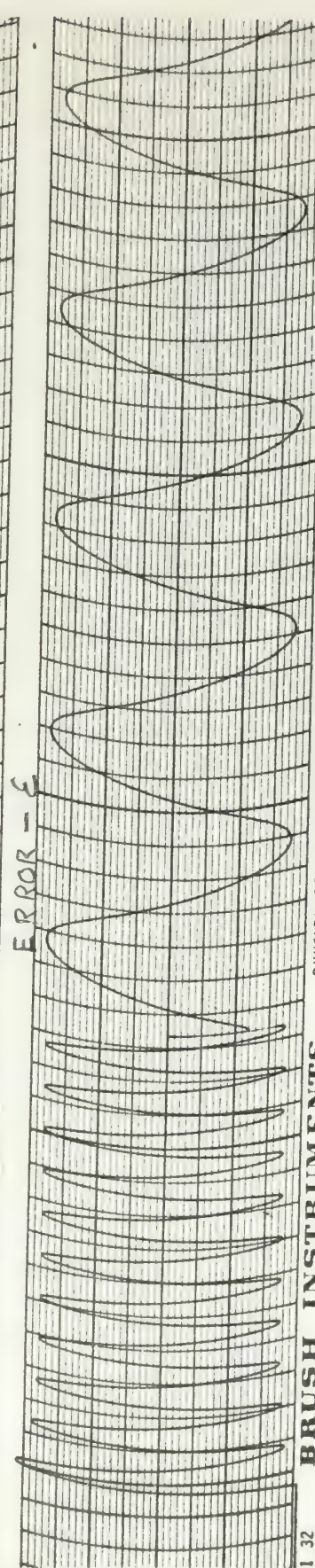
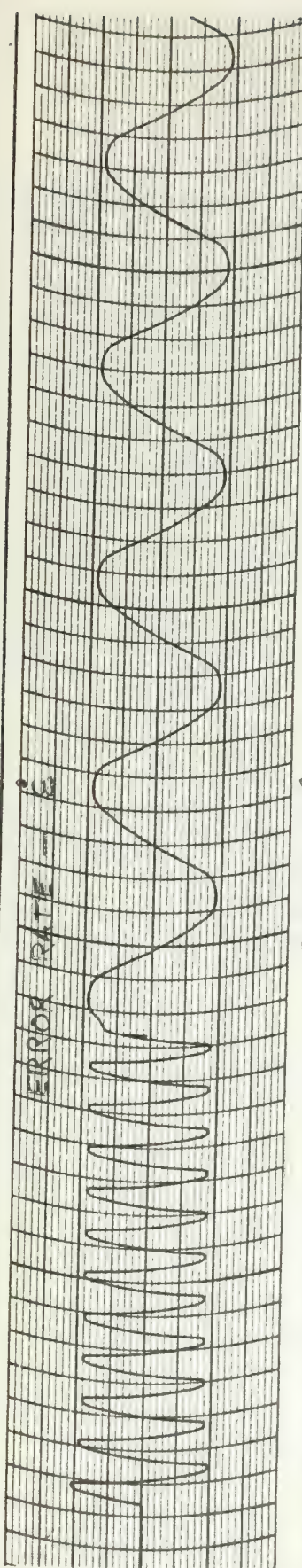


4th Order Loop W-4.1

Relay with Dead Zone in Error Signal Loop 2/10/51a

Scale: $\dot{\epsilon}$ - 3 volts/min ϵ - 0.1 volts/min X - 0.1 volts/min

Time 1.30 sec/division
0.2 sec/division



Model: D-100 v1-E-4.2

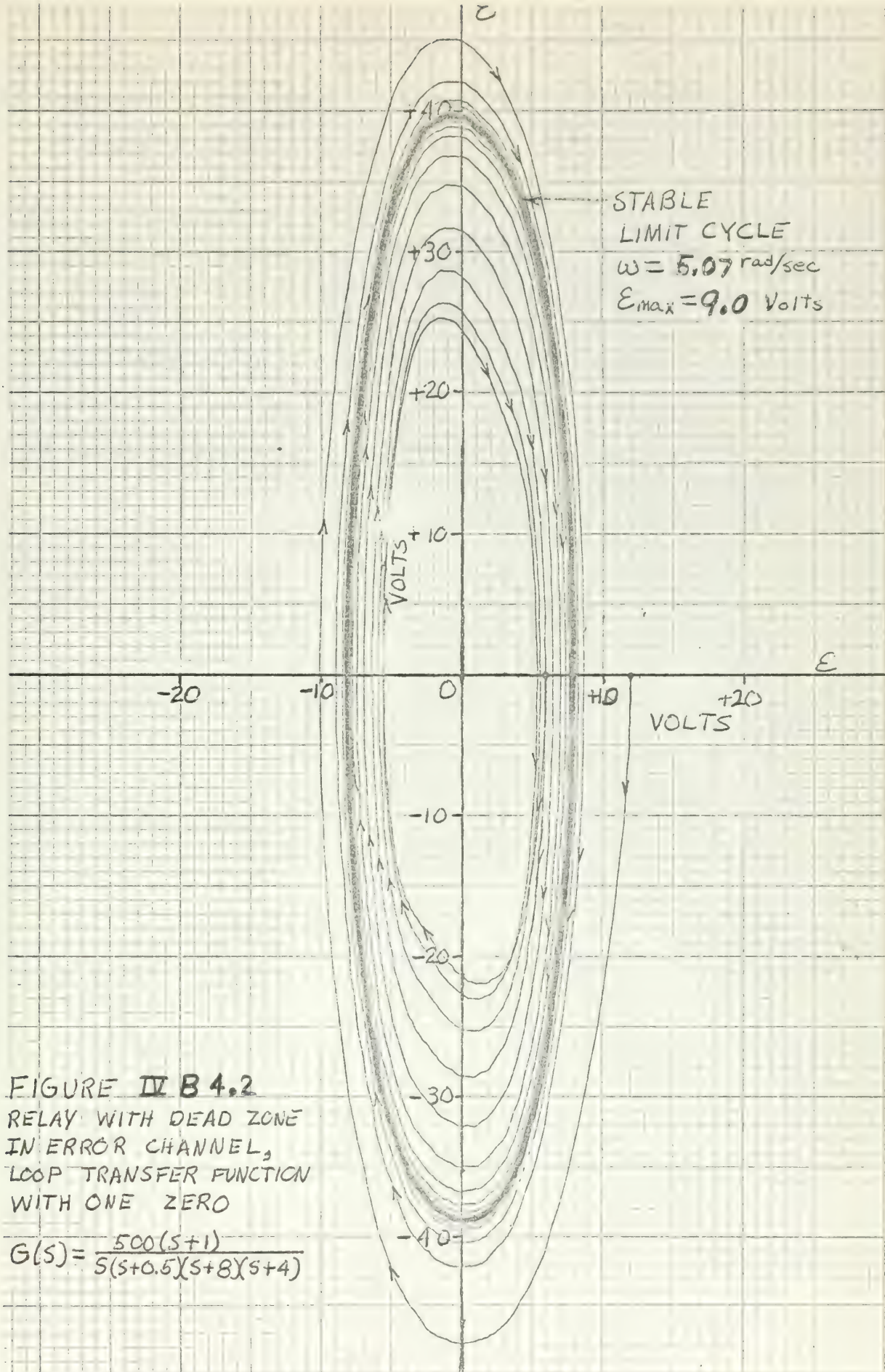
Relay with Dead Zone in Error Channel. Loop Transfer Function with One Zero, 12 Volts Step Input.

0.001: E - 5 volts/line

E - 0.5 volts/line

X - 0.5 Volts/line

Time - 1 second/division
0.001 seconds/division



IV-B-5 Comparison of the Results of the Four Methods for the System
of Figure IV-6.

| Method | Frequency rad/sec. | amplitude (volts) |
|---------------------|-----------------------|----------------------|
| Matthiessen's | 5.11 | 8.014 |
| Root locus | 5.11 | 8.014 |
| Describing Function | 5.1 | 8.91 |
| Analog simulation | 5.0 | 9.0 |

CHAPTER V

NONLINEARITY IN A FEEDBACK PATH

V-A Saturation in Velocity Feedback Path.

The system chosen to analyze is given in Figure V-A.

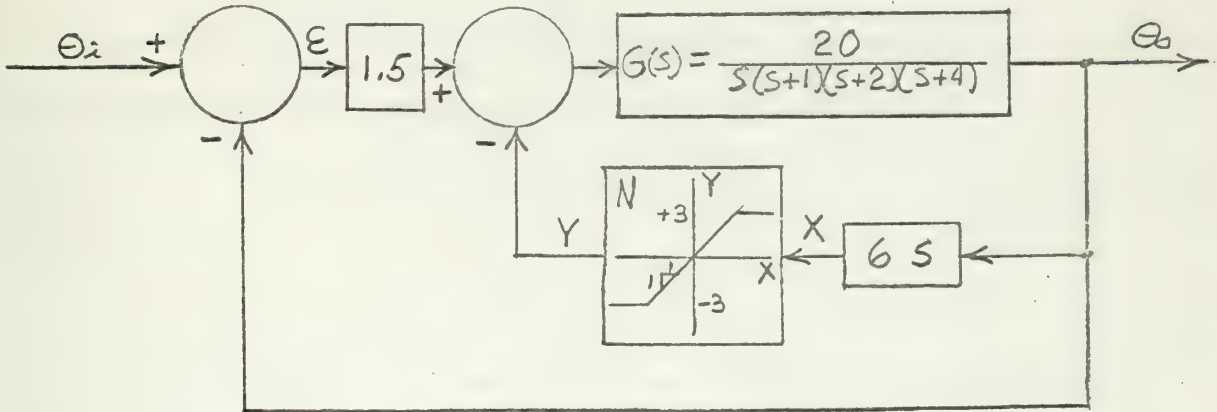


FIGURE V-A
SATURATION IN VELOCITY FEEDBACK PATH

V-A-1 Mitrovic's Method.

Assigning N as the instantaneous gain of the nonlinearity, the characteristic equation can be written as,

$$s^4 + 7s^3 + 14s^2 + (8 + 120N)s + 30 = 0. \quad (\text{V-A-1.1})$$

Assuming the last two coefficients variable, the characteristic equation is rewritten as,

$$s^4 + 7s^3 + 14s^2 + B_1s + B_0 = 0 \quad (\text{V-A-1.2})$$

where

$$B_1 = 8 + 120N \quad (\text{V-A-1.3})$$

and

$$B_0 = 30. \quad (\text{V-A-1.4})$$

From Appendix A, Mitrovic's equations for B_0 and B_1 are,

$$B_0 = -[14\omega_n^2\phi_1(\xi) + 7\omega_n^3\phi_2(\xi) + \omega_n^4\phi_3(\xi)] \quad (\text{V-A-1.5})$$

and

$$B_1 = 14\omega_n\phi_2(\xi) + 7\omega_n^2\phi_3(\xi) + \omega_n^3\phi_4(\xi). \quad (\text{V-A-1.6})$$

Substituting the values of the ϕ functions from Appendix A for $\xi = 0$ gives the parametric equations of the stability curve as

$$B_0 = 14\omega_n^2 + \omega_n^4 \quad (\text{V-A-1.7})$$

and

$$B_1 = 7\omega_n^2. \quad (\text{V-A-1.8})$$

From equations V-A-1.3 and V-A-1.4 the M-point locus is seen to be a straight line segment parallel to the B_1 axis. At the intersections of the M-point locus with the stability curve, equation V-A-1.4 equals V-A-1.7 and equation V-A-1.3 equals equation V-A-1.8. Thus at the intersections

$$\omega_n^4 + 14\omega_n^2 = 30 \quad (\text{V-A-1.9})$$

and

$$7\omega_n^2 = 8 + 120N. \quad (\text{V-A-1.10})$$

Solving equation V-A-1.9 for ω_n^2 gives

$$\omega_n^2 = 2.6411$$

and

$$\omega_n^2 = 11.3589,$$

from which

$$\omega_{n1} = 1.625 \text{ rad/sec}$$

and

$$\omega_{n2} = 3.370 \text{ rad/sec.}$$

Since the system is fourth order, the stability curve is a parabola with its axis parallel to the B_0 axis. Consequently, both values of ω_n must be considered since the M-point locus, a straight line parallel to the B_1 axis, can intersect the parabola in two places.

For $\omega_{n1} = 1.625$ rad/sec, the average gain of the nonlinearity over a cycle is found from equation V-A-1.10 to be

$$N_{1ave} = 0.0874,$$

from which the approximate amplitude of signal X in Figure V-A is determined to be

$$X_{1max} = 34.325 \text{ volts.}$$

For $\omega_{n2} = 3.370$ rad/sec, the average gain of the nonlinearity over a cycle is determined to be

$$N_{2ave} = 0.5958,$$

from which the average amplitude of signal X is determined to be

$$X_{2max} = 5.035 \text{ volts.}$$

However, the signal X is proportional to the output velocity and not the output angle. To obtain an approximate amplitude of the limit cycle in terms of output angle, θ_o , one must assume the signal X is relatively sinusoidal. With this assumption, the amplitude of the output angle can be obtained from

$$\theta_o = \frac{X_{max}}{6.0 \omega} \quad (V-A-1.11)$$

From equation V-A-1.11, the approximate amplitudes of the output angle for both limit cycles are

$$\theta_{o1max} = 3.52 \text{ volts}$$

and

$$\theta_{o2max} = 0.249 \text{ volts.}$$

The graphical presentation of the solution by Mitrovic's method is shown in Figure V-A-1.1.

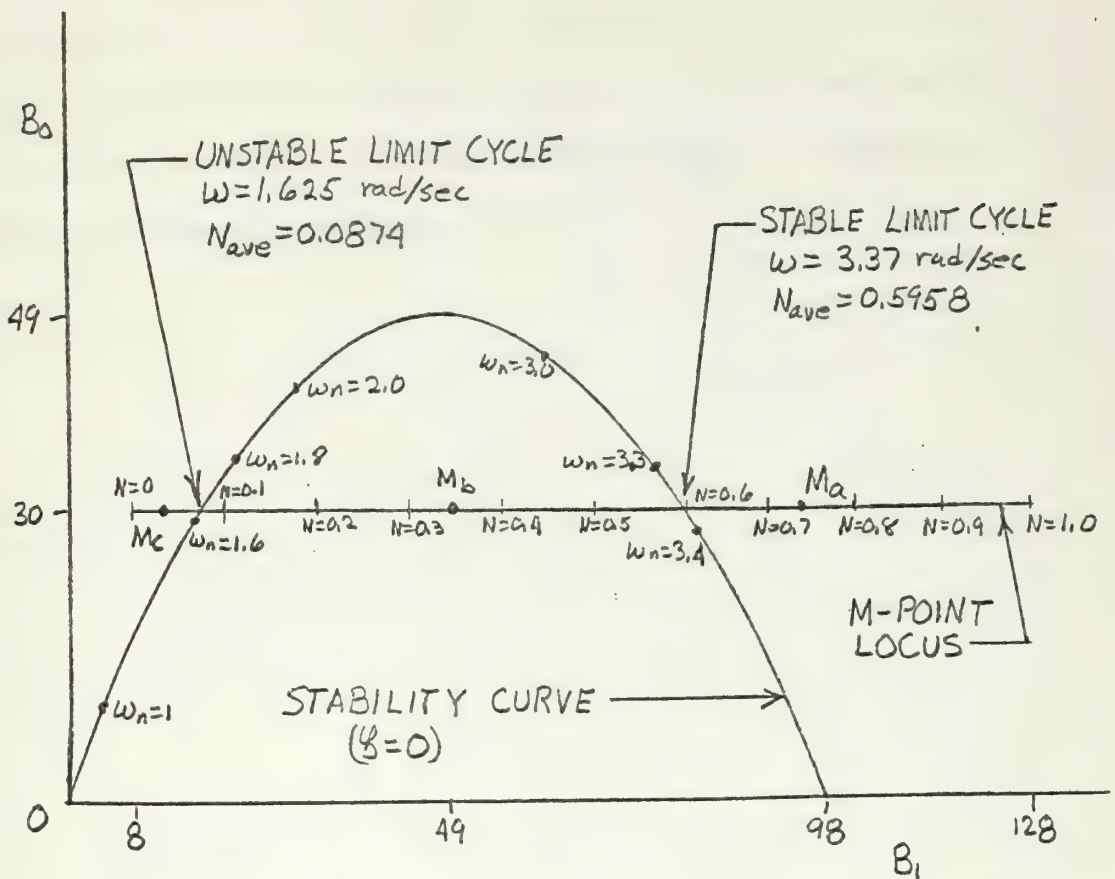


FIGURE V-A-1.1
GRAPHICAL SOLUTION FOR SATURATION IN
VELOCITY FEEDBACK PATH

Mitrovic's method predicts that the limit cycle at $\omega_{n1} = 1.625$ rad/sec is an unstable one and that the limit cycle at $\omega_{n2} = 3.37$ rad/sec is a stable limit cycle by the following arguments. For the stable limit cycle at $\omega_{n2} = 3.37$ the same arguments used in Chapter I, Section I-A-1 can be applied to Figure V-A-1.1. For the unstable limit cycle assume Θ_i is such that the first peak of signal X causes the instantaneous M-point to be at M_b . The system is then stable and the oscillations decrease. As the oscillations decrease N increases moving the M-point to the right.

Eventually, the "average" M-point will lie at the intersection of the stable limit cycle at $\omega_{n2} = 3.37$. Now assume that θ_2 is large enough to cause the first peak of signal X to be large enough to place the instantaneous M-point at M_c . The system is unstable and the oscillations increase. As the oscillations increase, N decreases causing the M-point to move even farther to the left into the unstable region. Consequently the oscillations increase indefinitely.

V-A-2 Root Locus Method.

Substituting $S = j\omega$ into equation V-A-1.1 and evaluating the higher powers of j gives,

$$\omega^4 - j7\omega^3 - 14\omega^2 + j(8 + 120N)\omega + 30 = 0. \quad (\text{V-A-2.1})$$

By requiring that the real and imaginary parts of equation V-A-2.1 go to zero independently, then

$$\omega^4 - 14\omega^2 + 30 = 0 \quad (\text{V-A-2.2})$$

and

$$-j7\omega^3 + j(8 + 120N)\omega = 0. \quad (\text{V-A-2.3})$$

Dividing equation V-A-2.2 by $j\omega$ the above two equations are exactly the same as equations V-A-1.9 and V-A-1.10 developed in Mitrovic's method. The solutions of these simultaneous equations are again given

$$\omega_1 = 1.625 \text{ rad/sec}$$

$$\omega_2 = 3.370 \text{ rad/sec}$$

$$N_{1\text{ave}} = 0.0874$$

$$N_{2\text{ave}} = 0.5958$$

$$X_{1\text{max}} = 34.325 \text{ volts}$$

and

$$X_{2\text{max}} = 5.035 \text{ volts.}$$

Also applying equation V-A-1.11 gives

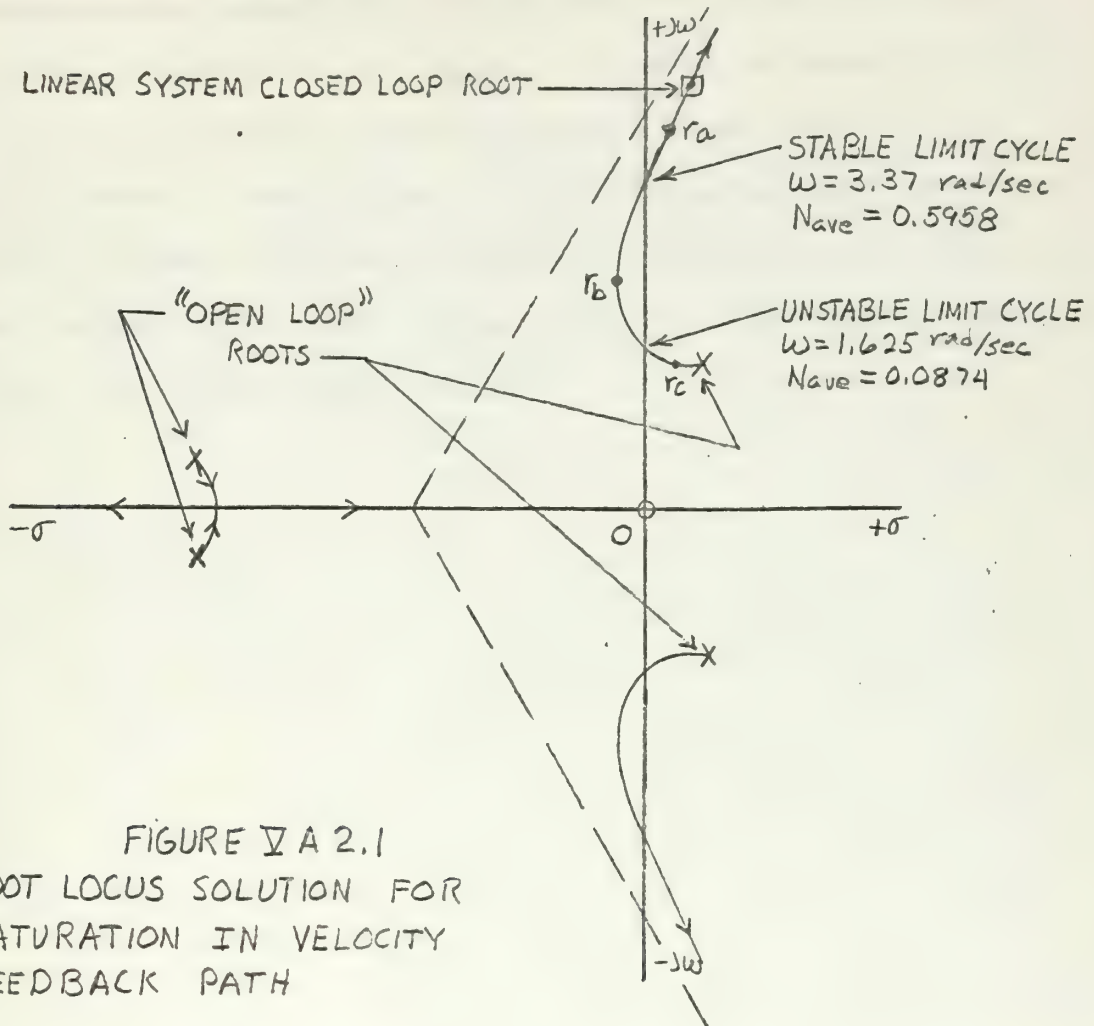
$$\Theta_{o1\text{max}} = 3.52 \text{ volts}$$

and

$$\Theta_{o2\text{max}} = 0.249 \text{ volts.}$$

The graphical solution of the root locus solution is given in Figure V-A-2.1. In the figure, the "open loop poles" are the poles of the transfer function obtained when the position feedback loop is closed on the

plant, first manipulating the 1.5 gain block out of the error channel.



The root locus method predicts the limit cycle at $\omega_1 = 1.625 \text{ rad/sec}$ will be an unstable limit cycle and the limit cycle at $\omega_2 = 3.37 \text{ rad/sec}$ will be a stable one. The arguments of Chapter I, Section I-A-2 can be applied to the $\omega_2 = 3.37 \text{ rad/sec}$ crossover to determine a stable limit cycle at that point. At the $\omega_1 = 1.625 \text{ rad/sec}$ crossover, assume the input signal, θ_i , is large enough to cause the first peak of signal X to be large enough to place the instantaneous root at r_b . The system is stable and the oscillations decrease. As the oscillations decrease, N increases causing the instantaneous closed loop root to move up the

locus toward the linear closed loop root.

Eventually, the average root location over a cycle will lie at the stable limit cycle crossover. If θ_c is large enough to cause the first peak of signal X to be large enough to place the instantaneous root at r_c , then the system is unstable and the oscillations increase. As the oscillations increase, N decreases, driving the closed loop root farther into the right-half plane toward the open loop root. Consequently, the oscillations will increase indefinitely.

V-A-3. Describing Function Method.

The describing function for saturation is given in Equation I-A-3.1 of Chapter I.

To obtain an equivalent loop transfer function, the gain of the error channel was first made unity by moving the gain block to the input channel and to the unity feedback path as shown in Figure V-A-3.1.

Reduction of the outer position feedback thus yields

$$G'(s) = \frac{20}{s^4 + 7s^3 + 14s^2 + 8s + 30} \quad (V-A-3.1)$$

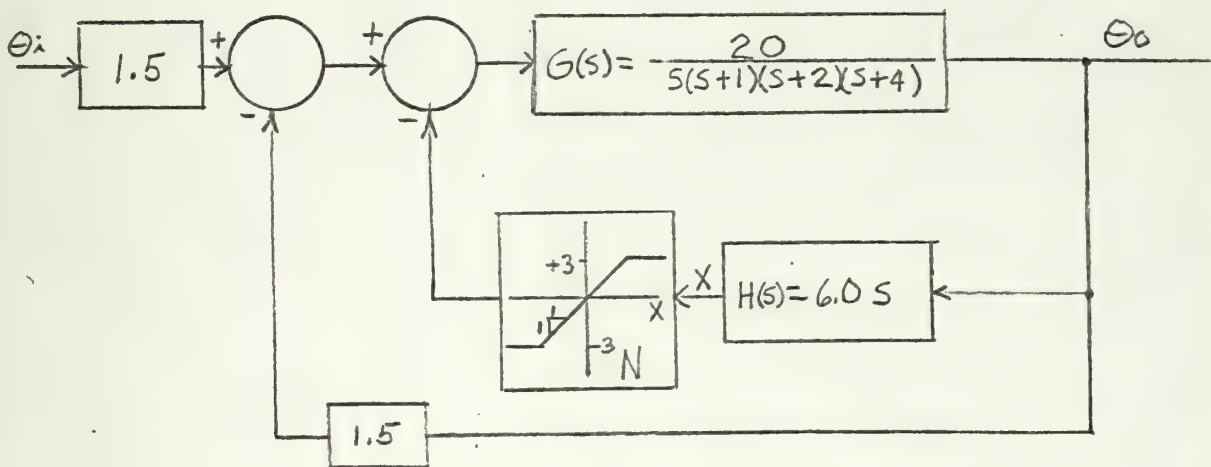


FIGURE V-A-3.1

A digital computer program was used to find the roots of the denominator of equation V-A-3.1, which are,

$$\begin{aligned} r_1 &= 0.2168 - j1.3854 \\ r_2 &= 0.2168 + j1.3854 \\ r_3 &= -3.7168 - j1.2011 \\ r_4 &= -3.7168 + j1.2011. \end{aligned}$$

Thus the equivalent open loop transfer function becomes,

$$G'H(s) = \frac{120s}{(s - 0.2168 \pm j1.3854)(s + 3.7168 \pm j1.2011)} \quad (V-A-3.2)$$

With $S = j\omega$, the magnitude and angle of equation V-A-3.2 were calculated using a digital computer program with ω varying between 0.1 rad/sec and 100 rad/sec. The results of this program with angles in the neighborhood of -180° are given in Table V-A-3.1. These results are plotted on the gain-phase of Figure V-A-3.2.

TABLE V-A-3.1

| ω | $ G'H(j\omega) $ db | $\angle G'H(j\omega)$ deg |
|----------|---------------------|---------------------------|
| 1.60 | 21.65 | -182.57 |
| 1.61 | 21.46 | -181.51 |
| 1.62 | 21.27 | -180.50 |
| 1.63 | 21.08 | -179.54 |
| 1.64 | 20.89 | -178.64 |
| 1.65 | 20.71 | -177.79 |
| 3.30 | 4.903 | -179.02 |
| 3.35 | 4.605 | -179.72 |
| 3.36 | 4.556 | -179.86 |
| 3.37 | 4.498 | -179.995 |
| 3.38 | 4.441 | -180.134 |
| 3.39 | 4.384 | -180.27 |
| 3.40 | 4.327 | -180.41 |

Values of the $1/G_D$ locus are given in the two areas of interest in Table V-A-3.2. These values are calculated from Equation I-A-3.1.

TABLE V-A-3.2

| R | G_D | $1/G_D$ db |
|-------|---------|------------|
| 0.060 | 0.07635 | 22.34 |
| 0.066 | 0.08397 | 21.52 |
| 0.068 | 0.08651 | 21.26 |
| 0.070 | 0.08905 | 21.01 |
| 0.072 | 0.09159 | 20.53 |
| 0.074 | 0.09413 | 20.53 |
| 0.46 | 0.5643 | 4.969 |
| 0.47 | 0.5756 | 4.798 |
| 0.48 | 0.5868 | 4.630 |
| 0.484 | 0.5935 | 4.532 |
| 0.488 | 0.5957 | 4.499 |
| 0.490 | 0.5979 | 4.467 |
| 0.50 | 0.6090 | 4.308 |

By interpolation of Figure V-A-3.2 and the tables, two limit cycles are seen to exist at

$$\omega_1 = 1.625 \text{ rad/sec}$$

$$R_1 = 0.0686$$

$$X_{1\max} = 43.7 \text{ volts}$$

and

$$\omega_2 = 3.37 \text{ rad/sec}$$

$$R_2 = 0.488$$

$$X_{2\max} = 6.15 \text{ volts}$$

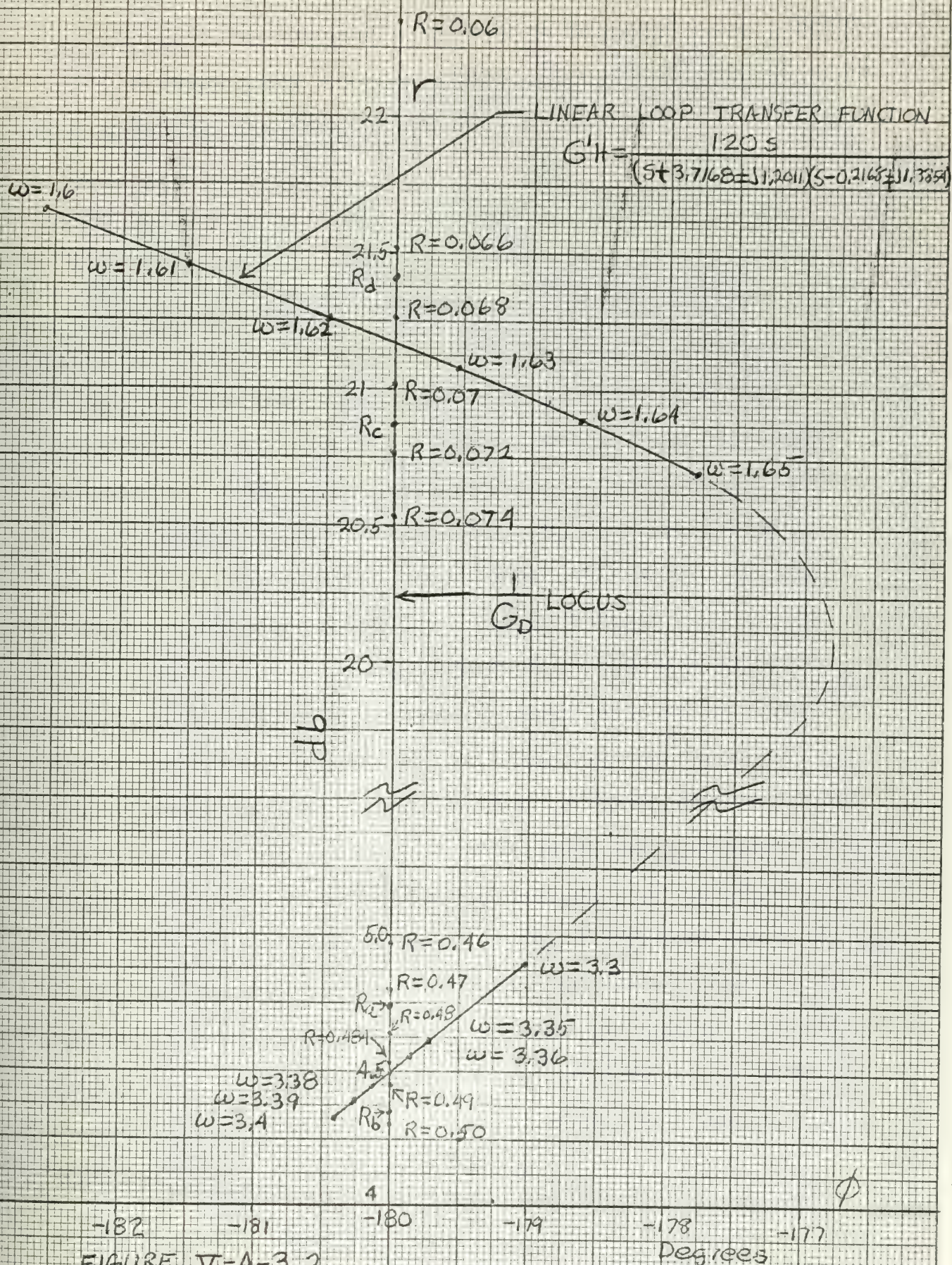


FIGURE V-A-3.2

GAIN-PHASE PLANE - SATURATION IN TACHOMETER CHANNEL

To determine the approximate amplitude of the output angle, sinusoidal variations of the signal X must be assumed. Thus equation V-A-1.11 can be used to give, for the limit cycle at $\omega_1 = 1.625$ rad/sec

$$\theta_{01\max} = 4.48 \text{ volts}$$

and for the limit cycle at $\omega_2 = 3.37$ rad/sec

$$\theta_{02\max} = 0.304 \text{ volts.}$$

The describing function method predicts a stable limit cycle at $\omega_2 = 3.37$ rad/sec and an unstable limit cycle at $\omega_1 = 1.625$ rad/sec. At $\omega_2 = 3.37$ the limit cycle is determined to be stable by applying the same reasoning given in Chapter I, Section I-A-3 to Figure V-A-3.2 using the signal X . At $\omega_1 = 1.625$ the limit cycle is determined to be unstable by the following reasoning. If the input, θ_i , is large enough to cause the first peak of signal X to be large R will be small and the instantaneous critical point will lie at say R_d in Figure V-A-3.2. The system is unstable due to a negative phase margin and the oscillations increase. As the oscillations increase, R becomes even smaller driving the critical point farther up the -180° axis and increasing the negative phase margin. Thus the system is always unstable and the oscillations increase indefinitely. If θ_i is small enough such that the first peak of signal X is small enough, the instantaneous critical point will lie at say R_c of Figure V-A-3.2. The system is stable due to positive phase margin and the oscillations decrease. As the oscillations decrease R becomes smaller driving the critical point down the -180° axis and increasing the positive phase margin. Eventually the positive phase margin begins to decrease due to the shape of the $G'H(j\omega)$ curve and the system reverts to the stable limit cycle at $\omega_2 = 3.37$ rad/sec.

V-A-4 Analog Computer Simulation.

The analog computer simulation of the given system is shown in Figure V-A-4.1. The coefficient pot settings and the associated resistances and capacitances for real time and magnitude scaling are given in Table V-A-4.1.

TABLE V-A-4.1

| Pot Setting | Associated Elements |
|-------------------------------|--|
| | For input of E_i Volts and $K_e = 1.5$ |
| $a_1 = \frac{0.75 E_i}{100}$ | $R_1 = 0.5 \text{ Meg}, \quad R_{f1} = 1 \text{ Meg}$ |
| $a_2 = 0.75$ | $R_2 = 0.5 \text{ Meg}, \quad R_{f1} = 1 \text{ Meg}$ |
| $a_3 = 1.0$ | $R_3 = 1 \text{ Meg}, \quad R_{f2} = 1 \text{ Meg}$ |
| $a_4 = 1.0$ | $R_4 = 1 \text{ Meg}, \quad R_{f2} = 1 \text{ Meg}$ |
| $a_5 = 1.0$ | $R_5 = 1 \text{ Meg}, \quad C_{f1} = 1 \text{ uf}$ |
| $a_6 = 1.0$ | $R_6 = 1 \text{ Meg}, \quad C_{f1} = 1 \text{ uf}$ |
| $a_7 = 1.0$ | $R_7 = 0.5 \text{ Meg}, \quad C_{f2} = 1 \text{ uf}$ |
| $a_8 = 1.0$ | $R_8 = 0.5 \text{ Meg}, \quad C_{f2} = 1 \text{ uf}$ |
| $a_9 = 1.0$ | $R_9 = 0.1 \text{ Meg}, \quad C_{f3} = 1 \text{ uf}$ |
| $a_{10} = 0.4$ | $R_{10} = 0.1 \text{ Meg}, \quad C_{f3} = 1 \text{ uf}$ |
| $a_{11} = 1.0$ | $R_{11} = 1 \text{ Meg}, \quad R_{f3} = 1 \text{ Meg}$ |
| $a_{12} = 0.6$ | $R_{12} = 0.1 \text{ Meg}, \quad R_{f4} = 1 \text{ Meg}$ |
| $a_{13} = 1.0$ | $R_{13} = 1 \text{ Meg}, \quad R_{f5} = 1 \text{ Meg}$ |
| $a_{14} = 1.0$ | $R_{14} = 1 \text{ Meg}, \quad C_{f4} = 1 \text{ uf}$ |
| $a = 0.03$ Initial Setting | For a 3 Volt Saturation Voltage |

To accurately set the back-bias pots "a", a sine wave generator was connected to the input of the nonlinearity simulation and the output monitored. Pots "a" were then adjusted until the output was limited to

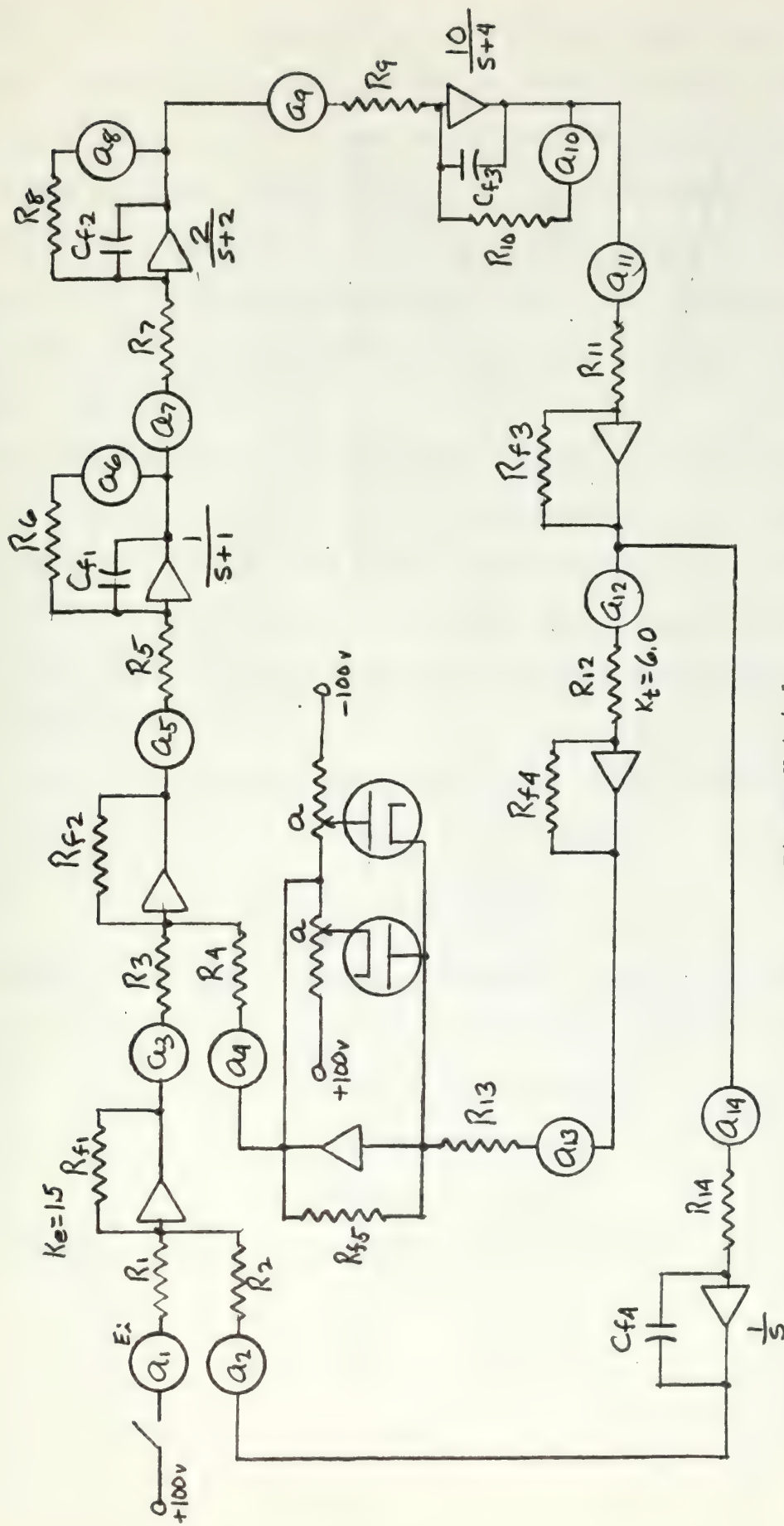


Figure V-A-4.1

Analog Computer Simulation of Saturation in Velocity Feedback Path

3 volts. The static characteristic curve is the same as that in Figure I-A.4.2, except the saturation voltage is 3 volts instead of 5 volts.

A step input signal of 1 volt was first impressed on the system and the system was found to build up into the limit cycle shown in recorder trace V-A-4.1. A step input signal of 5.8 volts was then impressed and the system was found to go into the same limit cycle as shown in recorder trace V-A-4.2. An expanded portion of the stable limit cycle is shown in recorder trace V-A-4.3.

A visual presentation of the unstable limit cycle was difficult to obtain. For a step input of 6.21 volts the system was only slightly damped before reverting to the stable limit cycle as shown in recorder trace V-A-4.4. For step input of 6.22 volts the system was slightly unstable with the oscillations eventually increasing indefinitely as shown in recorder trace V-A-4.5.

From the recorder traces, the stable limit cycle was determined to be,

$$\omega_2 = 3.35 \text{ rad/sec}$$

$$X_{1\max} = 6.2 \text{ volts}$$

$$\theta_{01\max} = 0.30 \text{ volts.}$$

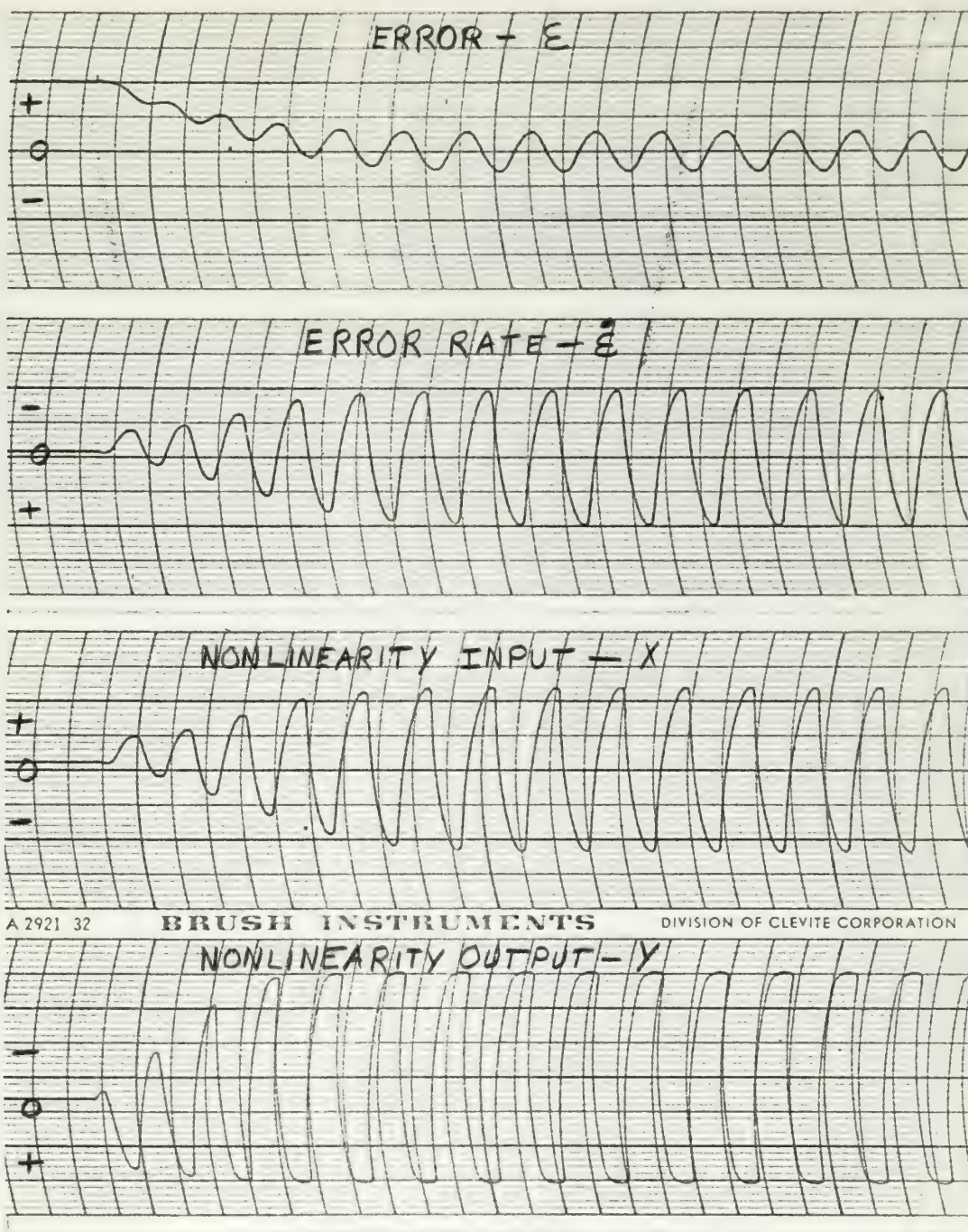
The unstable limit cycle was determined by averaging recorder traces V-A-4.4 and V-A-4.5 with measurements taken on the first few cycles only,

$$\omega_1 = 1.618 \text{ rad/sec}$$

$$X_{1\max} = 42.3 \text{ volts}$$

$$\theta_{01\max} = 4.29 \text{ volts.}$$

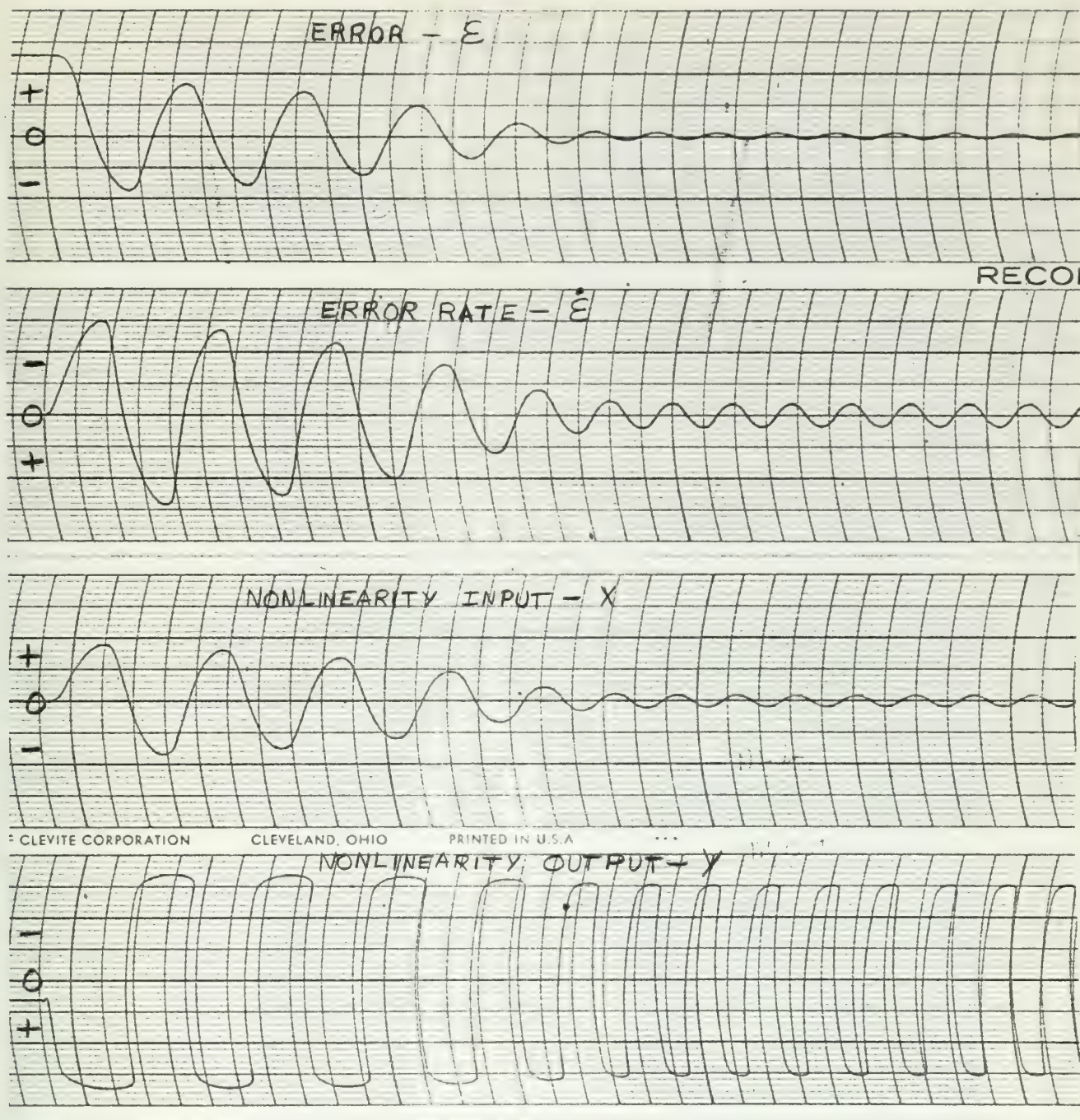
The phase portrait of the system is shown in Figure V-A-4.2.



Recorder Trace V-A-4.1

Saturation in Velocity Feedback Path, 1 Volt Step Input.

SCALES; E - 0.1 Volts/Line \dot{E} - 0.1 Volts/Line X - 0.5 Volts/Line
 Y - 0.2 Volts/Line Time - 1 Second/Division

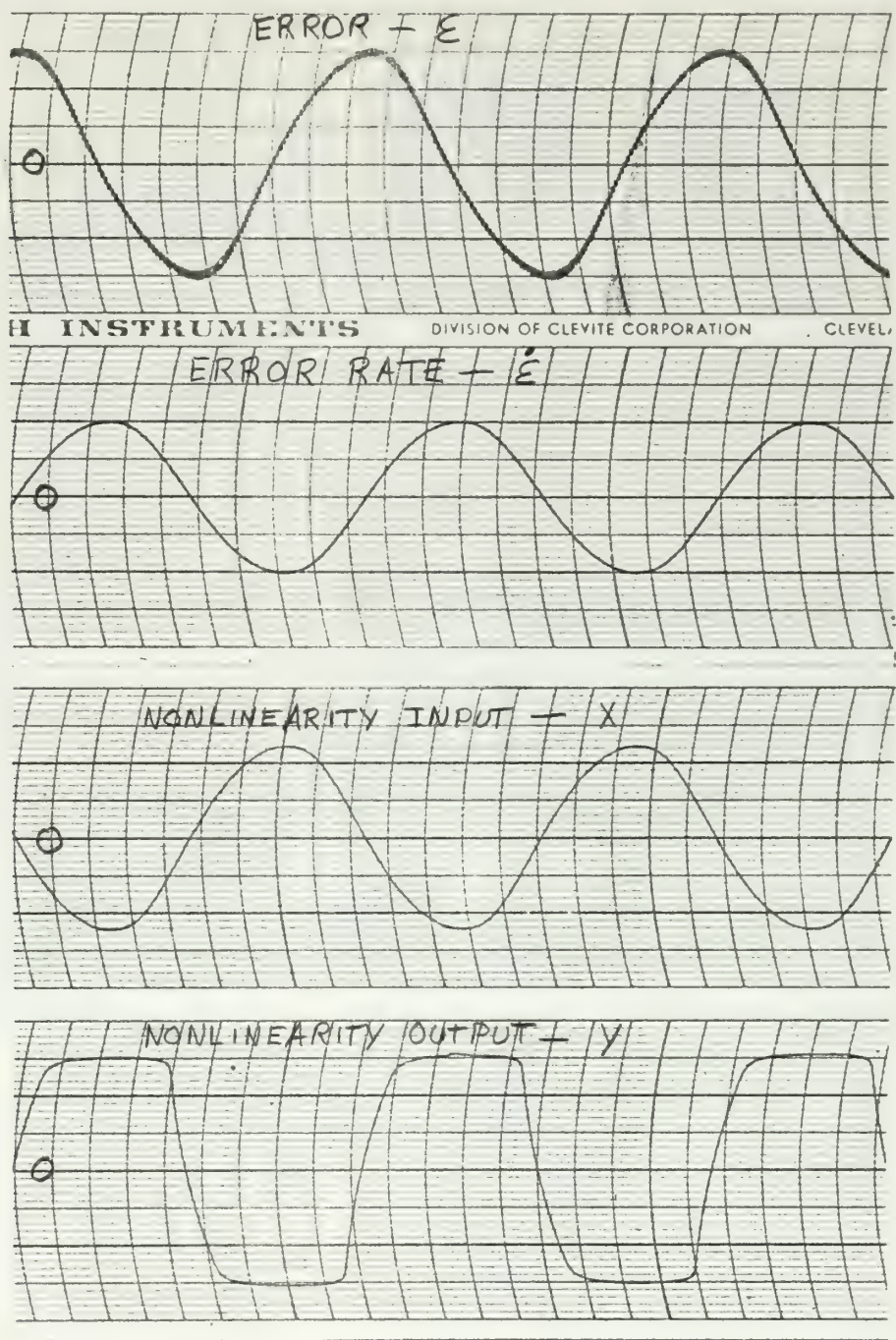


Recorder Trace V-A-4.2

Saturation in Velocity Feedback Path, 5.8 Volt Step Input.

SCALES: ϵ - 0.5 Volts/Line $\dot{\epsilon}$ - 0.5 Volts/Line X - 5 Volts/Line

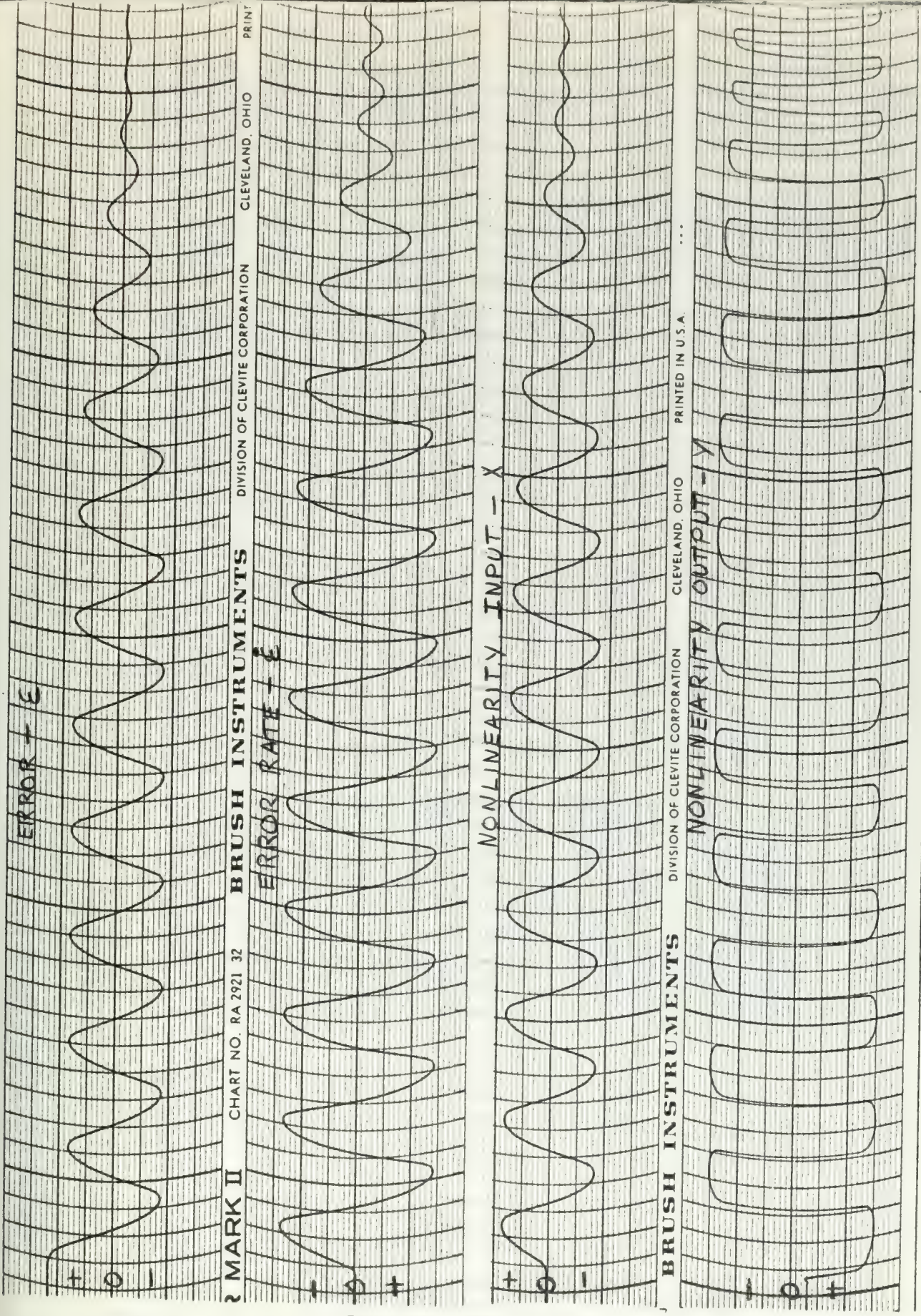
Y - 0.2 Volts/Line Time - 1 Second/Division



Recorder Trace V-A-4.3

Saturation in Velocity Feedback Path, Limit Cycle.

SCALES: E - 0.02 Volts/Line \dot{E} - 0.1 Volts/Line X - 0.5 Volts/Line
 Y - 0.2 Volts/Line Time - 0.2 Seconds/Division



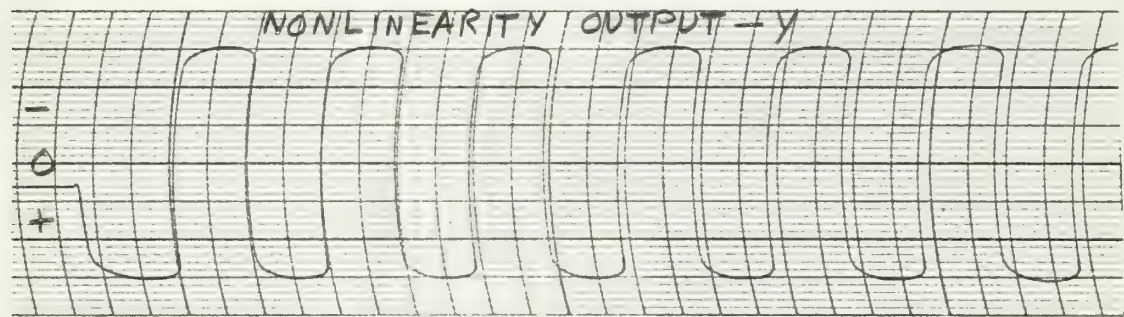
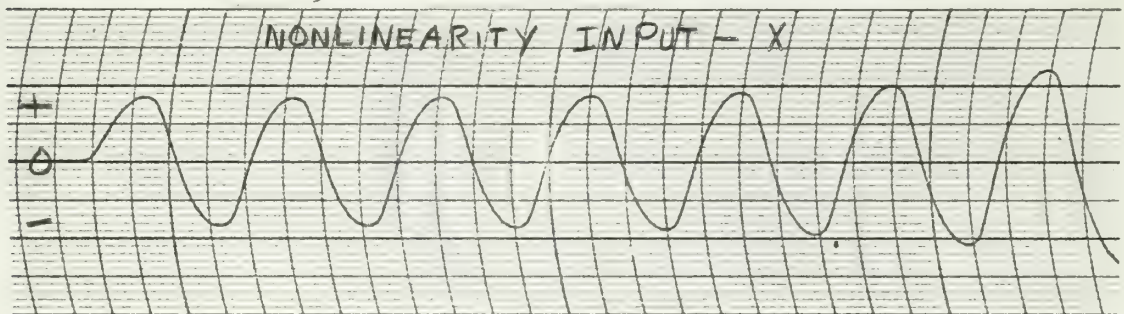
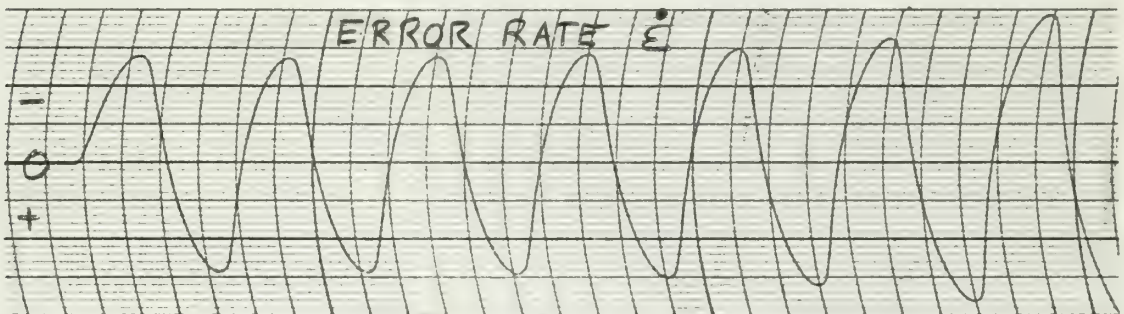
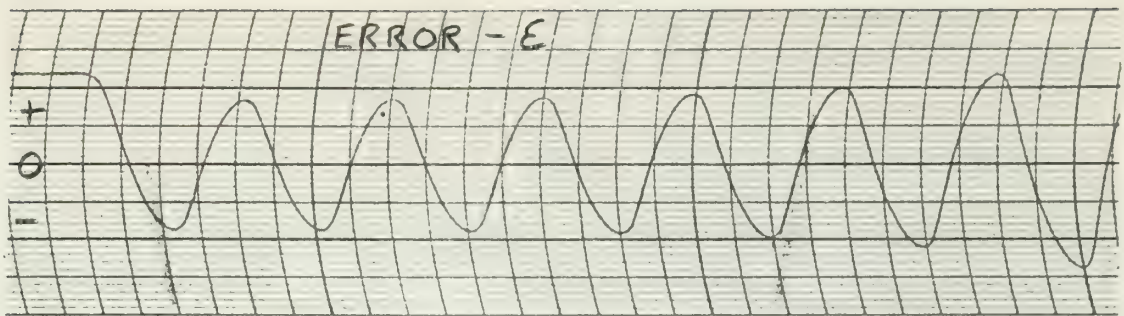
MARK II CHART NO. RA 2921 32 BRUSH INSTRUMENTS DIVISION OF CLEVITE CORPORATION CLEVELAND, OHIO PRINT

BRUSH INSTRUMENTS DIVISION OF CLEVITE CORPORATION CLEVELAND, OHIO PRINTED IN U.S.A.

Recorder Trace V-A-4.4

Saturation in Velocity Feedback Path, 6.21 Volts Step Input.

SCALES: E - 0.5 Volts/Line \dot{E} - 0.5 Volts/Line X - 5 Volts/Line
 Y - 0.2 Volts/Line Time - 1 Second/Division



Recorder Trace V-A-4.5

Saturation in Velocity Feedback Path, 6.22 Volts Step Input.

SCALES: E - 0.5 Volts/line \dot{E} - 0.5 Volts/line X - 5 Volts/line
 Y - 0.2 Volts/line Time - 1 Second/Division

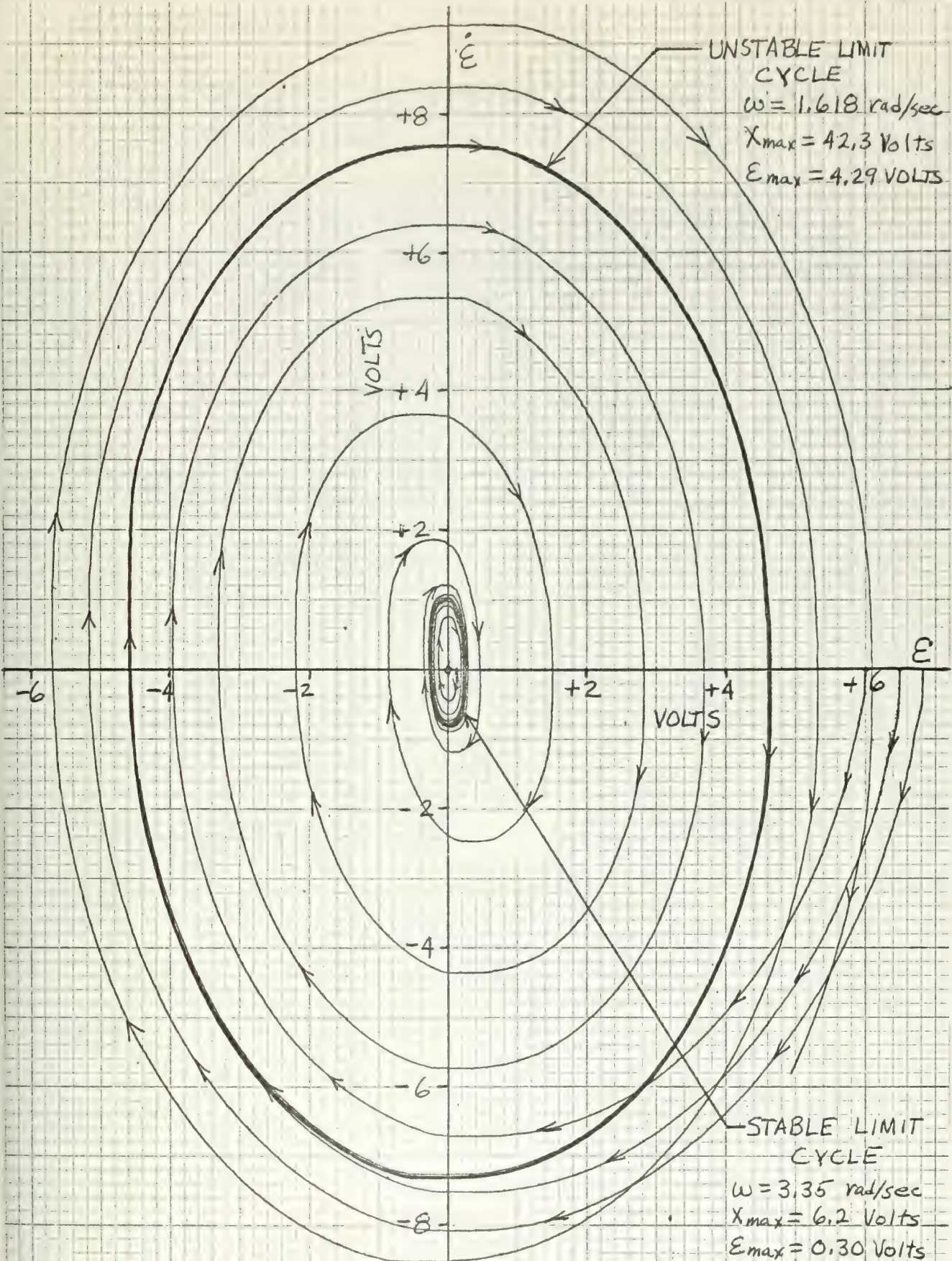


FIGURE V-A-4.2

PHASE PORTRAIT - SATURATION IN TACHOMETER CHANNEL

V-A-5 Comparison of the Four Methods in Predicting Limit Cycles of the System of Figure V-2.

| Method | Angular Frequency | | Amplitude (volts) | | | |
|---------------------|-------------------|----------|-------------------|----------|--------|----------|
| | rad/sec | | X max | | E max | |
| | Stable | Unstable | Stable | Unstable | Stable | Unstable |
| Mitrovic's | 3.37 | 1.618 | 5.03 | 34.33 | 0.249 | 3.52 |
| Root Locus | 3.37 | 1.618 | 5.03 | 34.33 | 0.249 | 3.52 |
| Describing Function | 3.37 | 1.618 | 6.17 | 43.7 | 0.304 | 4.48 |
| Analog Simulation | 3.35 | 1.618 | 6.2 | 42.3 | 0.30 | 4.29 |

V-B Saturation in Acceleration Feedback Path.

The system chosen to analyze is shown in Figure V-B.

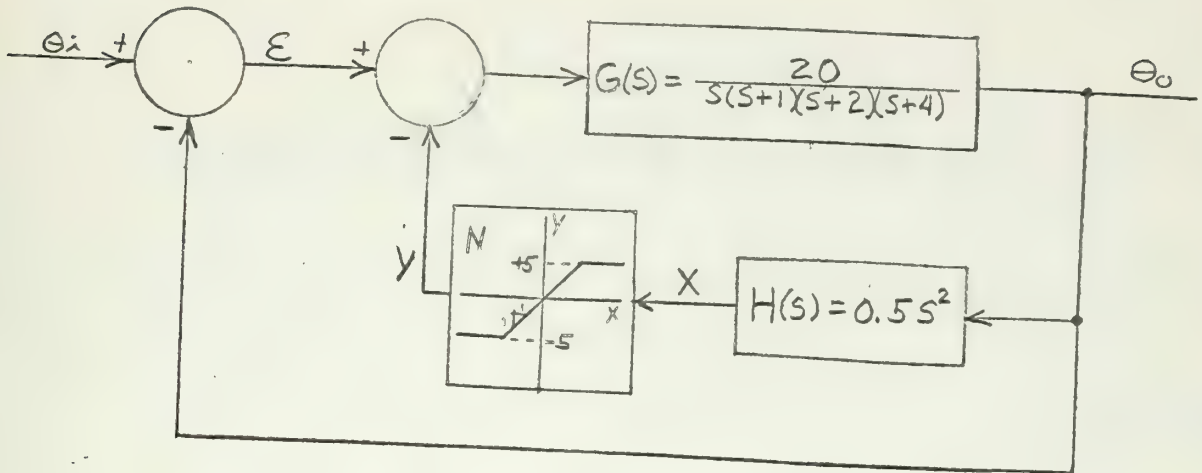


Figure V-B

Saturation in Acceleration Feedback Path

V-B-1. Mitrovic's Method.

Assigning N as the gain of the non-linearity the characteristic equation is:

$$s^4 + 7s^3 + (14 + 10N)s^2 + 8s + 20 = 0 \quad (V-B-1.1)$$

Assuming the s^1 and s^2 coefficients to be variable the characteristic equation becomes

$$s^4 + 7s^3 + B_2s^2 + B_1s + 20 = 0 \quad (V-B-1.2)$$

where

$$B_1 = 8 \quad (V-B-1.3)$$

and

$$B_2 = 14 + 10N \quad (V-B-1.4)$$

From Appendix A, Mitrovic's equations for B_1 and B_2 are

$$B_1 = \frac{1}{\omega_n} [20\phi_2(\gamma) - 7\omega_n^3\phi_1(\gamma) - \omega_n^4\phi_2(\gamma)] \quad (\text{V-B-1.5})$$

and

$$B_2 = \frac{1}{\omega_n^2} [-20\phi_1(\gamma) + 7\omega_n^3\phi_2(\gamma) + \omega_n^4\phi_3(\gamma)] \quad (\text{V-B-1.6})$$

Substitution of the B functions from Appendix A for $\gamma = 0$ gives the parametric equations of the stability curve as

$$B_1 = -\omega_n^2 \quad (\text{V-B-1.7})$$

and

$$B_2 = \frac{20}{\omega_n^2} + \omega_n^4. \quad (\text{V-B-1.8})$$

The shape of the stability curve in the B_1 versus B_2 plane is not easily recognized. However, at the intersection of the stability curve and the M-point locus, equation V-B-1.7 must equal equation V-B-1.3 or

$$7\omega_n^2 = 8$$

from which the frequency of the limit cycle is determined to be

$$\omega_n = 1.067 \text{ rad/sec.}$$

Also at the intersection equation V-B-1.8 must equal equation V-B-1.4 or

$$14 + 10N = \frac{20}{\omega_n^2} + \omega_n^4.$$

Substitution of ω yields the average gain of the nonlinearity over a cycle of

$$N_{avg} = 0.4674$$

from which the approximate amplitude of signal x is determined to be

$$X_{\max} = 10.82 \text{ volts}$$

To obtain an approximate amplitude of the angular oscillations, one must assume X to be sinusoidal. Then the amplitude of the error signal may be determined by

$$\varepsilon_{\max} = \frac{X_{\max}}{0.5 \omega_n^2} \quad (\text{V-B-1.9})$$

or

$$\varepsilon_{\max} = 18.94 \text{ volts.}$$

The graphical solution by Mitrovic's method is sketched in Figure V-B-1.1.

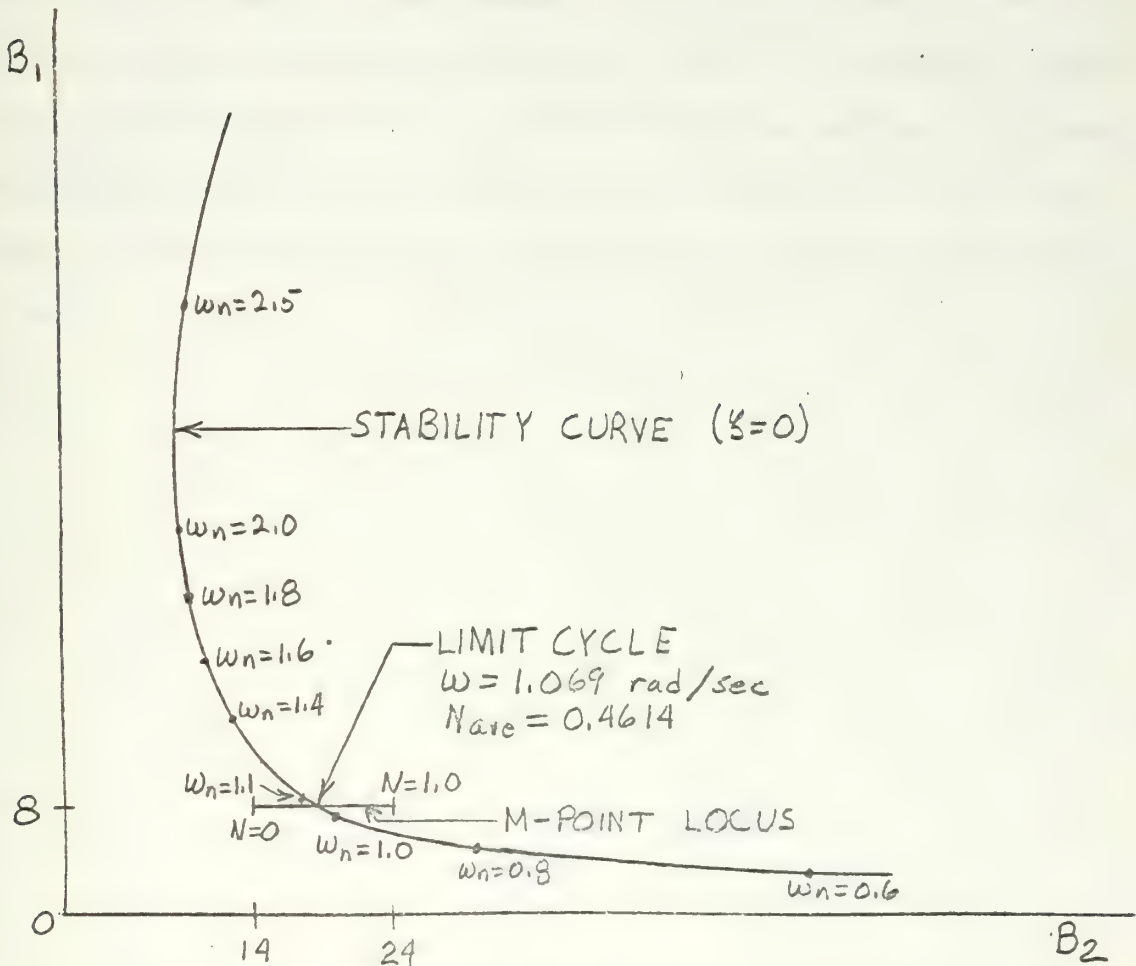


FIGURE V-B-1.1
GRAPHICAL SOLUTION OF SATURATION IN
ACCELERATION FEEDBACK PATH

Mitrovic's method predicts an unstable limit cycle by the following reasoning. If the input signal is large enough such that the first peak of signal X is large enough, the instantaneous nonlinear gain will be small enough to place the M-point at M_a in Figure V-B-1.1 the system is unstable and the oscillations increase. As the oscillations increase N decreases moving the M-point further into the unstable region. Thus the average M-point can never be in the stable region and the oscillations increase indefinitely. If the input signal is small enough such that the first peak of signal X is small enough, N will be relatively large placing the instantaneous M-point at M_b in figure V-B-1.1. The system is stable and the oscillations decrease. As the oscillations decrease N increases approaching one and moving the average M-point farther into the stable region. Thus the system is always stable and all oscillations eventually die out.

V-B-2. Root Locus Method.

Substitution of $S = j\omega$ into the characteristic equation and evaluation of the higher powers of j yields

$$\omega^4 - j7\omega^3 - (14 + 10N)\omega^2 + j8\omega + 20 = 0. \quad (\text{V-B-1.1})$$

Requiring that both the real and imaginary parts of equation V-B-1.1 go to zero independently

$$\omega^4 - (14 + 10N)\omega^2 + 20 = 0 \quad (\text{V-B-1.2})$$

and

$$-j7\omega^3 + 8\omega = 0. \quad (\text{V-B-1.3})$$

By dividing equation V-B-1.3 by $j\omega$, the frequency of the limit cycle is obtained directly as

$$\omega = \sqrt{8/7} = 1.069 \text{ rad/sec.}$$

Substituting ω into equation V-B-1.2, the average gain of the non-linearity is obtained as

$$N_{\text{ave}} = 0.4614$$

from which the approximate amplitude of signal X is obtained as

$$X_{\text{max}} = 10.82 \text{ volts.}$$

To get the approximate amplitude of the error signal, X is assumed sinusoidal and equation V-B-1.9 is used,

$$e_{\text{max}} = 18.94 \text{ volts.}$$

The root locus solution is sketched in Figure V-B-2.1. Before sketching the figure, the unity feedback loop was first reduced and the poles of the reduced transfer function were used as the poles of the equivalent loop transfer function.

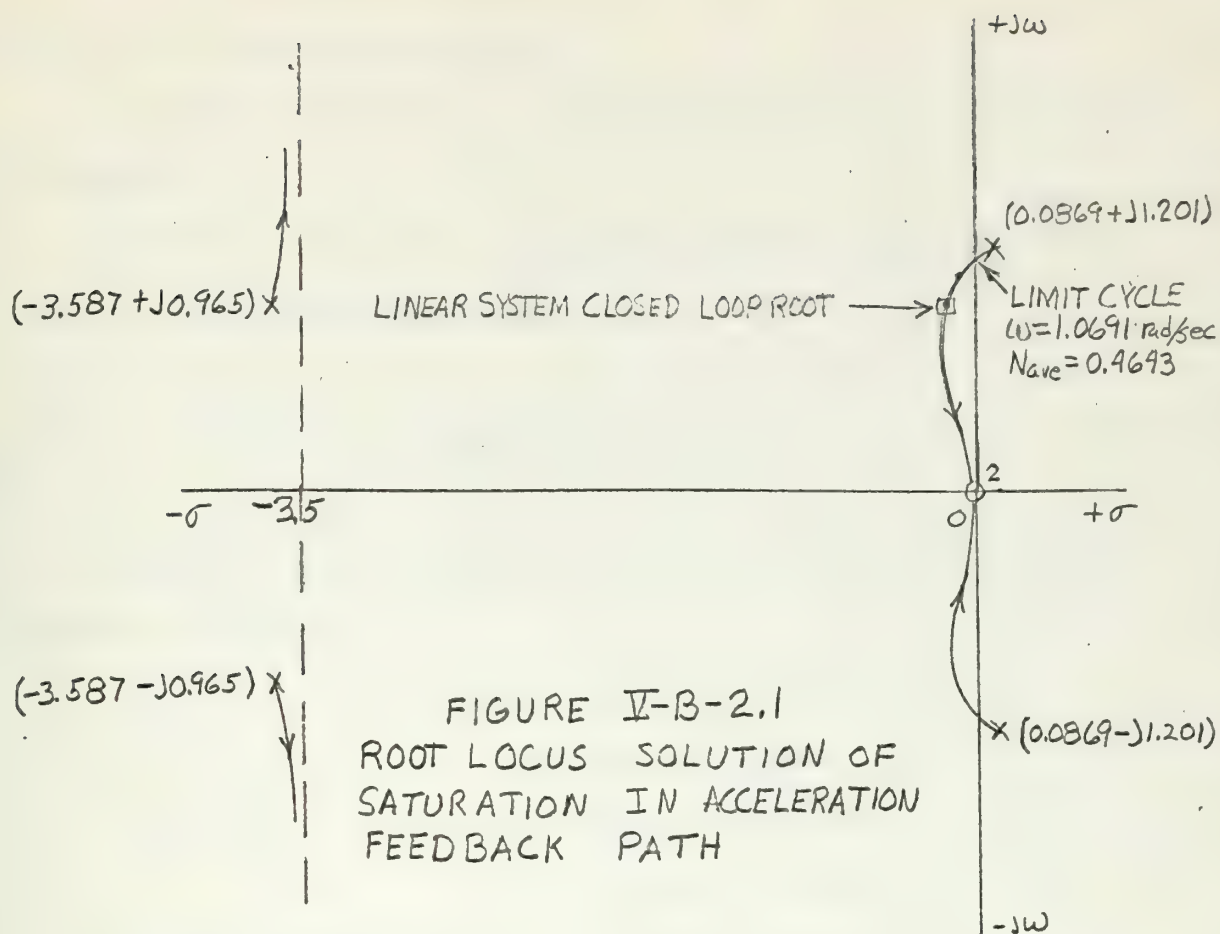


FIGURE V-B-2.1
ROOT LOCUS SOLUTION OF
SATURATION IN ACCELERATION
FEEDBACK PATH

The root locus predicts an unstable limit cycle by applying the same reasoning given in Section V-A-2 to Figure V-B-2.1.

V-B-3. Describing Function Method.

The describing function for saturation is given in equation I-A-3.1 of Chapter I.

To obtain an equivalent loop transfer function the unity feedback loop was first reduced which gives,

$$G'(s) = \frac{20}{s^4 + 7s^3 + 14s^2 + 8s + 20} \quad . \quad (V-B-3.1)$$

A digital computer program was used to find the roots of the denominator of $G'(s)$.

$$r_1 = 0.0869 + j 1.201$$

$$r_2 = 0.0869 - j 1.201$$

$$r_3 = -3.5869 + j 0.9652$$

$$r_4 = -3.5689 - j 0.9652$$

Thus the equivalent open loop transfer function becomes

$$G'H(s) = \frac{10s^2}{(s - 0.0869 \pm j1.201)(s + 3.5869 \pm j0.9652)} \quad , \quad (V-B-3.2)$$

With $s = j\omega$, the magnitude and angle of equation V-B-3.2 were calculated by a digital computer program with ω varying between 0.1 rad/sec and 100 rad/sec. The results of this program with angles in the neighborhood of -180° are given in Table V-B-3.1. These results are also plotted on the gain-phase plane of Figure V-B-3.1 as the linear loop transfer function.

TABLE V-B-3.1

| ω | $ G'H(j\omega) $ db | $\angle G'H(j\omega)$ deg |
|----------|---------------------|---------------------------|
| 1.05 | 5.599 | -182.94 |
| 1.06 | 6.153 | -181.48 |
| 1.07 | 6.721 | -179.83 |
| 1.08 | 7.301 | -177.97 |

The values of $1/G_D$ in the area of interest are given in Table V-B-3.2.

TABLE V-B-3.2

| R | G_D | $1/G_D$ db |
|-------|--------|------------|
| 0.30 | 0.3762 | 8.493 |
| 0.35 | 0.4364 | 7.203 |
| 0.37 | 0.4601 | 6.743 |
| 0.372 | 0.4625 | 6.698 |
| 0.374 | 0.4648 | 6.654 |
| 0.38 | 0.4719 | 6.523 |
| 0.40 | 0.4954 | 6.101 |

By interpolation of Figure V-B-3.1 and the tables, the limit cycle is at

$$\omega = 1.609 \text{ rad/sec}$$

and

$$R = 0.374$$

from which

$$X_{\max} = 13.37 \text{ volts.}$$

To obtain an approximate amplitude of the error signal, X is assumed sinusoidal and equation V-B-1.9 used,

$$\mathcal{E}_{\max} = 23.4 \text{ volts.}$$

The describing function method predicts an unstable limit cycle by applying the same reasoning given in Section V-A-3 to Figure V-B-3.1.

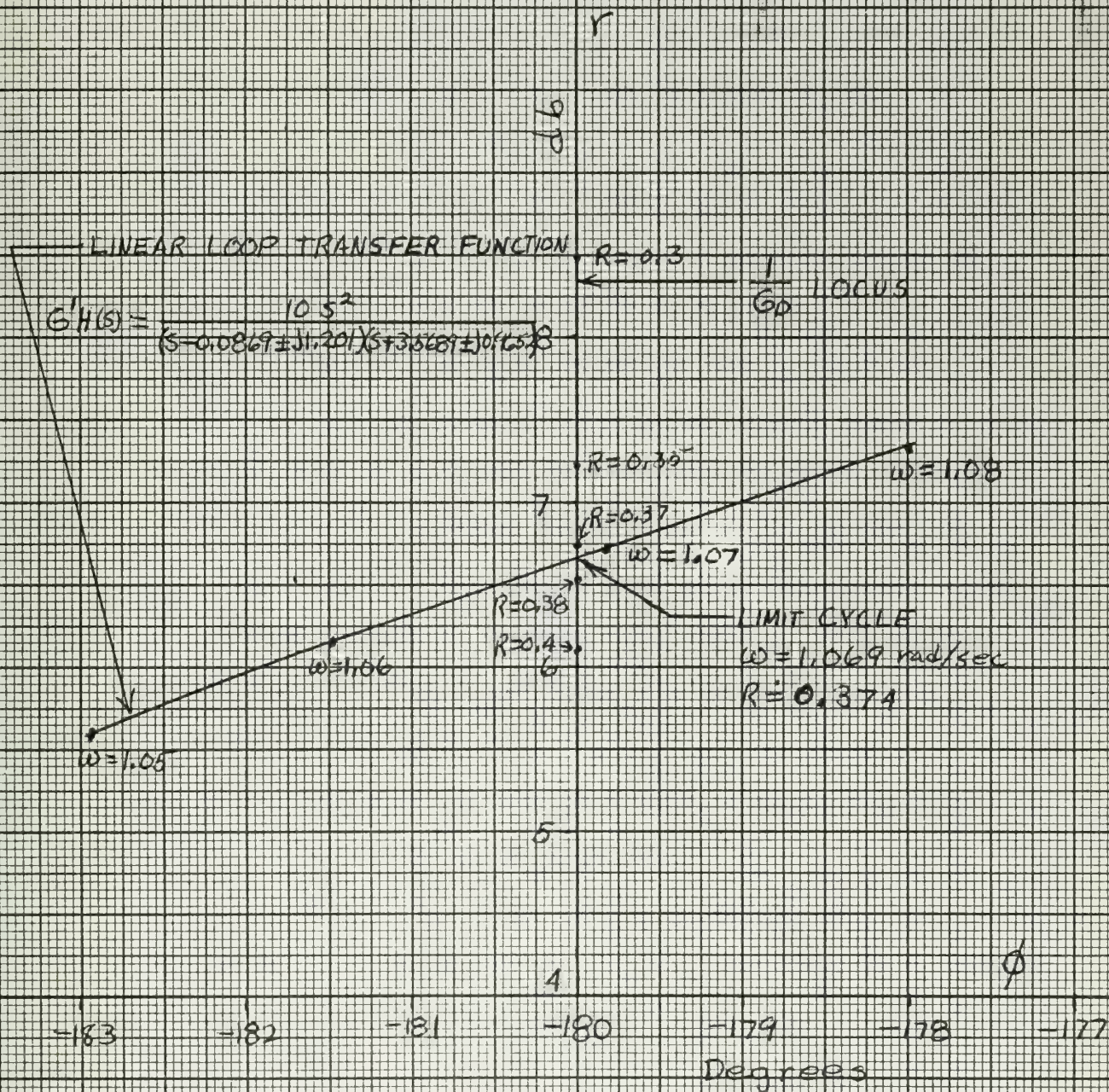


FIGURE V-B-3.1
 SATURATION IN ACCELERATION FEEDBACK PATH

V-B-4. Analog Computer Simulation.

A good simulation of the acceleration signal was difficult to obtain. The simulation that was finally decided upon was to use the velocity signal and approximately differentiate it by simulating $s/(s + 100)$. By using this transfer function an extra gain of 100 had to be simulated in the feedback path in order to maintain the D.C. gain constant of the path unaltered. Thus the simulated gain in the feedback path is $100 K_a$ or 50 instead of 0.5.

The analog computer simulation is shown in Figure V-B-4.1. The coefficient pot settings and associated resistances and capacitances for real time and magnitude scaling are given in Table V-B-4.1.

The diode back-biasing pots were set in the same way described in Chapter I. The static characteristic curve is the same as Figure I-A-4.2.

An input signal of 17 volts was first applied and the system was found to be stable but only slightly damped as shown in recorder trace V-B-4.1. An input signal of 23 volts was then applied and the system was found to be unstable as shown in recorder trace V-B-4.2. The unstable limit cycle was found to occur for an input step of 19.8 volts and is shown in recorder trace V-B-4.3.

From recorder trace V-B-4.3, the limit cycle is determined to have an amplitude of $X_{\max} = 10.6$ volts and a frequency of $\omega = 1.03$ rad/sec.

The phase portrait of the system is shown in Figure V-B-4.2.

The simulation of the acceleration signal is admittedly poor, especially since the amplitude of X differs considerably from that predicted by the describing function.



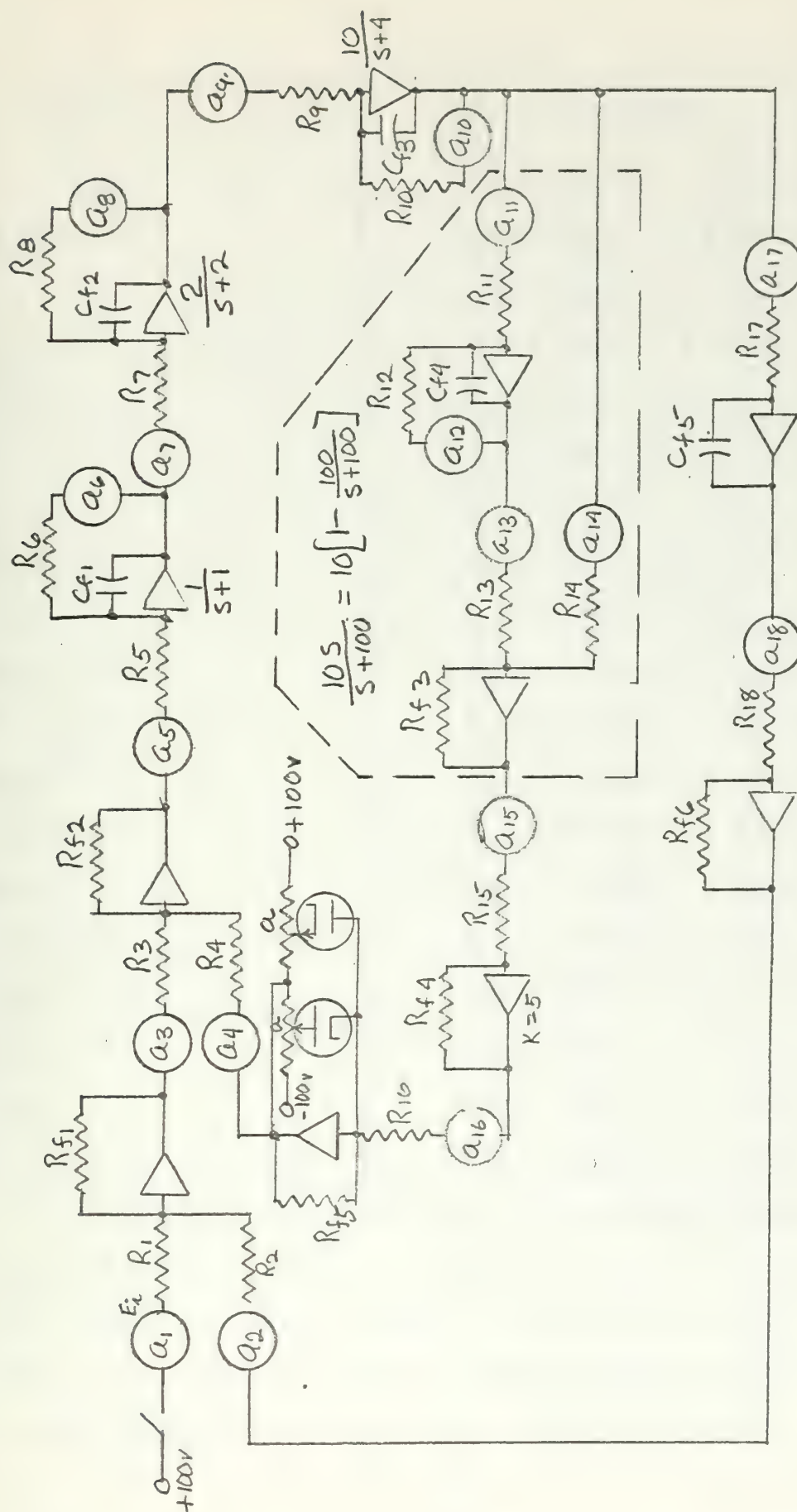


Figure V-B-4.1.
Analog Computer Simulation of Saturation in Acceleration Feedback Path



Table V-B-4.1

| Pot Setting | Associated Elements |
|----------------------------|--|
| $a_1 = \frac{E_i}{100}$ | For a step input of E_i Volts $R_1 = 1 \text{ Meg}, \quad R_{f1} = 1 \text{ Meg}$ |
| $a_2 = 1.0$ | $R_2 = 1 \text{ Meg}, \quad R_{f1} = 1 \text{ Meg}$ |
| $a_3 = 1.0$ | $R_3 = 1 \text{ Meg}, \quad R_{f2} = 1 \text{ Meg}$ |
| $a_4 = 1.0$ | $R_4 = 1 \text{ Meg}, \quad R_{f2} = 1 \text{ Meg}$ |
| $a_5 = 1.0$ | $R_5 = 1 \text{ Meg}, \quad C_{f1} = 1 \text{ uf}$ |
| $a_6 = 1.0$ | $R_6 = 1 \text{ Meg}, \quad C_{f1} = 1 \text{ uf}$ |
| $a_7 = 1.0$ | $R_7 = 0.5 \text{ Meg}, \quad C_{f2} = 1 \text{ uf}$ |
| $a_8 = 1.0$ | $R_8 = 0.5 \text{ Meg}, \quad C_{f2} = 1 \text{ uf}$ |
| $a_9 = 1.0$ | $R_9 = 0.1 \text{ Meg}, \quad C_{f3} = 1 \text{ uf}$ |
| $a_{10} = 0.4$ | $R_{10} = 0.1 \text{ Meg}, \quad C_{f3} = 1 \text{ uf}$ |
| $a_{11} = 1.0$ | $R_{11} = 0.1 \text{ Meg}, \quad C_{f4} = 0.1 \text{ uf}$ |
| $a_{12} = 1.0$ | $R_{12} = 0.1 \text{ Meg}, \quad C_{f4} = 0.1 \text{ uf}$ |
| $a_{13} = 1.0$ | $R_{13} = 0.1 \text{ Meg}, \quad R_{f3} = 1 \text{ Meg}$ |
| $a_{14} = 1.0$ | $R_{14} = 0.1 \text{ Meg}, \quad R_{f3} = 1 \text{ Meg}$ |
| $a_{15} = 0.5$ | $R_{15} = 0.1 \text{ Meg}, \quad R_{f4} = 1 \text{ Meg}$ |
| $a_{16} = 1.0$ | $R_{16} = 1 \text{ Meg}, \quad R_{f5} = 1 \text{ Meg}$ |
| $a_{17} = 1.0$ | $R_{17} = 1 \text{ Meg}, \quad C_{f5} = 1 \text{ uf}$ |
| $a_{18} = 1.0$ | $R_{18} = 1 \text{ Meg}, \quad R_{f6} = 1 \text{ Meg}$ |
| $a = 0.05$ Initial Setting | For a saturation of 5 volts |

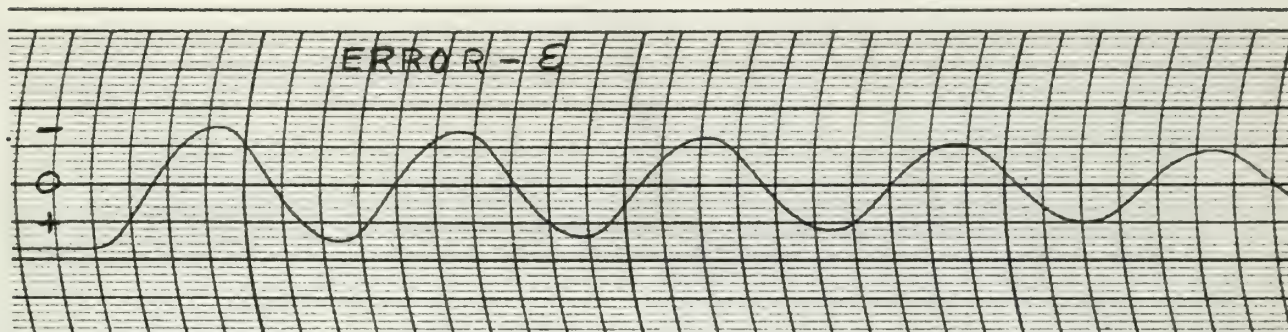
Although the nonlinearity input X is not strictly sinusoidal, it is not too far from a sinusoid. The large discrepancy can not be accounted for solely by wave shape. However, if a root locus solution similar to that of Section V-B-2 is done on the system assuming $50s^2/(s + 100)$ in the inner feedback path the following results are obtained:

$$\omega = 1.0725$$

$$X_{\max} = 13.6$$

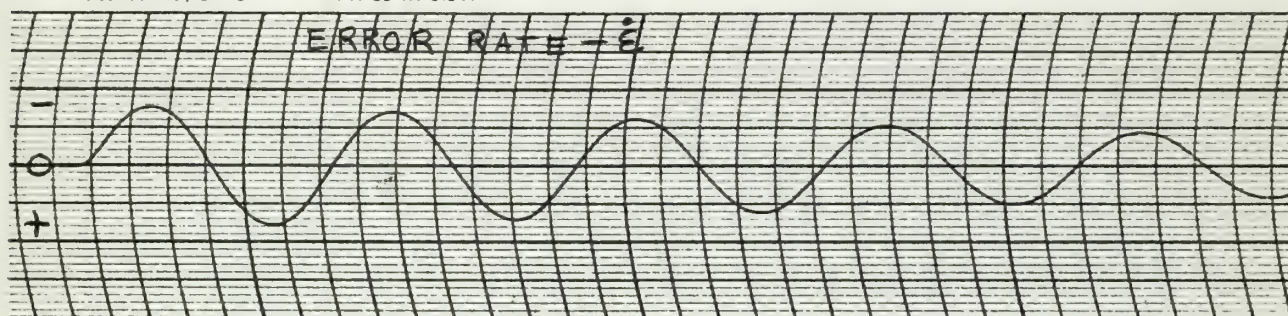
When the results are compared with those of the root locus solution, Section V-B-2, it is seen that the extra pole in the feedback path causes a slight increase in frequency and a significant increase in the approximate amplitude. Consequently, whatever it was in the actual analog simulation that caused the frequency to be less (1.03 rad/sec) than the predicted value (1.069 rad/sec) also caused the amplitude to be considerably less than predicted by the describing function.





CLEVELAND, OHIO

PRINTED IN U.S.A.



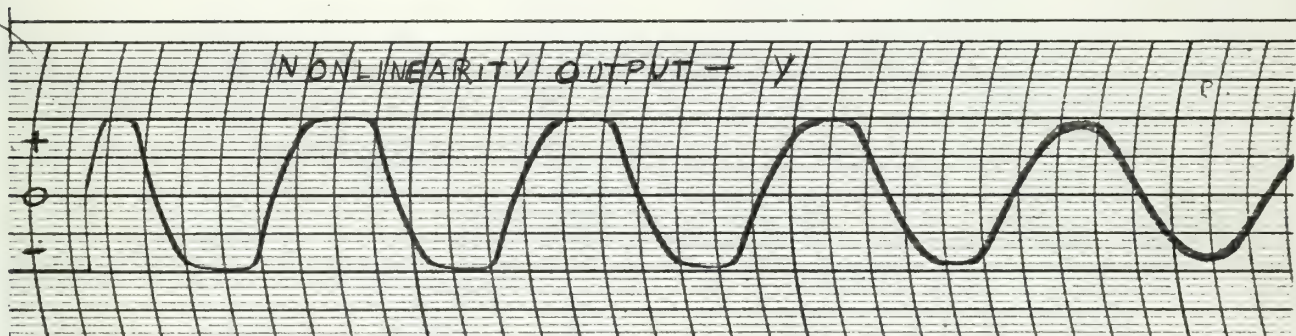
SCALES: E 2 volts/line

\dot{E} - 2 volts/line

y - 0.5 volts/line

X - 1 volt/line

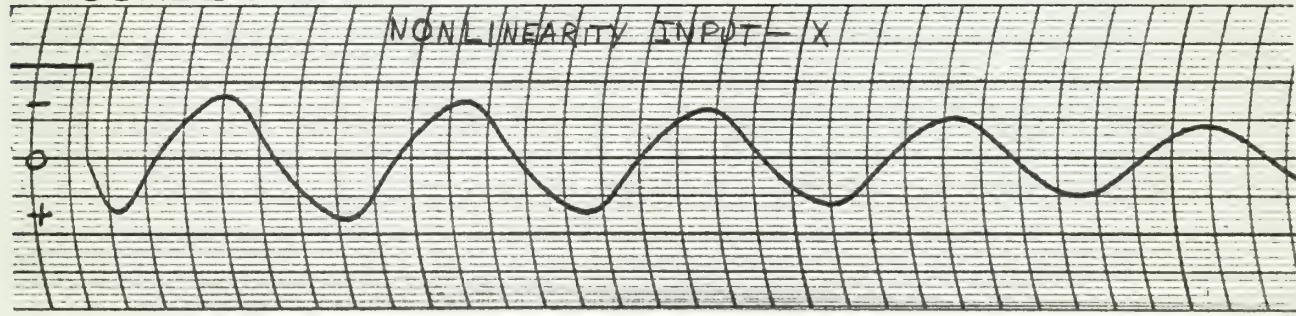
Time - 1 second/division



RECORDER MARK II

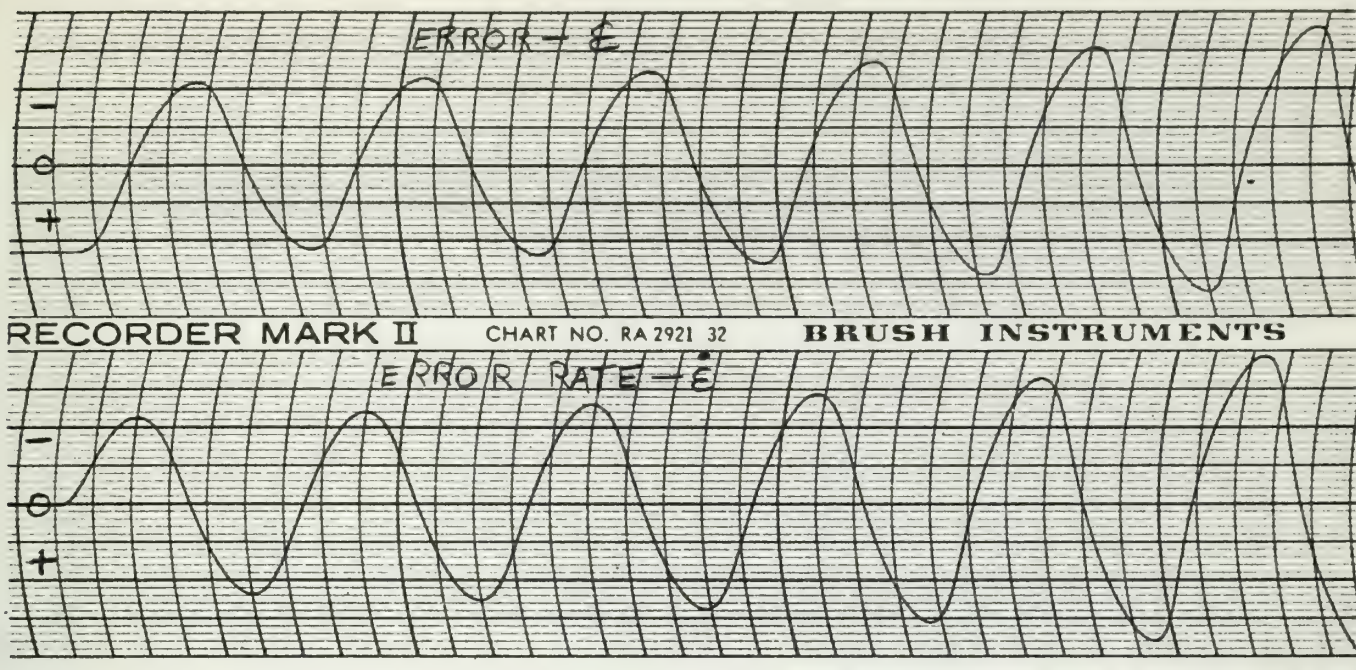
CHART NO. RA 2921 32

BRUSH INSTRUMENTS

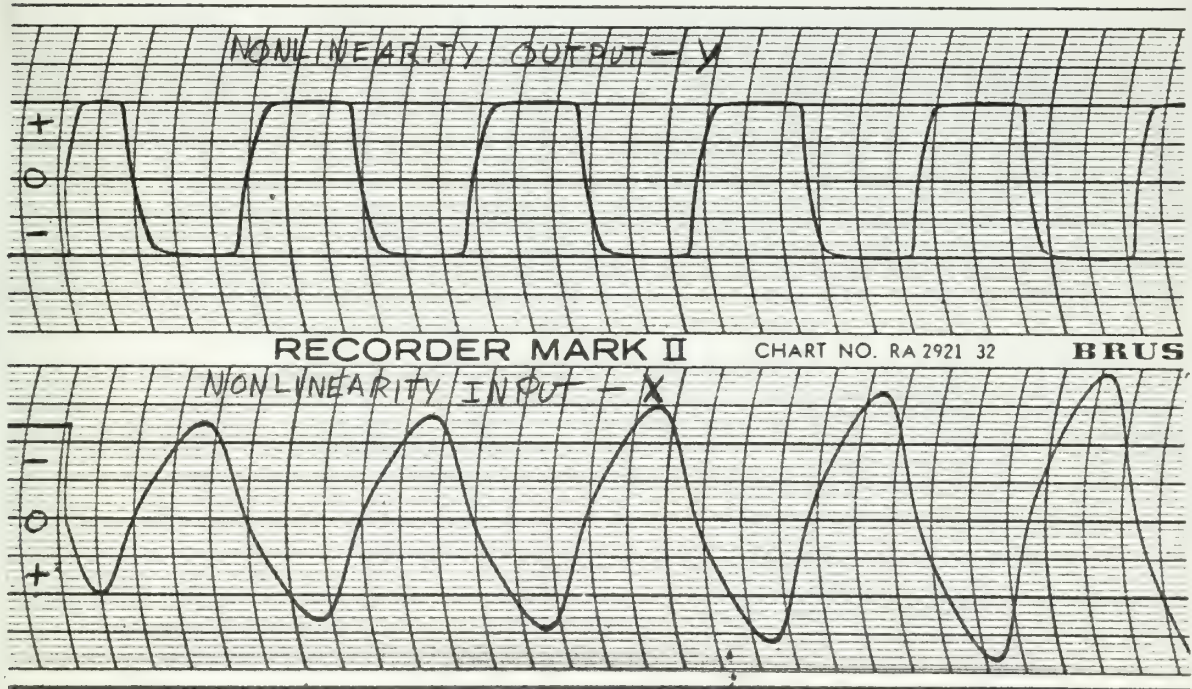


Recorder Trace V-B-4.1

Saturation in Acceleration Feedback Path, 17 volt Step Input



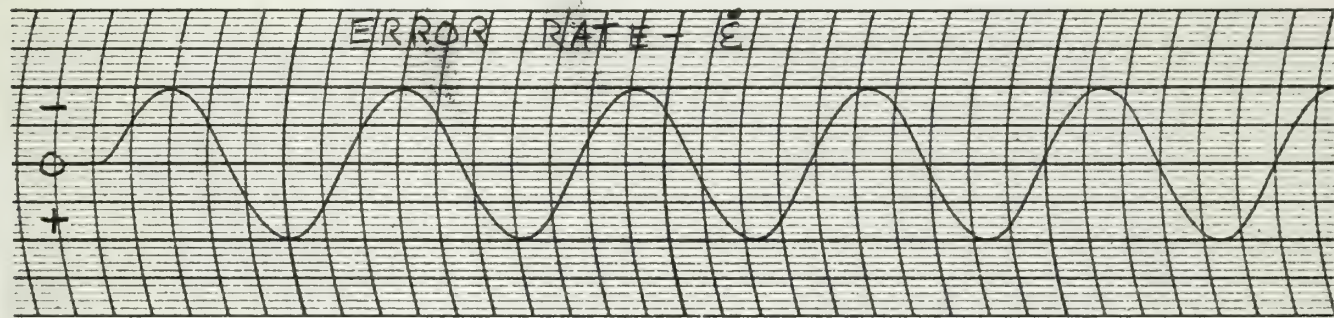
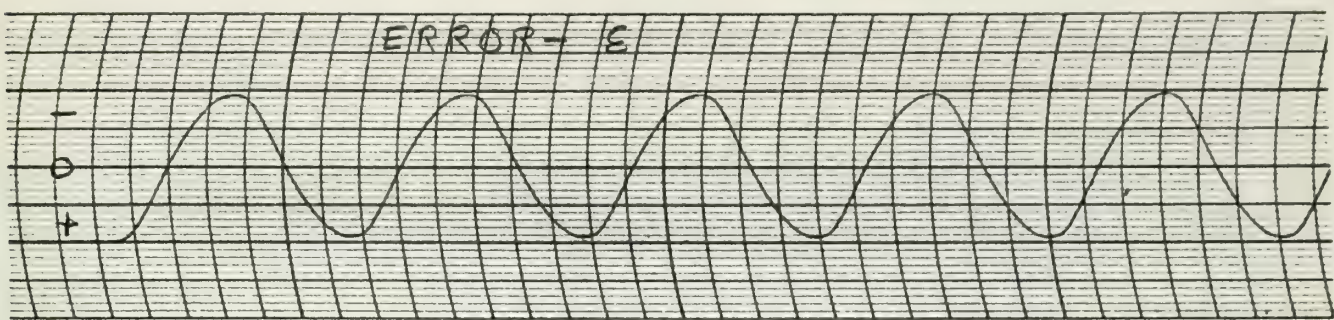
SCALES: ϵ - 2 volts/line $\dot{\epsilon}$ - 2 volts/line
 Y - 0.5 volts/line X - 1 volt/line
 Time - 1 second/division



Recorder Trace V-B-4.2

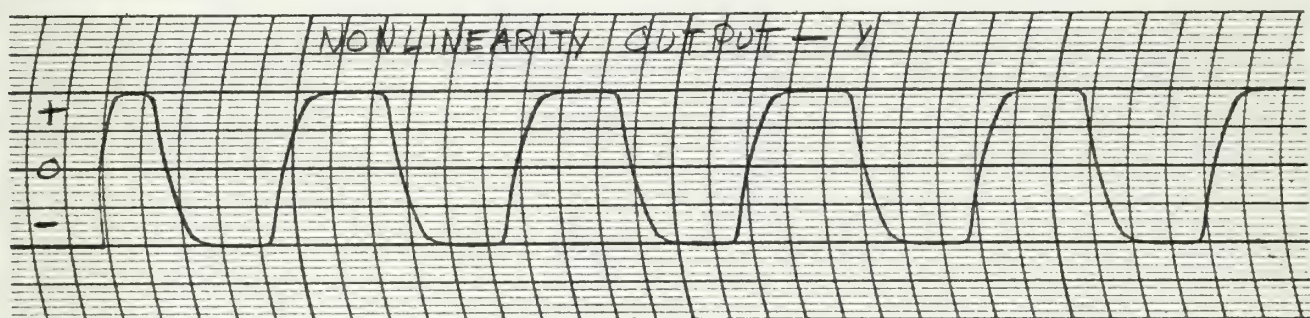
Saturation in Acceleration Feedback Path, 23 volt Step Input



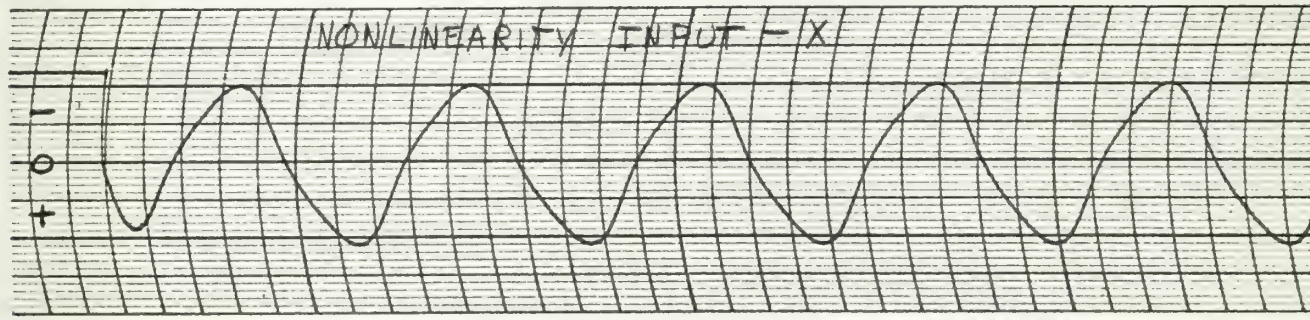


SCALES: E - 2 volts/line \dot{E} - 2 volts/line
 Y - 0.5 volts/line X - 1 volt/line

Time - 1 second/division



ATION CLEVELAND, OHIO PRINTED IN U.S.A. ...



Recorder Trace V-B-4.3

Limit Cycle, Saturation in Acceleration Feedback Path, 19.8 Volts Step Input



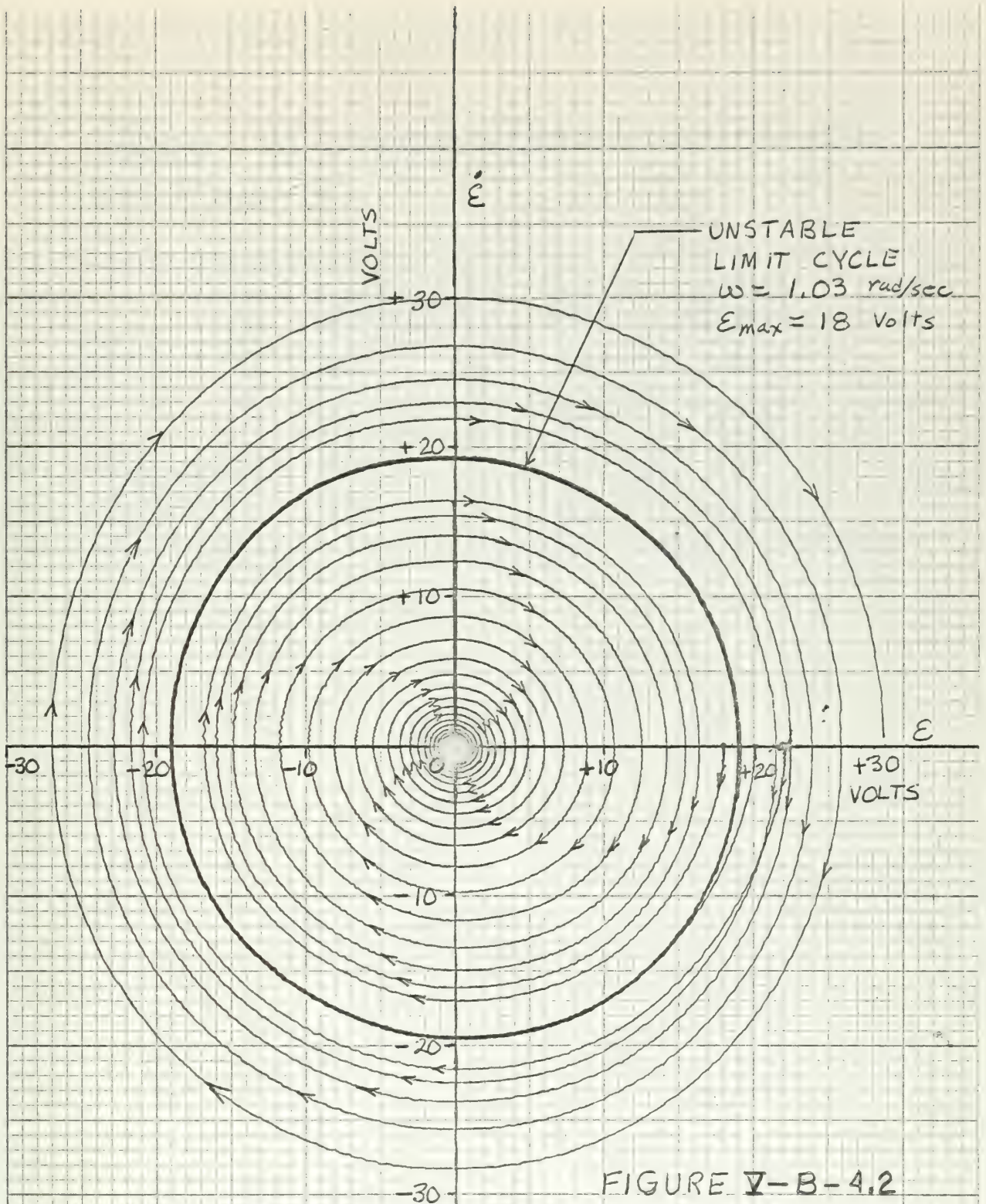


FIGURE V-B-4.2

SATURATION IN ACCELERATION
FEEDBACK PATH, NO ZEROS
IN FORWARD PATHS

$$G(s) = \frac{20}{s(s+1)(s+2)(s+4)}$$



V-B-5. Comparison of the Four Methods in Predicting Limit Cycles of the System of Figure V-B.

| Method | Frequency rad/sec | Amplitude (Volts) | |
|---------------------|----------------------|-------------------|----------------|
| | | X-Max | ϵ Max |
| Mitrovic's | 1.069 | 10.82 | 18.94 |
| Root Locus | 1.069 | 10.82 | 18.94 |
| Describing Function | 1.069 | 13.37 | 23.4 |
| Analog Simulation | 1.03 | 10.6 | 20.0 |



PART II

A STUDY OF LIMIT CYCLES OF A SYSTEM WITH TWO GAIN VARIABLE NONLINEARITIES USING MITROVIC'S METHOD

Introduction

The author had no experience in the problem of a system with two non-linearities and consequently had no idea of what performance to expect. Thus a system was arbitrarily chosen and an analog computer study of the system was started.

The system chosen is shown in Figure VI. This particular configuration was chosen primarily because each of the nonlinear gains appears alone in two of the coefficients of the characteristic equation, which is,

$$s^4 + 7s^3 + 14s^2 + (8 + KK_t N_2)s + KK_e N_1 = 0 \quad (\text{VI-a})$$

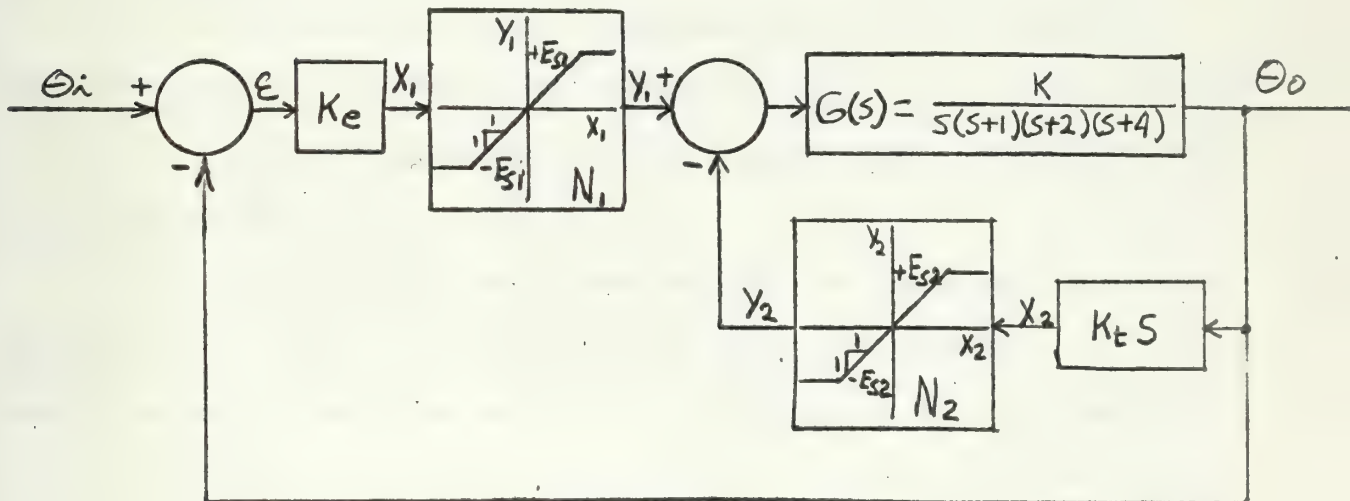


Figure VI

System with Two Saturation Nonlinearities

Assuming the last two coefficients variable, the characteristic equation becomes

$$s^4 + 7s^3 + 14s^2 + B_1s + B_0 = 0 \quad (\text{VI-b})$$

where

$$B_0 = KK_e N_1 \quad (\text{VI-c})$$

and

$$B_1 = 8 + KK_t N_2 \quad (\text{VI-d})$$

The equations of the stability curve are the same as those in Chapter V, Section V-A-1 and are repeated below

$$B_0 = 14 \omega_n^2 - \omega_n^4 \quad (\text{VI-e})$$

and

$$B_1 = 7 \omega_n^2 \quad (\text{VI-f})$$

This particular arrangement easily lends itself to presentation on the B_0 versus B_1 plane in that

1. The stability curve is independent of the gain K since the stability curve only depends on the coefficients of the s^4 , s^3 , and s^2 terms.

2. Once K is chosen a second rectangular grid of constant K_t and K_e can be drawn.

3. Once K_t and K_e are chosen then any instantaneous or average M-point is easily plotted using the $K_e - K_t$ grid. For example, if $K_e = 6$ and $K_t = 4$ and by some means an M-point is determined by $N_1 = 0.5$ and $N_2 = 0.25$, then this M-point is easily plotted at the intersection of the $K_e = 3$ line and the $K_t = 1$ line of the secondary grid.

In the study, three terms are used to describe certain parts of the system shown in Figure VI and need to be defined. These are:

Plant - that portion of the system represented by the linear transfer function

$$G(s) = \frac{K}{s(s+1)(s+2)(s+4)}$$

Linear System - the equivalent linear closed loop transfer function with both feedback loops reduced and no nonlinearities present, or the linear system described by the characteristic equation VI-a with N_1 and N_2 equal to 1.0.

Linear M-point - that point on the B_0 versus B_1 plane which is determined by equations VI-c and VI-d with N_1 and N_2 equal to 1.0.

Chapter VI

ANALOG COMPUTER STUDY AND STATEMENT OF RESULTS

Besides the poles of the plant, there are six parameters which directly or indirectly affect the two assumed variable coefficients of the characteristic equation. These are Θ_A , K_e , E_{s1} , K , K_t , and E_{s2} . As a starting point the plant gain, K , was made 20 and both saturation voltages were made equal to 3 volts. For these conditions the analog simulation is shown in Figure VI-1. The settings of the coefficient pots and their associated resistances and capacitances are given in Table VI-1.

The step input signal, E_i or Θ_A , was obtained by a pot reduction of a 100 volt d.c. source through an isolating amplifier. To change K_e various combinations of a_1 , R_1 , a_2 , and R_2 were used, however, both channels had to be the same. To change K_t various combinations of a_{13} and R_{13} were used.

Because the diode resistance is not zero during conduction and pot loading effects of pots "a" and "a'", the back bias pots were readjusted slightly as the amplitude of the limit cycle changed. The readjustments were made by eye such that on the average the output signals of both saturation simulators were 3 volts. A typical output signal of a saturation simulator for a large input signal is sketched in Figure VI-2.

First the stability curve was drawn on the B_0 versus B_1 plane and then a second grid of constant K_e and K_t lines was drawn as shown in Figure VI-3. From this figure, it is apparent that one should get a good indication of the limit cycles possible by taking many linear starting points located by K_e and K_t and observing the resulting limit cycles.

The initial study took exactly this form, that is, a K_e was chosen and several responses to a step input were observed for various values of K_t on

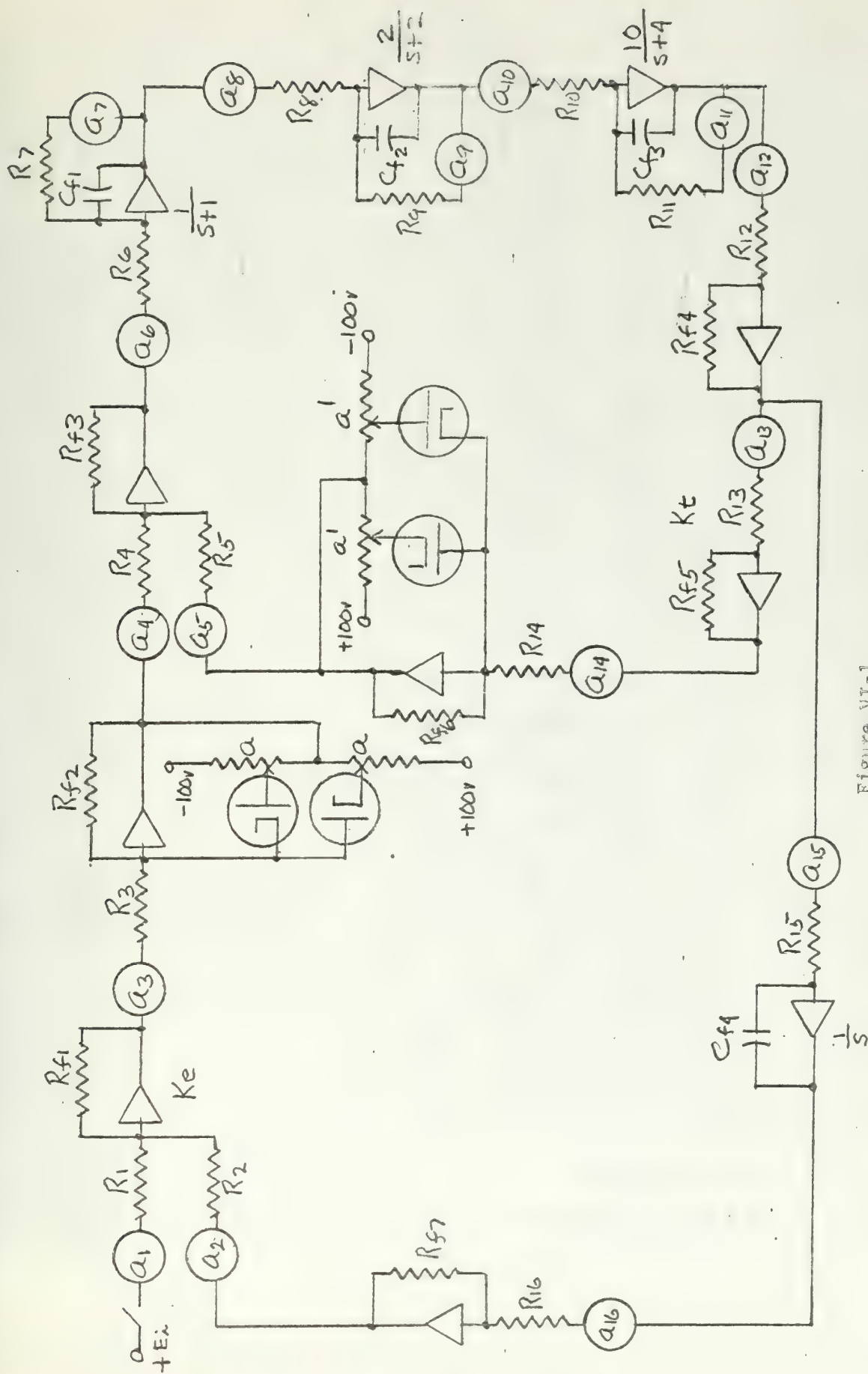


Figure VI-1

Analog Computer Simulation of Saturation in Both the Error Channel and the Velocity Feedback Path.

TABLE VI-1

| Pot Setting | Associated Elements |
|---|--|
| $a_1 = K_e$ for $K_e < 1.0$ | $R_1 = 1 \text{ Meg}, R_{f1} = 1 \text{ Meg}$ |
| $a_1 = \frac{K_e}{10}$ for $K_e > 1.0$ | $R_1 = 0.1 \text{ Meg}, R_{f1} = 1 \text{ Meg}$ |
| $a_2 = K_e$ for $K_e < 1.0$ | $R_2 = 1 \text{ Meg}, R_{f1} = 1 \text{ Meg}$ |
| $a_2 = \frac{K_e}{10}$ for $K_e > 1.0$ | $R_2 = 0.1 \text{ Meg}, R_{f1} = 1 \text{ Meg}$ |
| $a_3 = 1.0$ | $R_3 = 1 \text{ Meg}, R_{f2} = 1 \text{ Meg}$ |
| $a_4 = 1.0$ | $R_4 = 1 \text{ Meg}, R_{f3} = 1 \text{ Meg}$ |
| $a_5 = 1.0$ | $R_5 = 1 \text{ Meg}, R_{f3} = 1 \text{ Meg}$ |
| $a_6 = 1.0$ | $R_6 = 1 \text{ Meg}, C_{f1} = 1 \text{ uf}$ |
| $a_7 = 1.0$ | $R_7 = 1 \text{ Meg}, C_{f1} = 1 \text{ uf}$ |
| $a_8 = 1.0$ | $R_8 = 0.5 \text{ Meg}, C_{f2} = 1 \text{ uf}$ |
| $a_9 = 1.0$ | $R_9 = 0.5 \text{ Meg}, C_{f2} = 1 \text{ uf}$ |
| $a_{10} = 1.0$ | $R_{10} = 0.1 \text{ Meg}, C_{f3} = 1 \text{ uf}$ |
| $a_{11} = 0.4$ | $R_{11} = 0.1 \text{ Meg}, C_{f3} = 1 \text{ uf}$ |
| $a_{12} = 1.0$ | $R_{12} = 1 \text{ Meg}, R_{f4} = 1 \text{ Meg}$ |
| $a_{13} = K_t$ for $K_t < 1.0$ | $R_{13} = 1 \text{ Meg}, R_{f5} = 1 \text{ Meg}$ |
| $a_{13} = \frac{K_t}{10}$ for $K_t > 1.0$ | $R_{13} = 0.1 \text{ Meg}, R_{f5} = 1 \text{ Meg}$ |
| $a_{14} = 1.0$ | $R_{14} = 1 \text{ Meg}, R_{f6} = 1 \text{ Meg}$ |
| $a_{15} = 1.0$ | $R_{15} = 1 \text{ Meg}, C_{f4} = 1 \text{ uf}$ |
| $a_{16} = 1.0$ | $R_{16} = 1 \text{ Meg}, R_{f7} = 1 \text{ Meg}$ |
| $a = 0.03$ Initial Setting | For a 3 volt saturation level |
| $a' = 0.03$ Initial Setting | For a 3 volt saturation level |

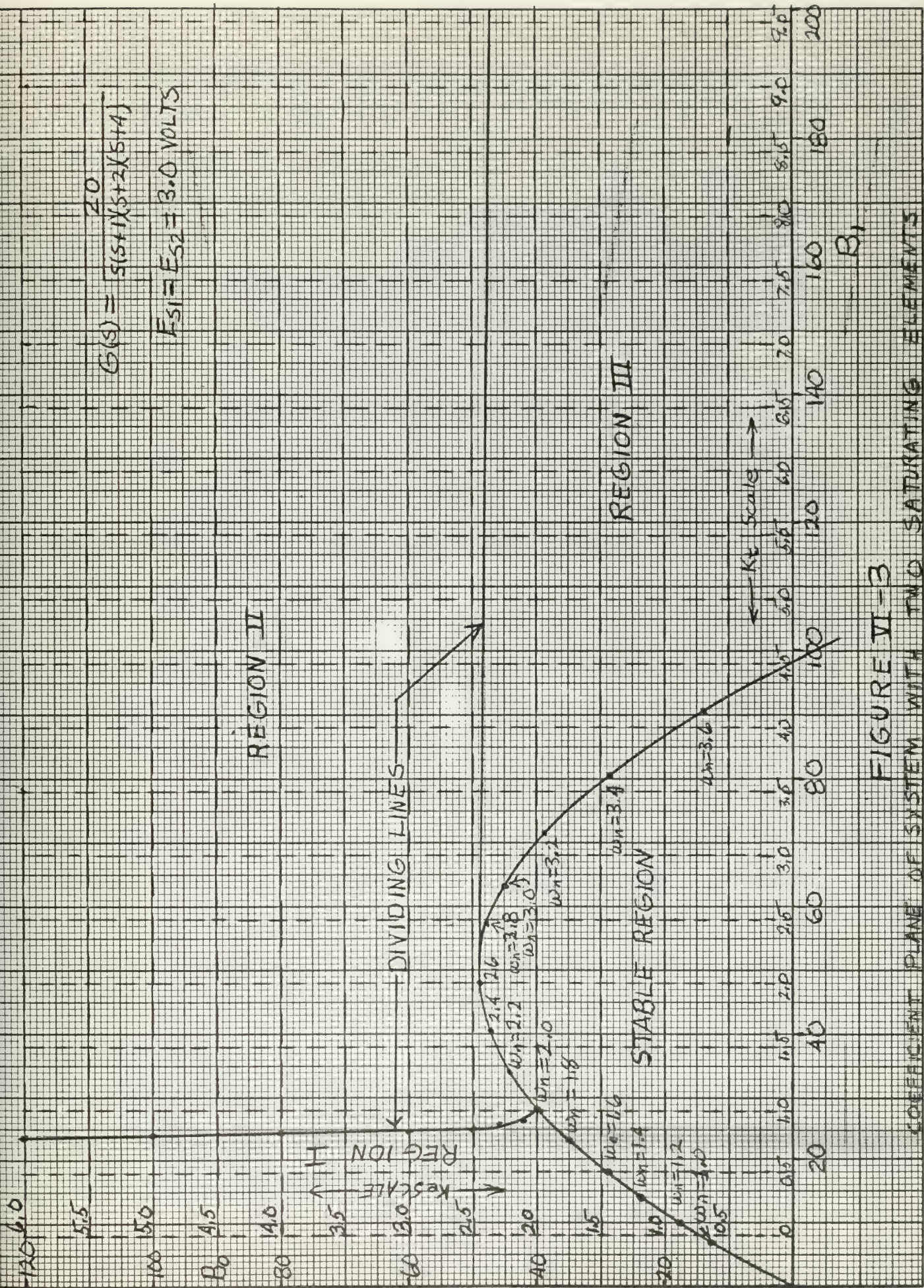


FIGURE VI-3
COEFFICIENT PLANE OF SYSTEM WITH TWO SATURATING ELEMENTS

a horizontal traverse across the plane. In the study, K_e was varied from $K_e = 0.5$ to $K_e = 6.0$. K_t was varied from $K_t = 0.5$ to $K_t = 10.0$. About every other value of K_t , the input step, E_i , was varied over several values to see if the resulting limit cycle was dependent on the magnitude of the step input signal. The only limitation placed on E_i was overloading of any one of the computer amplifiers; consequently, for certain linear starting points E_{imax} was as large as 200 volts. The results of these computer runs are tabulated in Table I of Appendix B.

From this first portion of the analog computer study several things were evident. These were:

1. No limit cycles were obtained from a step input signal when the linear system M-point was inside the stable region on the B_0 versus B_1 plane no matter what the input signal magnitude.
2. Limit cycles were only obtained for step input signals when the linear system M-point was outside the stable region and these limit cycles were independent of input signal magnitude and only dependent on the linear system M-point position.
3. The unstable region of the B_0 versus B_1 plane can be divided into three regions such that only one of the nonlinear elements saturate or both elements saturate for the linear system M-point lying in a given region.

Several runs were made for various linear M-points inside the stable region and for various step input signal magnitudes. From the results of Section V-A of Chapter V, one might expect for linear M-points close to the left portion of the stability curve that the system could be driven unstable for large step input signals. However, all linear M-points chosen showed some damping even for the linear point extremely close to the stability curve. A typical response for a linear M-point very close to the left

portion of the stability curve is shown in Recorder Trace VI-1 for a small step signal input and Recorder Trace VI-2 for a large step signal input. Typical responses for a linear M-point very close to the right side of the stability curve are shown in Recorder Trace VI-4 for a large step signal input. Typical responses for a linear M-point in the well damped portion of the stability region are shown in Recorder Trace VI-5 for a small step signal input and Recorder Trace VI-6 for a large step signal input.

Although it has been stated that no limit cycles were observed for a linear M-point in the stable region, the system could be driven into a limit cycle for repeated disturbances in the input signal after the initial step input. This type of response was only noted for linear M-points with a very small damping ratio and close to the left portion near the maximum of the stability curve. A typical response of this type is shown in Recorder Trace VI-7 for extremely little damping. In this trace, a limit cycle was achieved with only one disturbance after the initial step. Recorder Trace VI-8 shows the same type of response but with more damping. In this trace three disturbances were required to achieve a limit cycle.

To obtain these responses an initial step input signal was applied. Then with the system in a very oscillatory slightly damped condition the disturbance was applied. To apply the disturbance, the input pot was given a small quick twist to approximate a step change in input signal. It was found that the disturbances had to be (1) generally small in amplitude such that the error channel did not appreciably saturate, (2) applied at a definite time during a cycle and in a specific direction. It was found that the maximum effect was achieved when a positive disturbance was applied when the error was passing through zero from minus to plus. Also, the maximum effect

was observed for a negative disturbance as the error was passing through zero from plus to minus. This type of system performance was only found late in the experimental phase of the study and was not investigated thoroughly.

Recorder Traces VI-9 and VI-10 show that the resulting limit cycle for a linear M-point in the unstable region is independent of the magnitude of the step input signal. These are typical responses, and at all points where the effect of the step input signal was investigated, the limit cycle was the same for different input magnitudes. Comparison of Recorder Trace VI-9 or VI-10 with Recorder Trace VI-11 illustrates the effect of the relative position of the linear M-point and the stability curve on the resulting limit cycle. Recorder Trace VI-11 shows a limit cycle of higher frequency and much lower amplitudes than the one in Trace VI-10.

The most striking result of the initial computer study was that the unstable region of the B_0 versus B_1 plane can be divided into three subregions. These subregions are shown on the coefficient plane of Figure VI-3. For the linear M-point in Region I, only the error channel saturates and the limit cycle can be predicted from the intersection of the K_t coordinate of the linear M-point and the stability curve. For the linear M-point in Region II both channels saturate, but the resulting limit cycle frequency always indicated an intersection of an average M-point locus with the stability curve at a point to the left of the maximum point of the stability curve. For the linear M-point in Region III, only the tachometer channel saturates and the limit cycle can be predicted from the intersection of the K_e coordinate of the linear M-point and stability curve.

The dividing line which proceeds upward and to the left from the stability curve will be referred to as dividing line No. 1. The dividing line

which proceeds almost horizontally to the right from the top of the stability curve will be referred to as dividing line No. 2.

The approximate position of dividing line No. 1 was obtained from the results tabulated in Appendix B. To fix more accurately the position of the dividing line, more runs were taken on the analog computer simulation by choosing a K_e and varying K_t . A point on the dividing line was then determined when the amplitude of signal X_2 in the resulting limit cycle was equal to 3 volts, the saturation voltage. The results are tabulated in Table 2 of Appendix B. Typical changes in the limit cycle as K_t was increased across No. 1 dividing line are shown in Recorder Traces VI-12 and VI-13. The main feature to note from these two traces is the slight increase in the amplitude of signal X_2 from just under 3 volts to just over 3 volts.

The approximate position of dividing line No. 2 was obtained from the results of Table I in Appendix B. To fix more accurately the position of the dividing line, more computer runs were made by fixing K_t and varying K_e . The results are tabulated in Table 3 of Appendix B. Typical changes in the response as K_e was increased above the dividing line are shown in Recorder Traces VI-14 and VI-15. Recorder Trace VI-14 is a couple of oscillations of the limit cycle resulting from a linear M-point at $K_t = 8.0$ and $K_e = 2.38$. However, sufficient time was allowed to ensure that the system did not exhibit the same response as shown in Recorder Trace VI-15. Recorder Trace VI-15 is a series of three sections taken out of the response for a linear M-point at $K_t = 8.0$ and $K_e = 2.39$ to show the salient features of the entire response. The time intervals between the sections are indicated on the trace. Section one shows the build up to an apparently

stable limit cycle with only the tach channel saturating. However, closer inspection reveals that the amplitudes of signals X_1 and X_2 are increasing. Section 2 starts at approximately the same amplitudes as occur at the end of Section 1, but quickly builds up to the final stable limit cycle as shown in Section 3 at an expanded time scale. The salient features of these two recorder traces are as follows:

1. The sudden build up from an apparent limit cycle to a final stable limit cycle for a linear M-point just above dividing line No. 2.

2. The large difference in signal magnitudes between the limit cycles of the two traces and the difference in their frequencies.

3. The change in frequency of the oscillations during the build up to the final limit cycle in Recorder Trace VI-15. This point is not very noticeable on Trace VI-15 but it is noticeable on traces with an expanded time scale using dividers to measure the period.

4. The frequency and amplitude of Trace VI-14 is very nearly the frequency and amplitude of the apparent limit cycle of Trace VI-15.

Since the foregoing results allow one to predict the limit cycles for a large number of linear system M-points for 3 volt saturations, the next logical step was to see if the dividing lines are independent of saturation level. Thus both error channel and tach channel saturation voltages were adjusted to 10 volts. (pots "a" and "a'" equal to 0.1). The same analog computer procedures used to determine the dividing lines for $E_{s1} = E_{s2} = 3$ volts were again used. The resulting limit cycles for the linear starting points are tabulated in Tables 4 and 5 of Appendix B. A comparison of the dividing lines for the 3 volt and 10 volt saturation levels is given below in Tables VI-2 and VI-3.

TABLE VI-2

| No. 1 Dividing Line | | | |
|--------------------------|-------|-------------------------|-------|
| 10 volt Saturation Level | | 3 volt Saturation Level | |
| K_e | K_t | K_e | K_t |
| 2.1 | 0.875 | 2.1 | 0.92 |
| 2.2 | 0.855 | -- | -- |
| -- | -- | 2.3 | 0.89 |
| 2.4 | 0.84 | -- | -- |
| 2.5 | 0.83 | 2.5 | 0.85 |
| 3.0 | 0.795 | 3.0 | 0.83 |
| 4.0 | 0.785 | 4.0 | 0.81 |
| 5.0 | 0.775 | 5.0 | 0.80 |
| 6.0 | 0.77 | 6.0 | 0.785 |

TABLE VI-3

| No. 2 Dividing Line | | | |
|--------------------------|-------|-------------------------|-------|
| 10 volt Saturation Level | | 3 Volt Saturation Level | |
| K_e | K_t | K_e | K_t |
| 2.445 | 2.5 | -- | -- |
| -- | -- | 2.425 | 3.0 |
| 2.415 | 4.0 | 2.415 | 3.0 |
| -- | -- | 2.405 | 5.0 |
| 2.395 | 6.0 | 2.395 | 6.0 |
| 2.385 | 8.0 | 2.385 | 8.0 |
| 2.335 | 15.0 | 2.335 | 15.0 |

Tables VI-2 and VI-3 indicate that both dividing lines are essentially independent of saturation level, although dividing line No. 1 is more doubtful than dividing line No. 2. In order to definitely show this point, more saturation voltages will have to be used and more sophisticated measurement procedures should be used.

Practically all of the data given in Appendix B is graphically displayed in Figure VI-4 through VI-9. Figure VI-4 is a plot of the limit cycle amplitude of signal X_2 as K_t is varied with K_e fixed. Figure VI-5 is a plot of the limit cycle amplitude of signal X_1 for like K_t variations. Figure VI-6 is a plot of the limit cycle amplitude of signal X_2 as K_e is varied with K_t fixed. Figure VI-7 is a plot of the amplitude of signal X_1 for like variations of K_e . Figure VI-8 is a plot of the limit cycle frequency as K_t is varied with K_e fixed. Figure VI-9 is a plot of the limit cycle frequency as K_e is varied with K_t fixed.

These six figures essentially show the results as already stated. By correlation of these figures with the location of the linear M-point in Figure VI-3, one can see the regions in which only one element saturates. For example, the upper right portion of Figure VI-8 shows Region III of Figure VI-3 in which one would expect the frequency to remain constant as K_t is increased. Also, the transition across dividing line No. 2 is very apparent in all the figures because of the large discontinuity in the curve. Some curves for relatively small K_e and K_t abruptly stop and then start up again in a different portion of the graph. This is due to the variable being inside the region of stable linear M-points in Figure VI-3, thus no limit cycle. An important result to note which has not yet been pointed out is that for K_e greater than 3 and K_t greater than 3, the frequency of the

resulting limit cycle is essentially independent of variations in either K_e or K_t .

Figure VI-10 shows various instantaneous and "average" quantities plotted against the number of elapsed oscillation peaks for a linear M-point just above No. 2 dividing line. A better abscissa name would be "number of elapsed half cycles" although both are related to the elapsed time by the characteristics of the system. The quantities plotted in the figure are defined below:

B_{1min} = The minimum instantaneous value during a half cycle of the s^1 coefficient calculated by equation VI-d using the minimum instantaneous gain N_{2min} . N_{2min} occurs when the signal X_2 is maximum during the half cycle.

B_{1ave} = The "average" value of the s^1 coefficient over a half cycle as calculated from equation VI-d using the "average" gain of the nonlinearity N_{2ave} . The describing function was used to relate N_{2ave} to the maximum value of X_2 during the half cycle.

B_{omin} = The minimum instantaneous value of the s^0 coefficient calculated by equation VI-c using the minimum instantaneous gain N_{1min} . N_{1min} occurs when the signal X_1 is maximum during the half cycle.

B_{oave} = The "average" value of the s^0 coefficient calculated from equation VI-d using the "average" gain of the nonlinearity N_{1ave} . The describing function was used to relate N_{1ave} to the maximum value of X_1 during the half cycle.

ω_{ave} = The average frequency of the oscillation over a half cycle obtained by measuring the half-period of the oscillations.

Justification for using the describing function in the manner indicated above will be indicated in Chapter IX.

If the "average" M-point is assumed to indicate the stability of the system over the half cycle, then it is interesting to note that the "average" M-point, as defined by B_{lave} and B_{oave} , moves through a portion of the stable region on a constant B_o line. It is also noted that under limit cycle conditions at the extreme right side of Figure VI-10, the values of B_1 and B_o calculated using ω_{ave} in Mitrovic's stability curve equations are approximately equal to the end values of B_{lave} and B_{oave} curves which were calculated using the describing function and the amplitude of the limit cycle. A comparison is made below.

| From Stability Curve | From Figure VI-10 |
|----------------------|-------------------|
| $B_1 = 30.9$ | $B_{lave} = 31.4$ |
| $B_o = 43.2$ | $B_{oave} = 42.8$ |

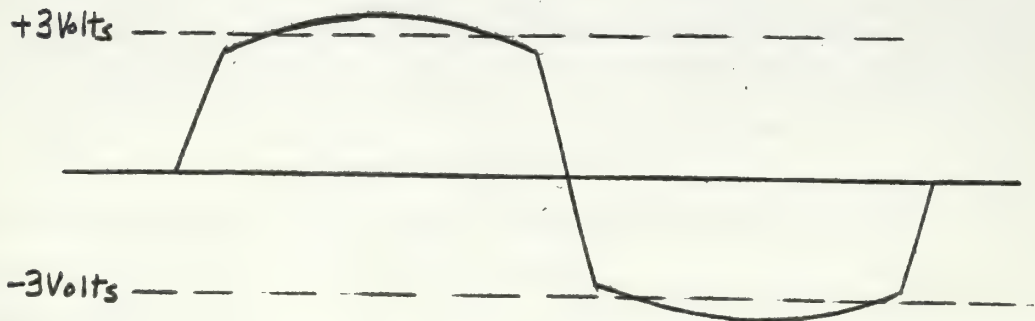
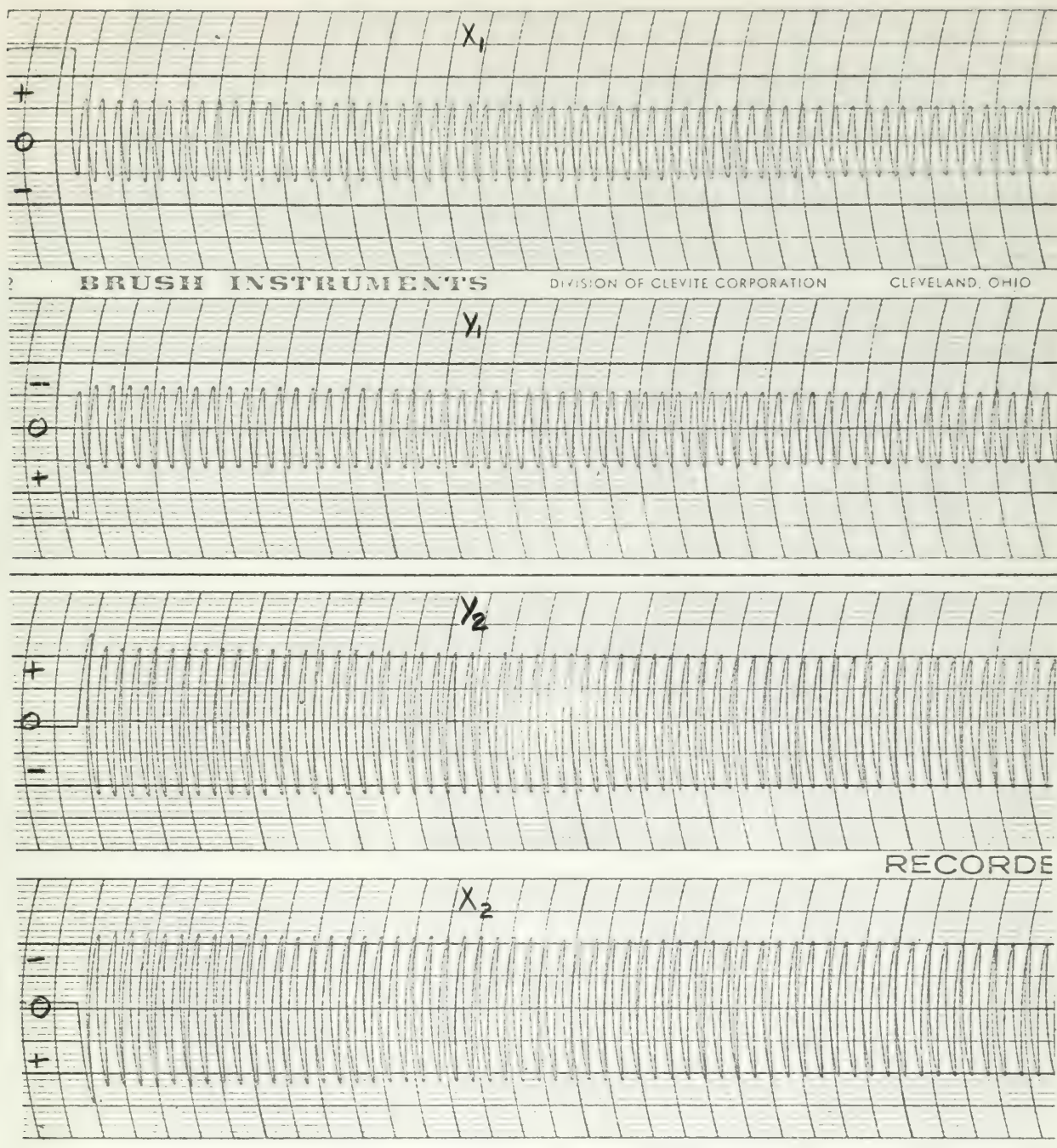


FIGURE VI-2



Recorder Trace VI-1

Linear M-Point Close to Left Side of Stability Curve,

$K_e = 2.4$, $K_t = 1.7$, 1.2 Volts Input Step

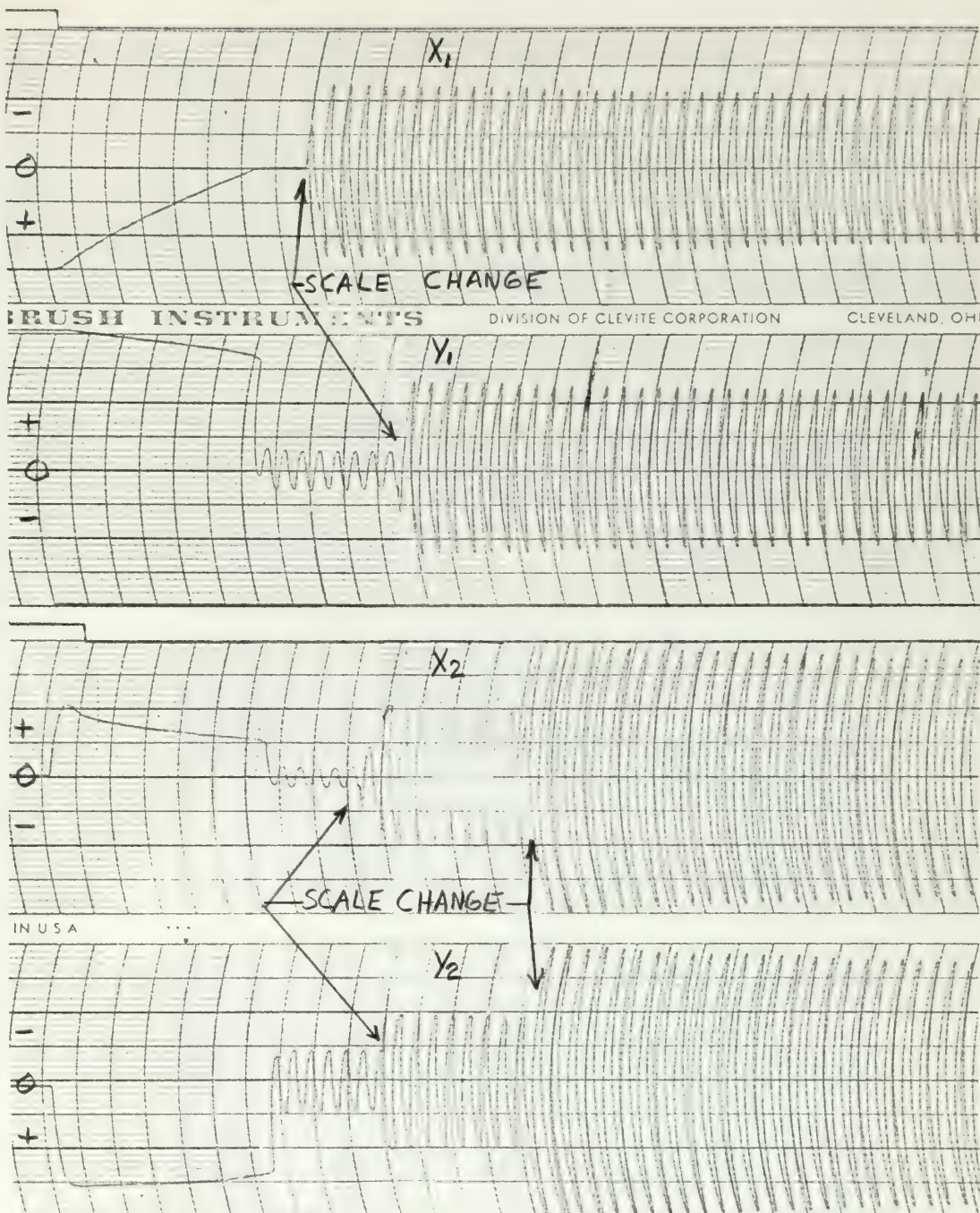
SCALES:

$X_1 = 0.2$ Volts/line

$Y_1 = 0.2$ volts/line

$X_2 = 0.2$ volts/line

$Y_2 = 0.2$ volts/line Time - 5 Seconds/Division



Recorder Trace VI-2

Linear M-Point Close to Left Side of Stability Curve, $K_e = 2.4$

$K_t = 1.7$, 62.5 Volts Input Step

SCALES:

X_1 - 10 Volts/Line

Y_1 - 0.2 Volts/Line

X_2 - 0.5 Volts/Line

-0.05 Volts/Line

-0.05 Volts/Line

-0.1 Volts/Line

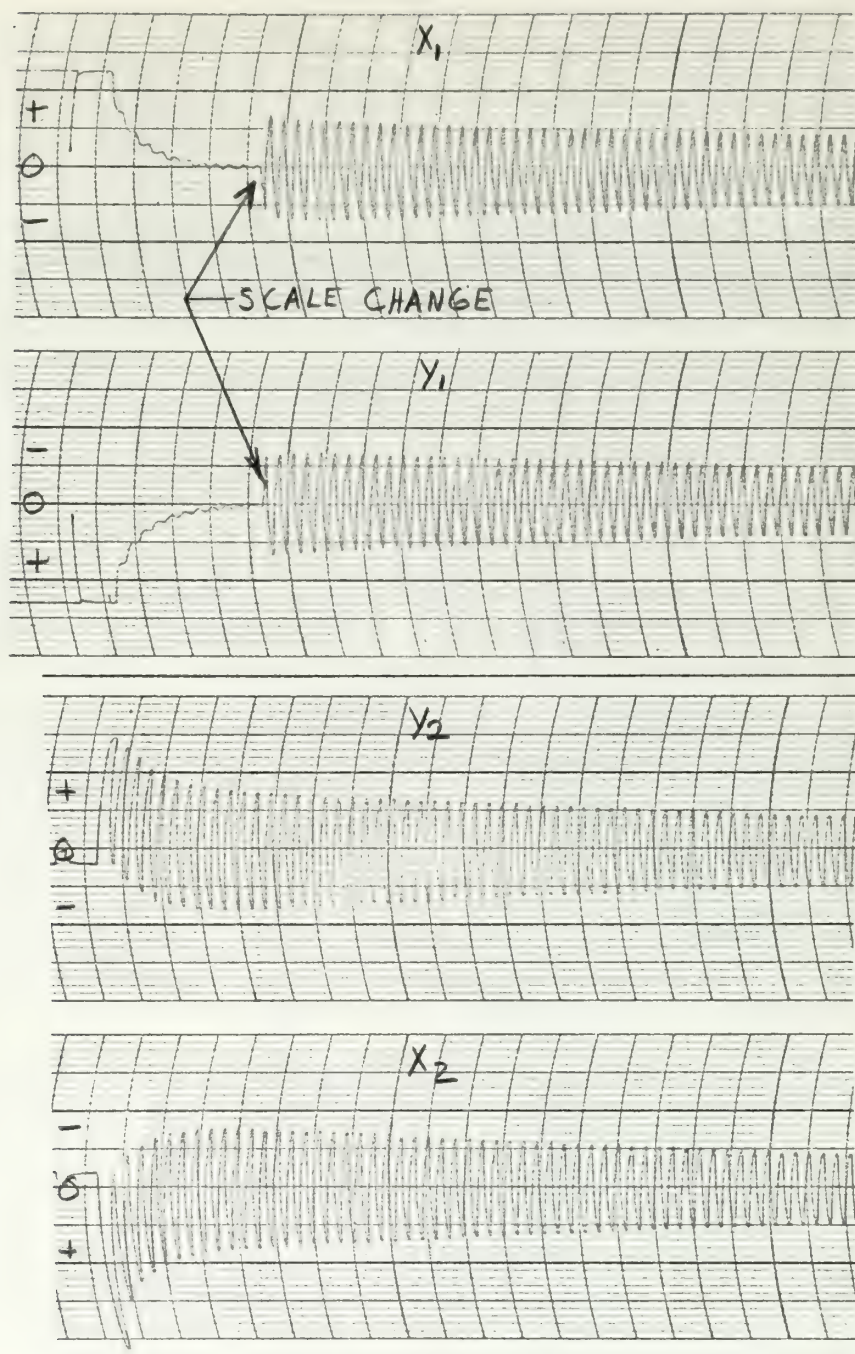
-0.05 Volts/Line

Y_2 - 0.2 Volts/Line

-0.1 Volts/Line

-0.05 Volts/Line

Time - 5 Seconds/Division



Recorder Trace VI-3

Linear M-point Close to Right Side of Stability Curve,
 $K_e = 1.0$, $K_t = 3.9$, 2.6 Volts Input Step.

SCALES:

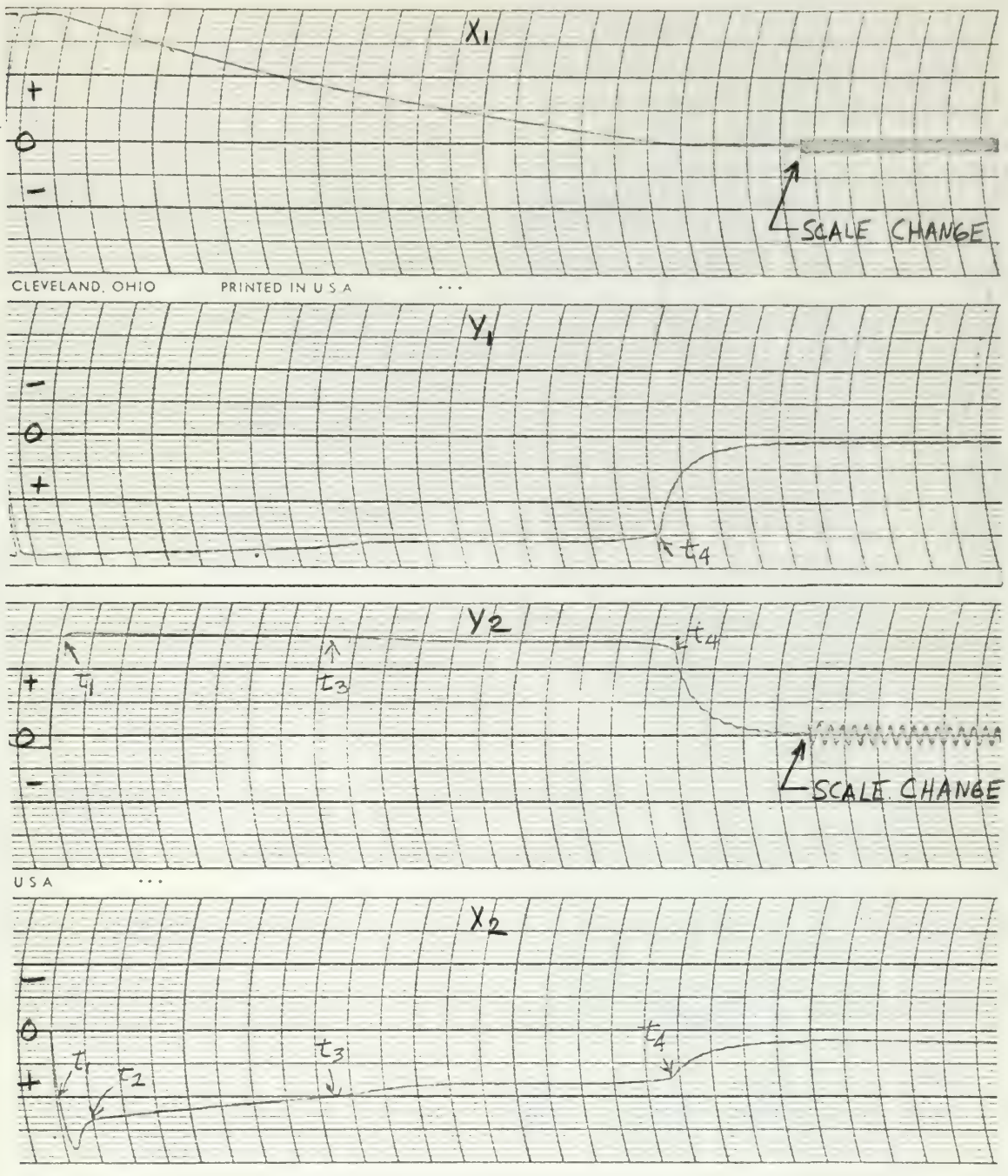
X_1 -0.2 Volts/Line
 -0.01

Y_1 -0.2 Volts/Line
 -0.01 Volt s/Line

Y_2 -0.2 Volts/
 Line

X_2 -0.2 Volts/Line

Time - 5 Seconds/Division



Recorder Trace VI-4

Linear M-point Close to Right Side of Stability Curve, $K_e = 1.0$,
 $K_t = 3.9$, 95 Volts Input Step.

SCALES

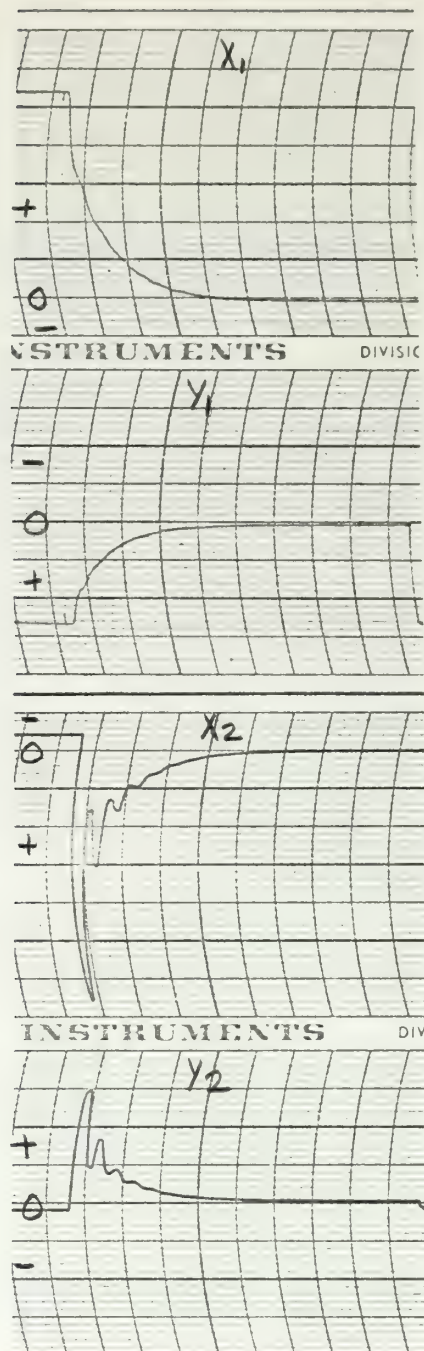
X_1 - 5Volts/Line
 -0.05 Volts/Line

Y_1 - 0.2 Volts/Line

Y_2 - 0.2 Volts/Line
 -0.05 Volts Line

X_2 - 0.3 Volts/Line

Time - 5 Seconds/Division



Recorder Trace VI-5

Linear M-point in Well Damped Region, $K_e = 0.5$, $K_t = 2.0$, 5.4 Volts Input Step.

SCALES:

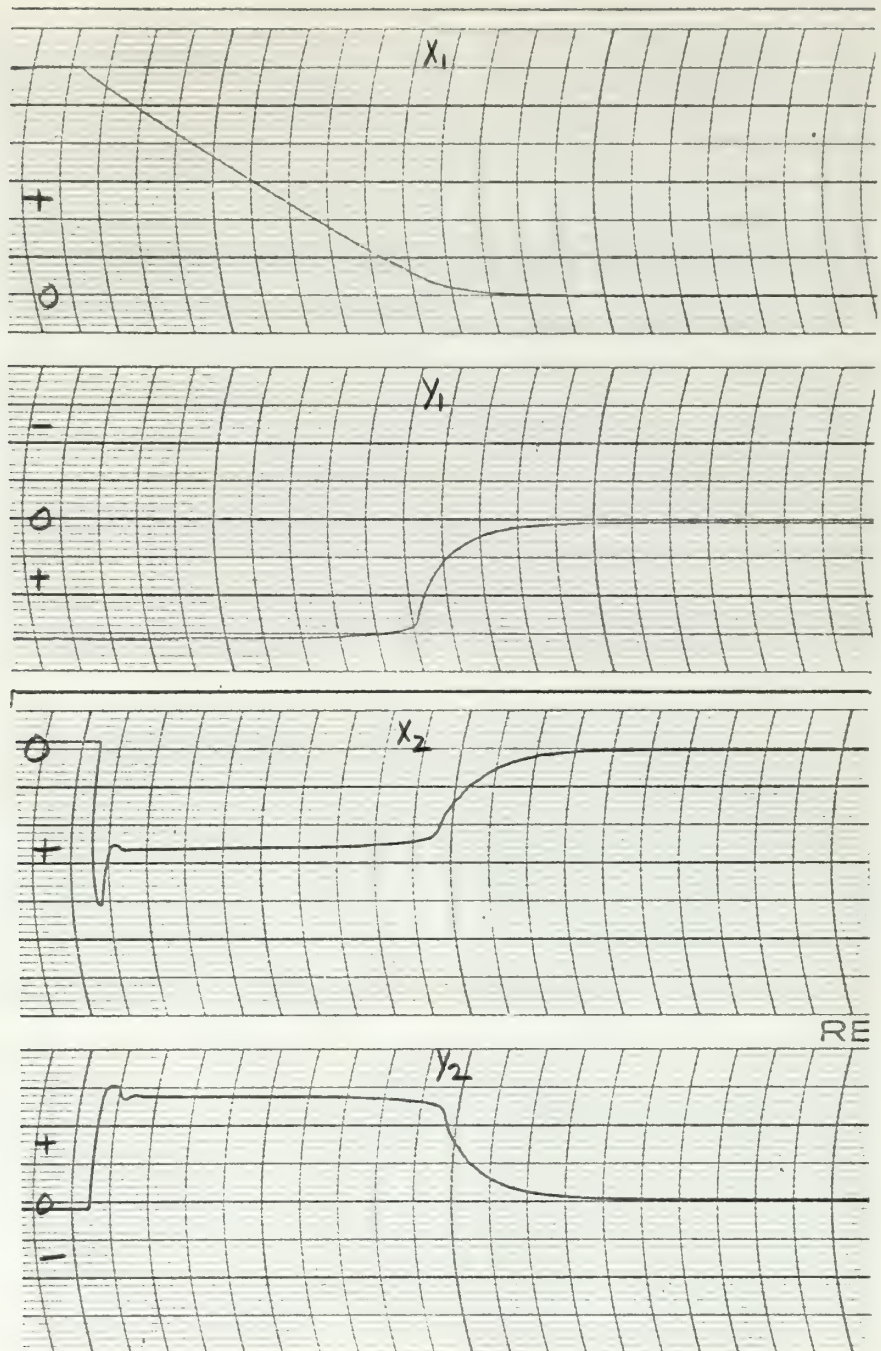
X_1 -0.1 Volts/Line

Y_1 -0.2 Volts/Line

X_2 -0.1 Volts/Line

Y_2 -0.2 Volts/Line

Time - 5 seconds/Division

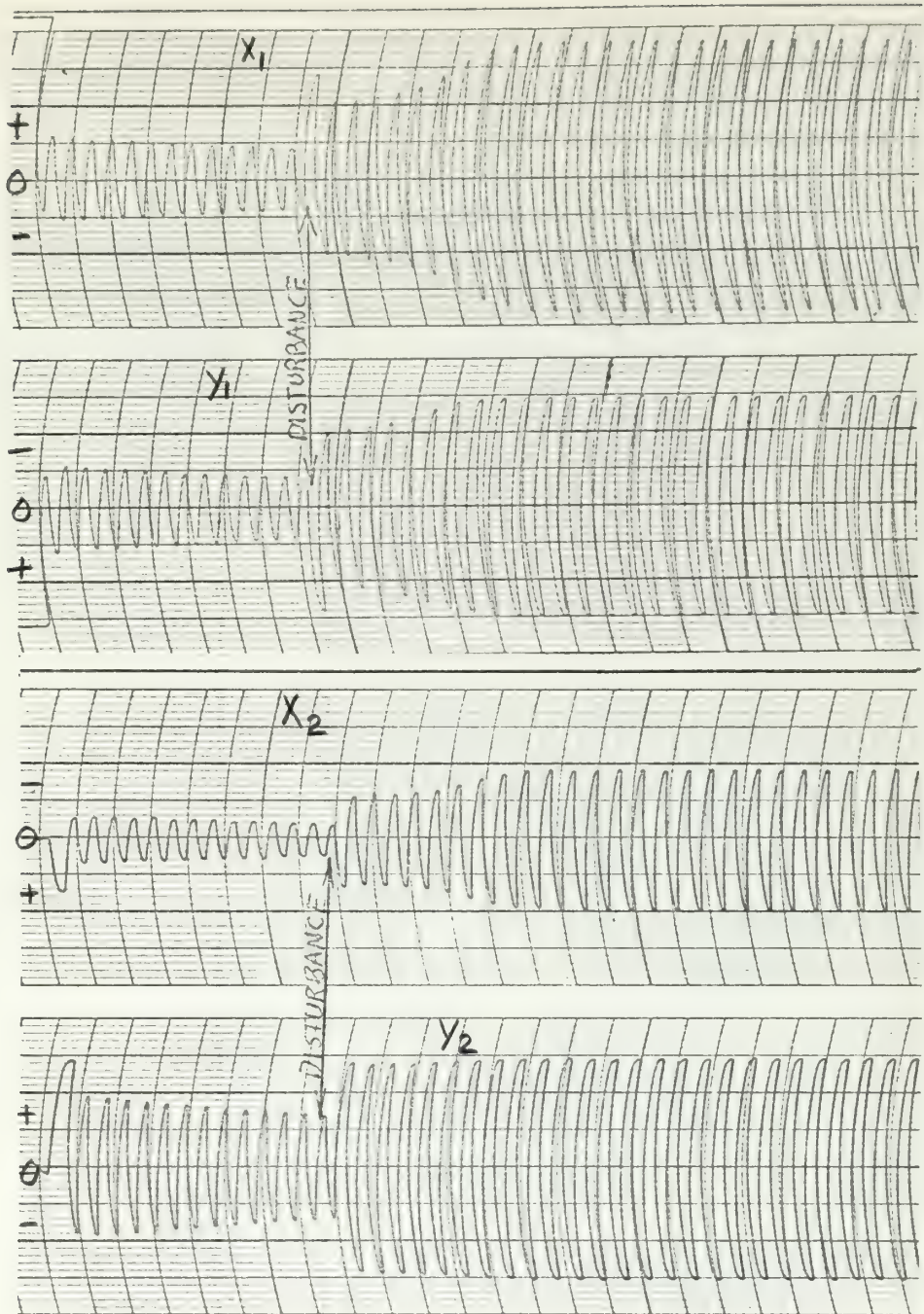


Recorder Trace VI-6

Linear M-point in Well Damped Region, $K_e = 0.5$, $K_t = 2.0$
60 Volt Input Step.

SCALES:

X_1 - 1 Volt/Line Y_1 - 0.2 Volt/Line X_2 - 0.2 Volt/Line
 Y_2 - 0.2 Volt/Line Time - 5 Seconds/Division



Recorder Trace VI-7

Repeated Sisturbances, M-Point at $K_e = 2.3$, $K_t = 1.5$

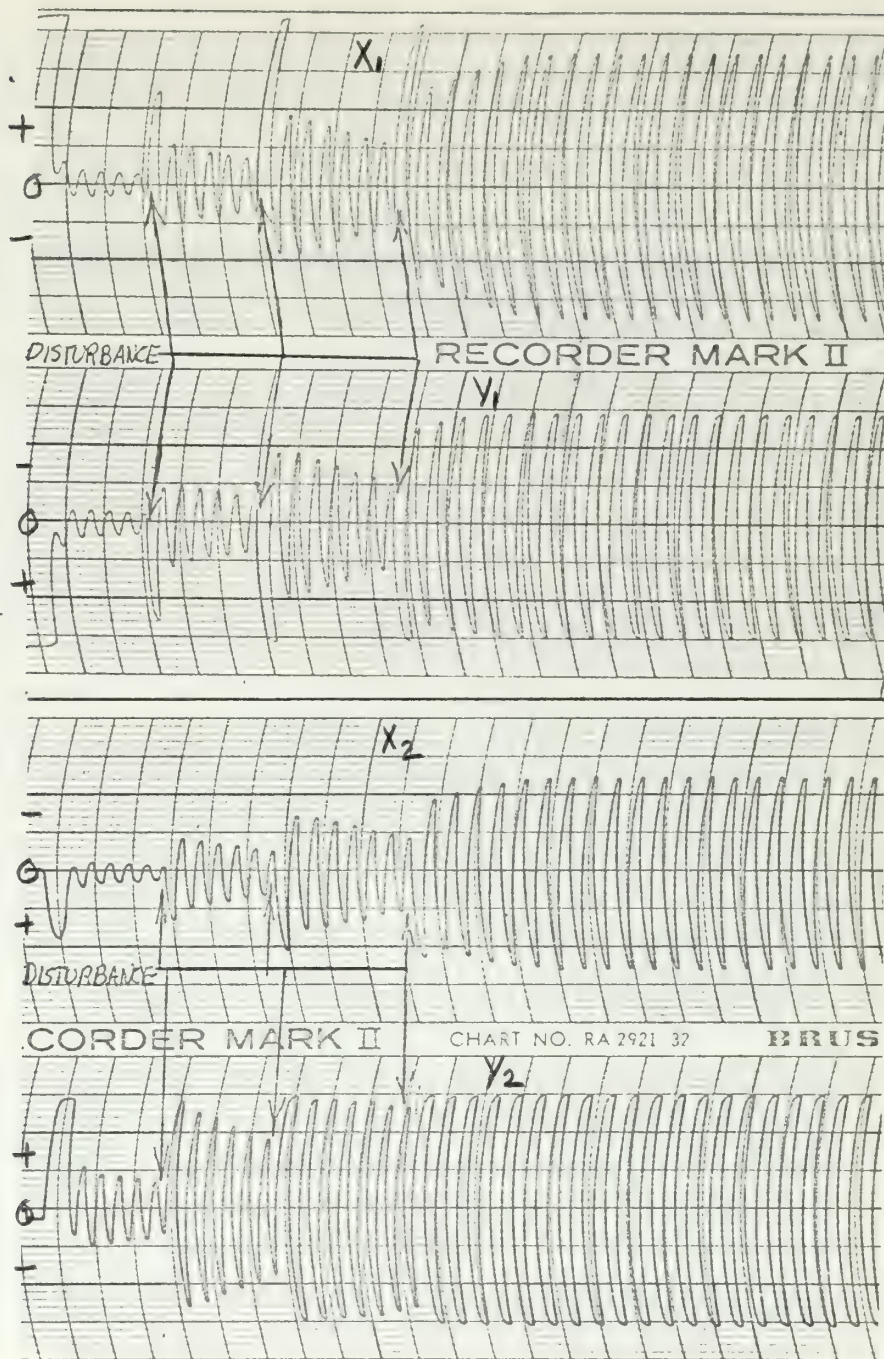
SCALES:

X_1 -0.2 Volts/Line

Y_1 -0.2 Volts/Line

X_2 -0.5 Volts/Line

Y_2 -0.2 Volts/Line Time - 5 Seconds/Division



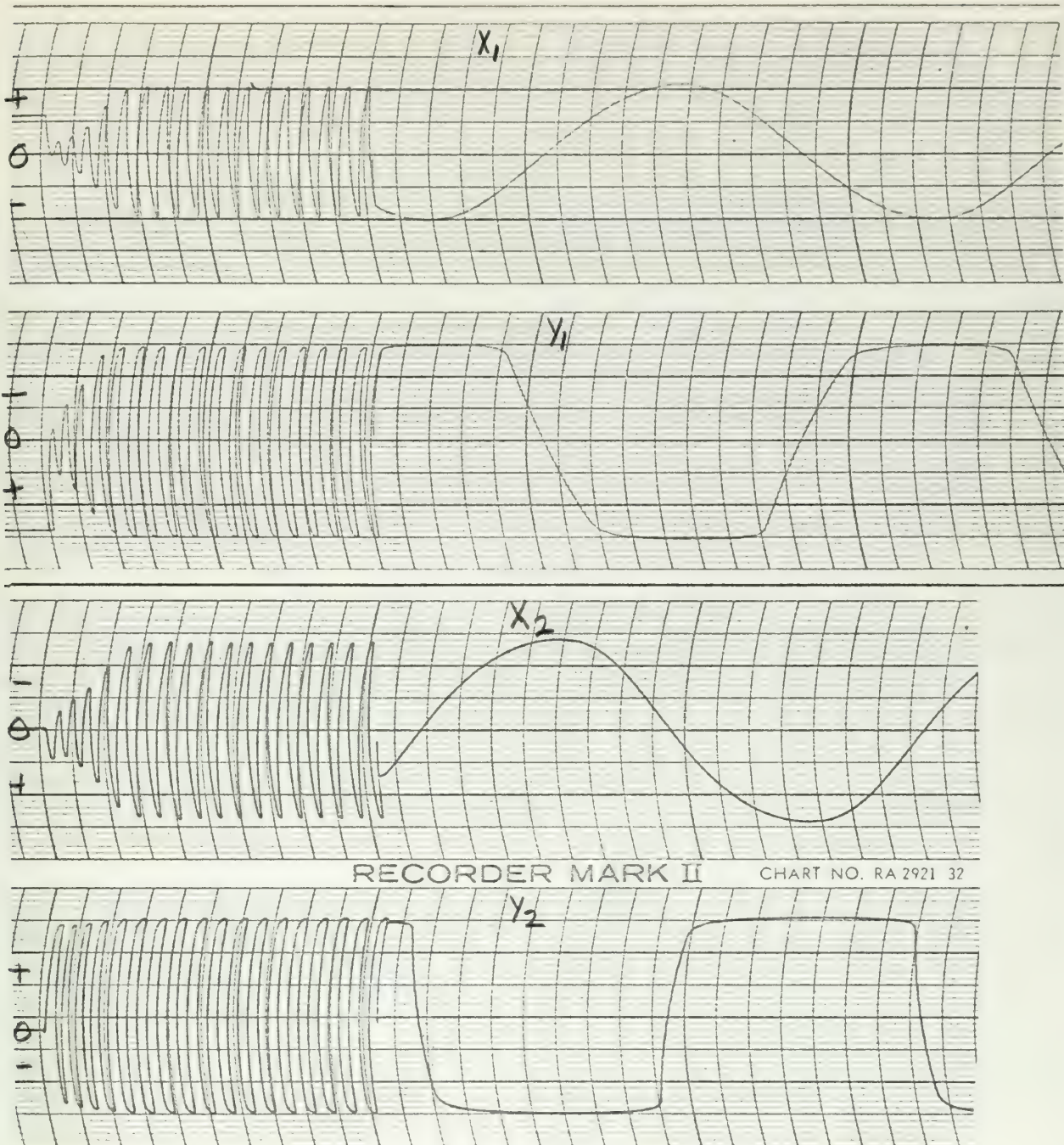
Recorder Trace VI-8

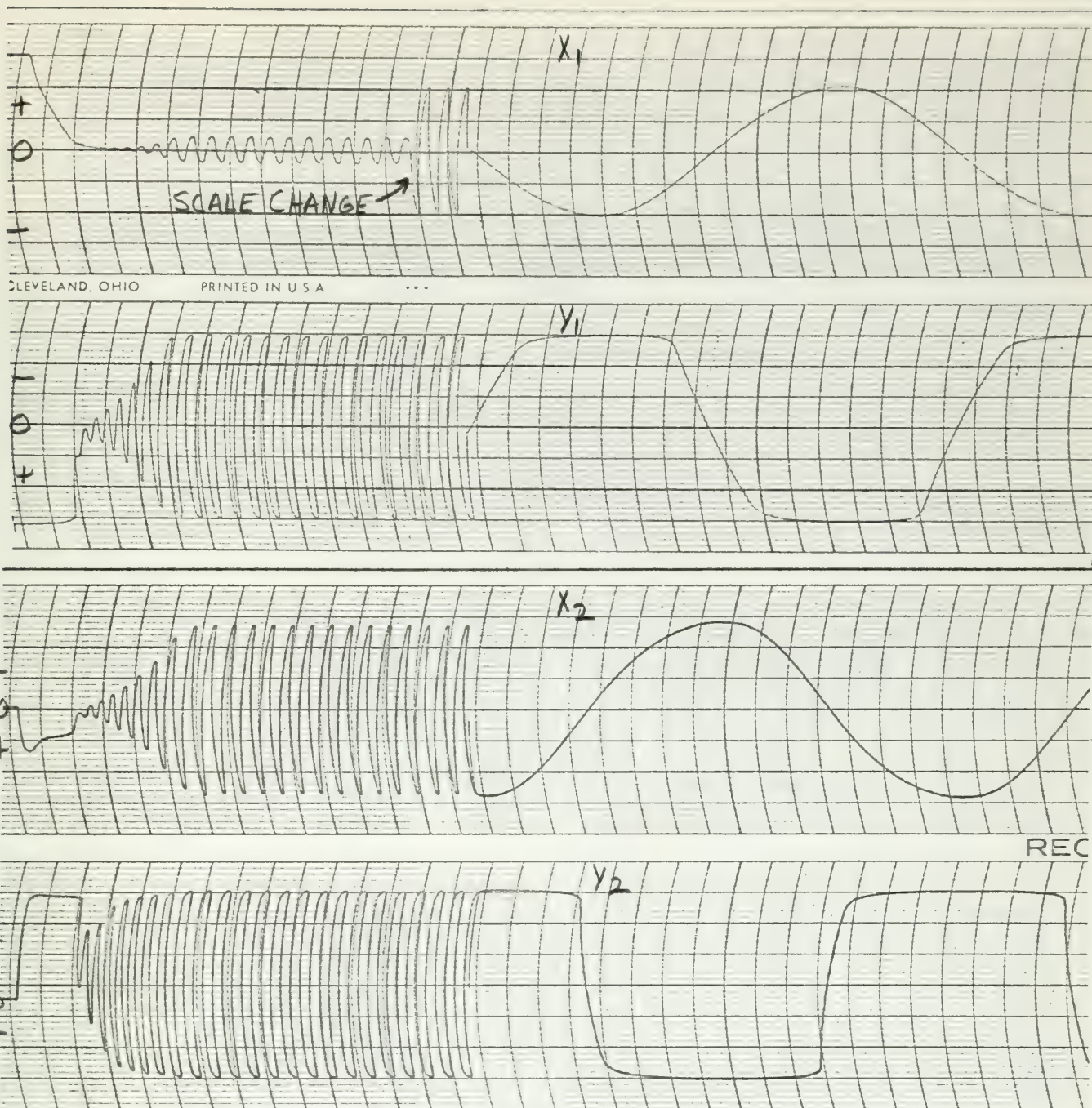
Repeated Disturbances, Linear M-Point at $K_e = 2.3$, $K_t = 2.0$

SCALES:

X_1 -0.2 Volts/Line Y_1 -0.2 Volts/Line X_2 -0.5 Volts/Line

Y_2 -0.2 Volts/Line Time - 5 Secnds/Division





Recorder Trace VI-10

Unstable Linear M-Point at $K_e = 3$, $K_t = 4$, 10 Volt Step Input.

SCALES:

$X_1 = 2 \text{ Volts/Line}$

$Y_1 = 0.2 \text{ Volts/Line}$

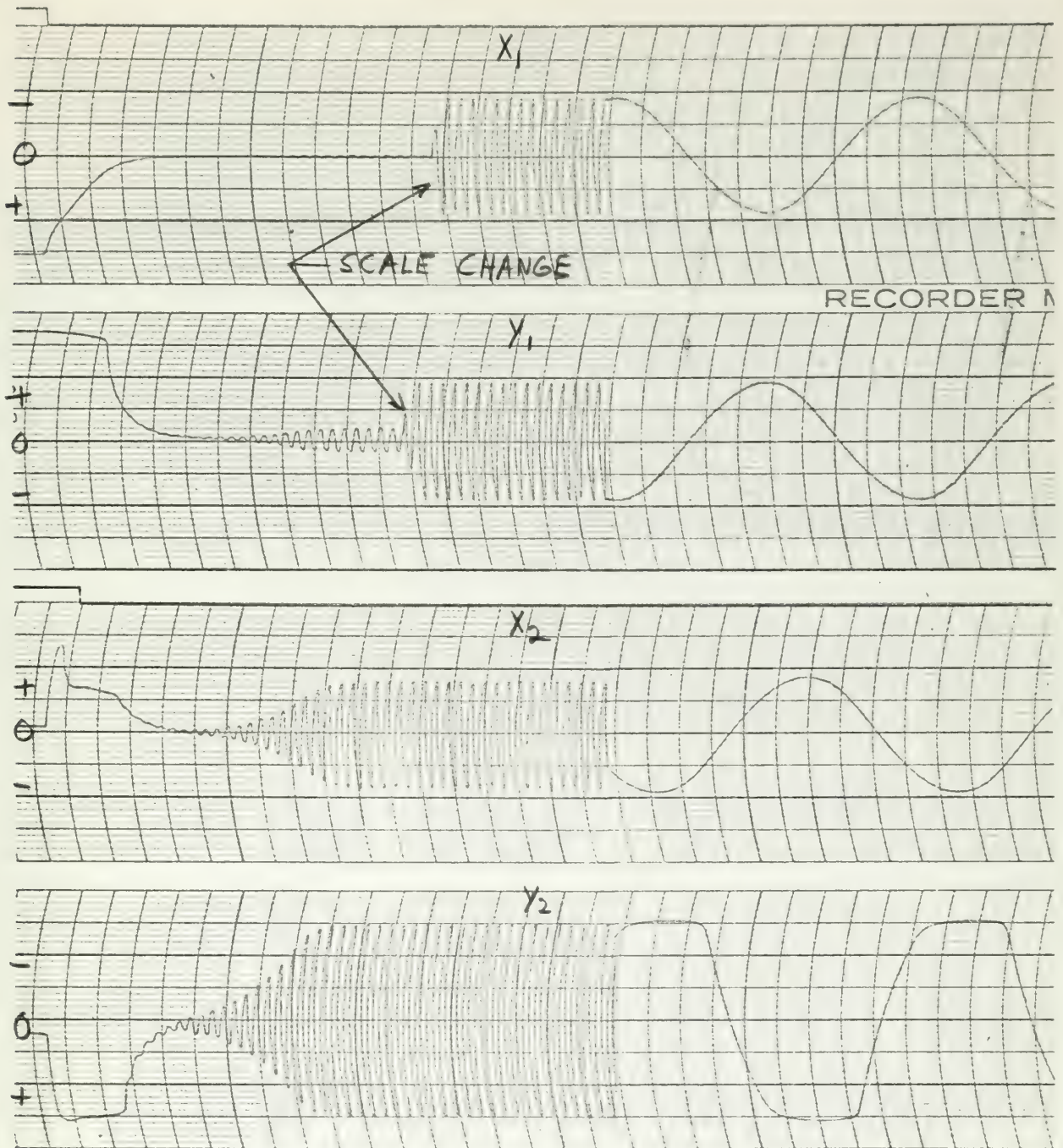
$X_2 = 1 \text{ Volt/Line}$

$1 = 0.5 \text{ Volts/Line}$

$Y_2 = 0.2 \text{ Volts/Line}$

Time - 5 Seconds/Division

-0.2 Seconds/Division



Recorder Trace VI-11

Unstable Linear M-Point Close to Stability Curve at $K_e = 1.5$, $K_t = 4.5$

SCALES:

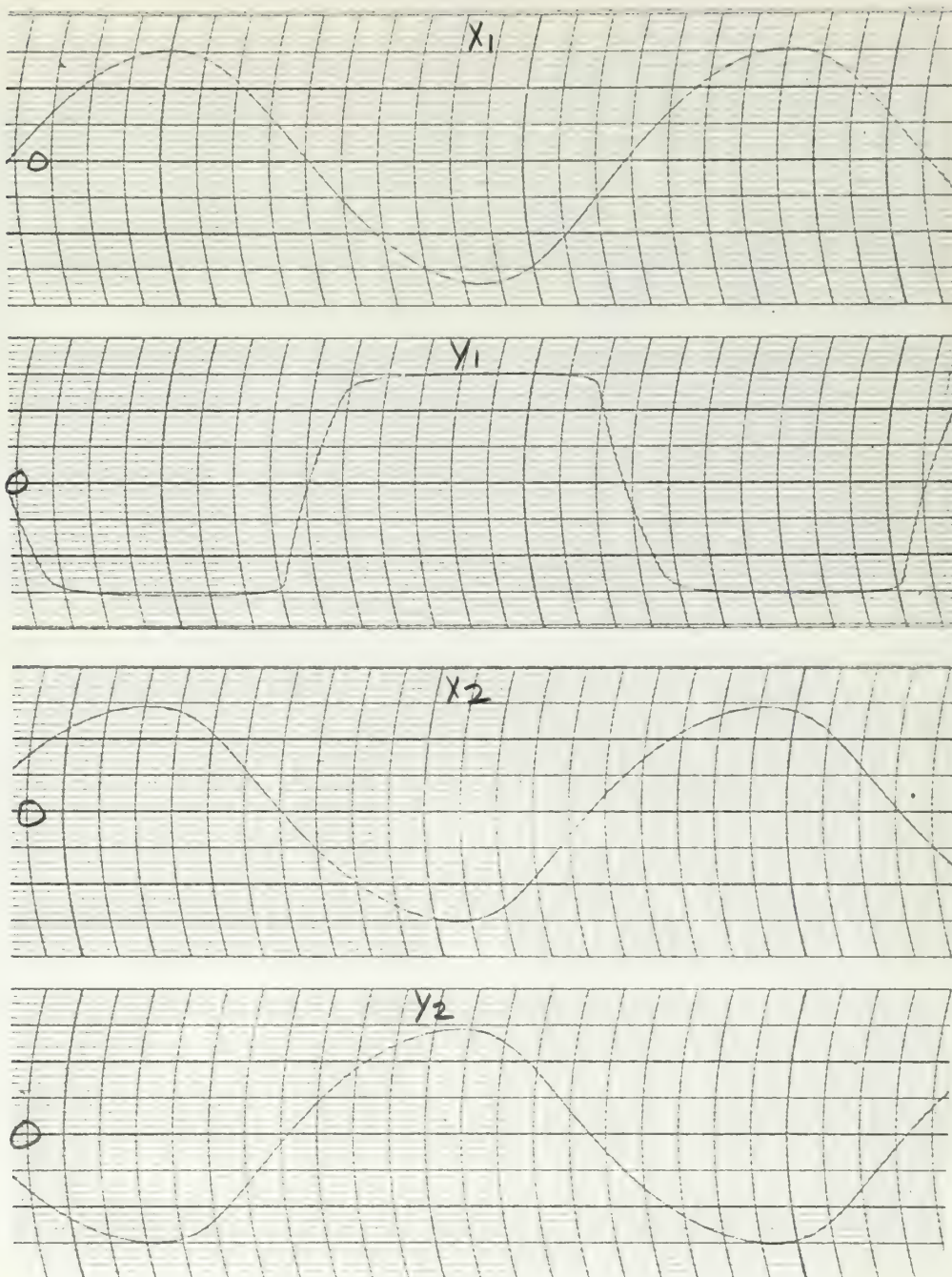
X_1 - 1 Volt/Line
-0.05 Volts/Line

Y_1 -0.2 Volts/Line
-0.05 Volts/Line

X_2 -0.5 Volts/Line

Y_2 -0.2 Volts/Line

Time - 5 Seconds/Division.
-0.2 Volts/Division



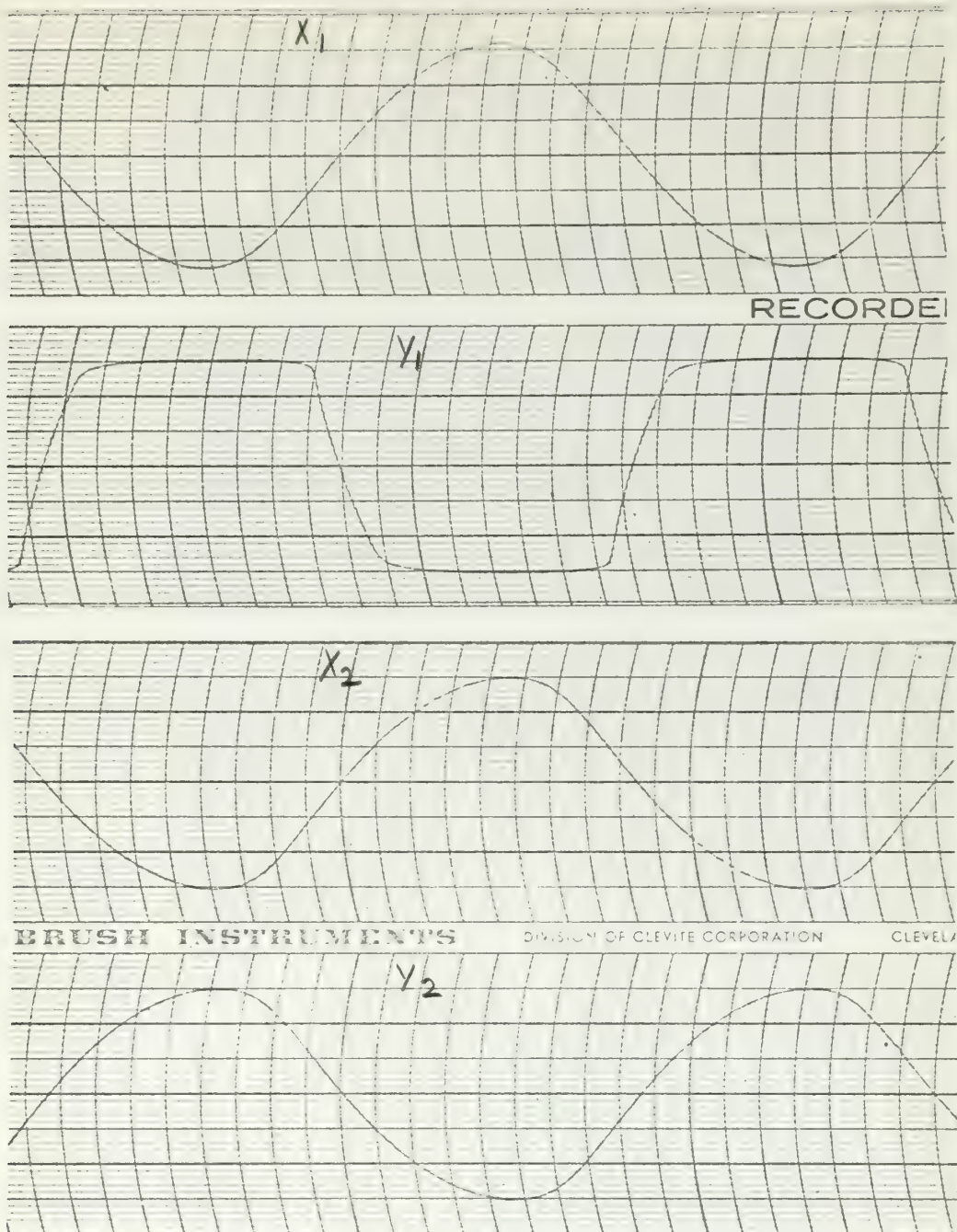
Recorder Trace VI-12

Limit Cycle for Unstable Linear M-Point to Left of No. 1

Dividing Line, $K_e = 4$, $K_t = 0.8$

SCALES: X_1 -0.5 Volts/Line Y_1 -0.2 Volts/Line X_2 -0.2 Volts/Line

Y_2 -0.2 Volts/Line Time -0.2 Seconds/Division

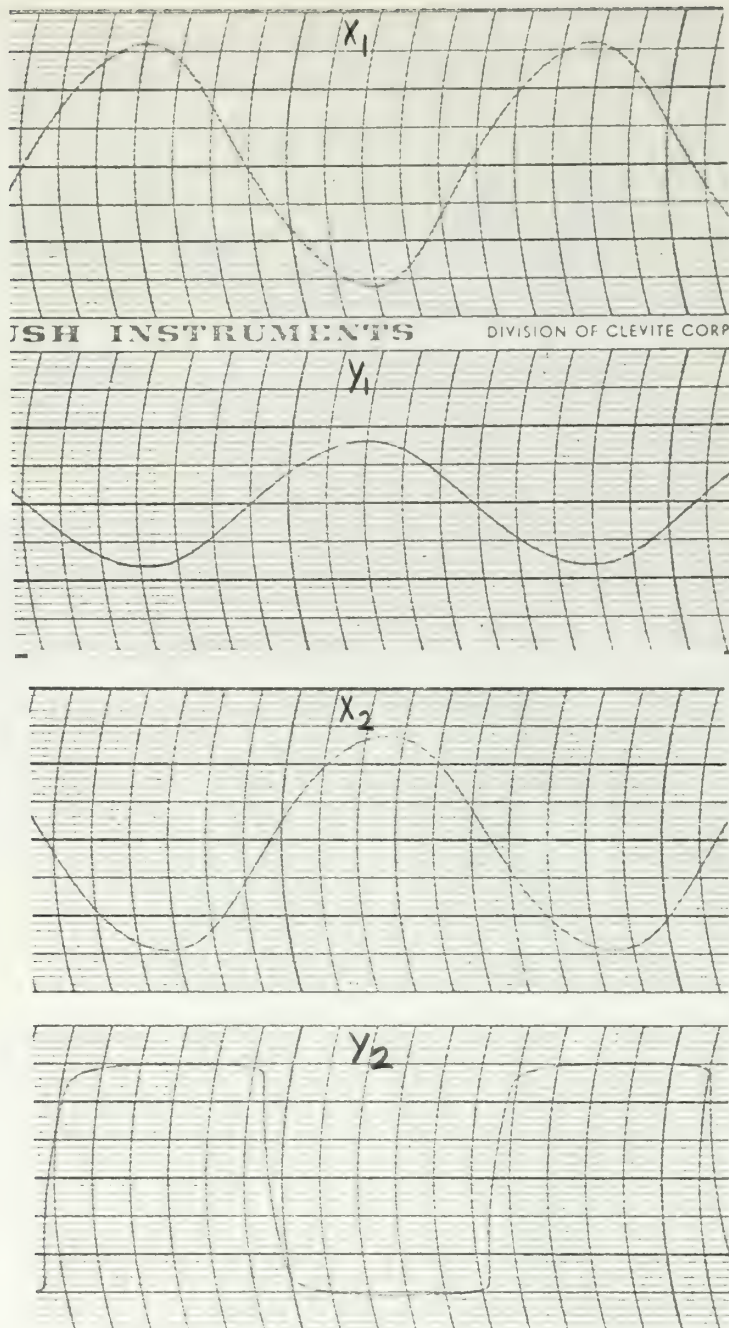


Recorder Trace VI-13

Limit Cycle for Unstable Linear M-Point to the Right of No. 1
Dividing Line, $K_e = 4$, $K_t = 0.82$.

SCALES:

X_1 -0.5 Volts/Line Y_1 -0.2 Volts/Line X_2 -0.2 Volts/Line
 Y_2 -0.2 Volts/Line Time -0.2 Seconds/Division

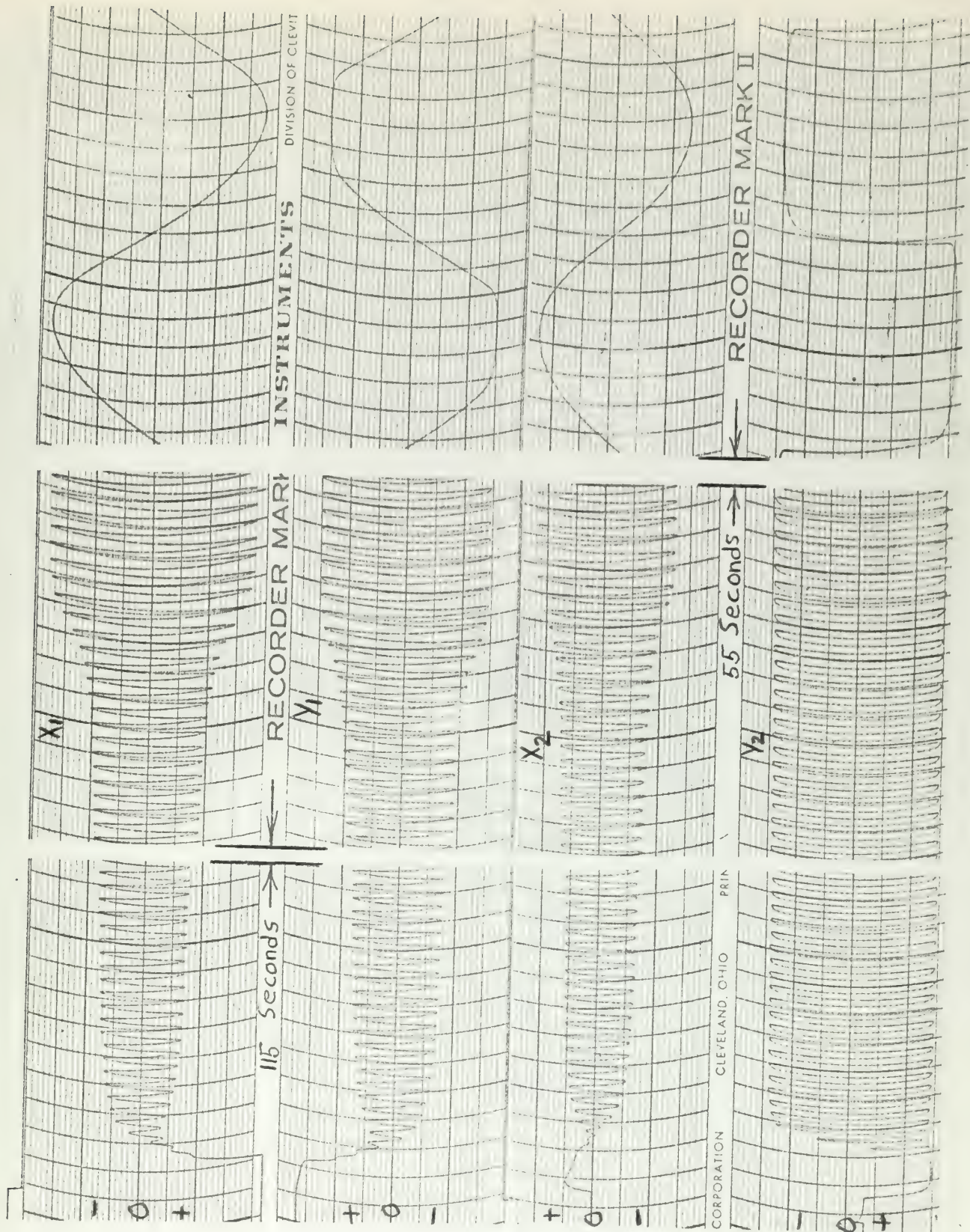


Recorder Trace VI-14

Limit Cycle for Unstable Linear M-point Below No. 2
 Dividing Line at $K_e = 2.38$, $K_t = 8$.

SCALES:

X_1 -0.1 Volts/Line Y_1 -0.2 Volts/Line X_2 -1 Volt/Line
 Y_2 -0.2 Volts/Line Time-0.2 Volts/Line



Recorder Trace VI-15

Unstable Linear M-Point Above No. 2 Dividing Line at $K_e = 2.40$, $K_t = 8$.

SCALES:

X_1 -0.2 Volts/Line

Y_1 -0.2 Volts/Line

X_2 -2 Volts/Line

Y_2 -0.2 Volts/Line

Time - 5 Seconds/Division

-0.2 Second/Division

FIGURE VI-4

VARIAION OF AMPLITUDE OF X_2 OF THE RESULTING
LIMIT CYCLE AS LINEAR TACH CHANNEL GAIN
IS VARIED, ERROR CHANNEL GAIN FIXED

LIMIT CYCLE PEAK X_{2max} (VOLTS)

NOTE 1

For small K_E and
For $K_E < 2.4$ the
curve segments
essentially lie on
the low portion
of the $K_E = 2.0$
curve.

LINEAR M-POINT K_E

E_2 SAT

35
30
25
20
15
10
5
0

2 3 4 5 6 7 8 9 10

$K_E = 0.5$
 $K_E = 1.0$
 $K_E = 1.5$
 $K_E = 2.0$
 $K_E = 2.5$
 $K_E = 3.0$

$K_E = 2.0$
 $K_E = 1.5$
 $K_E = 1.0$
 $K_E = 0.5$

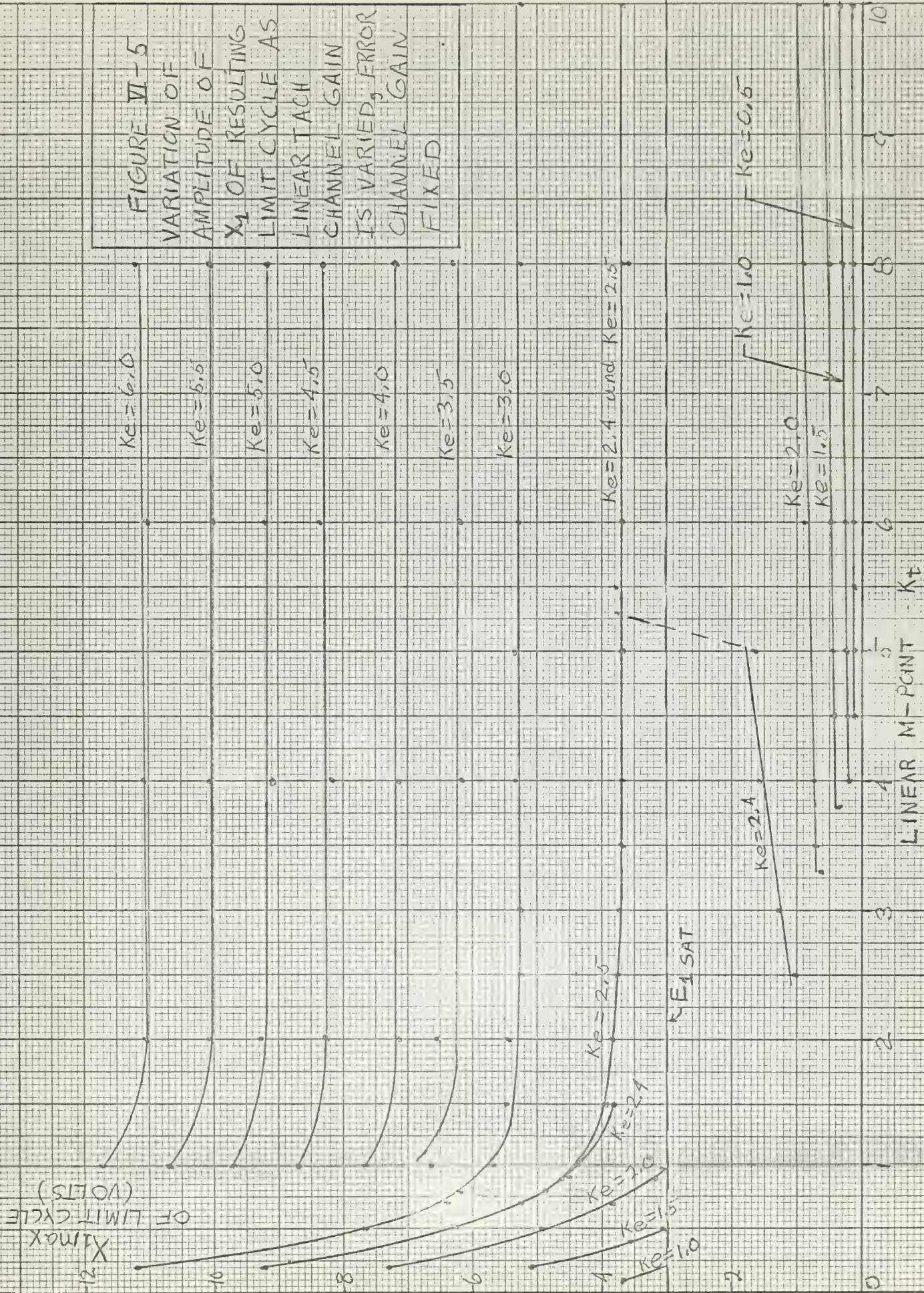


FIGURE VI-6
 VARIATION OF AMPLITUDE X_2 OF THE
 RESULTING LIMIT CYCLE AS THE
 ERROR CHANNEL GAIN IS VARIED,
 TACH CHANNEL GAIN FIXED

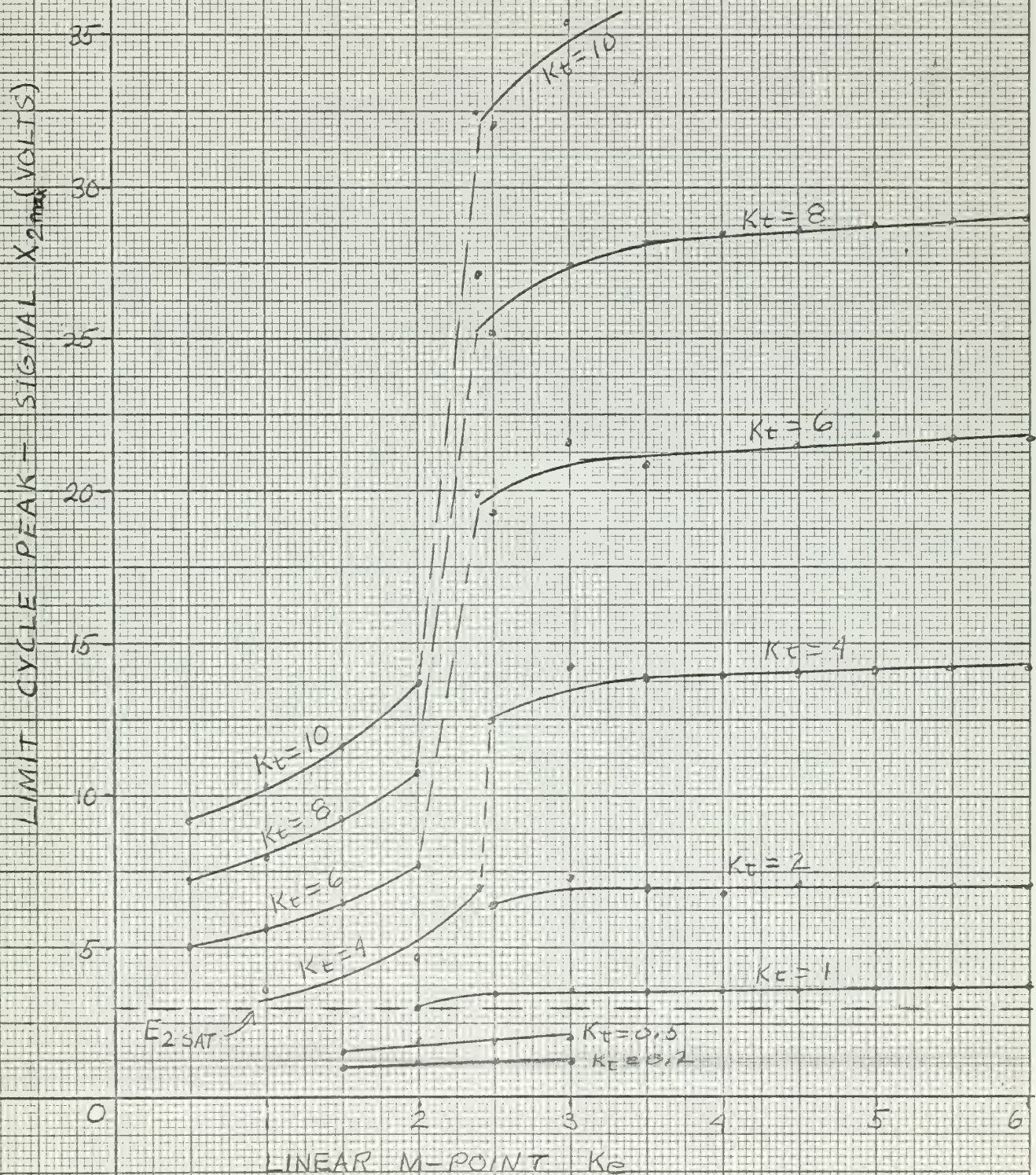
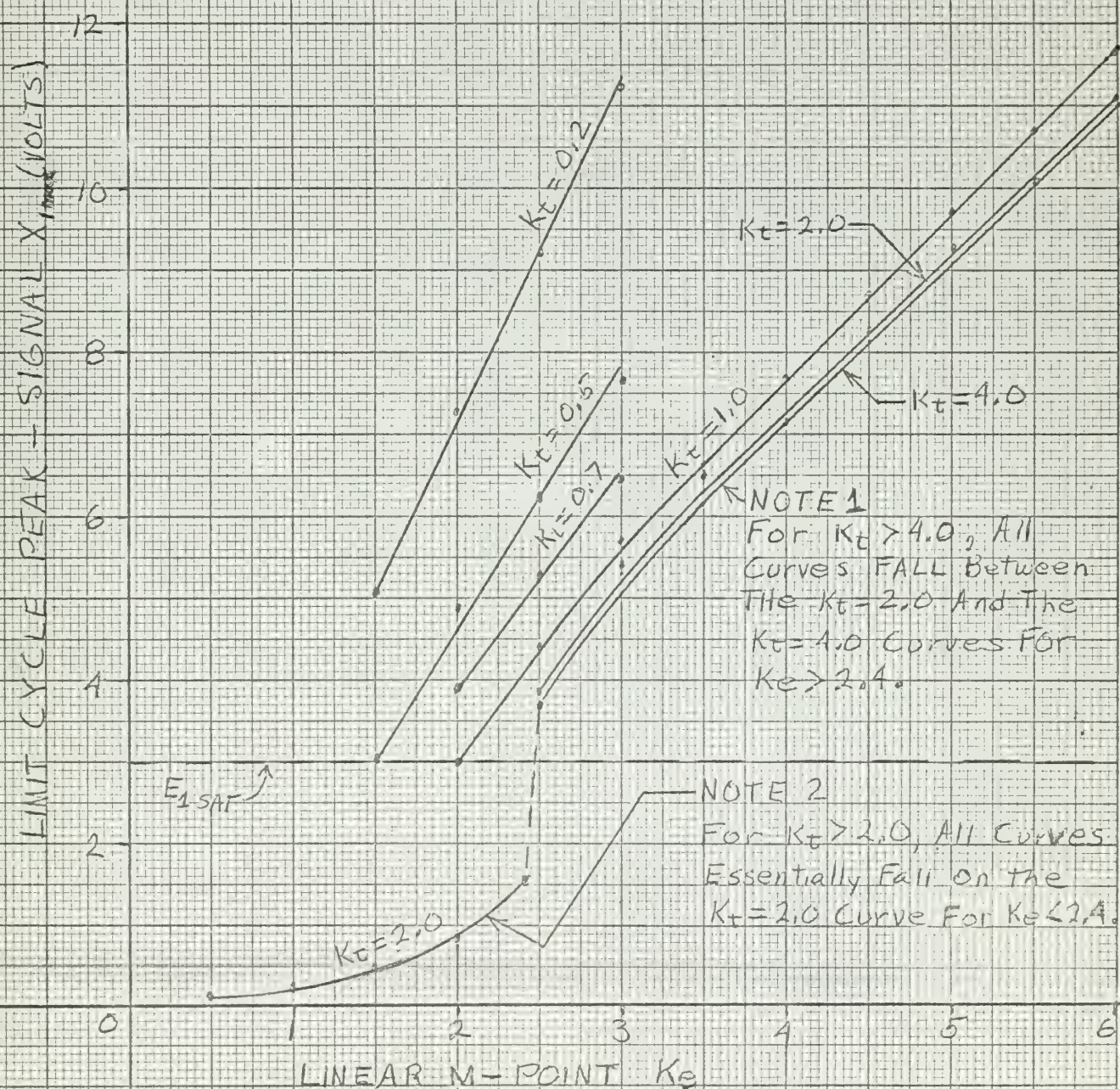
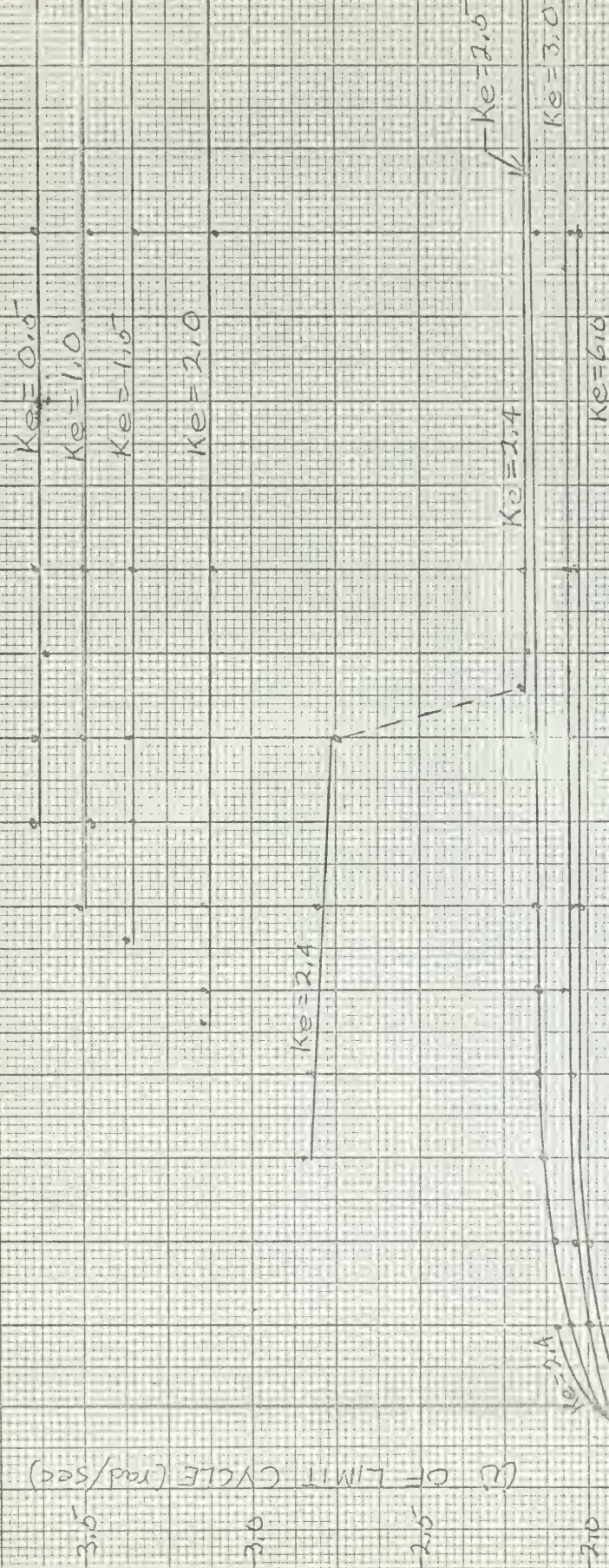


FIGURE VI-7
 VARIATION OF AMPLITUDE OF X_1 OF THE
 RESULTING LIMIT CYCLE AS THE ERROR
 CHANNEL GAIN IS VARIED, TACH
 CHANNEL GAIN FIXED.



(b) OF LIMIT CYCLE (rad/sec)



NOTE 1:

All curves for small K_t follow the $K_e = 2.4$ curve up to the stable region of $B_0 V_3 B_1$ plane

FIGURE VI-8

VARIATIONS OF THE LIMIT CYCLE FREQUENCY FOR VARIATIONS IN K_t , K_e REMAINING CONSTANT

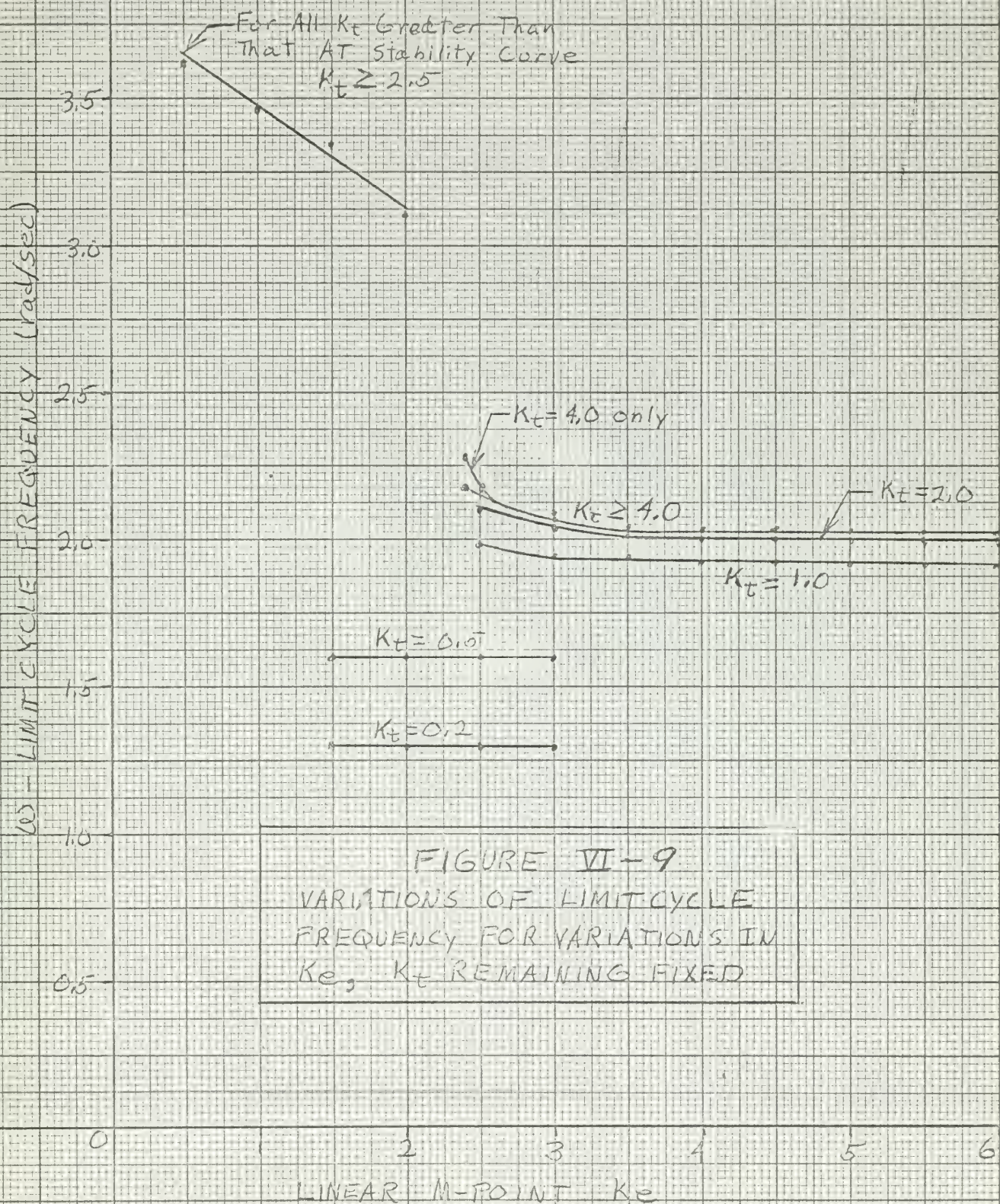
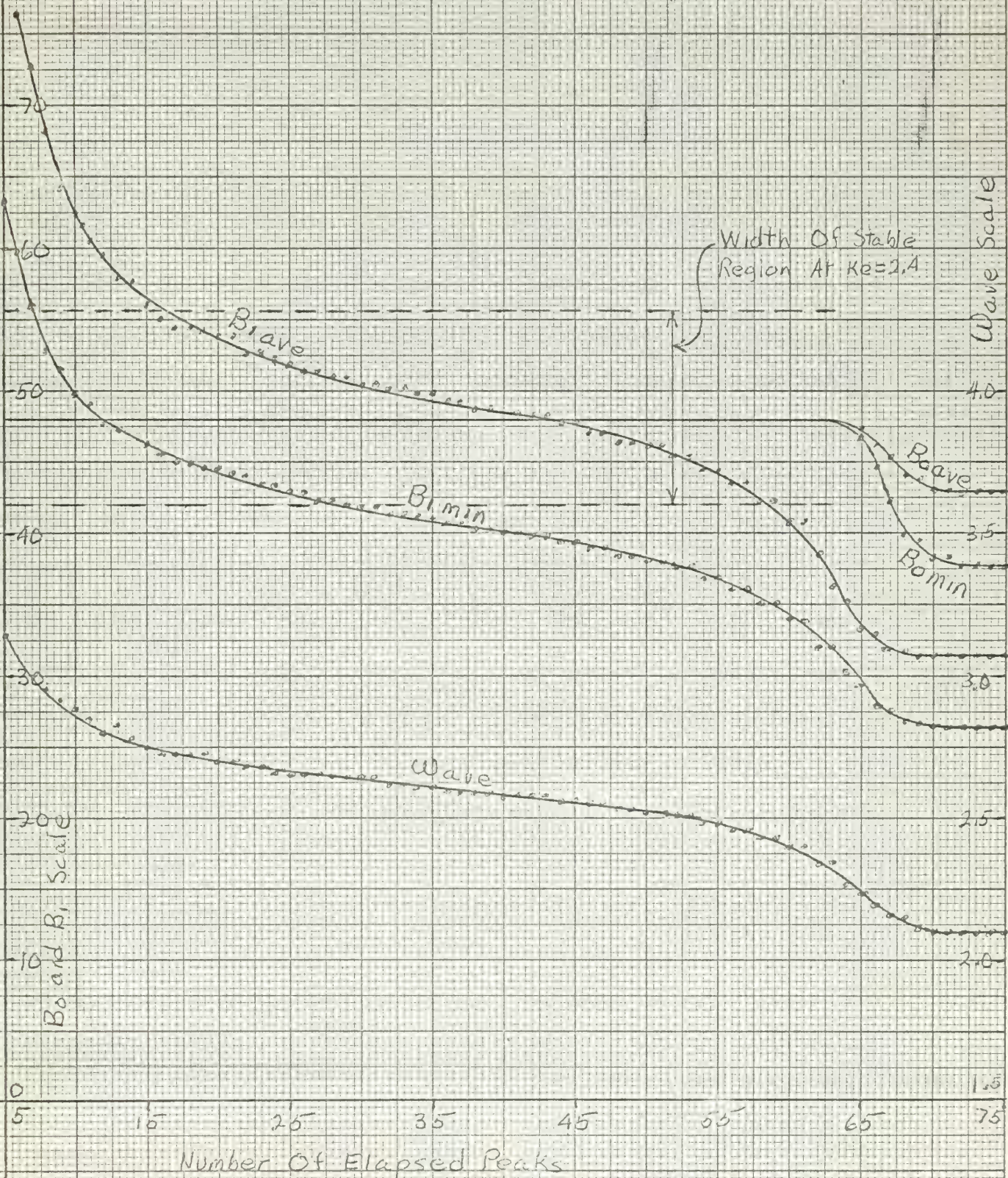


FIGURE VI-10
 VARIOUS QUANTITIES OF THE RESPONSE FOR A
 LINEAR M-POINT AT $K_e = 2.4$, $K_e = 8.0$ VERSUS
 THE NUMBER OF ELAPSED OSCILLATION PEAKS



CHAPTER VII

EXPLANATION OF THE RESULTS AND SOME METHODS OF PREDICTING THE RESULTS

An attempt is made in this chapter to explain the system responses and results given in Chapter VI by associating the responses obtained in the study with a corresponding M point motion on the K_2 versus K_1 plane of Figure VI-1.

Before attempting an explanation of any of the results, a helpful insight into the system can be obtained by first looking at the system as only having error channel saturation and then looking at the system as only having fast channel saturation. First, assuming only error channel saturation and applying the arguments given in Chapter I, Section I-A-1 to Figure VI-1, it is determined for any $K_2 < 4.5$ the error saturation produces a stable linear system. For $K_2 > 4.5$ the linear system can never be made stable by varying K_1 ; consequently, there is no possibility of a limit cycle with error channel saturation only and $K_2 > 4.5$. This fact is easily shown by a quick root locus analysis. The root locus of the inner loop is sketched in Figure VII-1. For a K_2 large enough to place the inner loop closed loop roots in the right half plane, no amount of K_1 can make the root locus swing into the left half plane. Starting with the closed loop roots of the inner loop as the open loop roots of the outer loop, the asymptotes remain at $\pm 60^\circ$ and -180° although their centroid is moved to the right. A rough check of the angle of emergence from the upper pole shows that this angle is a first quadrant angle. The 100 axis crossover of the inner loop root locus is determined to be $K_2 = 4.5$. Thus the outer loop root locus can only proceed as indicated in the figure and for $K_2 > 4.5$ the system is always unstable.

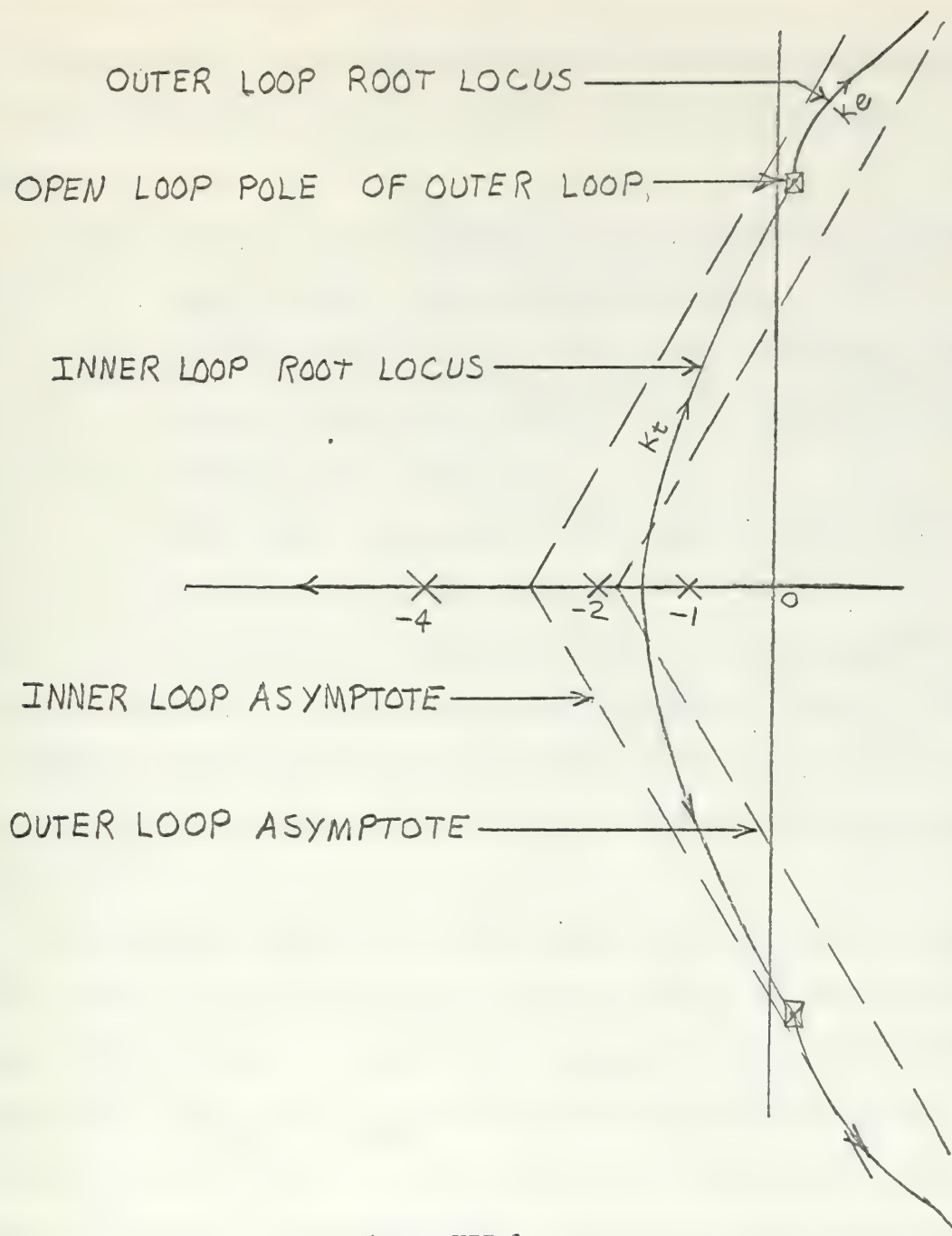


Figure VII-1

Root Locus of the Tachometer Feedback Path
then the Position Feedback Path.

Assuming only tach channel saturation and applying the arguments of Chapter V, Section V-A-1 to Figure VI-3, it is determined that for a $K_e < 2.45$;

1. The side of the stability curve to the right of the maximum ($\omega_n > 2.645$) yields stable limit cycles.
2. The side of the stability curve to the left of the maximum ($\omega_n < 2.645$) yields unstable limit cycles, at least for $0.75 < K_e < 2.45$.
3. Which limit cycle governs the response is entirely dependent upon the input signal magnitude.

For $K_e > 2.45$ Figure VI-3 indicates the linear system is always unstable no matter what the K_t , thus no limit cycle is possible. For $K_e < 0.75$, the absolute minimum gain of the nonlinearity, i.e., $N_2 = 0$, the M-point is still within the stable region, and thus an unstable limit cycle is impossible.

From the above discussion, one can safely say that with both saturations present a stable limit cycle will always result no matter where the linear M-point lies, even though individually each saturation has certain areas in which the single nonlinearity system is absolutely unstable. This statement is true because for large K_e and K_t the tach channel saturation moves the "average" M-point to the left such that the error channel saturation can move it downward to lie on the stability curve, or vice versa.

A result of the Chapters of Part I will also be helpful in being able to predict the results of Chapter VI. The magnitude of the describing function at the intersection at the intersection with the linear loop transfer function curve on the gain-phase plane is essentially equal to the magnitude of the "average" gain of the nonlinearity as obtained by Mitrovic's

and root locus methods. Table VII-1 gives a comparison of N_{ave} and G_D under the limit cycle condition for all the systems analyzed in Part I.

TABLE VII-1

| Nonlinearity | No. of Zeros | Root Locus N_{ave} | Mitrovic's N_{ave} | Describing Function(G_D) |
|----------------------------|--------------|----------------------|----------------------|------------------------------|
| Saturation | 0 | 0.60 | 0.60 | 0.604 |
| | 1 | 0.8051 | 0.8052 | 0.7953 |
| Dead Zone | 0 | 0.5951 | 0.590 | 0.5989 |
| | 1 | 0.4089 | 0.4072 | 0.3987 |
| Ideal Relay | 0 | 1.1053 | 1.1032 | 1.0976 |
| | 1 | 0.5573 | 0.5573 | 0.5629 |
| Relay with Dead Zone | 0 | 0.4568 | 0.4543 | 0.4225 |
| | 1 | 0.6208 | 0.6208 | 0.5757 |
| Tach FB Saturation | 0 | 0.08737 | 0.08739 | 0.08802 |
| | | 0.5958 | 0.5959 | 0.5957 |
| Acceleration FB Saturation | 0 | 0.4614 | 0.4614 | 0.4648 |

The number of significant figures listed for the describing function in Table VII-1 is misleading since G_D was calculated using at best three figure accuracy from a graphical plot of an intersection. Even with this uncertainty in G_D , the comparisons only differ greatly in the last two or three significant figures. With more accurate calculation of the intersections of the three methods, the numbers should be exactly equal. A non-rigorous proof of this equality follows:

The describing function method applies the Nyquist criterion and is basically a frequency response technique involving a variable system critical point. For this proof assume that the symbol, G_D , and the words, describing function, are undefined in terms of the amplitude of the input signal to nonlinearity. Then for gain variable nonlinearities, the Nyquist

criterion becomes

$$G_D G(j\omega) = -1 \quad (\text{VII-1})$$

This general equation can then be applied to any one of the systems analyzed in Part I.

For convenience apply the root locus criterion to the system of Section I-A, Chapter I which yields

$$\frac{10 N}{s(s+1)(s+2)} = -1 \quad (\text{VII-2})$$

But in equation VII-2

$$\frac{10}{s(s+1)(s+2)} = G(s)$$

which is the linear loop transfer function. Thus

$$NG(s) = -1 \quad (\text{VII-3})$$

where $G(s)$ can now be any linear loop transfer function.

In the root locus method of predicting limit cycles for gain variable nonlinearities, one is only interested in the limit of stability of the linear loop transfer function. Another way of saying the same thing is that one is interested in finding the point on the linear system root locus at which self sustained oscillations are possible. Of course, this occurs when the linear root locus crosses the $j\omega$ axis or when $s = j\omega$. Substituting $j\omega$ for s in equation VII-4,

$$NG(j\omega) = -1. \quad (\text{VII-4})$$

It is a well known fact that both the frequency response technique and the root locus accurately predict the absolute stability of a system. Consequently, equations VII-1 and VI-4 must be equivalent and therefore N and G_D must be equal since the $G(j\omega)$ is the same in both equations for any given system.

The fact that N_{ave} and G_D are equal under limit cycle conditions is really only useful when G_D as a number is related to the amplitude of the input signal to the nonlinearity. Of course this relationship is strictly valid only when the input signal is sinusoidal. Thus when the use of the describing function can be justified in a given system, root locus and Mitrovic's methods will also accurately predict the limit cycle amplitude. The limit cycle can then accurately and quickly be determined by substituting $s = j\omega$ in the characteristic equation, calculating the amplitude from the describing function relationship.

PROBABLE QUALITATIVE EXPLANATIONS

1. Stable responses to step inputs for which the linear system M-point lies within the stability region.

- a. For small signal inputs in which the error channel does not saturate, Recorder Traces VI-1, VI-3, and VI-5 are representative. Two of these traces show the first peak of signal X_2 is large enough to saturate the tach channel. However, after the first velocity peak, the X_1 and X_2 signals are well below the saturation levels of 3 volts and the oscillations die out according to the position of the linear M-point. Insight into an explanation is obtained if the instantaneous minimum M-points are calculated from X_{2max} of the first peak in Traces VI-3 and VI-5 and then plotted on the B_0 and versus B_1 plane. These instantaneous M-points are shown as M_1 and M_2 respectively in Figure VII-2. The starting point of the arrow is the linear M-point and the head of the arrow is the instantaneous minimum M-point. One trace which was not included in the results of Chapter VI showed that the first peak of X_2 saturated the tach channel sufficiently to drive the instantaneous minimum M-point into the unstable region as shown

by M_3 in Figure VII-2. However, the tachometer channel did come out of saturation and the system was stable. Thus for linear M-points close to the left portion of the stability curve the tach channel may saturate but the magnitude of signal X_2 is not large enough to cause the instantaneous M-point to be in the unstable region for a sufficient portion of the first oscillation to drive the average M-point to the stability curve. This was thought to be due to the relatively small values of K_t . As K_t is increased in an attempt to raise the magnitude of the first peak of signal X_2 , two effects combine to keep the response stable. First as K_t increases, the linear M-point moves to the right and the linear system damping is increased, at least the damping is increased until the M-point moves approximately across the axis of the parabolic stability curve. The increased damping tends to nullify the expected increase in $X_{2\max}$. Secondly and most important, the relative distance the average M-point must move to reach the left side of the stability curve increases. The left portion of the stability curve is the governing stability limit for the linear M-point in the stable region because only by tach saturation can the system be driven unstable. Thus, the increase in $X_{2\max}$ is not sufficient to offset the increase in this relative distance such that the instantaneous M-point can lie in the unstable region for a sufficient portion of the first oscillation to drive the average M-point to the stability curve.

As the linear M-point moves to the right past the approximate axis of the stability curve the damping begins to decrease but the relative distance between linear M-point and the left side of the stability curve is quite large and obviously overrides the increase in peak X_2 and keeps the system stable. This relative distance is in some manner related to the degree of saturation necessary to cause limit cycle operation since this is the graphical distance

the average M-point must move to reach the unstable limit cycle governing the tach channel.

b. For large input steps in which the error channel initially saturates, the same explanations given above also apply after the error channel comes out of saturation. Recorder Traces VI-2, VI-4, and VI-6 are applicable. It is constructive, however, to analyze the response prior to the error channel becoming linear. The effects to be discussed are most apparent in Recorder Trace VI-4. With the error channel initially saturated, the initial driving voltage of the plant is 3 volts. Since X_2 does not change instantaneously (it is proportional to velocity) the driving voltage remains at 3 volts for a short instant of time. The trace indicates that X_2 increases very rapidly and that Y_2 essentially jumps to the saturation value of 3 volts. Also, the output angle and X_1 have not changed during this short time interval. Thus because of the signs of the feedback voltages, the driving signal of the plant goes to zero after a very short time. This leads to the initial plant driving signal shape shown in Figure VII-4a as a first approximation. Second approximations might be as shown in Figure VII-4b and c. The solution for the output angle when the first signal approximation is applied to the plant is of the form,

$$\theta_0 = C_1 t + C_2 e^{-t} + C_3 e^{-2t} + C_4 e^{-4t} + C_5 (t-t_1) + C_6 e^{-(t-t_1)} + C_7 e^{-2(t-t_1)} + C_8 e^{-4(t-t_1)}$$

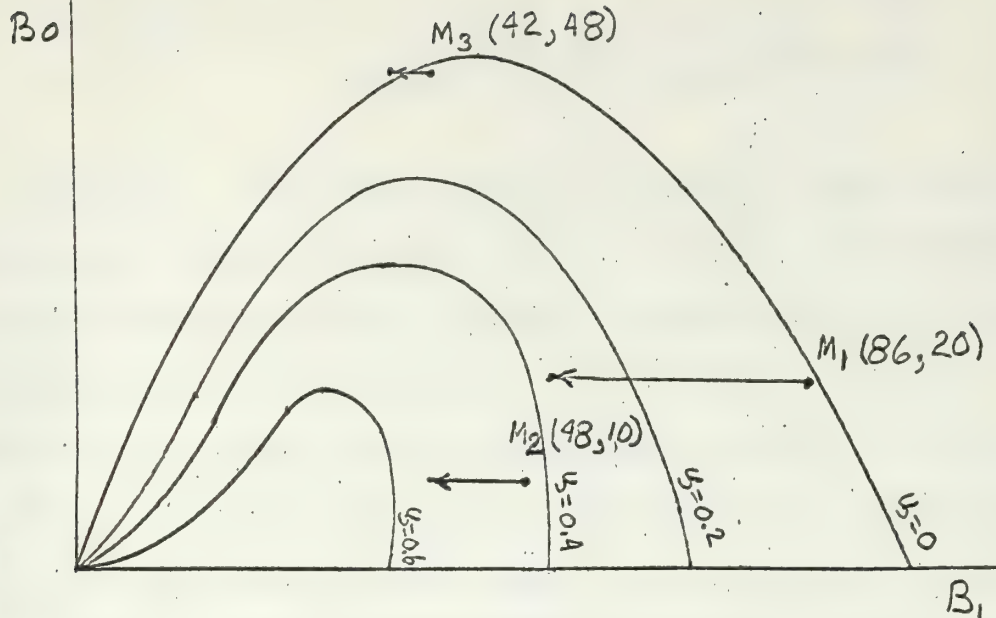


Figure VII-2

M-point Loci for Stable Linear Systems for Small Step Input Magnitude

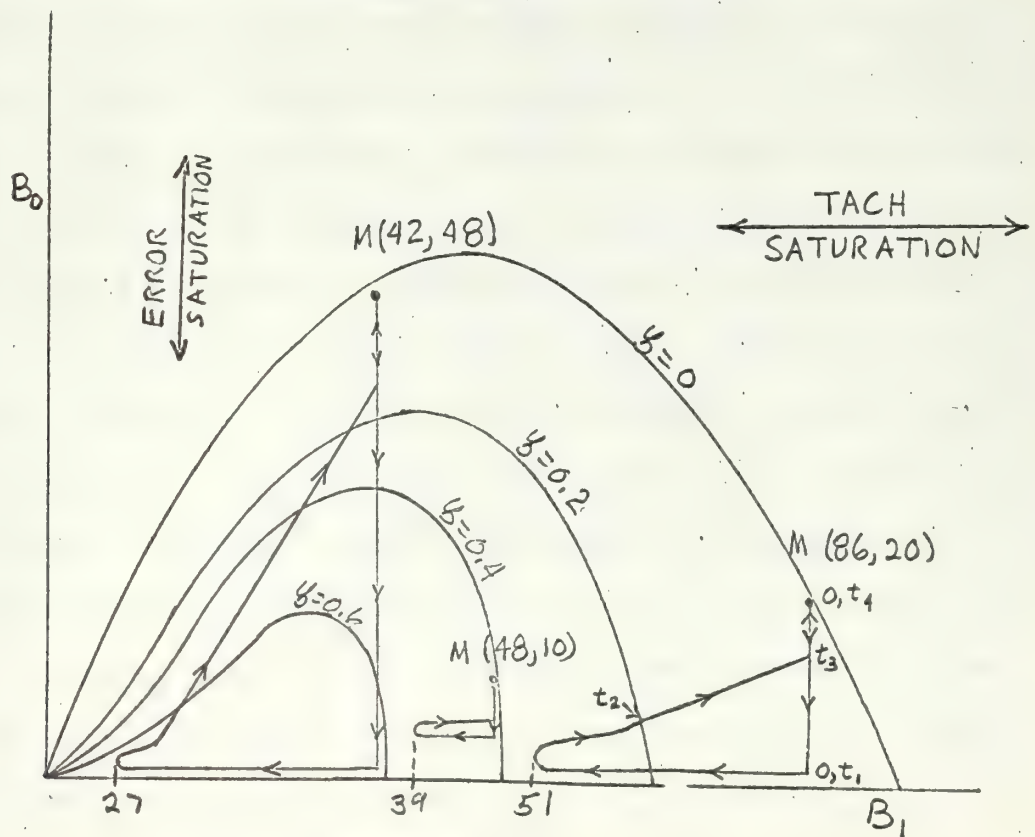


Figure VII-3

M-point Loci for Stable Linear Systems for Large Step Input Magnitude

Differentiation gives the output velocity as

$$\dot{\theta}_0 = C_1 + C_2' e^{-t} + C_3' e^{-2t} + C_4' e^{-4t} + C_5 + C_6' e^{-(t-t_1)} + C_7' e^{-2(t-t_1)} + C_8' e^{-4(t-t_1)}$$

Since $X_2 = K_T \dot{\theta}_0$, the initial portion of signal X_2 is easily explained by the sum of the exponential terms given above. Time t_1 is the time at which the tach channel saturates. At time t_2 , indicated on Recorder Trace VI-4, the response of the plant to the initial input has ended and the system is coasting because the plant driving signal is zero. At time t_3 , the velocity of the coasting system has decreased such that X_2 is less than 3 volts and the tach channel becomes linear. As X_2 slowly decreases below 3 volts, a slowly increasing positive voltage is applied to the plant because the error channel is still transferring a positive 3 volt signal. This is indicated on the Recorder Trace by the fact that X_2 levels out at about 2.8 volts instead of remaining in an exponential decay. The relatively sudden decrease in X_2 after time t_3 and before X_2 levels out can not be explained, except by noting that the saturation simulations do not strictly limit their outputs to three volts. This is due to a finite diode resistance and pot loading effects when the diode conducts. Signal Y_1 is initially 3.6 volts and signal Y_2 is 3.1 volts after saturation. Thus the plant of the analog simulation is actually being driven by about 0.5 volts or less during the period in which the author has assumed zero driving voltage. This fact may account for the relatively sudden decrease in X_2 after time t_3 . Eventually the output drives to within 3 volts of the input and the error channel comes out of saturation at time t_4 . From this time on the system responds according to the linear M-point.

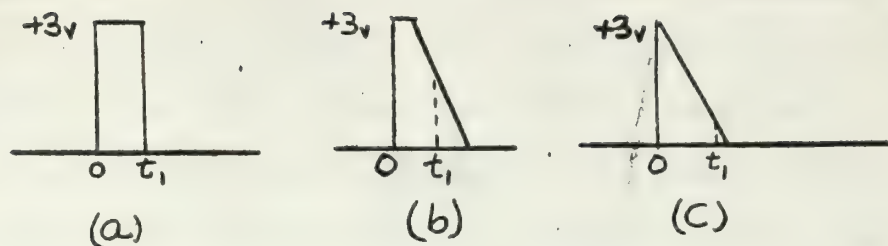


Figure VII-4

Possible Waveshapes of Initial Plant Driving Signals for Stable Linear M-point with Large Input Steps Applied.

The same response in Recorder Trace VI-4 can also be qualitatively explained strictly by the system M-point motion. With the error channel initially saturated the M-point immediately jumps downward along the linear M-point K_t coordinate. For Recorder Trace VI-4, this initial M-point jump moves the M-point to $K_e = 0.0316$ or $B_o = 0.632$ by equation VI-c. This M-point motion increases the system damping a small amount over the damping of the linear system. Within a very short time interval, the tach channel saturates and rapidly moves the M-point to the left, essentially along a constant K_e line since the error has not appreciably changed to cause an upward component in the M-point motion. The rapid movement of the M-point to the left greatly increases the system damping, possibly close to critical damping. With the M-point moving into a highly damped region within a short time, very few oscillations would be expected and would be damped out very quickly by say time t_2 in Recorder Trace VI-4. The peak velocity is more difficult to explain but is certainly dependent upon how soon the tach channel saturates since this is the controlling factor of the time required for M-point motion into the highly damped region. After time t_2 , it is difficult to explain the response strictly by M-point motion until time t_4 .

is reached when the error channel comes out of saturation. At this time the system is completely linear and the oscillations occur according to the ζ and ω_n of the linear M-point. These oscillations will be small since the disturbance as the error channel comes out of saturation is small. The estimated M-point motion corresponding to Recorder Trace VI-4 is sketched in Figure VII-3 along with those of Recorder Traces VI-2 and VI-6. The corresponding times from recorder trace VI-4 are indicated along the path. The lines of constant ζ were not calculated but their shape was sketched from those calculated for a different fourth order system. For the given fourth order system, the constant ζ lines will not differ greatly from those sketched. The objective of the constant ζ lines is to show that the instantaneous damping can increase or decrease either a small amount or a large amount for both horizontal and vertical motions of the system M-point. The entire figure is not to scale but the numbers listed are correct.

c. The fact that the system could be driven into a limit cycle by repeated disturbances and linear M-points close to the left portion of the stability curve cannot be explained satisfactorily by M-point motion. However, from Recorder Trace VI-8, it was noted that between disturbances and after the first saturated peak of X_2 , the signals X_1 and X_2 were slightly damped and below 3 volts but at a generally higher amplitude than before the disturbance. With little linear system damping the magnitude of X_2 oscillations decreases very little between disturbances. After several disturbances the X_2 oscillations are just below the saturation level. The next disturbance causes the first peak of X_2 to saturate N_2 to the degree required to move the average M-point from the linear point to the stability curve and the oscillations build up since tach saturation gives an unstable

limit cycle. The final limit cycle is stable because the error channel eventually saturates as the oscillations build up. It was stated in Chapter VI that the magnitude of the disturbance had to be small such that the error channel does not saturate appreciably, otherwise the magnitude of X_2 oscillations after the disturbance was less than the magnitude of the oscillations before the disturbance. This result is easily explained by the M-point motion. When the error channel saturates the M-point moves rapidly downward, greatly increasing the damping. The increased damping damps out the oscillations before the output has time to come into correspondence with the new input demand. Consequently, the disturbance causing the oscillations after the error channel comes out of saturation is much less than the disturbance which caused the error channel to saturate. The response is very similar to the response to a large step input applied at time zero as described previously.

2. Limit cycles were obtained only for linear M-points in the unstable region.

a. The result that the limit cycles were independent of the magnitude of the input signal was suspected because of the arguments given in the introduction to Part I. For saturation in the error channel limit cycles are only possible for an unstable linear system. Thus the existence of the limit cycle is entirely dependent on the linear system and not the step input signal because the linear poles and zeros determine the possibility of instability and the linear gain determines whether or not the linear system is stable or unstable. For saturation in the tach channel, an unstable limit cycle is possible with a stable linear system. However, the existence of this limit cycle is only dependent on the linear system. The magnitude of the step input signal determines only whether or not the non-linear system response is unstable or stable. Thus if the existence of a

limit cycle for each of the nonlinearities individually is independent of the magnitude of the input step function, then the existence of a limit cycle with both nonlinearities in the same system is independent of the step input.

b. The result that the limit cycle amplitudes of X_1 and X_2 are dependent on the relative distance between the linear M-point and the stability curve is explained by degrees of saturation. Degree of saturation means the relative magnitudes of N_{1ave} and N_{2ave} which are required to place the average M-point on the stability curve. For systems with linear M-points close to the stability curve, the average M-point has a small distance to travel either horizontally and/or vertically to reach the stability curve. For sinusoidal input waveshapes of signals X_1 and X_2 , it has been shown that N_{ave} can be related to the amplitude of the input signal through the describing function. For small average M-point motions N_{1ave} and N_{2ave} will be just less than 1.0 from equations VI-c and VI-d because B_{oave} and B_{1ave} will be very close to the linear M-point values. By the describing function relation for values close to one, the input amplitude is just slightly greater than the saturation voltage. Thus the amplitudes of X_1 and X_2 will be slightly greater than 3 volts. For linear M-points relatively distant from the stability curve, the values of B_{oave} and B_{1ave} will be greatly different from the linear M-point coordinates. Thus N_{1ave} and N_{2ave} are small fractions and through the describing function relationship the amplitudes of X_1 and X_2 are correspondingly large.

c. The result that for $K_t > 3$ and $K_e > 3$ the frequency of the limit cycle is essentially independent of K_e and K_t variations can be explained only in terms of other results which are apparent in Figures VI-4 through VI-7. From Figure VI-5 it is noted that for constant K_e above the

stability curve and for $K_t > 2$, the amplitude of X_1 is independent of K_t variations and only dependent on K_e variations. Thus as K_t increases above $K_t = 2$, the vertical distance the average M-point must move to reach the stability curve is relatively constant for K_e constant. This fact can be explained as follows. No matter what the K_e or K_t , the initial driving voltage of the plant remains at 3 volts, thus the initial changes in Θ_0 and $\dot{\Theta}_0$ are unaffected by K_e and K_t . Also Θ_0 is subject to an extra time lag which $\dot{\Theta}_0$ is not. Thus for $K_t > K_e > 3$, it can safely be said that the tach channel saturates before the error channel and the resultant average M-point motion is to the left instead of downward. Consequently, it is difficult to conceive of a limit cycle occurring on the right side of the stability curve. This fact is shown in experimental results since all the limit cycles obtained from linear M-points in Region II exhibited frequencies on the left side of the stability curve. Thus the tach channel first saturates to move the average M-point to the left past the maximum of the stability curve along a constant K_e line. Once the average M-point is in this position the vertical distance it must move to reach the stability curve by error channel saturation is relatively constant as long as the K_e coordinate of the linear M-point is kept constant. As K_e increases, Figure VI-7 shows that for $K_e > 3$, the limit cycle amplitude increases linearly with K_e and that K_t variations have little effect when $K_t > 2$. The linear variations of $X_{1\max}$ with K_e is reasonable since it has been shown that the relative vertical distance the average M-point must move is independent of K_t for a given K_e . Thus the B_{oave} coordinate of the average M-point of the limit cycle is relatively independent of the variations in the linear M-point for K_e and K_t greater than 3. Since the B_{oave} coordinate is always the same, it can intersect the left portion of

the stability curve at only one point and therefore the frequency of any limit cycle resulting from a linear M-point located by $K_e > 3$ and $K_t > 3$ is unaffected by variations of K_e and K_t . These same conclusions could be obtained by using $X_{2\max}$ and Figures VI-4 and VI-6. However, it must be pointed out that the limit cycle frequency and the signal amplitudes are not necessarily independent in Region II of Figure VI-3, thus the above explanation is somewhat trivial. In Regions I and III, the frequency is independent of amplitudes and the above result indicates that it is also essentially true in Region II for $K_e > 3$ and $K_t > 3$.

3. Division of the Unstable Region into Subregions.

The signals X_1 and X_2 are not independent of one another. That is, except for constants X_2 is the time derivative of X_1 . Consequently it is entirely reasonable for the system in limit cycle operation that the limit cycle amplitude of one of the signals is not large enough to allow the limit cycle amplitude of the other signal to be great enough to saturate the other channel. For example, a limit cycle with small velocity excursions will not drive the output angle far enough before the velocity changes sign to allow signal X_1 to be greater than the saturation level of the error channel. This is especially apparent in Recorder Trace VI-14 where the limit cycle amplitude of X_2 is 14.3 volts whereas the amplitude of X_1 is only 1.61 volts.

a. The explanation of dividing line No. 1 is this. Recorder Traces VI-12 and VI-13 are applicable. Recorder Trace VI-12 shows the limit cycle resulting from a linear M-point just to the left of dividing line No. 1 at $K_e = 4$ and $K_t = 0.8$. The amplitude of X_1 is 8.1 volts and the amplitude of X_2 is 2.95 volts. Recorder Trace VI-13 shows the limit cycle resulting from a linear M-point just to the right of dividing line

No. 1 at $K_e = 4$ and $K_t = 0.82$. The amplitude of X_1 is unchanged at 8.1 volts within the readable accuracy of the trace whereas the amplitude of X_2 has increased to 3.02 volts. In this case the amplitude of the velocity and output angle probably did not change enough to be readable had these signals been recorded because $\dot{\theta}_{012} = 2.95/0.8 = 3.69$ volts and $\dot{\theta}_{013} = 3.02/0.82 = 3.69$ volts. However, the increase in K_t was enough to cause $X_{2\max}$ to be greater than 3 volts.

b. Dividing line No. 2 is due to an entirely different phenomenon since from Figure VI-7 for $K_e < 2.4$ the amplitude of X_1 is well below saturation at about 1.5 or 1.6 volts. Also, since the maximum of the stability curve is at $K_e = 2.45$ and the amplitude of X_1 is about half the saturation voltage at $K_e = 2.38$, one would expect something quite drastic to occur as K_e is increased above 2.45 because the error channel must saturate for larger values of K_e . The phenomenon which occurs can be explained as follows. For a linear M-point just below No. 2 dividing line, Recorder Trace VI-14, only the tach channel saturates and the limit cycle average M-point lies on the right side of the stability curve. A quick calculation using the amplitude X_2 and equation VI-d shows the minimum instantaneous M-point of the limit cycle is at $B_{1\min} = 41.5$ and $K_e = 2.38$ where as an unstable tach channel limit cycle exists at $B_1 = 41.0$ for $K_e = 2.38$. Thus the minimum instantaneous M-point never crosses into the left unstable region and a dynamic equilibrium condition is established about an average M-point on the right side of the stability curve at the $K_e = 2.38$ line. As K_e is increased to place the linear M-point above No. 2 dividing line, two effects add together to cause the response and limit cycle of Recorder Trace VI-15. These two effects are sketched in Figure VII-5 along with $B_{1\min}$ of Recorder Trace VI-14. The first effect is that the increase in K_e increases the relative distance the average M-point must travel to reach the stability curve

from Δa to $\Delta a'$. As indicated previously, this causes the limit cycle amplitude of X_2 to increase slightly. Secondly, the increase in K_e causes the graphical distance between a stable tach channel limit cycle and an unstable tach channel limit cycle to decrease from Δb to $\Delta b'$. This change in Δb is easily calculated from Equation VI-e. For $K_e = 2.4$, Equation VI-e gives

$$\omega_n^4 - 14\omega_n^2 - 48 = 0$$

from which

$$\omega_n^2 = 6$$

$$\omega_n^2 = 8$$

The smaller of the values is the desired one. Substituting for ω_n^2 in Equation VI-f gives

$$B_1 = 42.$$

For $K_e = 2.38$, Equation VI-e becomes

$$\omega_n^4 - 14\omega_n^2 - 47.6 = 0$$

or

$$\omega_n^2 = 5.815$$

$$\omega_n^2 = 8.185.$$

Substituting the smaller value in Equation VI-f gives

$$B_1 = 40.705$$

Since a parabola is symmetric about its axis the change in Δb is then

$$\text{Change in } \Delta b = 2(42 - 40.705) = 2.59$$

It can be seen from the figure that the instantaneous minimum M-point for $K_e = 2.4$ would lie in the unstable region even if the amplitude of X_2 did not change by the first effect. Consequently, the small increase in K_e causes the instantaneous minimum M-point to move past the left portion of the stability curve into an unstable region. This in turn causes the dynamic equilibrium that would be attained at point 1 in Figure VII-5 to be upset and the signals increase in amplitude. As the signal X_2 increases

the average M-point moves through the stable region along a constant K_e line. Eventually the error channel saturates allowing the system to reach a new limit cycle described by an average M-point on the stability curve somewhere to the left and below point 2 in Figure VII-5.

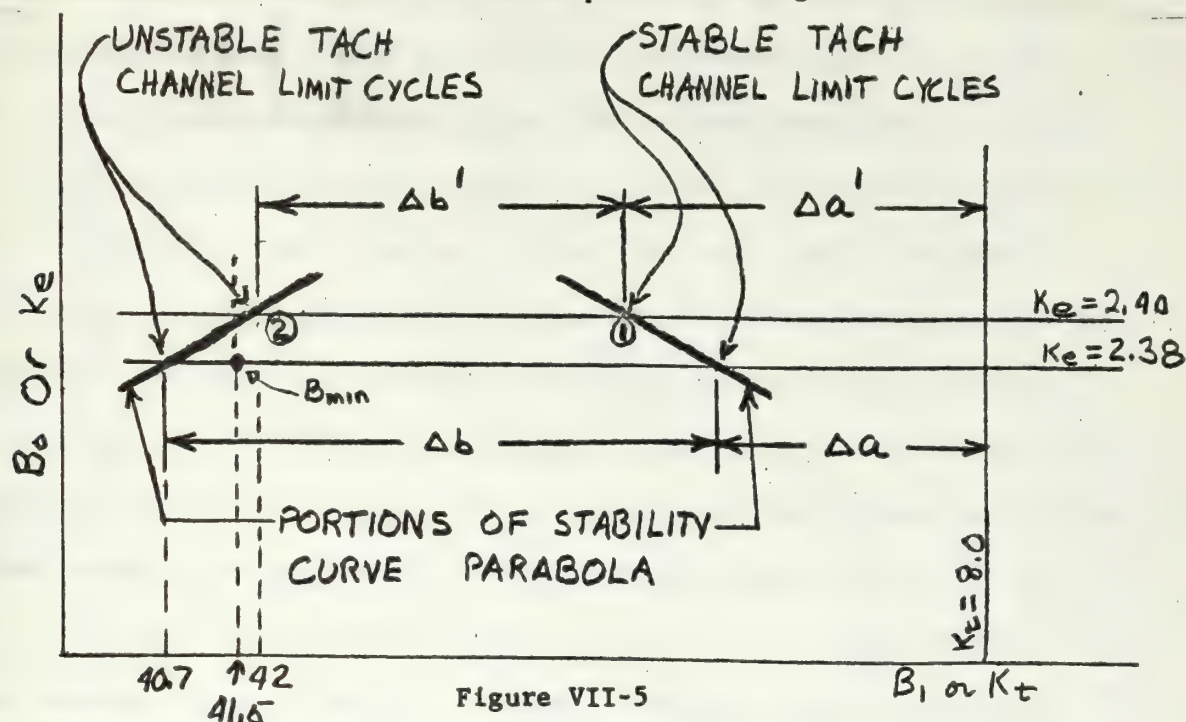


Figure VII-5

Sketch of Phenomenon Occurring at No. 2 Dividing Line

Another indication that the above explanation correctly describes the phenomenon is taken from Figure VI-4. It was noted that the constant K_e lines are linear with varying K_t for M-points below No. 2 dividing line. The line for $K_e = 2.4$ was extrapolated to $K_t = 8$ which should indicate X_{2max} if the limit cycle occurs on the right side of the stability curve. If this X_{2max} is used to obtain a B_{1min} from equation VI-d, one gets

$$B_{1min} = 8 + 160 \left(\frac{3}{X_{2max}} \right) = 35.8$$

If this B_{1min} is now plotted on the coefficient plane, it falls just to the left of the left side of the stability curve which has a B_1 coordinate of 42 for $K_e = 2.4$. Although this B_{1min} is further to the left than would be expected it could be considerably in error because the extrapolated

point is far from the last experimental point and the lower portion of the $K_e = 2.4$ line in Figure VI-4 is based on only four experimental points.

The above explanation either greatly conflicts with certain concepts already used or the author has failed to see the points that would resolve the conflicts. For instance, the concept that the average M-point over a cycle or half cycle indicates the stability of the system over the period or half period which the average M-point is valid. The average M-point has to move through the stable region to reach the left side of the stability curve since the linear value of K_e is the upper vertical limit any M-point can attain. Average M-point motion through the stable region indicates that the signals should decrease slightly in amplitude before increasing to their final limit cycle values. But all of the Recorder Traces exhibiting the same response as Trace VI-15 showed increasing amplitudes until the final limit cycle amplitude was reached. None of the traces showed even a slight decrease from one peak to the next. One explanation that might resolve the conflict is that the fictitious average M-point jumps from the right side to the left side of the stability curve. This is not very reasonable either since the average M-point must in some way be related to the instantaneous amplitude of signal X_2 and this does not change appreciably from peak to peak. Also the B_{lave} curve of Figure VI-10 indicates a smooth transition across the stable region, although the use of describing function when the system is not in a limit cycle is questionable.

c. Dividing lines independent of the magnitude of the saturation voltages.

In Region I just to the left of dividing line No. 1, only the error channel saturates. For linear M-points in this region the frequency of the limit cycle is completely determined by the stability curve which is independent of the saturation voltage. For linear M-points in

Region I, the M-point locus is always the vertical line which is the K_t coordinate of the linear M-point which again is independent of the saturation voltages. Thus the limit cycle is completely determined by the intersection of a curve which is dependent on ω_n and a straight line which is only dependent on the linear M-point. From the intersection, the frequency of the limit cycle and a quantity called N_{lave} are determined. Only when N_{lave} is related to X_{1max} does the saturation voltage play a part. Thus the relative distance the average M-point must move to reach the stability curve is unaltered by E_{s1} as long as the linear M-point remains unchanged and in Region I. As shown in the statement of results and in the explanation of No. 1 dividing line, the dividing line occurs when X_{2max} equals E_{s2} and K_t is increased from low values. Whatever the exact relationship between X_{1max} and X_{2max} in the limit cycle is, it should remain unaltered as long as $E_{s1} = E_{s2}$. Consequently, No. 1 dividing line should be independent of the saturation voltages as long as they remain equal.

The same arguments can be applied in explaining why dividing line No. 2 is apparently independent of the saturation voltages. In explaining the phenomenon that occurs at dividing line No. 2 it was stated that in the process of building up toward a stable tach channel limit cycle on the right side of the stability curve, the amplitude of X_2 became large enough with increasing K_e to drive the instantaneous minimum M-point past the left portion of the stability curve. The pertinent relative distances in this explanation are independent of E_{s2} , that is distances $\Delta a + \Delta b$ and Δa in Figure VII-5. N_{2ave} as a number is completely determined by the distance Δa . N_{2min} is defined as E_{s2}/X_{2max} and a specific N_{2min} is defined by an infinite number of combinations of E_{s2} and X_{2max} . It is noted that N_{2min} is defined exactly the same as the quantity R in the describing function of Equation I-A-3.1 in Chapter I. Thus once N_{2ave} is determined for

a limit cycle the N_{2min} or R can be uniquely determined by the describing function. The dividing line is then determined when N_{2min} as found in the above manner is equal to the N_{2min} required to place the instantaneous minimum M-point on the left side of the stability curve. Since both N_{2min} 's are independent of E_{s2} and only on the characteristics of the linear system, No. 2 dividing line must be independent of E_{s2} .

PROPOSED METHODS OF PREDICTING THE RESULTS OF CHAPTER VI

1. Linear M-point Inside Stable Region.

a. Small step inputs which do not initially saturate the error channel.

In order to predict the response of the nonlinear system under these conditions, the initial peak of $\dot{\Theta}_0$ for the linear system must be found. This can always be found by factoring the total characteristic equation with N_1 and N_2 equal to 1.0 and then solving the linear differential equation for a step of E_{s1} or less. Certain linear system prediction aids may be available such that the actual solution is unnecessary.

Then calculate X_{2max} from

$$X_{2max} = K_t \dot{\Theta}_{0max}$$

If X_{2max} is greater than E_{s2} then calculate B_{1min} from N_{2min} . If B_{1min} plots to the left of the left side of the stability or on it, a limit cycle could result and the linear system should be redesigned. If B_{1min} plots to the right of the left side of the stability curve then the response of the nonlinear system is essentially that of the linear system.

b. A large step input such that the error channel initially saturates.

The first velocity peak again must be found. This could easily be done by using one of the shapes of Figure VII-4 as applied to the plant

if the time t_1 could be determined. However, more study of the problem is required to determine reasonable values of t_1 . Since time t_1 is indefinite an alternative is to solve the differential equation by a two part piecewise linear solution. In this method assume a step input of magnitude E_{s1} is applied to the plant with the linear tach channel feedback included. The differential equation obtained applies up to time t_1 or when $X_2 = E_{s2}$. This differential equation must be solved for θ_0 and its derivatives up to the point of the previous criteria. The values of θ_0 and its derivatives at this time are then used as the initial conditions in the second differential equation which is obtained from the plant alone. The plant driving voltage is zero when the second differential equation applies. With the first velocity peak known B_{1min} can be calculated and plotted on the coefficient plane. If B_{1min} plots to the left of the left side of the stability curve a limit cycle may be possible. If B_{1min} plots in the stable region the response will be similar to those of Recorder Traces VI-2, VI-4, and VI-6.

A second approximate method to find the first velocity peak is now proposed. The author has not had time to think through the method but it does show possibilities. The method basically defines a new equivalent instantaneous transfer function which should be applicable, approximately at least, through the first velocity peak. First the lines of constant ζ with ω_n as a parameter must be calculated from Mitrovic's equations of Appendix A and then plotted on the coefficient plane. Knowing the step input magnitude, the initial degree of error channel saturation can be calculated from

$$N_{1i} = \frac{E_{s1}}{E_i}$$

Knowing N_{1i} the initial M-point which governs the system can be calculated by equation VI-c, the other coordinate is the K_t of the linear M-point since $N_2 = 1.0$ initially. Plotting this M-point, the ζ and ω_n which initially govern the response can be found from the constant ζ lines. This ζ and ω_n are for the dominant closed loop roots only. To find the remaining closed loop roots the instantaneous characteristic equation,

$$s^4 + 7s^3 + 14s^2 + (8 + KK_t)s + KK_e N_{1i} = 0$$

and the quadratic factor,

$$s^2 + 2 \zeta \omega_n s + \omega_n^2$$

must be formed and the first divided by the second. Thus all of the roots of an equivalent instantaneous closed loop transfer function are known.

The gain of the equivalent closed loop transfer function is just $KK_e N_{1i}$.

This equivalent transfer function is shown in Figure VII-6. Two assumptions must now be made in order to use the initial equivalent transfer function.

These are:

1. The nonlinear error channel gain N_{1i} cannot change appreciably until the first velocity peak is reached.

2. The nonlinear tach channel gain N_2 cannot change appreciably.

The first assumption is shown to be approximately true in the recorder traces. The second assumption is not true but must be made in order to proceed. The primary question now becomes what value of E_i' to use with the equivalent transfer function of Figure VII-5. The author has no answer.

A guess might be

$$E_i' = E_i - K_e E_{s1}$$

since the initial error channel saturation has already been taken care of by formulating the transfer function.

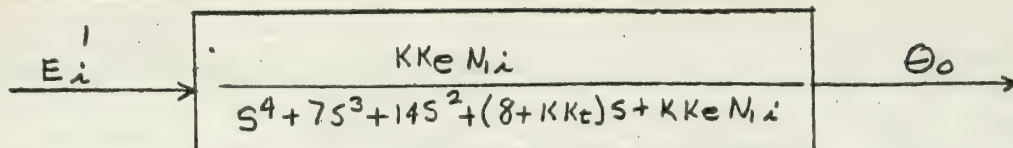


Figure VII-6

Initial Instantaneous Equivalent Closed Loop Transfer Function for Stable Linear M-point with Large Input Steps Applied.

The reason for including the above method was to illustrate an idea which may or may not be applicable to the two nonlinearity problem. Only further study and development will show if the idea has merit. Certainly the instantaneous equivalent closed loop transfer function is easily obtained from Mitrovic's method.

c. The author was unable to predict when the system could be driven into a limit cycle by repeated disturbances. However, it was noted that for any reasonable damping the system should remain stable. One trace was taken for $K_e = 2$ and $K_t = 1.5$, which is still quite close to the left side of the stability curve. The ζ at this point was roughly $\zeta = 0.1$. The disturbances applied were considered quite drastic. They consisted of 6 to 10 disturbances alternating in sign on succeeding half cycles. The tach channel saturated to quite a high degree but the system did remain stable.

2. Prediction of Dividing Lines.

a. No. 1 Dividing Line.

The criterion governing No. 1 dividing line stems from the relationship that must be true between signals X_1 and X_2 under steady state limit cycle operation. This relationship is

$$X_2(t) = \frac{K_t}{K_e} \frac{d}{dt} X_1(t)$$

The only quantity available from Mitrovic's or the root locus methods which is related to the input signal to the nonlinearity is N_{ave} . Without knowing the waveshapes of X_1 and X_2 , the above equation is practically useless for prediction. If sinusoidal waveshapes can be assumed, the above equation can be stated in a useful form. That is, on an amplitude basis

$$X_{2m} = \frac{Kt}{Ke} \omega X_{1m}$$

For sinusoids, X_{1m} and X_{2m} occur a quarter cycle apart but this is immaterial in the dividing line prediction because of the manner in which the dividing lines are defined. From the amplitude relationship, the criterion for No. 1 dividing line is easily formed as

$$\frac{Kt}{Ke} \omega X_{1m} = E_{s2}$$

Consequently, it is apparent that an accurate relationship between X_{1m} and N_{lave} is needed. If the relationship used in Part I, $N_{lave} = E_{s1}/X_{1m}$, is used, the amplitudes obtained differ greatly from the observed amplitudes. However, using this relationship in the criterion, the dividing line is predicted to be a vertical line starting from $\omega = 2.0$ on the stability curve, although the use of ω in the criterion then becomes questionable. In a search for a more accurate relationship, the equivalency of N_{ave} and G_D in Part I was noted. Also the use of the describing function is indicated by the fact that sinusoidal signals had to be assumed to put the criterion into a useable form. Thus the criterion for No. 1 dividing line can be written as

$$\frac{Kt}{Ke} \omega G_{D1}^{-1}(X_{1m}) = E_{s2}$$

where $G_{D1}(X_{1m}) = N_{lave}$ and the symbol $G_{D1}^{-1}(X_{1m})$ is the inverse function of

of $G_{D1}(X_{1m})$ or just $X_{1m}(G_D)$. To find the point on the stability curve where the dividing line starts the same criterion is used but written in a different way, that is

$$\frac{K_t \omega E_{s1}}{K_e} = E_{s2}$$

E_{s1} replaces X_{1m} by the following reasoning. For linear M-points very close to the stability curve, the degree of saturation required to move the average M-point to the stability curve is very small. Thus X_{1max} is essentially equal to E_{s1} . It is then just a matter of trial and error to find the point at which K_e , K_t , and ω satisfy the criterion. It should be noted that for this particular point on the dividing line waveshapes are unimportant if ω is considered the average limit cycle for frequency obtained from the average period.

In applying the criterion to calculate the dividing line, the following procedure was used. A linear M-point was chosen and error channel saturation only was assumed. From the intersection of the K_t coordinate of the linear M-point and the stability curve the ω and N_{lave} of the resulting limit cycle were read. A table of X_{1m} and the resulting G_D was calculated by a digital computer program. Entering the table with N_{lave} , the limit cycle amplitude X_{1m} was obtained. Using ω and X_{1m} along with the linear M-point coordinates in the criterion, a value of X_{2m} was obtained. If this value of X_{2m} was less than E_{s2} , K_t was increased and a new X_{2m} calculated using the same procedure. This procedure was continued until E_{s2} was bracketed by X_{2m} . The procedure rapidly converges to give the K_t for the chosen K_e which results in $X_{2m} = E_{s2}$. Table VI-1 gives a comparison of the calculated and experimental linear M-points which define dividing line No. 1. The results of Table VI-1 were considered quite good since the analog computer

TABLE VI-1

| K_e | Calculated K_t | Experimental K_t |
|-------|---------------------|-----------------------|
| 2.1 | 0.883 | 0.92 |
| 2.3 | 0.855 | 0.89 |
| 2.5 | 0.838 | 0.85 |
| 3.0 | 0.818 | 0.82 |
| 4.0 | 0.79 | 0.81 |
| 5.0 | 0.783 | 0.80 |
| 6.0 | 0.778 | 0.785 |

results are subject to 3-5% error.

The criterion can be put into a form in which once choosing a linear M-point K_e , the linear M-point K_t of the dividing line can be found directly but the algebra is quite involved due to getting $X_{1m}(G_D)$ from equation I-A-3.1 of Part I. The inverse sine and square root terms of Equation I-A-3.1 can be expanded in an infinite series form. If the two infinite series are added, reversion of the series sum can be accomplished to give X_{1m} as a function of G_D . At the intersection of the linear M-point K_t coordinate and the stability curve, N_2 assumed 1.0, Equation VI-c equals Equation VI-e and Equation VI-d equals VI-f. From these equations expressions for N_{ave} , which equals G_D , can be obtained in terms of K_e and K_t . Substitution for the various quantities results in a statement of the criterion in terms of K_e and K_t of the linear M-point only. The expression is very complicated and includes a power series whose argument contains both K_e and K_t .

b. Prediction of No. 2 Dividing Line.

From Figure VI-5 and the explanation of the phenomenon occurring at the dividing line, the criterion governing the dividing line can be stated as follows:

"For the linear M-point on the dividing line, B_{1min} , as calculated for a stable tach channel limit cycle on the right side of the stability curve must equal the B_1 coordinate of the stability curve on the left side where the linear M-point K_e coordinate intersects."

Calculation of the dividing line is again a trial and error procedure. One such procedure using B_1 coordinates is as follows. Choose a K_t and a K_e . Reading the B_1 coordinate of the K_e line intersections from the graph was found to be too inaccurate to give adequate results. Thus the B_1 coordinates of the intersections of the K_e line with the stability curve had to be calculated from Equations VI-e and VI-f. From Equation VI-e, ω_n^2 is found by solving,

$$14 \omega_n^2 - \omega_n^4 = B_o = KK_e$$

Substitution of the two values of ω_n^2 into Equation VI-f gives the desired B_1 coordinates. The following symbols will be used:

B_{1r} = The coordinate of the right intersection at which a stable tach channel limit cycle exists,

B_{1L} = The coordinate of the left intersection at which an unstable tach channel limit cycle exists.

Using B_{1r} , N_{2ave} can be calculated from Equation VI-d. From $N_{ave} = G_D$ and using the pre-calculated table, the value of N_{2min} can be determined. It is noted that the definition of N_{2min} , $N_{2min} = E_{s2}/X_{2max}$, is exactly the definition of the quantity R used in the describing function in Part I, Equation I-A-3.1. Having N_{2min} , B_{1min} can be calculated using

Equation VI-d. A comparison of B_{1min} and B_{1L} can be made. If B_{1min} is greater than B_{1L} , the linear M-point was below the dividing line and K_e must be increased. If B_{1min} is less than B_{1L} , the linear M-point was above the dividing line and K_e must be decreased. Table VII-2 gives a comparison of the experimental dividing line and the calculated dividing line using the procedure outlined above.

TABLE VII-2

| K_t | Calculated K_e | Experimental K_e |
|-------|------------------|--------------------|
| 3 | 2.431 | 2.425 |
| 4 | 2.429 | 2.415 |
| 5 | 2.430 | 2.405 |
| 6 | 2.429 | 2.395 |
| 8 | 2.427 | 2.385 |
| 10 | 2.425 | 2.335 |

The last significant figure shown in the calculated K_e was interpolated between the differences existing in the comparison of B_{1min} with B_{1L} for the calculations at $K_e = 2.42$ and $K_e = 2.43$. The results are surprisingly good considering the calculated K_e is subject to slide rule accuracy and considering the analog results are inherently subject to the 3-5% accuracy. The worst percentage difference between calculated K_e and experimental K_e is less than 4%.

CHAPTER VIII

SOME PREDICTIONS OF RESULTS FOR DIFFERENT SYSTEMS

WITH TWO GAIN VARIABLE NONLINEARITIES

An attempt is made in this chapter to extend certain of the ideas developed in study of the system of Figure VI with equal saturation voltages. However, it must be pointed out that the extension of the ideas is mostly speculation with no specific experimental results to back up the ideas.

An attempt will first be made to indicate the expected results when different parameters of the system of Figure VI are changed. In Chapter VII it has already been shown that both dividing lines are independent of the saturation voltages as long as they remain equal. It is then reasonable to expect the same types of responses for linear M-points in the stable region as the equal saturation voltages are changed. The argument applied is that the relative distances between a given linear M-point and the stability curve remain unaffected by the saturation voltages, thus the degree of saturation required is unchanged. Only the amplitudes of the signals are changed to cause the required degrees of saturation.

For the same linear system with $E_{s2} > E_{s1}$ certain results seem evident. When the linear M-point lies in the stable region and for small input steps in which the error channel does not initially saturate, it should become increasingly difficult to find a linear M-point at which the tach channel saturates as the difference between E_{s2} and E_{s1} is increased. A point should be reached at which E_{s2} exceeds E_{s1} by such a large amount that the response remains linear throughout. By the same reasoning that the tach channel saturates less and less as the difference between E_{s2} and E_{s1} is increased, it should be more difficult to drive the system into a

limit cycle by repeated disturbances. For large signal inputs such that the error channel initially saturates, it should be found that the entire response approaches error channel saturation only as the difference between E_{s2} and E_{s1} is increased.

For $E_{s2} > E_{s1}$, the dividing lines in the unstable regions should be predictable by the criterion as stated in Chapter VII. For dividing line No. 1, the criterion can be rewritten as

$$\frac{K_t \omega}{K_e} = \frac{E_{s2}}{X_{1m}}$$

Assuming only error channel saturation, X_{1m} is independent of E_{s2} since the vertical distance from linear M-point to the stability curve is independent of E_{s2} . Thus for a given K_e , one would expect the dividing line to shift to the right where K_t and ω are larger as E_{s2} is increased and E_{s1} is kept constant. A minimum of calculations show that for $E_{s1} = 3$ and $E_{s2} = 5$, the dividing line starts at $\omega_n = 2.42$ on the stability curve by applying the criteria in the form

$$\frac{K_t \omega}{K_e} E_{s1} = E_{s2}$$

Another point for the same saturation voltages was calculated for $K_e = 5$ and was found to be about $K_t = 1.4$. The criterion in the form useful at the stability curve, indicates that the difference of E_{s2} and E_{s1} is unimportant to the placement of the dividing line. It does, however, indicate that the ratio of E_{s2} to E_{s1} is the quantity which determines the placement of dividing line No. 1. It has already been shown in Chapter VII that for equal saturation voltages, a ratio of 1.0, the dividing line is independent of their magnitude.

This same reasoning also applies to the case where $E_{s2} < E_{s1}$ only the dividing line would shift to the left of the position for $E_{s1} = E_{s2}$.

Thus for any given linear plant and any saturation voltages, dividing line No. 1 should be predictable. The only restriction is that the plant and the feedback paths have the same configuration as Figure VI. Postulating even farther, if the linear plant can be normalized, which has already been done for a third order plant,¹ then a master set of curves should be possible defining dividing line No. 1 in terms of the ratio of E_{s2} to E_{s1} . For the system of Figure VI, described by the coefficient plane of Figure VI-3, it is unclear what happens when the ratio of E_{s2} to E_{s1} becomes large enough such that the starting point of dividing line No. 1 moves to the right of the stability curve maximum. At the maximum for $E_{s1} = 3$, the criteria gives $E_{s2} = 6.64$ or a ratio of 2.213. For this ratio and $K_e = 5$, another point on the dividing line is at $K_t = 1.72$. The criterion applied at the stability curve keeps giving reasonable values of E_{s2} for points to the right of the maximum. For example, for $E_{s1} = 3$ and $\omega_n = 3$, the required E_{s2} is 11 volts.

It was shown in Chapter VII that dividing line No. 2 was independent of the saturation voltages. Although it was not stated explicitly the criterion for the dividing line is only dependent on N_{2ave} and N_{2min} as degrees of saturation. Since the dividing line is independent of the error channel and it has already been shown to be independent of E_{s2} in Chapter VII, it is therefore the same for any combination of saturation voltages.

Since No. 2 dividing line depends only on the degree of saturation in the tach channel, the error channel may saturate as E_{s2} becomes greater than

¹Thaler, G. J. and Brown, R. G., Analysis and Design of Feedback Control Systems, McGraw-Hill, 2nd Ed., 1960: 380-383.

E_{s1} . It was implied for equal saturation that No. 2 dividing line separated linear M-points with tach channel saturation from linear M-points with both channels saturating. A better description of the dividing line No. 2 is that it separates linear M-points for which limit cycles occur on the right side of the stability curve with the tach saturation producing the stable limit cycle from linear M-points for which limit cycles occur on the left side of the stability curve with the error channel producing the stable limit cycle. Thus for linear M-points below No. 2 dividing line it is entirely possible to get both channels saturating for $E_{s2} > E_{s1}$ although the error channel saturation is incidental to the stable limit cycle. Consequently, a third dividing line must be postulated. The description of the third dividing line would be that it separates linear M-points for which only the tach channel saturates from linear M-points for which both channels saturate. For a linear M-point in the region between No. 2 dividing line and No. 3 dividing line the limit cycle will occur on the right side of the stability curve with the stable limit cycle produced solely by the tach channel. The criterion for No. 3 dividing line has to be the same as that for No. 1 dividing line only applied in reverse. In general terms the limit cycle relationship between X_1 and X_2 is

$$\frac{K_e}{K_t} \int X_2(t) dt = X_1(t)$$

Assuming sinusoidal waveshapes of $X_1(t)$ and $X_2(t)$, then

$$\frac{K_e}{\omega K_t} X_{2m} = X_{1m}$$

Then forming the dividing line criterion yields,

$$\frac{K_e}{\omega K_t} X_{2m} = E_{s1}$$

At the stability curve the criterion would simply be

$$\frac{K_e}{\omega K_t} E_{s2} = E_{s1}$$

Since dividing line No. 1 and dividing line No. 3 are obtained by different ways of applying the same criterion, it is reasonable to say they are the same dividing line at least for an E_{s2}/E_{s1} ratio large enough for the right hand portion to be below No. 2 dividing line. With this assumed true, for a few points on the right side stability curve the E_{s2} voltage required to just make $X_{1\max} = E_{s1} = 3$ were calculated by the criterion. Then a few points on the dividing line at three of these voltages were calculated at $K_t = 8$. A very rough sketch of what the complete set of curves might look like is given in Figure VIII-1. The points actually calculated are circled. The dividing lines are labeled in terms of the ratio E_{s2}/E_{s1} , but were calculated assuming $E_{s1} = 3$ and E_{s2} necessary to satisfy the criterion at the stability curve. The dividing lines with no calculated points other than at the stability curve are estimated from the shape of the ones with calculated points. The shape of the dividing lines from the left side of the stability curve were estimated by the shape for $E_{s2}/E_{s1} = 1.0$ although the value of E_{s2}/E_{s1} was calculated by the criterion at the stability curve. If the above postulation of dividing lines proves correct, then for a dividing line such as $E_{s2}/E_{s1} = 8.77$ the only meaningful portion of dividing line No. 2 is the portion to the right of the 8.77 dividing line. The shape of the dividing lines close to stability curve has not been determined. Figure VIII-2 shows three possibilities which may occur. If these postulated dividing lines can be confirmed by analog computer results, then it should be interesting to see if the dividing lines for $E_{s2}/E_{s1} < 2.233$ stop at the stability curve. For $E_{s2}/E_{s1} > 2.33$ the dividing lines at worst have a discontinuity at the stability curve. Thus it may be reasonable that the other dividing lines may enter the stable region. If this is true then they

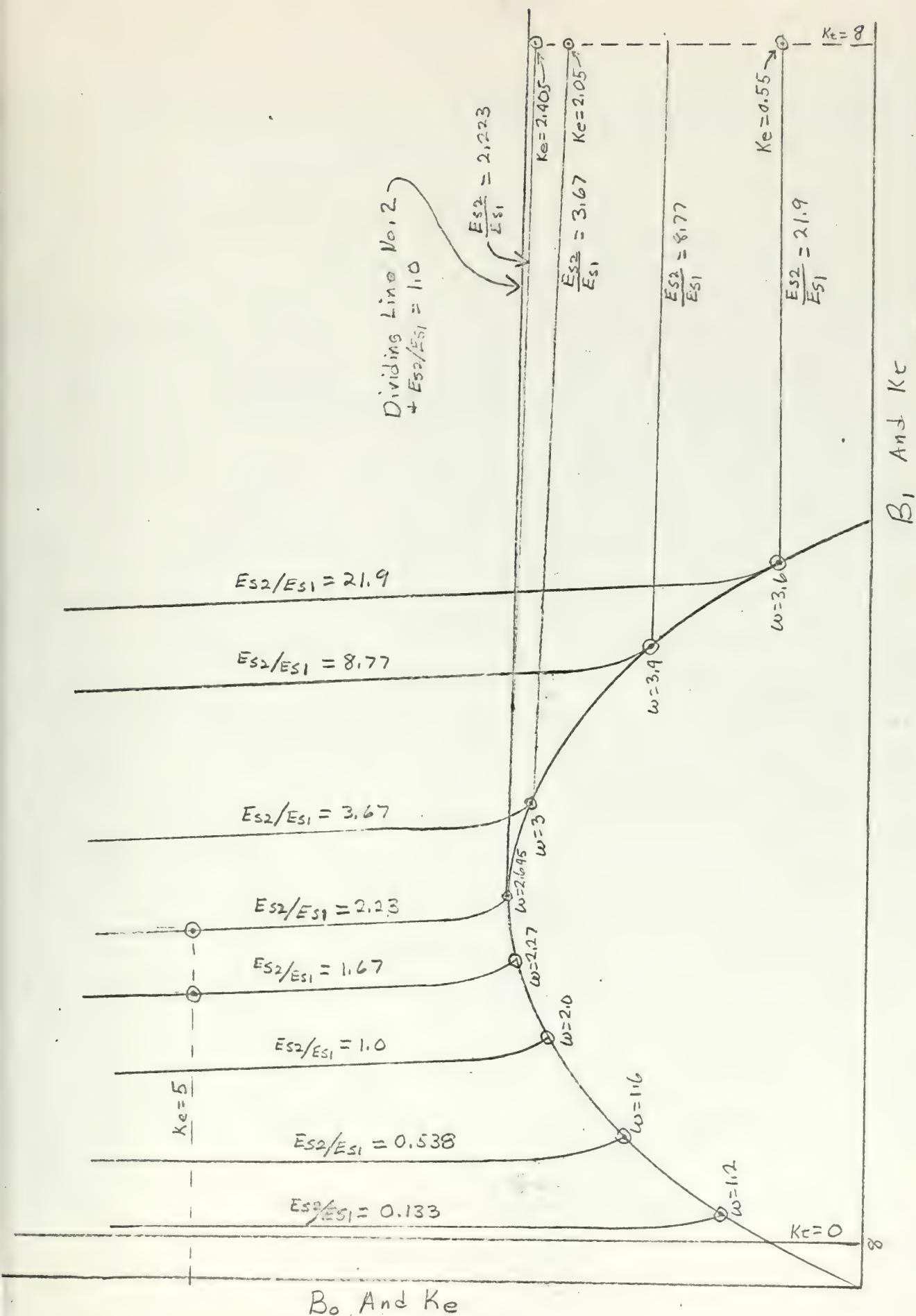


Figure VIII-1

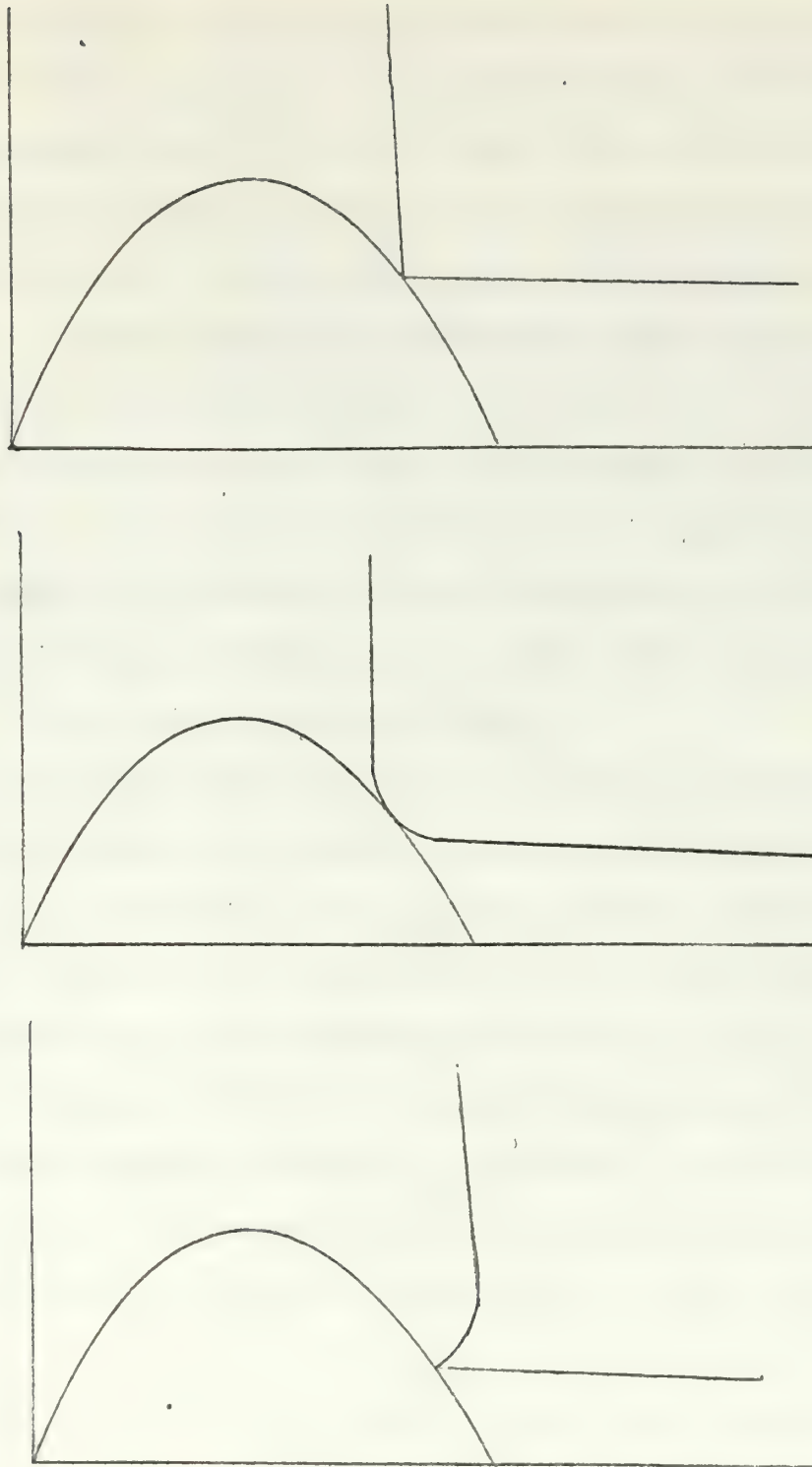


Figure VIII-2

Possible Shapes of the Dividing Lines at the Stability
Curve for Large E_{s2}/E_{s1} Ratios.

should have more than a casual association with possible limit cycle operation of systems whose M-point lies in the stable region. In the small amount of investigation done in driving a stable linear system into a limit cycle with repeated disturbances, all the points investigated were close to the upper part of the stability curve and not much lower than $K_e = 2.0$ or $\omega_n = 2.0$. This may indicate that the dividing line for $E_{s2}/E_{s1} = 1.0$ may circle through the stable region and leave at dividing line No. 2. The author just did not have the time to see if the dividing line criterion could give answers for M-points in the stable region. Certainly from the concepts of degrees of saturation and relative distances it should be easier to drive the instantaneous M-point past the unstable tach channel limit cycle for $E_{s2}/E_{s1} < 1.0$ on the first velocity peak.

When the plant gain K is changed, not very much should change as far as Figure VI-3 is concerned. The stability curve does not change since it is independent of K . The scales on the K_e - K_t grid will vary inversely with K . That is, if K is doubled, the scales will be halved. The all important relative distances between linear M-point and the stability curve will not change as K increases, they will only have different K_e and K_t coordinates. Since the relative distances determine N_{ave} , then No. 1 and No. 2 dividing lines are unchanged as far as the B_0 - B_1 coordinate system is concerned. If the above extension of the dividing lines proves to be valid, then they will be unchanged.

The author can conceive of no reason why most of the concepts discussed in connection with the plant of Figure VI can not be applied with different plants in the block except for second order systems. Mitrovic's method does not lend itself easily to the analysis of second order systems. For a third order plant the stability curve is a straight line and thus dividing

line No. 2 could not exist. Also, with a third order system, the filtering may be insufficient such that the signal X_2 is not sinusoidal in which case the criterion for dividing line No. 1 would give poor predictions since it makes use of the describing function.

With different types of gain variable nonlinearities in the blocks the concept of dividing lines and a knowledge of the type of limit cycles produced by each nonlinearity individually should give a good indication of the actual responses. For example, assume two elements with dead zone in the nonlinear blocks of Figure VI. In this case the entire stability curve represents unstable limit cycles for the error channel dead zone. For the dead zone in the tach channel, the right side of the stability curve represents unstable limit cycles and the left side represents stable limit cycles. It cannot be definitely concluded that a system with a linear M-point in the unstable region will always go into a stable limit cycle. For instance, consider a linear M-point well above the stability curve. If the average value of signal X_1 over a half cycle is initially large, then N_{1ave} can never be small enough to move the average M-point downward below the maximum of the stability curve where the tach channel N_{2ave} can act to move the average M-point to the left side of the stability curve. At this same linear M-point, it should be possible to obtain a stable response for small input signals, that is, N_{1max} and N_{2max} never get large enough to move the instantaneous M-point outside the stable region. Thus it can be seen that the analysis is much more complicated than for two saturations primarily because the initial M-point starts at the point (0,0) of the K_e - K_t grid. However, with more study, one should be able to relate certain M-point motions to the position of the linear M-point and thereby be able to describe certain dividing lines. If dividing lines can be found, then

their position should be dependent only on a ratio of the two amounts of dead zone because N_{ave} and N_{max} would only be dependent on the appropriate relative distances between linear M-point and stability curve.

In all of the previous discussion, a reliance on the describing function is strongly implied. It should be point out at this point that in general the describing function and the requirement of sinusoidal waveshapes are not necessary. The only necessary quantities are the relative distances involved in the coefficient plane since these distances can be related to various phenomena occurring in the experimental results. The relative distances can be described and measured entirely by the somewhat nebulous quantities N_{ave} and N_{min} or N_{max} . The author has only been able to give N_{ave} and N_{min} meaningful interpretations for prediction purposes through the use of the describing function. It should be stressed again that N_{ave} is just a symbol which is used for lack of a better symbol. Even for a sinusoidal signal, a straight integral time average of the instantaneous gain, N , over a cycle does not corrolate with the observed maximum signals. However, for sinusoidal signals the describing function does corrolate N_{ave} with maximum observed signal. Consequently, the relation between the amplitude of the input signal and N_{ave} is much more complicated than a time average of the instantaneous gain and for non sinusoidal waveshapes this relation must certainly be dependent on the waveshape. If a relationship between N_{ave} and the input signal can be found which is independent of waveshape, then all of the prediction methods should be valid.

CHAPTER IX

MISCELLANEOUS IDEAS AND CONCEPTS

In studying the two nonlinearity problems, the author had a few ideas which were not particularly concerned with the problem or which did not give pertinent results. These ideas are considered to have possibilities but were not developed.

The first idea to be discussed concerns a general method for calculating the limit cycles in any system with any number of nonlinearities if any limit cycles exist in the system. If no limit cycle exists, then the method should give no non-trivial solutions. The only restrictions on the method are these:

1. Each nonlinearity must be such that it can be described by a describing function.
2. The linear system must provide enough filtering between the nonlinearities such that the describing function description can be justified.

The basis of the method is application of the stability criterion to the total nonlinear system. In Chapter VII it was indicated that the criterion for the root locus method degenerates into the Niquist criterion at the limit of stability or when $s = j\omega$. In applying the root locus criterion to the total nonlinear system, each nonlinearity must somehow be included as a magnitude and angle. At the stability limit or under limit cycle conditions, the describing function provides the description of the nonlinearity as a magnitude and angle. In other words, the describing function can be thought of as linearizing the nonlinearity on the average over a cycle. Thus the root locus criterion can be formed for the total system

including the nonlinear effects by the magnitude and angle of their describing function. Since the root locus criterion is just a method of rearranging the total characteristic equation, one may as well start with the characteristic equation. It then becomes convenient to express the describing functions as a real part and an imaginary part.

For illustration purposes consider the system configuration of Figure VI. Also let the plant be fourth order, although any order plant can be used, and let the two nonlinear elements be any general nonlinear elements. That is, the nonlinear elements can be gain variable only, hysteretic, or frequency sensitive. The describing function of the nonlinearities can be written as

$$N_1(X_{1m}, \omega) = N_{1r}(X_{1m}, \omega) + j N_{1i}(X_{1m}, \omega)$$

and

$$N_2(X_{2m}, \omega) = N_{2r}(X_{2m}, \omega) + j N_{2i}(X_{2m}, \omega)$$

The total characteristic equation is then

$$a_4 s^4 + a_3 s^3 + a_2 s^2 + (a_1 + K K_t N_2) s + K K_e N_1 = 0$$

substitution of the above describing functions for N_1 and N_2

$$a_4 s^4 + a_3 s^3 + a_2 s^2 + \{a_1 + K K_t [N_{2r}(X_{2m}, \omega) + j N_{2i}(X_{2m}, \omega)]\} s + K K_e [N_{1r}(X_{1m}, \omega) + j N_{1i}(X_{1m}, \omega)] = 0$$

At the stability limit for the total system, $s = j\omega$, thus

$$a_4 \omega^4 - j a_3 \omega^3 - a_2 \omega^2 + j \omega \{a_1 + K K_t [N_{2r}(X_{2m}, \omega) + j N_{2i}(X_{2m}, \omega)]\} + K K_e [N_{1r}(X_{1m}, \omega) + j N_{1i}(X_{1m}, \omega)] = 0$$

Thus two independent equations can be obtained from the above equation each containing the three variables, ω , X_{1m} , and X_{2m} .

Clearly a third equation must be obtained and this equation must come from the physical configuration of the system and must relate X_{1m} to X_{2m} . For other than gain variable nonlinearities, the phase difference must be maintained between X_1 and X_2 . Thus for the configuration of Figure VI, the relationship is

$$s \frac{X_1(s) K_t}{K_e} = X_2(s)$$

or for limit cycle operation,

$$j\omega \frac{K_t}{K_e} X_{1m} = X_{2m}$$

Substitution of this relationship into the characteristic equation will give one equation in two unknowns which can be broken up into two independent equations in the same two unknowns. Of course the nature of the describing functions will make the algebra very messy especially manipulating the terms containing j into real and imaginary terms. Conceivably this can be done and then the single equation can be broken up into the two independent equations, the solutions of which will not be simple.

Thus, in theory anyway, the method is not restricted to the number of nonlinearities as long as a sufficient number of relationships between the individual nonlinearity input signals can be determined from the physical configuration of the system. The only limitation is the justification of the use of the describing function for each nonlinearity, which in itself will eliminate a vast number of multiple nonlinearity system configurations.

A second idea came about in trying to predict the limit cycle for the configuration of Figure VI for a linear M-point in Region II where both channels saturate. The limit cycle must surely be described by the intersection of an average M-point locus and the stability curve. The problem becomes one of predicting the average M-point locus from the linear M-point

to the stability curve. It has been demonstrated that in limit cycle conditions the amplitude of the nonlinearity input signal can adequately be related to N_{ave} through the describing function. Consequently, it was reasoned that in a highly oscillatory condition other than the limit cycle condition, the system can be thought of as being in a quasi-limit cycle at least over a half cycle of oscillation. Thus, it appeared logical that the describing function could be used to relate the average M-point to the maximum amplitude over the half cycle in question. The envelope of the oscillations then becomes important since this determines amplitude of the oscillations. It was then theorized that the total envelope could be approximated by a series of exponential segments with each segment dependent only on the real part of the average root over the half cycle as determined by the average M-point of the half cycle.

For linear M-points in the unstable region, the highly oscillatory condition is assured since for the system studied a stable limit cycle always results. Thus the following method was evolved. For a chosen linear M-point, the resultant closed loop transfer function can be formed and its denominator factored. The linear differential equation is easily solved by operational methods to give the initial linear response. An impulse forcing function of such a magnitude was assumed such that the linear envelope of signals X_1 and X_2 essentially retained symmetry about zero. The amplitude of successive peaks of both signals X_1 and X_2 were calculated until a peak of one of the signals was greater than the saturation voltage. When a signal peak was found that exceeded the saturation voltage, the average M-point was calculated for that half cycle by using the peak magnitude in the describing function to determine the N_{ave} for the saturated channel. This new average M-point was plotted on the coefficient plane.

In order to obtain the information necessary to calculate the next exponential segment of the envelope, a curvilinear grid of constant ζ and ω_n lines had to be superimposed on the coefficient plane. This curvilinear grid was calculated from Mitrovic's mapping equations of Appendix A for negative values of ζ . From the position of the average M-point with respect the ζ and ω_n grid, a new average ζ and ω_n was read which were assumed to govern the response over the next half cycle. Thus the envelope equations for signals X_1 and X_2 for the next half cycle can be written as

$$X_1 = X_{1i} e^{-\zeta \omega_n t}$$

and

$$X_2 = X_{2i} e^{-\zeta \omega_n t}$$

The quantities X_{1i} and X_{2i} are the values of the envelope calculated from the linear solution, or the end points of each preceding exponential segment. The average frequency over a half cycle changes as the governing ζ and ω_n of the half cycle change as

$$\omega = \omega_n \sqrt{1 - \zeta^2}$$

From this relation a new period, T_{ave} , can be obtained. Since the next peak of the signal under consideration occurs a half cycle later, the magnitude of the new envelope segment at the end of the next half cycle was calculated by setting $t = T_{ave}/2$ in the envelope equations. Thus new values of X_{1max} and X_{2max} were determined which were used in the describing function to determine a new M-point to be used over the next half cycle. Thus by successive calculations the average M-point locus was constructed.

Several average M-point loci were calculated in this manner but none of them ever crossed the stability curve. A typical locus calculated in this manner is shown in Figure IX-1. As can be seen the locus approaches but never reaches the stability curve. It appears to continue indefinitely

past the experimental limit cycle while never quite reaching the stability curve. The behavior of the locus calculated in the manner described is reasonable since the average M-point can approach the stability curve as close as one pleases but the ζ to be used in the next half cycle is always negative causing the next peak to be slightly greater than the previous peak. The method as outlined does not take into account the phase difference between the signals. One improvement would be to take the phase difference into account possibly by using quarter cycle increments instead of half cycle increments.

An observation made in the application of the method for the several M-points tried is that the manner of making the transition from the linear M-point to the first average M-point does not affect the locus appreciably for succeeding average M-points. That is, it apparently made no difference whether the exact linear M-point equation was solved completely to calculate the first peak greater than the saturation voltage or that the first peak greater than the saturation was calculated by $X = e^{-\zeta \omega_n t}$ where the linear system ζ and ω_n are used. Thus an initial amplitude of the dominant channel signal greater than saturation could be assumed as long as this amplitude does not cause saturation in the other channel through the relationship

$$\frac{K_T}{K_e} \frac{d}{dt} X_1(t) = X_2(t)$$

Another observation to be noted was that after both channels saturate, the average locus departs from a horizontal or vertical line as the case may be. If a straight line is drawn through the next couple of calculated points, this straight line intersects the stability curve quite close to the experimental limit cycle. This observation is indicated in Figure IX-1. This observation is probably coincidental, but some interpretation may be made in the future.

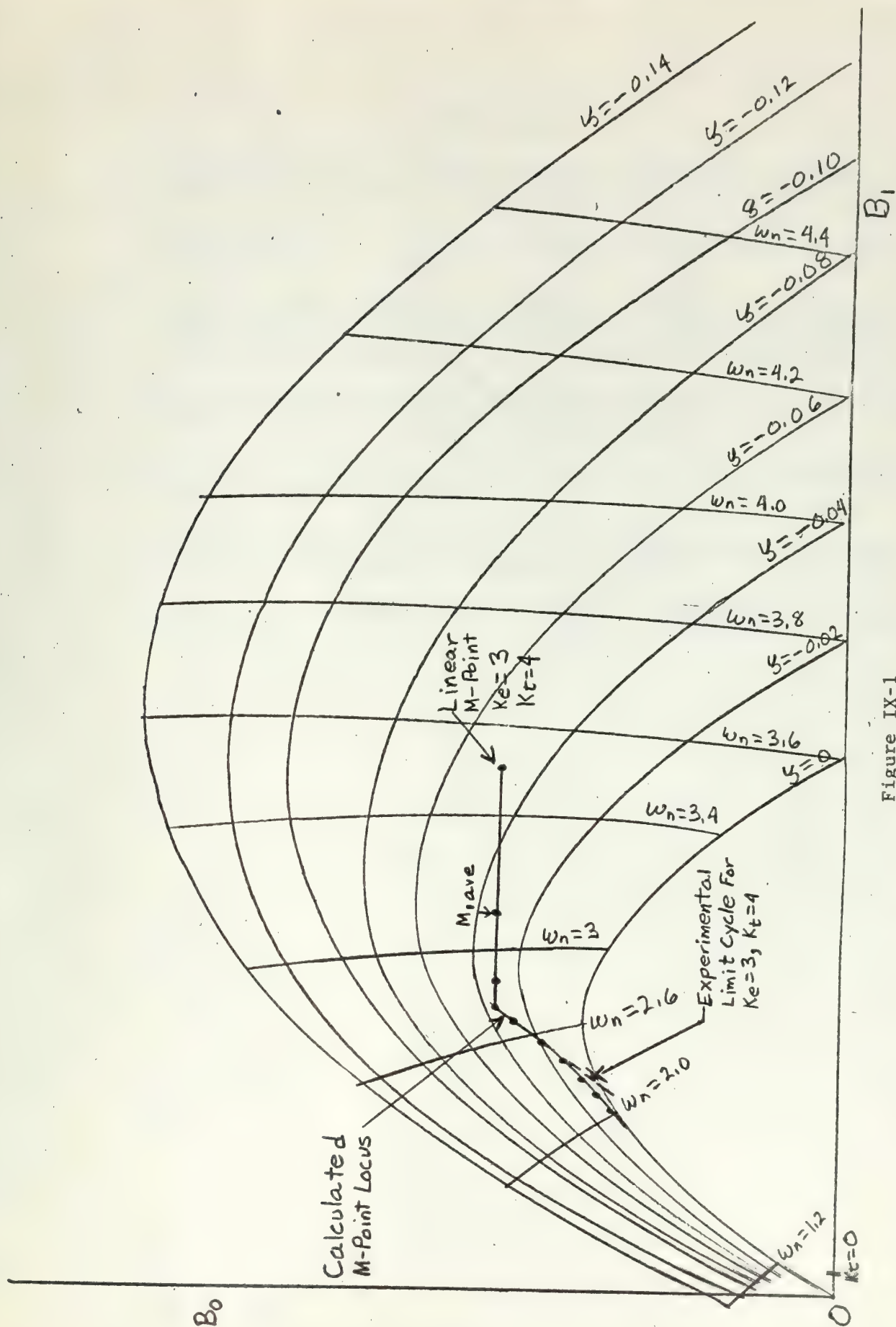


Figure IX-1

Proposed Method of Calculating the Average M-point Locus for a Linear System M-point in Region II.

BIBLIOGRAPHY

1. Kochenburger, R. J., A Frequency Response Method for Analyzing and Synthesizing Contractor Servomechanisms. AIEE Transactions, 1949.
2. Kochenburger, R. J., Limiting in Feedback Control Systems. AIEE Transactions, Pt. II, 1953.
3. Mitrovic, Dusan., Graphical Analysis and Synthesis of Feedback Control System. Part I-Theory and Analysis. AIEE Transaction, Pt. II (Applications and Industry), Vol. 77, 1958 (Jan. 1959 Section) : 476-487.
4. Mitrovic, Dusan., Graphical Analysis and Synthesis of Feedback Control Systems. Part II - Synthesis. Ibid. 487-496.
5. Thaler, G. J. and Brown, R. G., Analysis and Design of Feedback Control Systems. McGraw-Hill, 1960.
6. Thaler, G. J. and Pastel, M. P., Analysis and Design of Nonlinear Feedback Control Systems. McGraw-Hill, 1962.
7. Truxal, J. G., Automatic Feedback Control System Synthesis. McGraw-Hill, 1955.

APPENDIX A

General Equations of Mitrovic's Method¹.

If the overall system characteristic equation is,

$$a_n s^n + a_{n-1} s^{n-1} + a_{n-2} s^{n-2} + \dots + a_1 s + a_0 = 0$$

then Mitrovic's general mapping equations required in this thesis are:

1. For coefficients a_0 and a_1 assumed variable,

$$B_0 = -[a_2 \omega_n^2 \phi_1(y) + a_3 \omega_n^3 \phi_2(y) + \dots + a_{n-1} \omega_n^{n-1} \phi_{n-2}(y) + a_n \omega_n^n \phi_{n-1}(y)]$$

and

$$B_1 = a_2 \omega_n \phi_2(y) + a_3 \omega_n^2 \phi_3(y) + \dots + a_{n-1} \omega_n^{n-2} \phi_{n-1}(y) + a_n \omega_n^{n-1} \phi_n(y).$$

2. For coefficients a_1 and a_2 assumed variable,

$$B_1 = \frac{1}{\omega_n} [a_0 \phi_2(y) - a_3 \omega_n^3 \phi_1(y) - a_4 \omega_n^4 \phi_2(y) - \dots - a_{n-1} \omega_n^{n-1} \phi_{n-3}(y) - a_n \omega_n^n \phi_{n-2}(y)]$$

and

$$B_2 = \frac{1}{\omega_n^2} [a_0 + a_3 \omega_n^3 \phi_2(y) + a_4 \omega_n^4 \phi_3(y) + \dots + a_{n-1} \omega_n^{n-1} \phi_{n-2}(y) + a_n \omega_n^n \phi_{n-1}(y)].$$

The ϕ functions in the above equations are various functions of y only which occur in the derivation of Mitrovic's mapping equations. The ϕ functions are as follows:

$$\begin{aligned} \phi_0(y) &= 0 \\ \phi_1(y) &= -1 \\ \phi_2(y) &= 2y \\ \phi_3(y) &= 1 - 4y^2 \\ \phi_4(y) &= -4y + 8y^3 \\ \phi_5(y) &= -1 + 12y^2 - 16y^4 \\ &\vdots \end{aligned}$$

¹Thaler, G. J. and Ohta, T., Mitrovic's Method - Some Fundamental Techniques, United States Naval Postgraduate School, Research Paper, No. 39, Jan 1964.

From the above listing, a general formula evolves from which next ϕ function can be formed by knowing the two preceding ϕ functions. This formula is:

$$\phi_m(y) = -[2y\phi_{m-1}(y) + \phi_{m-2}(y)] \quad m \geq 2.$$

For convenience, the values of the ϕ functions for $y = 0$ are given below.²

$$\phi_1(0) = -1$$

$$\phi_2(0) = 0$$

$$\phi_3(0) = +1$$

$$\phi_4(0) = 0$$

$$\phi_5(0) = -1$$

$$\phi_6(0) = 0$$

$$\phi_7(0) = +1$$

|
|
|
|
|

²Thaler, G. J. and Brown, R. G., Analysis and Design of Feedback Control Systems, McGraw-Hill, 1960, Ch 10.

APPENDIX B

Tabulated Results of Analog Computer Study with $E_{s1} = E_{s2} = 3$ volts.

Table I gives the results of the first set of computer runs traversing the B_0 versus B_1 plane with a linear system M-point.

TABLE I

| Linear System M-Point | | Resulting Limit Cycle | | | | |
|--------------------------|-------|----------------------------------|------------|------------|------------|------------|
| K_e | K_z | ω | X_{1max} | N_{1min} | X_{2max} | N_{2min} |
| 0.5 | 0.1 | Stable for E_i up to 200 volts | | | | |
| | 0.5 | Stable for E_i up to 200 volts | | | | |
| | 4.5 | 3.65 | 0.101 | 1.0 | 3.31 | 0.907 |
| | 5.0 | 3.64 | 0.106 | 1.0 | 3.97 | 0.756 |
| | 5.5 | 3.63 | 0.111 | 1.0 | 4.6 | 0.653 |
| | 6.0 | 3.63 | 0.118 | 1.0 | 5.0 | 0.60 |
| | 8.0 | 3.63 | 0.126 | 1.0 | 7.2 | 0.417 |
| | 10.0 | 3.62 | 0.132 | 1.0 | 9.22 | 0.326 |
| 1.0 | 0.1 | 1.19 | 3.62 | 0.829 | 0.435 | 1.0 |
| | 0.2 | Stable for E_i up to 150 volts | | | | |
| | 4.0 | 3.51 | 0.207 | 1.0 | 3.62 | 0.807 |
| | 4.5 | 3.49 | 0.242 | 1.0 | 3.8 | 0.789 |
| | 5.0 | 3.49 | 0.266 | 1.0 | 4.45 | 0.674 |
| | 6.0 | 3.49 | 0.283 | 1.0 | 5.65 | 0.531 |
| | 8.0 | 3.48 | 0.302 | 1.0 | 8.0 | 0.375 |
| | 10.0 | 3.47 | 0.314 | 1.0 | 10.3 | 0.291 |
| 1.5 | 0.2 | 1.3 | 5.08 | 0.591 | 0.895 | 1.0 |
| | 0.4 | 1.51 | 3.58 | 0.838 | 1.48 | 1.0 |
| | 0.5 | 1.6 | 3.02 | 0.994 | 1.57 | 1.0 |
| | 0.55 | Stable for E_i up to 100 volts | | | | |
| 1.5 | 1.0 | Stable for E_i up to 100 volts | | | | |
| | 3.8 | 3.37 | 0.384 | 1.0 | 3.35 | 0.92 |
| | 4.5 | 3.36 | 0.45 | 1.0 | 4.5 | 0.667 |
| | 5.0 | 3.36 | 0.465 | 1.0 | 5.2 | 0.577 |
| | 6.0 | 3.36 | 0.49 | 1.0 | 6.46 | 0.464 |
| | 8.0 | 3.35 | 0.515 | 1.0 | 9.25 | 0.324 |
| | 10.0 | 3.34 | 0.525 | 1.0 | 11.6 | 0.269 |

Table I (Cont'd)

| Linear System M-Point | | Resulting Limit Cycle | | | | |
|--------------------------|-------|-----------------------------------|-------------|-------------|-------------|-------------|
| K_e | K_t | ω | $X_{1\max}$ | $N_{1\min}$ | $X_{2\max}$ | $N_{2\min}$ |
| 2.0 | 0.2 | 1.3 | 7.28 | 0.413 | 0.95 | 1.0 |
| | 0.5 | 1.595 | 4.9 | 0.613 | 1.94 | 1.0 |
| | 0.7 | 1.76 | 3.89 | 0.772 | 2.46 | 1.0 |
| | 0.9 | 1.92 | 3.19 | 0.94 | 2.79 | 1.0 |
| | 0.97 | 1.97 | 3.04 | 0.987 | 2.82 | 1.0 |
| | 1.1 | Stable for E_i up to 75 volts | | | | |
| | 2.0 | Stable for E_i up to 75 volts | | | | |
| | 3.3 | 3.15 | 0.655 | 1.0 | 3.32 | 0.904 |
| | 3.5 | 3.15 | 0.705 | 1.0 | 3.72 | 0.806 |
| | 4.0 | 3.14 | 0.755 | 1.0 | 4.63 | 0.648 |
| | 6.0 | 3.12 | 0.86 | 1.0 | 7.72 | 0.388 |
| | 8.0 | 3.11 | 0.9 | 1.0 | 10.7 | 0.28 |
| | 10.0 | 3.11 | 0.925 | 1.0 | 13.7 | 0.219 |
| 2.4 | 0.7 | 1.755 | 5.25 | 0.572 | 2.72 | 1.0 |
| | 0.8 | 1.84 | 4.88 | 0.614 | 3.0 | 1.0 |
| | 0.9 | 1.9 | 4.55 | 0.659 | 3.28 | 0.915 |
| | 1.5 | 2.09 | 3.82 | 0.785 | 5.0 | 0.6 |
| | 1.7 | Stable for E_i up to 62.5 volts | | | | |
| | 2.5 | 2.84 | 1.03 | 1.0 | 3.07 | 0.977 |
| | 3.0 | 2.82 | 1.28 | 1.0 | 4.5 | 0.667 |
| | 4.0 | 2.78 | 1.53 | 1.0 | 6.95 | 0.432 |
| | 5.0 | 2.75 | 1.6 | 1.0 | 9.5 | 0.316 |
| | 5.3 | 2.20 | 3.75 | 0.759 | 17.8 | 0.1686 |
| | 5.5 | 2.18 | 3.79 | 0.772 | 18.5 | 0.1622 |
| | 6.0 | 2.19 | 3.7 | 0.811 | 19.8 | 0.1515 |
| | 8.0 | 2.17 | 3.59 | 0.837 | 27.2 | 0.1102 |
| | 10.0 | 2.18 | 3.72 | 0.817 | 32.4 | 0.0926 |
| 2.5 | 0.2 | 1.29 | 9.2 | 0.326 | 0.96 | 1.0 |
| | 0.5 | 1.595 | 6.25 | 0.48 | 1.98 | 1.0 |
| | 0.7 | 1.76 | 5.25 | 0.572 | 2.6 | 1.0 |
| | 0.8 | 1.83 | 4.85 | 0.619 | 2.88 | 1.0 |
| | 0.9 | 1.89 | 4.6 | 0.652 | 3.14 | 0.955 |
| | 1.0 | 1.98 | 4.4 | 0.682 | 3.4 | 0.883 |
| | 1.5 | 2.05 | 3.96 | 0.758 | 4.85 | 0.618 |
| | 2.0 | 2.1 | 3.82 | 0.785 | 6.45 | 0.465 |
| | 2.5 | 2.13 | 3.76 | 0.798 | 8.0 | 0.375 |
| | 3.0 | 2.14 | 3.72 | 0.807 | 9.5 | 0.316 |
| | 3.5 | 2.145 | 3.7 | 0.811 | 11.1 | 0.27 |
| | 4.0 | 2.16 | 3.7 | 0.811 | 12.5 | 0.24 |
| | 5.0 | 2.17 | 3.68 | 0.815 | 15.9 | 0.1887 |
| | 6.0 | 2.2 | 3.7 | 0.811 | 19.3 | 0.1555 |
| | 8.0 | 2.15 | 3.68 | 0.815 | 25.2 | 0.119 |
| | 10.0 | 2.14 | 3.68 | 0.815 | 32.0 | 0.0937 |

Table I (Cont'd)

| Linear System M-Point | | Resulting Limit Cycle | | | | |
|--------------------------|-------|-----------------------|------------|------------|------------|------------|
| K_e | K_t | ω | X_{lmax} | N_{lmin} | X_{2max} | N_{2min} |
| 3.0 | 0.2 | 1.295 | 11.2 | 0.268 | 0.965 | 1.0 |
| | 0.5 | 1.595 | 7.65 | 0.392 | 2.04 | 1.0 |
| | 0.7 | 1.755 | 6.4 | 0.469 | 2.78 | 1.0 |
| | 0.8 | 1.83 | 6.3 | 0.477 | 3.08 | 0.974 |
| | 1.0 | 1.94 | 5.7 | 0.527 | 3.68 | 0.815 |
| | 1.5 | 2.0 | 5.5 | 0.545 | 5.55 | 0.54 |
| | 2.0 | 2.04 | 5.45 | 0.55 | 7.25 | 0.413 |
| | 2.5 | 2.025 | 5.25 | 0.597 | 9.0 | 0.333 |
| | 3.0 | 2.06 | 5.27 | 0.569 | 10.8 | 0.278 |
| | 3.5 | 2.075 | 5.25 | 0.582 | 12.5 | 0.24 |
| | 4.0 | 2.05 | 5.35 | 0.56 | 14.2 | 0.211 |
| | 5.0 | 2.05 | 5.35 | 0.56 | 18.3 | 0.164 |
| | 6.0 | 2.065 | 5.3 | 0.567 | 21.6 | 0.139 |
| | 8.0 | 2.07 | 5.25 | 0.582 | 27.4 | 0.1095 |
| | 10.0 | 2.085 | 5.22 | 0.574 | 35.4 | 0.0847 |
| 3.5 | 1.0 | 1.935 | 6.65 | 0.451 | 3.55 | 0.845 |
| | 2.0 | 2.02 | 6.55 | 0.458 | 6.98 | 0.43 |
| | 4.0 | 2.05 | 6.15 | 0.488 | 13.9 | 0.216 |
| | 6.0 | 2.05 | 6.2 | 0.484 | 20.8 | 0.1445 |
| | 8.0 | 2.045 | 6.3 | 0.476 | 28.2 | 0.1065 |
| 4.0 | 1.0 | 1.92 | 7.65 | 0.392 | 3.59 | 0.836 |
| | 2.0 | 2.03 | 7.15 | 0.387 | 6.75 | 0.444 |
| | 4.0 | 2.045 | 7.15 | 0.42 | 13.9 | 0.216 |
| | 8.0 | 2.03 | 7.2 | 0.417 | 28.4 | 0.1055 |
| 4.5 | 1.0 | 1.925 | 8.7 | 0.345 | 3.59 | 0.836 |
| | 2.0 | 2.01 | 8.25 | 0.364 | 7.1 | 0.423 |
| | 4.0 | 2.04 | 8.15 | 0.368 | 14.1 | 0.213 |
| | 6.0 | 2.035 | 8.35 | 0.359 | 21.4 | 0.1405 |
| | 8.0 | 2.035 | 8.3 | 0.361 | 28.6 | 0.105 |
| 5.0 | 1.0 | 1.915 | 9.7 | 0.309 | 3.62 | 0.829 |
| | 2.0 | 2.00 | 9.25 | 0.324 | 7.15 | 0.42 |
| | 4.0 | 2.035 | 9.1 | 0.33 | 14.1 | 0.213 |
| | 6.0 | 2.025 | 9.2 | 0.326 | 21.6 | 0.139 |
| | 8.0 | 2.025 | 9.15 | 0.328 | 28.8 | 0.1045 |
| 5.5 | 1.0 | 1.915 | 10.7 | 0.28 | 3.62 | 0.829 |
| | 2.0 | 2.00 | 10.07 | 0.298 | 7.15 | 0.42 |
| | 4.0 | 2.03 | 10.05 | 0.299 | 14.2 | 0.211 |
| | 6.0 | 2.03 | 10.0 | 0.30 | 21.5 | 0.1395 |
| | 8.0 | 2.025 | 10.02 | 0.294 | 28.9 | 0.104 |

Table I (Cont'd)

| Linear System M-Point | | Resulting Limit Cycle | | | | |
|--------------------------|-------|-----------------------|------------|------------|------------|------------|
| K_e | K_t | ω | X_{lmax} | N_{lmin} | X_{2max} | N_{2min} |
| 6.0 | 1.0 | 1.915 | 11.7 | 0.256 | 3.63 | 0.827 |
| | 2.0 | 2.00 | 11.07 | 0.271 | 7.15 | 0.42 |
| | 4.0 | 2.025 | 11.05 | 0.272 | 14.2 | 0.211 |
| | 6.0 | 2.035 | 11.0 | 0.273 | 21.4 | 0.1405 |
| | 8.0 | 2.025 | 11.2 | 0.268 | 29 | 0.1035 |

Table II gives the resulting limit cycle for linear M-point close to dividing line No. 1.

TABLE II

| Linear System M-point | | Resulting Limit Cycle | | |
|--------------------------|-------|-----------------------|------------|------------|
| K_e | K_t | ω_{ave} | X_{1max} | X_{2max} |
| 2.1 | 0.90 | 1.92 | 3.52 | 2.98 |
| | 0.92 | 1.93 | 3.50 | 3.0 |
| | 0.96 | 1.955 | 3.42 | 3.08 |
| | 1.0 | 1.99 | 3.34 | 3.19 |
| 2.3 | 0.86 | 1.895 | 4.2 | 2.97 |
| | 0.88 | 1.91 | 4.1 | 2.99 |
| | 0.90 | 1.915 | 4.05 | 3.03 |
| | 0.92 | 1.925 | 4.0 | 3.07 |
| 2.5 | 0.80 | 1.85 | 4.9 | 2.89 |
| | 0.82 | 1.87 | 4.83 | 2.95 |
| | 0.84 | 1.88 | 4.75 | 2.99 |
| | 0.86 | 1.89 | 4.7 | 3.03 |
| | 0.88 | 1.91 | 4.65 | 3.08 |
| | 0.90 | 1.915 | 4.6 | 3.12 |
| 3.0 | 0.80 | 1.83 | 6.0 | 2.96 |
| | 0.82 | 1.85 | 5.85 | 2.98 |
| | 0.84 | 1.865 | 5.8 | 3.02 |
| 4.0 | 0.80 | 1.83 | 8.05 | 2.96 |
| | 0.82 | 1.85 | 8.0 | 3.02 |
| 5.0 | 0.79 | 1.82 | 10.35 | 2.92 |
| | 0.80 | 1.83 | 10.25 | 3.0 |
| | 0.81 | 1.84 | 10.2 | 3.04 |
| 6.0 | 0.78 | 1.815 | 12.1 | 2.98 |
| | 0.79 | 1.83 | 12.4 | 3.02 |
| | 0.80 | 1.84 | 12.5 | 3.03 |

Table III gives the resulting limit cycles for linear M-points close to dividing line No. 2.

TABLE III

| Linear System M-point | | Resulting Limit Cycle | | |
|--------------------------|-------|-----------------------|------------|------------|
| K_t | K_e | ω_{ave} | X_{1max} | X_{2max} |
| 3.0 | 2.40 | 2.78 | 1.31 | 4.5 |
| | 2.42 | 2.73 | 1.49 | 4.68 |
| | 2.43 | 2.08 | 3.83 | 9.65 |
| | 2.45 | 2.08 | 3.88 | 9.75 |
| 4.0 | 2.35 | 2.83 | 1.25 | 6.1 |
| | 2.38 | 2.74 | 1.42 | 6.51 |
| | 2.39 | 2.71 | 1.57 | 6.7 |
| | 2.41 | 2.68 | 1.58 | 6.85 |
| | 2.42 | 2.09 | 3.68 | 12.8 |
| 5.0 | 2.40 | 2.68 | 1.51 | 8.6 |
| | 2.41 | 2.11 | 3.7 | 16.0 |
| | 2.42 | 2.12 | 3.68 | 16.5 |
| 6.0 | 2.39 | 2.73 | 1.52 | 10.3 |
| | 2.40 | 2.11 | 3.66 | 19.0 |
| 8.0 | 2.38 | 2.75 | 1.60 | 14.3 |
| | 2.39 | 2.13 | 3.62 | 27.4 |
| | 2.40 | 2.15 | 3.65 | 27.8 |
| 10 | 2.38 | 2.74 | 1.62 | 18.7 |
| | 2.39 | 2.16 | 3.7 | 32.8 |

thesW6415

Use of Mitrovic's method in predicting l



3 2768 000 98673 1
DUDLEY KNOX LIBRARY